

Base Metal Complexes of Ketone and Imine Ligands:

Metal-Ligand Cooperativity and Catalytic Hydrosilylation

Onedele Metaalcomplexen van Keton- en Imineliganden:

Metaal-Ligand Coöperativiteit en Katalytische Hydrosilylering

(met een samenvatting in het Nederlands)

Proefschrift

ter verkrijging van de graad van doctor aan de Universiteit Utrecht op  
gezag van de rector magnificus, prof.dr. G.J. van der Zwaan, ingevolge het  
besluit van het college voor promoties in het openbaar te verdedigen op  
woensdag 14 maart 2018 des middags te 12.45 uur

door

**Dide Gertruda Adriana Verhoeven**

geboren op *3 september 1990*  
te *Utrecht*

Promotor: Prof.dr. R. J. M. Klein Gebbink

Copromotor: Dr. M. -E. Moret

The work described in this Ph. D. thesis was financially supported by the Sectorplan Natuur- en Scheikunde.

# Base Metal Complexes of Ketone and Imine Ligands:

Metal-Ligand Cooperativity and Catalytic Hydrosilylation

*Hoe ver je gaat,  
Heeft met afstand niets te maken.  
Hoogstens met de tijd.*

– Bløf

Verhoeven, Dide Gertruda Adriana

Title: Base Metal Complexes of Ketone and Imine Ligands: Metal-Ligand Cooperativity and Catalytic Hydrosilylation

Utrecht, Utrecht University, Faculty of Science

Ph. D. thesis Utrecht University – with ref. – with summary in Dutch

ISBN: 978-90-393-6946-3

The work described in this thesis was carried out at the Organic Chemistry & Catalysis group, Debye Institute for Nanomaterials Science, Faculty of Science, Utrecht University, Utrecht, the Netherlands.

Front cover: *Het Overkomen* – Catalytic profile represented by a floral pathway.

The activation energy of a chemical reaction is represented by the cold mountain in the background, the pathway as followed in a catalytic reaction is shown in front by the lower laying hills and the path is given by the flowers. The figure on the hills is a representation of the cooperative theme of the thesis with assistance from the butterfly on the hand.

Artist: Frans Geenen, *Just Frans Art*, [www.justfransart.nl](http://www.justfransart.nl)

# Table of Contents

<b>Preface</b>	7
<b>Chapter 1</b> Metal-Ligand Cooperativity at Tethered $\pi$ -Ligands	11
<b>Chapter 2</b> Coordination of a Diphosphine-Ketone Ligand to Ni(0), Ni(I), and Ni(II): Reduction-Induced Coordination	47
<b>Chapter 3</b> Periodic Trends in the Binding of a Phosphine-Tethered Ketone Ligand to Fe, Co, Ni, and Cu	61
<b>Chapter 4</b> Cobalt-Catalyzed Hydrosilylation of Olefins and Ketones	81
<b>Chapter 5</b> Nickel Complexes of Diphosphine-Tethered Imine Ligands	99
<b>Chapter 6</b> Nickel Complexes with Diphosphine-Tethered Imine Ligands: Silane Activation, Hydrosilylation and Mechanistic Insights	119
<b>Appendices</b>	143
A: The Crystal Structure of Na[B(Ar <sup>F</sup> ) <sub>4</sub> ]	
B: Additional Experimental Section to Chapter 2	
C: Additional Experimental Section to Chapter 3	
D: Additional Experimental Section to Chapter 4	
E: Additional Experimental Section to Chapter 5	
F: Additional Experimental Section to Chapter 6	
<b>Summary</b>	183
<b>Samenvatting</b>	189
<b>Dankwoord</b>	197
<b>Résumé</b>	203
<b>Publication list</b>	205



## Preface

The incorporation of cooperative ligands in metal complexes is gaining interest for the development of new homogeneous catalysts. Productive elementary reactions in catalysis, such as bond-making and bond-breaking processes, are often two-electron transformations which are generally well mediated by late second and third row transition metals. However, economic and environmental considerations warrant the investigation of catalysts based on first row transition metals such as Fe, Co, Ni and Cu, which tend to undergo one-electron reactions. Employing cooperative ligands, i.e. ligands that directly participate in chemical reactions, in base metal catalysis can lead to enhanced reactivity and selectivity, overcoming often undesired one-electron pathways. The use of  $\pi$ -ligands for such processes is a promising strategy, as these ligands can adapt their bonding in versatile ways and therewith stabilize the metal center during reactivity. In this thesis, the synthesis, complexation, and reactivity of two phosphine tethered  $\pi$ -ligand frameworks, containing a ketone or an imine backbone, are investigated.

In **Chapter 1**, current examples of tethered  $\pi$ -bound complexes are reviewed, including C=C, C=O, C=N, and boron containing moieties. The synthesis and reactivity of these systems is discussed, especially focusing on possible metal-ligand cooperativity.

**Chapter 2** focusses on the use of the diphosphine-ketone ligand  $^{\text{Ph}}\text{dppb}$  ( $^{\text{Ph}}\text{dppb}$  = 2,2'-bis(diphenyl-phosphino)benzophenone). A series of nickel complexes is formed, with varying oxidation states of II, I and 0. The ketone functionality in this series is shown to possess hemilabile behavior, with noncoordination in the Ni(II) complex ( $^{\text{Ph}}\text{dppb}$ )NiCl<sub>2</sub> and  $\eta^2(\text{C},\text{O})$ -coordination upon reduction of the metal center to Ni(I) or Ni(0). The electronic structure of these complexes is further investigated by DFT calculations, indicating that bonding in the coordinating structures is dominated by  $\pi$ -backdonation, and the ligand acts as an acceptor ligand.

The coordination chemistry of the  $^{\text{Ph}}\text{dppb}$  ligand is extended to base metals Fe, Co, and Cu in **Chapter 3**. Again, noncoordination is obtained in the M(II) structures (M = Fe, Co and Ni), and in a dimeric Cu(I) complex. Synthesis of the M(I) complexes (M = Fe, Co and Ni) leads to  $\eta^2(\text{C},\text{O})$ -coordination of the C=O fragment. Special attention is paid to the latter binding mode and periodic trends are observed throughout the series. A study of the geometrical and computational parameters allows for an improved understanding of the binding of ketones to late first row transition metals. In **Chapter 4**, the catalytic activity of the Co(I) complex towards hydrosilylation is described. To increase solubility, a slightly modified ligand is used, in which the phenyl substituents on the phosphines are replaced by *p*-tolyl groups. ( $^{\text{pTol}}\text{dppb}$ )CoCl is an active catalyst in the hydrosilylation of alkenes and ketones with phenylsilane. Mild conditions are employed, being 1 mol% Co(I), room temperature, 1 h, and neat conditions for the hydrosilylation of benchmark substrate 1-octene.

In **Chapter 5**, an imine-based  $\pi$ -ligand is explored. The ligand consists of two diphosphine substituted *o*-phenylene linkers bound to the C=N backbone (PCNP), which is readily synthesized *via* imine condensation of the amine and aldehyde building blocks. Synthesis of Ni(II) complex  $(P^{Ph}CNP^{Ph})NiCl_2$  with phenyl substituents on the diphosphine linkers results in an  $\eta^1(N)$ -coordination of the ligands' imine backbone. The less common  $\eta^2(C,N)$ -coordination is obtained by synthesis of its Ni(0) analogue  $(P^{Ph}CNP^{Ph})Ni(PPh_3)$ , with additional coordination of both phosphine arms and a  $PPh_3$  ligand. The influence of additional bulk on the ligand was investigated by substitution of the phenyl groups by *o*-tolyl groups, forming a mixed diphenyl/di-*o*-tolyl and a tetra *o*-tolyl substituted complex. The latter leads to an adjusted coordination, only binding one phosphine arm of the PCNP ligand next to the imine backbone, and  $PPh_3$ . Coordination of  $P^{Ph}CNP^{Ph}$  to Ni(0) without the addition of a co-ligand results in a dimeric  $\mu-\eta^1(N)\eta^2(C,N)$ -coordinating complex, in a mixture with a species that is suggested to arise from C–C coupling of the two imine-carbon atoms in a Ni(0)/Ni(II) mixed valence complex. A crystalline Ni(0)/Ni(II) compound is obtained upon exposure to CO.

**Chapter 6** expands on the nickel complexes of the PCNP ligands, and reactivity with hydrosilanes is described. The complexes selectively activate one equivalent of diphenylsilane, resulting in formal hydrosilylation of the imine backbone. One hydride binds to the imine-carbon atom and the remaining  $-SiHPh_2$  binds to the imine-nitrogen. The Si–H bond of the latter fragment also coordinates in an  $\eta^2(Si,H)$ -fashion to Ni. The activation mechanism is detailed with stoichiometric reactions and DFT calculations. The formed Si–Ni-complexes are active precatalysts in the hydrosilylation of 1-octene with diphenylsilane, and the mechanism of this reaction is investigated using stoichiometric reactions, indicating, amongst other findings, that the Si–N bond is formed reversibly under catalytic conditions.







*When we dream alone it's only a dream,  
But when many dream together it is the beginning of a new reality.*  
- F. Hundertwasser

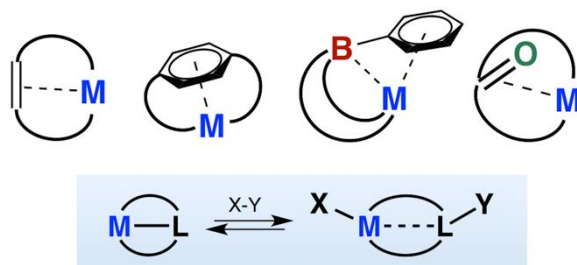


# | Chapter 1 |

## Metal-Ligand Cooperation at Tethered $\pi$ -Ligands

**Abstract** Metal-ligand cooperativity in homogeneous catalysis is emerging as a powerful tool for the design of efficient transition-metal catalysts. This chapter highlights recent advances in the use of neutral  $\pi$ -coordinating ligands, tethered to a transition-metal center by other donor ligands, as cooperative reaction centers. The state-of-the-art organometallic complexes, including  $\pi$ -coordinating ligands originating from C=C, C=E (E = O, N) and boron containing moieties, are described here, with special attention on their specific reactivity. Geometric and electronic aspects of ligand design and their influence on the coordination mode and reactivity of the  $\pi$ -system are discussed.

*Recent advances in the use of tethered  $\pi$ -coordinating ligands for metal-ligand cooperation*



---

Published as: D. G. A. Verhoeven, M.-E. Moret, *Dalton Trans.*, **2016**, 45, 15762–15778.

## 1.1 Introduction

Metal-ligand cooperativity is a fertile area of investigation for the development of modern homogeneous catalysts.<sup>[1,2]</sup> Cooperative ancillary ligands do not only stabilize and tune the coordination environment of a metal center, but also engage in chemical reactions with substrate molecules, opening new reactive pathways. In particular, they are proving useful in controlling the reactivity of base metals in view of substituting widely used precious metals catalysts.<sup>[2,3]</sup>

Metal-ligand cooperativity can take a number of forms. First, perhaps the simplest of those is hemilability,<sup>[4,5]</sup> i.e. reversible dissociation of an electron donor (or acceptor) moiety that allows the coordination environment of the metal to adapt to the steric and electronic requirements of different reaction intermediates along a reaction mechanism. Then, redox-active ligands,<sup>[3]</sup> which act as electron reservoirs during catalysis due to the presence of low lying empty orbitals and/or high-lying filled orbitals at energies comparable to that of the metal d orbitals. This property has been used to facilitate multi-electron processes at metals that tend to undergo one-electron processes or even at redox inactive metals, maintaining the metals oxidation state throughout the process (Figure 1).<sup>[1,6-10]</sup> Finally, the category of bifunctional ligands broadly encompasses ligands that engage in bond-forming and bond-breaking events, working together with the metal in substrate activation via functional groups positioned at the ligand. A prominent example of bifunctional ligands are tethered amido ligands ( $R_2N-M$ ) as found in Noyori-type catalysts for transfer hydrogenation,<sup>[11]</sup> which can accept a proton to become amine ligands ( $R_2N(H)-M$ ). This allows dihydrogen to be split heterolytically, leaving a hydride ligand on the metal center, to be subsequently transferred to an unsaturated substrate. Similar mechanisms have been proposed for many of the most efficient catalysts for the hydrogenation of polar bonds, via bifunctional  $H_2$  activation involving a variety of internal bases such as deprotonated acidic  $CH_2$  groups<sup>[12-14]</sup> or a coordinated cyclopentadienone<sup>[15-20]</sup> ligand. Bifunctional substrate activation is of interest for performing bond-making and bond-breaking processes with non-precious metals. In particular, this design principle has recently

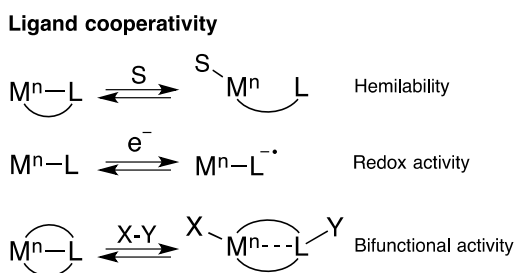
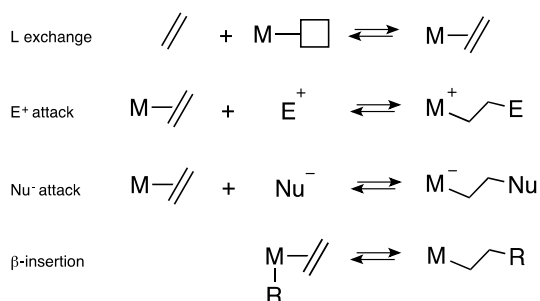


**Figure 1.** Ligand cooperativity in substrate activation.

been used in the development of highly efficient iron-based catalysts for the (de)hydrogenation of polar substrates.<sup>[14,21-25]</sup>

The coordination of olefins and other  $\pi$ -ligands to transition metals is a staple of organometallic chemistry. Upon binding, electron density is transferred from the  $\pi$ -bonding orbital to the metal ( $\sigma$ -donation) and, concomitantly, d electrons are partially donated to the  $\pi$ -antibonding orbital. This reduces the bond order and activates the double bond towards both nucleophilic and electrophilic attack. As a result, several elementary steps are available to metal-bound olefins (Scheme 1): a) ligand exchange where an olefinic substrate binds to the metal via a vacant site, b) electrophilic or c) a nucleophilic attack while the olefin is already bound to the metal, or d) concerted processes such as  $\beta$ -insertion (Scheme 1). While these elementary steps are part of the mechanism of many catalytic transformations of unsaturated substrates, anchoring such motifs to a metal in a multidentate ligand represents an attractive design principle for cooperative ligand systems.

The relative lability of simple  $\pi$ -ligands requires them to be tethered via the ligand backbone, so that dissociation of the ligand will not occur. A stable and robust option are the tridentate pincer type ligands,<sup>[26-37]</sup> which gained much attention as robust redox-active or bifunctional ligands. Paralleling the elementary steps outlined in Scheme 1, anchored  $\pi$ -ligands may display a range of cooperative processes. Weakly bound ligands may display hemilability and adaptive coordination. Upon binding of a substrate, the multiple bond can accept either an electrophilic or a nucleophilic fragment, proton ( $H^+$ ) and hydride ( $H^-$ ) being prototypical examples. Hence, a small molecule  $X-Y$  can split in a heterolytic fashion, adding part of the substrate to the metal center and part to the ligand backbone, and so performing a two-electron bond-breaking process, split over both the ligand and the metal (Figure 1).



**Scheme 1.** Types of olefin activation on a metal center.

This Chapter highlights recent advances in the use of  $\pi$ -coordinating ligands in the design of cooperative ligands. First, pincer ligands incorporating  $\pi$ -coordinating C=C moieties, including aromatic systems, are discussed (Section 1.2). Systems containing an activating borane moiety conjugated with a carbon-based  $\pi$ -system are covered in

the Section 1.3. Finally,  $\pi$ -interactions of C=E bonds (E = O, NR) are described, including carboxyl and imine based systems (Section 1.4).

## 1.2 $\pi$ -Coordinating C=C bonds

### 1.2.1 Olefin complexes

A first class of ligands that can be envisioned to act as cooperative ligands in catalysis are olefins. This well-known class of ligands has been studied in detail, starting from the first organometallic complex ever reported, i.e. Zeise's salt ( $K[PtCl_3(C_2H_4)] \cdot H_2O$ ).<sup>[38]</sup> A metal can bind to an olefinic C=C bond via its  $d_\sigma$  orbital to the ligands  $\pi$ -electrons, forming the  $\sigma$ -bond. Next to this, the metal  $d_\pi$  orbitals can donate electrons to the LUMO of the ligand, the C=C  $\pi^*$ , via  $\pi$ -backdonation. Lengthening of the olefinic C=C bond is obtained to which both factors contribute, but the latter effect predominates. The resonance structures that can be drawn for these interactions, shown in Figure 2a, follow the Dewar-Chatt-Duncanson model; the side-on bound adduct which gives an L type ligand and the metallacyclopropane adduct which gives an  $X_2$  type ligand.<sup>[7]</sup> The difference in the binding mode causes a change in the oxidation state of the metal center, i.e. the metal oxidation state remains the same in the L-type bound ligand and it increases by two in the  $X_2$ -type binding, causing ambiguity in the oxidation state of the metal. Throughout this Chapter the lower oxidation state as generally referred to.

Strong bonds are formed with electron rich metal centers, as backdonation will be most efficient.<sup>[39]</sup> This bond can be formed or broken depending on the metal oxidation state, possibly functioning as a hemilabile ligand and directing the system toward bifunctional behavior. One way of activating a small molecule X–Y on such systems is via changing the ligands coordination mode, forming a  $\sigma$ -bond with one of the olefinic carbons and adding X to the metal center, together with addition of Y to the second olefinic carbon (Figure 2b). Internal alkenes and alkynes are classes of ligands that have shown to be suitable as  $\pi$ -coordinating ligands.



**Figure 2.** a) Resonance extremes of an alkene binding to a metal center, left: side-on adduct, right: metallacyclopropane adduct. b) Addition of a substrate X–Y to this bond, altering the binding mode to form a  $\sigma$ -bond with one of the olefinic carbons.

The use of phosphine-substituted *trans*-stilbenes as  $\pi$ -coordinating ligands was investigated in detail by several groups. The *ortho*-diphosphine *trans*-stilbene ligand *tPCH=CHP* contains two phosphorus groups to bind the metal center in a bidentate fashion bridged *via* the olefinic ligand backbone which can coordinate to the metal center in an  $\eta^2$ -fashion (Figure 3). The incorporation of this ligand in metal complexes was first described by the group of Bennett in 1976.<sup>[40,41]</sup> The complexation to rhodium and iridium was described, in which the desired  $\eta^2$ -coordination of the olefinic backbone was indeed observed, as was shown by NMR analysis and the elongation of the C–C bond in X-ray crystal structure analysis of the  $^o\text{Tol-Rh-Cl}$  complex. The coordination to group 10 metals Ni, Pd and Pt in the oxidation state of two was shown to result in a different coordination mode, in which a  $\sigma$ -bond was formed with one of the olefinic carbon atoms under elimination of HX.<sup>[40]</sup>

The Rh and Ir complexes were shown to bind CO and subsequently cleave HCl in a heterolytic fashion over the metal–olefin fragment. This results in the addition of chloride to the metal center and a proton to the ligand backbone, inducing the formation of a C–M  $\sigma$ -bond with one of the olefinic carbon atoms (Scheme 2).<sup>[41]</sup> The reaction can formally be seen as an electrophilic attack of  $\text{H}^+$  at the olefin (Scheme 1). It shows an early example of cooperative behavior of the olefin ligand with the metal center.

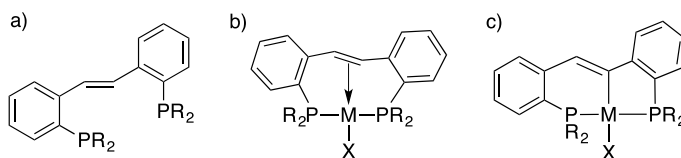
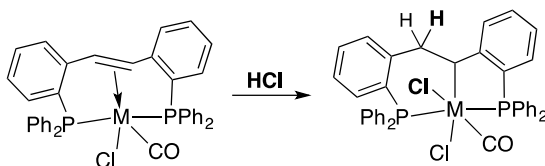
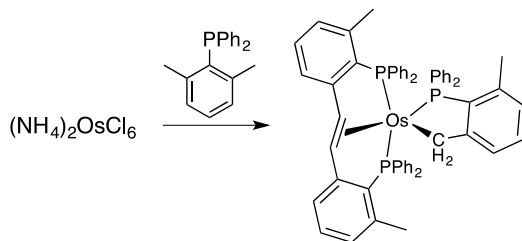


**Figure 3.** a) *trans*-Stilbene-type ligand: *tPCH=CHP*, R = *o*Tol or Ph. b)  $\eta^2$ -Coordination complexes M = Rh, Ir, R = Ph, X = Cl, Br, I. c)  $\sigma$ -Coordination complexes M = Ni, Pd, Pt, R = ph, *o*Tol, X = Cl.



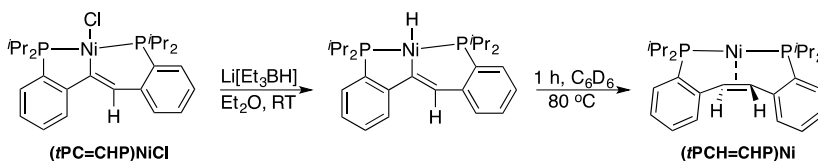
**Scheme 2.**  $\sigma$ -Complexes after addition of CO and subsequent cooperative addition of HCl, M = Rh, Ir.

A different approach for making a similar ligand was reported by Baratta *et al.* Here, the carbon-carbon double bond was formed from two *o*-methyl groups of two phosphines, as a result of activation of four C–H bonds, leaving an *ortho*-tolyl substituted *trans*-stilbene-type ligand,  $^o\text{Tol}t\text{PCH=CHP}$  (Scheme 3). An osmium(II) complex was synthesized of which the X-ray crystal structure showed an elongation of the C=C bond (1.437(4) Å), as a result of  $\eta^2$ -coordination to Os.<sup>[42]</sup>



**Scheme 3.** Synthesis of an Os(I) complex of the  $\sigma^{\text{Tot}}t\text{PCH}=\text{CHP}$  ligand from 2,6-xyllyl-PPh<sub>2</sub> and (NH<sub>4</sub>)<sub>2</sub>OsCl<sub>6</sub> upon activation of four C-H bonds.<sup>[42]</sup>

The use of the  $t\text{PCH}=\text{CHP}$  ligand was extended in the group of Iluc, with the aim of using its backbone as an hydrogen atom reservoir, i.e. noncoordination and  $\eta^2$ -coordination in the neutral form and  $\eta^1$ -coordination in the vinyl form which could store hydrogen.<sup>[43]</sup> After modification of the ligand by incorporating di-iso-propylphenyl ligands,  $\sigma$ -coordination metal complexes were synthesized with Ni, Pd and Pt resulting from C-H activation of the backbone, followed by rapid reductive elimination of HCl. Interestingly, H transfer was observed for the nickel analogue ( $t\text{PC}=\text{CHP}$ )NiCl upon addition of Li[Et<sub>3</sub>BH], first forming a hydride ligand on the metal center which was then transferred to the backbone resulting in a Ni(0) complex ( $t\text{PCH}=\text{CHP}$ )Ni with  $\eta^2$ -binding of the olefin (Scheme 4).



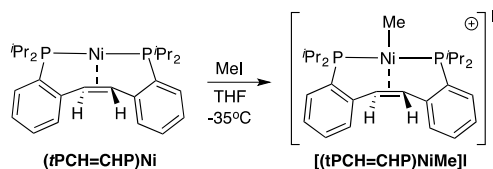
**Scheme 4.** The ( $t\text{PC}=\text{CHP}$ )NiCl complex and the observed H-transfer upon addition of Li[Et<sub>3</sub>BH] to ( $t\text{PCH}=\text{CHP}$ )Ni.

$\eta^2$ -Coordination of the ligand was also established for nickel(II), upon substitution of the olefinic protons for methyl groups, eliminating the possibility of HCl loss. 2 eq of  $t\text{PCMe}=\text{CMeP}$  were mixed with 3 eq of NiCl<sub>2</sub>(dme), resulting in a cationic mono chloride species with a NiCl<sub>4</sub><sup>2-</sup> counteranion, [( $t\text{PCMe}=\text{CMeP}$ )NiCl]<sub>2</sub>[NiCl<sub>4</sub>]. The complex displays a square-planar geometry around the Ni(II) center and an elongated C-C bond distance for the olefinic backbone (1.398(3) Å vs. 1.330(4) Å).

Synthesis of the more electron-rich analogues Ni(I)  $t\text{PCH}=\text{CHP}$  complex, without a counterion, was performed next by a comproportionation reaction using the nickel(II) and nickel(0) precursors NiCl<sub>2</sub>(dme) and Ni(cod)<sub>2</sub> (Figure 4). Analysis by single crystal X-ray spectroscopy showed a tetrahedral geometry around the nickel(I) center and an olefinic C-C bond distance of 1.394(3) Å indicative of an  $\eta^2$ -interaction, without the need to incorporate methyl groups on the ligand backbone.  $\eta^2$ -Coordination was also



observed for the previously described Ni(0) complex  $(tPCH=CHP)Ni$ , now directly synthesized from the ligand and  $Ni(cod)_2$ , which showed activity upon addition of 1 eq MeI, forming a cationic methyl nickel complex,  $[(tPCH=CHP)NiMe]^+$  (Scheme 5).<sup>[43]</sup>



**Scheme 5.** Reaction of the  $\eta^2$ -coordinated Ni(0) complex  $(PCH=CHP)Ni$  with MeI resulting in  $[(tPCH=CHP)NiMe]^+$ .

The hemilability of this system was shown with the Fe and Co analogues.<sup>[44]</sup> The Fe(II) and Co(II) complexes  $(tPCH=CHP)MX_2$  were synthesized, both containing a non-coordinated olefin moiety, with distances from the metal center to the ligand centroid of 3.596 Å for  $LFeBr_2$  and 3.501 Å for  $LCoCl_2$  (Figure 4). A weak interaction was obtained after halide abstraction of both complexes with  $Na[BAR^F_4]$ , shown by the slight elongation of the olefinic C–C ligand backbone (ligand: 1.330(4) Å; Fe: 1.332(14) Å; Co: 1.397(6) Å, Figure 4). A strong interaction was obtained after synthesis of the analogous neutral Co(I) complex  $(tPCH=CHP)MCl$  by reduction of the Co(II) complex with  $LiAlH_4$  (Figure 4). The  $^1H$  NMR spectrum shows a significant upfield shift for the olefinic protons to  $\delta$  2.01 ppm (for  $tPCH=CHP$  at  $\delta$  8.53 ppm), which is consistent with a bound olefinic moiety with significant  $\pi$ -backdonation. The bond distances were found to be in line with this observation, as an elongation was found for the C–C backbone from 1.397(6) Å in the unbound Co(II) complex to 1.442(5) Å in the bound Co(I) complex. The higher degree of backbonding was attributed to the more electron rich Co(I) system compared to the cationic Co(II) species. A similar system was found for the square-planar rhodium analogue  $(tPCH=CHP)RhCl$ , in which significant  $\pi$ -backdonation of the bound olefin was shown by upfield shifted olefin protons and an elongated C–C distance of 1.432(8) Å (Figure 4). Group 11 metals were explored by the synthesis of the Cu and Ag analogues. Bonding of the olefin was in both cases not observed, although a weak interaction could not be excluded for the Cu(I) complex  $(tPCH=CHP)Cu(OTf)$ : a relatively short distance between the metal and the ligand centroid was observed (2.426 Å), but the olefinic C=C bond lacked elongation (1.294(5) Å). Also the synthesis of cationic divalent complexes, without a halide or triflate ligand, did not lead to interaction with the backbone but afforded linear complexes.<sup>[44]</sup>

Overall it was observed that the olefinic C=C bond of  $tPCH=CHP$  elongates upon coordination to a metallic center, predominantly upon binding to an electron rich metal. Bond lengths ranging from 1.40 to 1.44 Å were observed for olefin bound metal complexes, of which the longest C=C length of 1.442(5) Å was observed for

(*t*PCH=CHP)CoCl, showing efficient coordination to the electron rich cobalt center. A large upfield shift in both  $^1\text{H}$  and  $^{13}\text{C}$  NMR was observed in all cases for coordination of the olefin backbone, showing the increased electron density on the ligand backbone. *t*PCH=CHP is a promising ligand for the activation of small molecules as it is observed to bind to numerous metal centers and the ligand binding mode shows great versatility.

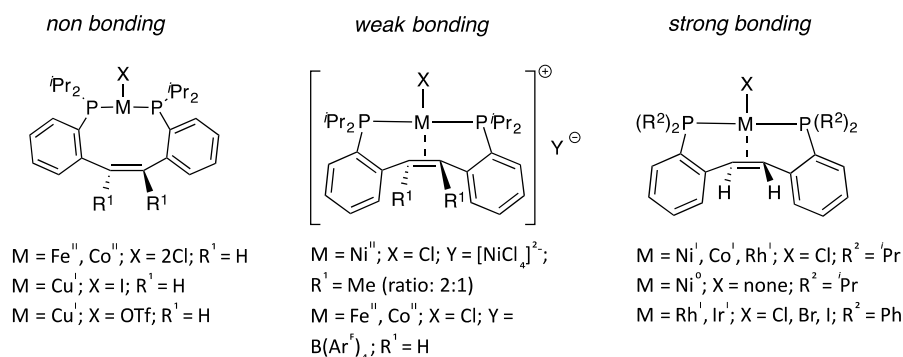
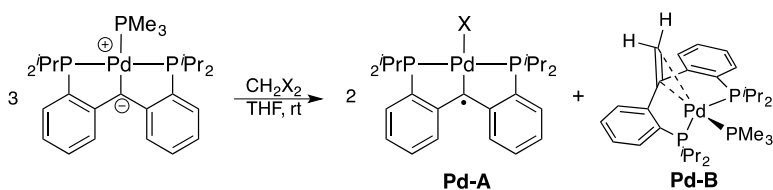


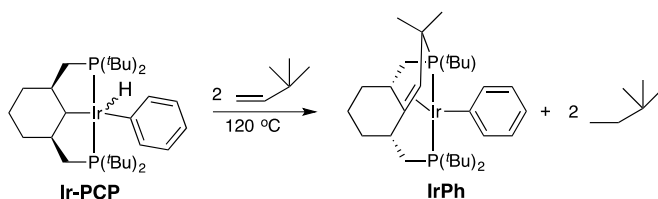
**Figure 4.** Overview of the non-bonding and  $\eta^2$ -bonding *trans*-stilbene complexes, arranged by their binding mode.

In a separate study in the group of Iluc toward radical trapping, a Pd complex was obtained with an  $\eta^2$ -coordinating olefinic moiety in the backbone of the ligand. This complex was synthesized, among others, from a Pd-PCP pincer complex that reacted with  $\text{CH}_2\text{X}_2$  to obtain **Pd-B** after  $\text{CH}_2$  transfer to the coordinated nucleophilic carbon atom (Scheme 6). This novel type of  $\text{CH}_2$  transfer was characterized by X-ray crystal structure analysis, next to other techniques, after direct synthesis of the complex, in which the elongation of the C–C bond was observed probably due to  $\pi$ -backbonding (1.398(3) Å vs. 1.34 Å for a C(sp<sup>2</sup>)–C(sp<sup>2</sup>)).<sup>[45]</sup> Complex **Pd-B** could also be independently synthesized by dehydrogenation of the corresponding saturated diphosphine ligand upon coordination to Pd. The 1,1-disubstitution pattern found in this ligand, contrasting with the 1,2-disubstitution pattern in the *trans*-stilbene derivatives, may open up distinct reactive pathways and certainly warrants further investigation.



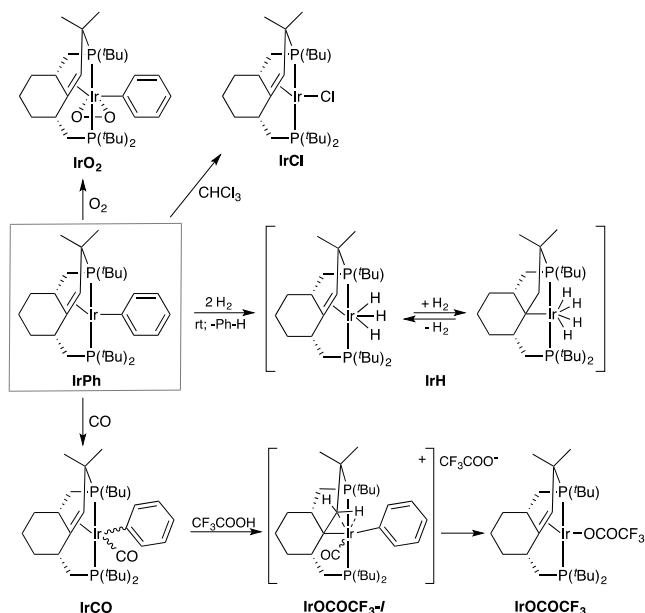
**Scheme 6.** Reaction of the Pd-PCP pincer complex with  $\text{CH}_2\text{X}_2$  to form the expected halide complex **Pd-A** and unexpected  $\text{CH}_2$  transfer product **Pd-B**.

An iridium-based system in which an internal olefin connected to a cyclohexyl ring binds in an  $\eta^2$ -fashion was synthesized in the group of Wendt (Scheme 7). The olefin binds in a similar fashion as was found for **Pd-B**, but having both carbon atoms bound to the ligand. The complex was formed from a PCP-pincer complex with a cyclohexyl backbone bound to Ir(III) with a phenyl and a hydride co-ligand. Upon heating in the presence of *tert*-butylethylene as a hydrogen acceptor, the  $\alpha$ -carbon of one of the methyl groups of the *t*-butyl substituent was coupled to the Ir-bound carbon atom to form a new coordinated olefin functionality, **IrPh**. This bond-making process was found to be reversible under a  $H_2$  atmosphere at 140 °C.<sup>[46]</sup> The formed Ir(I) complex has a distorted square-planar geometry around the metal center, average Ir–C bond lengths of 2.16 and 2.20 Å and a C=C bond length of 1.42 Å, which are all in line with other electron rich Ir-olefin complexes<sup>[47]</sup> and the before mentioned distances for the elongation of the olefin backbone.



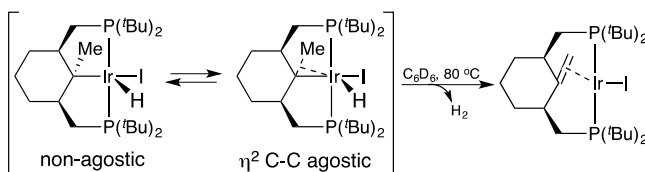
**Scheme 7.** The iridium based PCP-pincer complex and its subsequent reaction toward the  $\eta^2$ -bound complex.

The olefinic iridium complex was found to be active (Scheme 8) toward the addition of  $O_2$ , performing an oxidative addition over Ir cleaving the Ir–Ph bond (**IrO<sub>2</sub>**), to  $CHCl_3$  by replacing the phenyl ligand for a chloride (**IrCl**), and to CO by addition of a CO molecule to the metal center (**IrCO**). The product of the last reaction was shown to react with trifluoroacetic acid in an interesting way. First the Ir(I)-bound olefinic moiety was protonated, resulting in the unstable Ir(III) alkyl complex **IrOCOCF<sub>3</sub>-I**. A similar type of protonation of the backbone was shown before in the example of Bennett with the *trans*-stilbene-type ligands where addition of HCl lead to protonation of the backbone and the addition of Cl to the metal center (vide supra). **IrOCOCF<sub>3</sub>-I** reacted further cleaving both the phenyl and CO bonds with iridium, forming benzaldehyde together with the proton and forming a bond between Ir and the trifluoroacetate anion (**IrOCOCF<sub>3</sub>**).<sup>[48]</sup> Further reactivity of **IrPh** was explored with  $CO_2$  and  $N_2$ , but no reaction was observed.<sup>[48]</sup> Exposure to  $H_2$  showed the formation of hydride complexes that are in equilibrium, i.e. an olefinic complex with three hydride ligands on Ir and a PCP-pincer complex that added another  $H_2$  molecule, split over the metal center and the ligand backbone **IrH**. This addition constitutes an interesting example of cooperative  $H_2$  activation over a metal-olefin reactive center.<sup>[46]</sup>



**Scheme 8.** Reactivity study of the  $\eta^2$ -bound iridium complex with O<sub>2</sub>, CHCl<sub>3</sub>, H<sub>2</sub>, and CO with the subsequent reaction of CF<sub>3</sub>COOH.

Recently, a related PCP-Ir based complex with a terminal olefin was synthesized. Starting from the ligand with a methyl substituted cyclohexyl-group, an equilibrium was observed between an agostic  $\eta^2$  C–C bond and the non-agostic structure (Scheme 9). Heating of the complex to 80 °C lead to the formation of H<sub>2</sub> *via*  $\beta$ -elimination, and an  $\eta^2$ -interaction with the olefin. Analysis by X-ray crystallography showed a C=C distance of 1.438(15) Å, which is in line with previously described  $\eta^2$ -bound complexes.<sup>[49]</sup>



**Scheme 9.** PCP-Ir complex and its reaction to the  $\eta^2$ -bound complex.

Besides the previously described systems based on a diphosphine/olefin architecture, related ligands have recently been studied using sulfur as the anchoring ligands, or an alkyne as the  $\pi$ -coordinating ligand.

A family of complexes containing an internal alkene moiety in a thione based ligand was developed in the groups of Han and Jin (SCCS, Figure 5a).<sup>[50]</sup> The metallic center, Ir, Rh or Pd, was bound to the ligand in a bidentate fashion *via* the sulfur atoms and a coordination of the olefinic part was established either directly or after halide

abstraction (Figure 5b,c). The carbon-carbon double bond was found to elongate from 1.325(5) Å to 1.411(5) upon interaction with the metal center in  $[(^{\text{me}}\text{SCCS})\text{Ir}(\text{Cp}^*)]_2\text{Cl}$  ( $M = \text{Ir}$ ,  $X = \text{Cl}$ ,  $R = \text{Me}$ , Figure 5b and Figure 6, C(5)–C(6)).

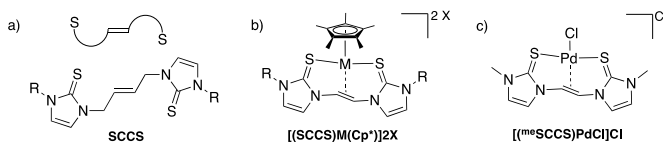


**Figure 5.** a) Schematic (top) and chemical structure (bottom) of SCCS.  $R = \text{Me}$ ,  $\text{CH}=\text{CH}_2$ . b) General structure of the Ir and Rh complexes.  $M = \text{Ir}$ ,  $X = \text{Cl}$ ,  $R = \text{Me}$ ,  $\text{CH}=\text{CH}_2$ ;  $M = \text{Ir}$ ,  $X = \text{OTf}$ ,  $\text{NO}_3$ ,  $R = \text{Me}$ ;  $M = \text{Rh}$ ,  $X = \text{OTf}$ ,  $R = \text{Me}$ ,  $\text{CH}=\text{CH}_2$ . c) Structure of the Pd complex.

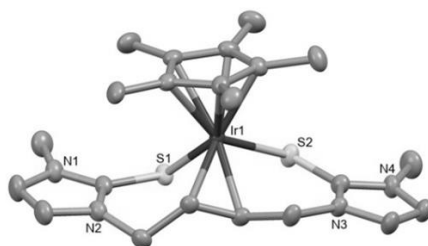


**Figure 6.** X-ray crystal structure of  $[(^{\text{me}}\text{SCCS})\text{Ir}(\text{Cp}^*)]_2\text{Cl}$ .<sup>[50]</sup>

The coordination of an alkyne ligand can be envisioned in a similar way, *via*  $\pi$ -coordination of the triple bond to the metal center. Such a system was explored by Ohe et al. using *ortho*-diphenylphosphinodiphenylacetylene (PCCP) as the ligand. This ligand contains an internal alkyne moiety connected to two phosphorus groups *via* phenyl rings (Figure 7a).<sup>[51]</sup> The reaction of PCCP with an equimolar amount of  $[\text{RhCl}(\text{cod})]_2$  ( $\text{cod} = 1,5$ -cyclooctadiene) resulted in the  $\eta^2$ -alkyne-rhodium(I) complex  $\text{Rh}(\text{PCCP})\text{Cl}$ , binding PCCP in a pincer-like multidentate fashion ( $L_3$ ), and a chloride ligand (Figure 7b). The Rh(I) complex adopts a square planar geometry in which the alkyne carbons lie parallel to the  $\text{ML}_3$  plane. When the mixture of PCCP and rhodium precursor was heated for longer time and at higher temperatures (48 h,  $50^\circ\text{C}$ ) a dimeric-rhodium species was synthesized ( $[\text{Rh}(\text{PCCP})\text{Cl}]_2$ ), and X-ray crystallography showed the formation of a cyclobutadiene ligand generated by the dimerization of the chloride-complex. The cyclobutadiene ring was shown to have two  $\eta^2$ - coordinations to the rhodium atoms located on the opposite faces (Figure 7b). Upon exchanging the chloride ligand of  $\text{Rh}(\text{PCCP})\text{Cl}$  for CO, leaving a cationic complex after halide abstraction with  $\text{NaPF}_6$  ( $\text{Rh}(\text{PCCP})\text{CO}$ ) backdonation from Rh to the alkyne ligand was weakened due to the stronger *trans* influence of CO, as shown in the X-ray crystal structure by longer Rh–C bond distances with the acetylenic carbons C(2)–C(3) compared to the chloride bound complex (2.203(7) and 2.199(6) for the Cl vs. 2.107(3) and 2.114(3) for the CO complex, Figure 8).

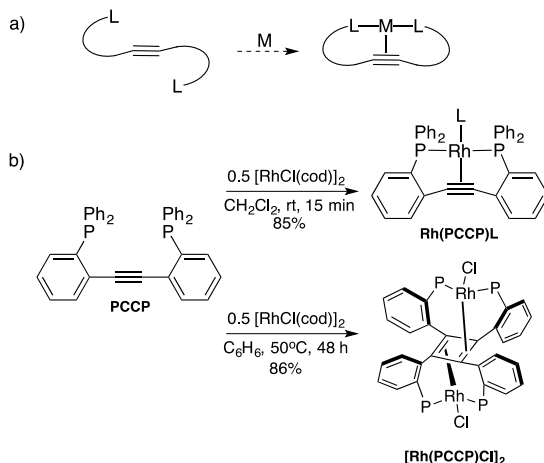


**Figure 7.** a) Schematic representation of the alkyne-M binding. b) The coordination of PCCP to Rh and the formation of a dimeric-Rh species, L = Cl or L = CO with  $\text{PF}_6^-$ ; P =  $\text{PPh}_2$ . Figures adopted from Ohe et al.<sup>[51]</sup>

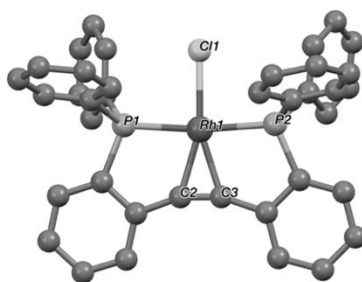


**Figure 8.** X-ray crystal structure of  $\text{Rh}(\text{PCCP})\text{Cl}$ .<sup>[51]</sup>

Next to olefinic C=C bond coordination,  $\pi$ -coordinating arene groups are also of interest and are discussed next.

### 1.2.2 Aromatic complexes

Aromatic ligands containing a six-membered ring can bind to a metal center, forming an  $\eta^2$ ,  $\eta^4$  or  $\eta^6$ -bound complex. Interactions of an aromatic ring with a metal center are in general strong in comparison to hemilabile binding of olefin complexes, and  $\eta^6$ -arene ligands are often used as robust ancillary ligands. Cooperative activity can nevertheless be observed in such systems if the M–arene interaction is destabilized by strain in the ligand system and/or bulky substituents, or in the case of late transition metals which cannot easily accommodate a 6-electron donor in their valence shell. Heterolytic activation of a small molecule can occur in arene-based systems *via* splitting a molecule, X–Y, over the metal center and the aromatic ring, and so these systems are of interest to explore for their cooperative behavior.

Hemilabile arene coordination was used to prepare two-legged piano stool rhodium complexes that display unusual reversible electrochemical conversion between the oxidation states of I and II, using a 1,4-bis[4-(diphenylphosphino)butyl]-2,3,5,6-tetramethylbenzene ( $^{\text{Ph}}\text{PArP}$ ) ligand. The ligand was designed to have a long tether between the anchoring phosphine groups close to the metal center and the arene ring, in the form of the butyl chain, to accommodate flexibility of the ligand and its binding mode upon structural or electronic changes of the complex.<sup>[52]</sup> A Rh(I) complex was synthesized using  $^{\text{Ph}}\text{PArP}$  and  $[\text{Rh}(\text{THF})_2(\text{COE})_2][\text{PF}_6]$ , resulting in a complex with a rhodium center bound to two phosphorus atoms and an  $\eta^6$ -coordinated arene ring (Figure 9a). The complex,  $(^{\text{Ph}}\text{PArP})\text{Rh}(\text{I})$ , was chemically oxidized using  $\text{AgPF}_6$ , resulting in the dicationic Rh(II) analogue  $(^{\text{Ph}}\text{PArP})\text{Rh}(\text{II})$  (Figure 9a). The arene ring coordinates to the metal center in both oxidation states, but it was shown that the Rh(II) complex contains generally shorter Rh–C bond distances.  $(^{\text{Ph}}\text{PArP})\text{Rh}(\text{I})$  showed reactivity toward small molecules, such as CO, acetonitrile and *tert*-butyl isocyanide, in a way that the interaction with the arene ligand was broken upon addition of other ligands (Figure 9a).<sup>[53]</sup> A tricarbonyl species was formed upon exposure of the Rh(I) piano-stool complex to 1 atm CO, although reaction was slow and took over 20 days at room temperature.<sup>[53]</sup> Reactions with CO in acetonitrile resulted in binding of a CO and an acetonitrile molecule, and reaction with *tert*-butyl isocyanide resulted in binding of two of these ligands, again breaking the Rh–arene interaction in both cases. Similar reactivity was observed for the  $(^{\text{Ph}}\text{PArP})\text{Rh}(\text{II})$  analogue with both CO and *tert*-butyl isocyanide, although reactions proceeded faster as explained by a generally higher reactivity of 17-electron complexes toward substitution reactions compared to their 18-electron counterparts (Figure 9a). The Rh(II) complex was additionally reduced under a CO atmosphere or upon addition of *tert*-butyl isocyanide, forming the same complexes as obtained before by reaction of the Rh(I) analogue,  $(^{\text{Ph}}\text{PArP})\text{Rh}(\text{I})(\text{CO})_3$  and  $(^{\text{Ph}}\text{PArP})\text{Rh}(\text{I})\text{L}_2$ , respectively. One of the key features to obtain this interaction was indeed found to be the tether length, as it needed to be long enough to accommodate structural changes upon complex oxidation. This shows that an arene-based system can contain hemilability in the sense of making and breaking the interaction with the ligand backbone when needed. The interaction between the metal center and the  $\pi$ -electron cloud is broken upon addition of substrates, resulting in vacant sites for these extra incoming ligands. In a next example of an envisioned M–arene interaction an *m*-terphenyl scaffold was used as the ligand (Figure 9b). Here, no interaction with the explored metals was obtained as M–L distances of 3.51, 3.48 and 3.37 Å were obtained for the nickel, palladium<sup>[54]</sup> and rhodium<sup>[55]</sup> complexes, respectively. In this case, the distance from the metal center to the closest arene–H is mentioned, due to its geometry. Nevertheless, for the rhodium complex containing the significantly shorter M–L distance, an interaction between the metal center and the  $\pi$ -electron cloud is

observed as shown in the corresponding  $^1\text{H}$  NMR spectrum where the aromatic protons of the central arene ring were distributed in a range of  $\delta$  6.18–8.04 ppm.<sup>[55]</sup>

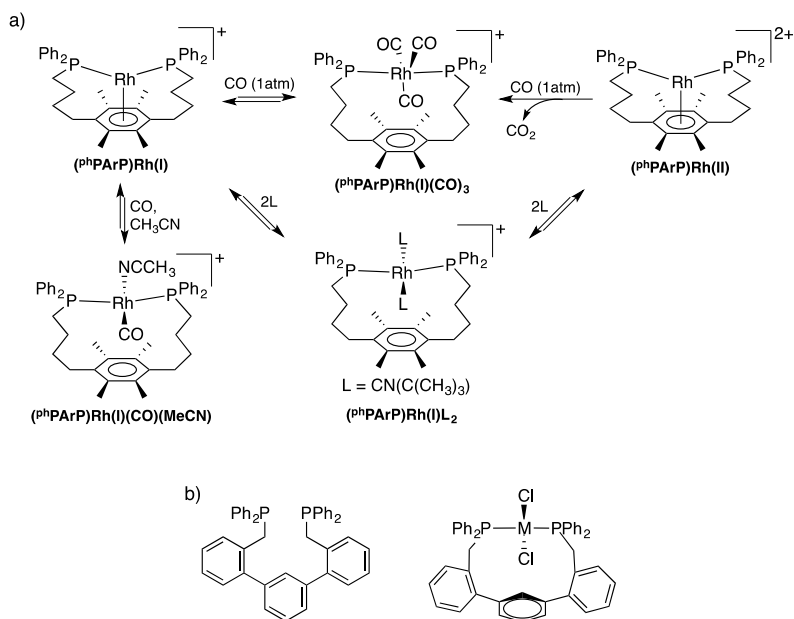
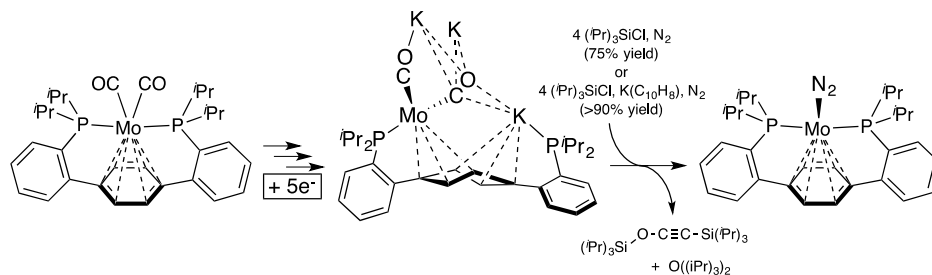


**Figure 9.** a) Two-legged piano stool based rhodium complexes and their reactivity. b) *m*-Terphenyl based ligand (left) and the corresponding divalent metal complexes (right) M = Ni, Pd or Rh.

Another strategy to obtain an Ar–M interaction is to keep the tether sufficiently short in combination with a flexible ligand backbone, so that the arene moiety is forced in close proximity to the metal center. The combination with a late transition metal (such as Ni(0)) that cannot readily accept 6 electrons from the aromatic ring results in enhanced reactivity. The use of a *p*-terphenyl diphenylphosphine ( $\text{P}_2\text{terph}$ , Figure 10) ligand was designed and explored in the group of Agapie. The phosphorus groups are on the *ortho* positions of the two peripheral phenyl rings, creating a geometry with a short M–L distance upon coordination to a metal. Several systems with this ligand are explored,<sup>[56–59]</sup> but only selected cases are described here. In general, two ways of cooperative behavior are described, in which a) the ligand acts as an electron reservoir in combination with coordinative flexibility to stabilize different oxidation states, or b) the ligand backbone is activated and can form bonds with H-atoms or small molecules. A prominent recent example of the first case is a Mo-based complex, in which the *p*-terphenyl ligand stabilizes the formal oxidation states of Mo<sup>II</sup>, Mo<sup>0</sup>, Mo<sup>-II</sup>, and Mo<sup>-III</sup> (Scheme 10),<sup>[60]</sup> allowing for a remarkable deoxygenative reductive coupling of two metal-bound CO molecules. The redox active behavior of the tethered aromatic ring



holds promise for catalytic reactions involving multi-electron transformations, such as the valorization of carbon dioxide.



**Scheme 10.** *p*-Terphenyl based Mo-complexes.

Chemical cooperativity at the aromatic ring was demonstrated with nickel-based systems. The solid state structure of a **Ni(0)(P<sub>2</sub>terph)** complex, formed from a reaction of P<sub>2</sub>terph with Ni(cod)<sub>2</sub>, showed an interaction of the nickel center with both phosphines and a double bond of the arene backbone with Ni–C lengths of 1.992(1) and 2.002(1) Å. The chelation of the nickel center induced a bend of the peripheral aryl rings of 14° inwards relative to *p*-terphenyl.<sup>[61]</sup> The **Ni(0)(P<sub>2</sub>terph)** complex was exposed to Ni(II)Cl<sub>2</sub>(dme) to perform a comproportionation reaction, resulting in a dinuclear Ni<sup>I</sup>–Ni<sup>I</sup> complex **Ni<sub>2</sub>(P<sub>2</sub>terph)Cl<sub>2</sub>**, coordinated *via* the phosphines in an almost linear PNiNiP fashion. To accommodate this binding, the peripheral aryl rings bent outwards with 16°. Furthermore, two bridging chloride ligands are bound to the nickel centers next to an arene–M interaction *via* two neighboring double bonds in the arene backbone.

Addition of HCl to **Ni(0)(P<sub>2</sub>terph)** resulted in oxidative addition of the substrate to the nickel center and loss of the arene–nickel bond (Ni–C<sub>arene</sub>: >2.5 Å) with only a weak interaction with the arene π-system.<sup>[62]</sup> Another dinuclear complex was formed upon heating of **Ni(P<sub>2</sub>terph)HCl**, resulting in a **Ni<sub>2</sub>(P<sub>2</sub>terphH<sub>2</sub>)Cl<sub>2</sub>** with two bridging chloride ligands and the phosphorus ligands bound to the Ni(I) centers in a PNiNiP fashion, similar to the previously described dinuclear structure. The protons that were bound to nickel migrated to one of the double bonds of the aromatic rings, resulting in a single bond with a C<sub>ar</sub>–C<sub>ar</sub> distance of 1.5198(1) Å breaking the aromaticity. The Ni<sub>2</sub>Cl<sub>2</sub> center interacts with the remaining four conjugated carbon atoms in the ring. To study the H-migration, a halide abstraction was performed starting from **Ni(P<sub>2</sub>terph)HCl**, affording the positively charged **Ni(P<sub>2</sub>terph)H** complex. Only a H was bound to the nickel center, which was stabilized by an η<sup>2</sup>-interaction of the arene ring (Ni–C<sub>Ar</sub>: 2.142(3) and 2.157(3) Å). Analysis by NMR and X-ray crystallography in combination with isotopic labeling experiments shows that the metal hydride can migrate to the aromatic ring, either to the *ipso* or *ortho* carbon (Figure 10), demonstrating the possibilities of this system to store part of the substrate in the ligand backbone, which is a possible way of introducing cooperative behavior in the system.

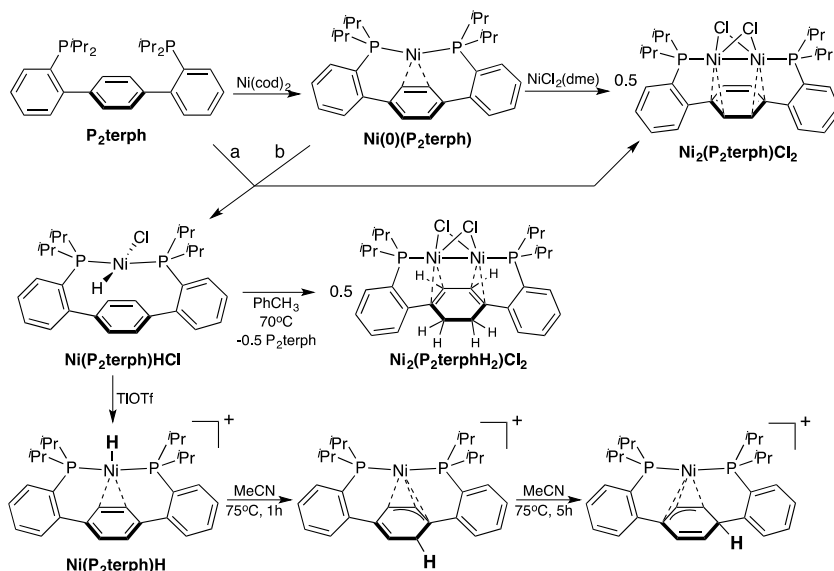


**Figure 10.** The *p*-terphenyl based ligand  $P_2terph$  and its coordination to nickel. a:  $Ni(cod)_2$ ,  $NiCl_2(dme)$ , b:  $HCl$ ,  $Et_2O$ .

Besides the incorporation of a C–H based aromatic ring, the use of heteroatom containing rings is of interest. The incorporation of pyridine in the ligand backbone was investigated, binding the phosphorus tethers on the *meta* positions, keeping a symmetrical ligand system. A diphosphine pyridine (PPyP) ligand was designed, in which the ligand can bind to the metallic center *via* its phosphorus atoms positioned on the *ortho* positions of the peripheral rings, as well as the heterocycle  $\pi$  system (Figure 11).<sup>[63,64]</sup> Nickel and palladium complexes were synthesized in which the aromaticity was disrupted due to an interaction with one of the carbon–carbon double bonds of the pyridine backbone. This was shown by a significant upfield shift in the  $^1H$  NMR spectrum of  $Ni(PPyP)$  in which the central pyridine protons shifted, i.e. the *ortho*-pyridyl shifted to  $\delta$  7.82 ppm and the *para*-pyridyl protons to  $\delta$  4.35 ppm (respectively  $\delta$  8.96 and 7.89 ppm in the free ligand), indicating a severe change in the electronic environment. Binding of a Lewis acidic group such as  $B(C_6F_5)_3$  to the pyridine nitrogen atom enhanced the strength of this interaction between the ring and the metal center further, as was evident in further upfield shift of the *para*-pyridyl proton shifted to  $\delta$  3.18 ppm in  $Ni(PPyBP)$  (Figure 11b). The electron-withdrawing  $B(C_6F_5)_3$  group enhances the  $\pi$ -acceptor feature of the ligand, and so enhances the bond strength from the electron rich  $Ni^0$  center to the  $\pi$ -system of the pyridine ligand. Activation of small molecules, such as  $HBpin$ ,  $PhSiH_3$  and  $[Na][HBet_3]$  was shown to take place in a stoichiometric fashion by breaking the aromaticity of the pyridine ring. In case of  $HBpin$  and  $PhSiH_3$  the heteroatom binds to nitrogen and hydrogen to the carbon at the *ortho*

position (Figure 11c). In case of  $[\text{Na}][\text{HBET}_3]$  the activation took place on a methylated version of the nickel complex **Ni(PPyMeP)**, which was synthesized by addition of methyl triflate resulting in the methylated nitrogen atom and a triflate counter ion. Subsequent reaction with  $[\text{Na}][\text{HBET}_3]$  resulted in the breaking of the aromaticity by addition of a hydrogen atom to the carbon at the *ortho* position of nitrogen (Figure 11d). This ligand-based reactivity was attributed to the metal-ligand bond, in which the pyridine aromaticity was disrupted resulting in a somewhat activated ligand backbone.<sup>[63]</sup>

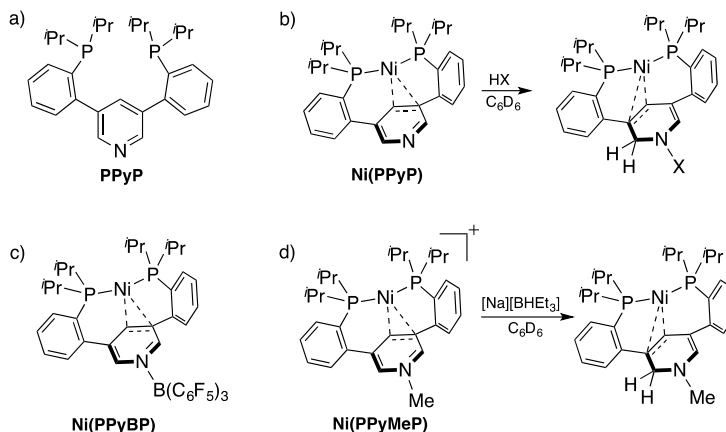


**Figure 11.** a) PPyP ligand. b) Ni(PPyP) and its activation of HX, HX = HBPin or H<sub>3</sub>PhSi. c) The Ni(PPyBP) complex with B(C<sub>6</sub>F<sub>5</sub>)<sub>3</sub> bound to the nitrogen atom of the pyridine ring. d) Ni(PPyMeP) and its reaction with [Na][BHEt<sub>3</sub>].

### 1.3 $\pi$ -Systems incorporating a boron atom

The last example showed how introducing an electronegative element in a conjugated  $\pi$ -systems can be used to increase its affinity for hydrides and enhance reactivity. A similar, maybe stronger, effect can also be achieved by conjugation with an electron deficient group such as a borane.

Boranes themselves can act as Z-type,  $\sigma$ -acceptor ligands that bind to a metal center *via* accepting an electron pair of the metal center, formally forming a retrodonative bond.<sup>[65]</sup> They are often tethered to L-type ligands such as a phosphines for stabilization on the metal center, forming so called ambiphilic ligands.<sup>[66]</sup> Following the discovery of the first metallaboratrane by Hill in 1999,<sup>[67]</sup> ambiphilic ligands have attracted much interest because of their ability to stabilize unusual electronic structures and to act as cooperative ligands, as has been covered in several excellent reviews.<sup>[68-71]</sup> In many cases, the boron atom bears conjugated aromatic substituents that can also engage in binding to the metal, resulting in  $\eta^2(\text{BC})$  or  $\eta^3(\text{BCC})$  coordination modes. The chemistry

of acyclic boron-containing  $\pi$ -ligand complexes has been reviewed in 2012 by the group of Emslie.<sup>[72]</sup> Here, selected recent examples highlighting the specific reactivity of this motif are discussed.

The use of ambiphilic phosphine-borane based ligands in Pd catalyzed Suzuki-Miyaura reactions was explored in the group of Bourissou.<sup>[73,74]</sup> Boron-based ligands containing three aromatic substituents, of which one phosphorus-substituted, were synthesized (**PB1** and **PB2**, Figure 12) and their activity as co-ligands was explored. The addition of **PB1** or **PB2** to a standard cross-coupling reaction with a Pd(II) precursor, such as PdCl<sub>2</sub>(cod), Pd(ma)(nbd) or Pd<sub>2</sub>dba<sub>3</sub>, resulted in good yields for 2-chloropyridine, chloro-N-heterocycles and amino-2-chloropyridines. To better understand the effect of adding a Lewis acidic substituent in the form of a borane to this catalytic reaction, a closer look was taken at the in situ formed Pd-complexes. **Pd-PB1** was isolated in which an extra coordinated maleic acid ligand was coordinated to Pd. Ligand **PB1** was found to have an  $\eta^3$ -interaction with the metal center, *via* the phosphorus atom and an  $\eta^2$ -interaction with an aromatic double bond of a mesityl substituent (Figure 12). A new complex was formed upon addition of PhI, **Pd'-PB1**, in which the ligand was still bound *via* the phosphorus atom, but now also with an  $\eta^4$ (BCCCH<sub>2</sub>)-interaction of the mesityl bound boron atom, forming an extended  $\pi$ -coordination. This latter complex showed to be significantly less active in catalysis, and is expected to be a product of decomposition. Analysis of a single crystal by X-ray spectroscopy, and NMR analysis both confirm the formation of **Pd'-PB1**, which was formed *via* a C-H activation on one of the mesityl rings, resulting in a CH<sub>2</sub> group and loss of 1 equivalent of benzene. An upfield shift of about 10 ppm was found in the <sup>11</sup>B NMR spectra, from  $\delta$  69.4 ppm for **Pd-PB1** to  $\delta$  52.8 ppm for **Pd'-PB1**, suggesting the presence of some Pd  $\rightarrow$  B interaction. This structure shows a rare example of an  $\eta^4$ -boratabutadiene complex.

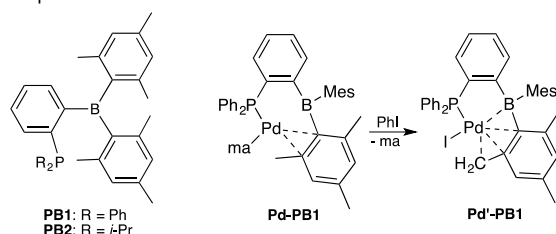


**Figure 12.** Left: phosphine-borane based ligands as synthesized in the group of Bourissou.<sup>[73]</sup> Right: Pd based complex **Pd-PB1** and its reaction with PhI to **Pd'-PB1**.

To explore the possibilities of borane-based ligands as supporting ligands in catalysis, the group of Emslie designed multidentate ambiphilic ligands with a phosphine donor and a borane acceptor, aiming for  $\pi$ -coordinating systems. The phosphine-borane based TXPB ligand (Figure 13a) was designed to anchor the metal center *via* the thioxanthene backbone and explored with a variety of metals, amongst which nickel,

palladium and rhodium. The ligand was shown to be versatile and gave rise to a broad variety of complexes, but problems were encountered as the central thioether donor group was shown to be easily replaced from the metal center.<sup>[66,75,76]</sup> Therefore, a new ligand system was designed containing a bisphosphine moiety instead. A ferrocene group was included to provide increased flexibility, while still remaining a firmly bound complex. The ligand **FcPPB** ( $\text{FcPPB} = \text{Fe}(\eta^5\text{-C}_5\text{H}_4\text{PPh}_2)(\eta^5\text{-C}_5\text{H}_4\text{PtBu}\{\text{C}_6\text{H}_4(\text{BPh}_2)\text{-ortho}\})$ , Figure 13b) was bound to platinum using  $\text{Pt}(\text{nb})_3$  ( $\text{nb} = \text{norbornadiene}$ ), affording an arylborane complex that binds the two phosphorus atoms, and the borane-phenyl moiety *via* an  $\eta^3\text{-BCC}$  interaction with both the *ipso* and *ortho* carbon atoms.<sup>[75]</sup> Similar structures were obtained when performing the metallation with either  $\text{Ni}(\text{cod})_2$  or  $\text{Pd}_2(\text{dba})_3$ , resulting in **Ni(FcPPB)** and **Pd(FcPPB)**, respectively, both containing the  $\eta^3\text{-BCC}$  interaction with the phenyl-boron moiety.<sup>[77]</sup>

The reactivity of **Pt(FcPPB)** with small molecules was explored. A CO molecule was bound to the Pt center upon exposure to a CO atmosphere, resulting in **Pt(FcPPB)(CO)**, which was characterized as an **FcPPB** complex connected to the ligand *via* the two phosphorus atoms and an  $\eta^2\text{-BC}$  interaction with the borane moiety, next to a CO molecule. Exposure of **Pt(FcPPB)** to an atmosphere of  $\text{H}_2$  afforded **PtH( $\mu\text{-H}$ )(FcPPB)** by inserting a H in the Pt–B bond and adding the other H to Pt. It was shown that  $\text{H}_2$  was only weakly bound, as **Pt(FcPPB)** was regained slowly upon storing the complex under argon and rapidly upon applying vacuum. Furthermore, it was possible to gain **Pt(FcPPB)(CO)** upon exposure to a CO atmosphere, and also its reverse reaction was possible.

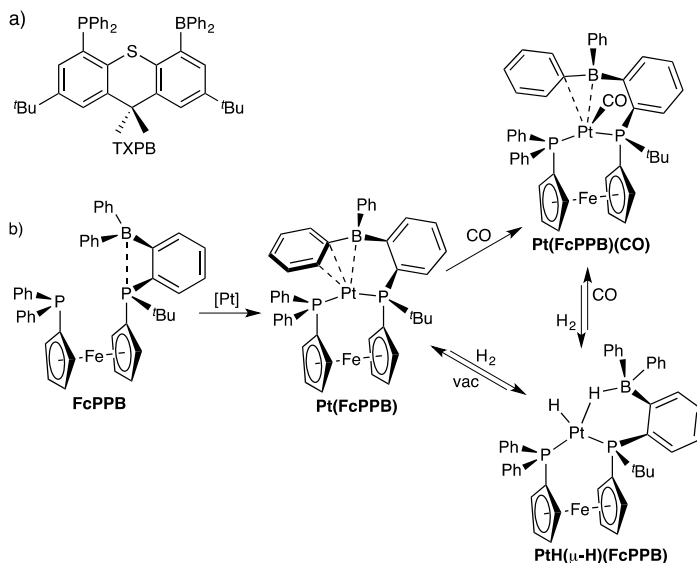


**Figure 13.** a) TXPB ligand. b) Bisphosphine-ferrocene based ligand **FcPPB**, the Pt based complexes and their reactivity with CO and  $\text{H}_2$ .

Ambiphilic, tridentate diphosphanylborane (DPB) ligands, were originally introduced by Bourissou and co-workers in 2006.<sup>[78]</sup> In their work on rhodium complexes, only a Rh  $\rightarrow$  B coordination mode was observed. Subsequently, Cu(I) coordination chemistry revealed that this ligand scaffold could also accommodate  $\eta^2$ (BC) or  $\eta^3$ (BCC) coordination modes.<sup>[79]</sup> Further research on the rhodium system was performed by Ozerov and co-workers, in which the coordination of the borane unit was shown to bind *via* the  $\pi$ -system of the borabenzyl moiety.<sup>[80]</sup> Next to this, the product of oxidative addition of the B–C bond was obtained, forming a PBP-pincer complex. The group of Peters explored further possibilities of these ligands. In particular, substitution of the boron-phenyl moiety for the more bulky boron-mesityl group was found to strongly impact the coordination chemistry and the reactivity of the ligand. A nickel-borane complex was formed from a comproportionation reaction with NiBr<sub>2</sub> and Ni(cod)<sub>2</sub>.<sup>[81]</sup> Analysis by X-ray crystallography showed a coordination of the (<sup>Mes</sup>DPB<sup>Ph</sup>) ligand *via* the two phosphorus atoms and an  $\eta^2$ (B,C) coordination of the boron atom and the *ipso*-carbon atom of the mesityl ring, next to a bound bromide ligand ((<sup>Mes</sup>DPB<sup>Ph</sup>)NiBr, Figure 14). The complex was reduced using Na/Hg resulting in the Ni(0) complex (<sup>Mes</sup>DPB<sup>Ph</sup>)Ni, which surprisingly did not bind a solvent molecule. Both of the phosphorus atoms were bound to nickel, as for the Ni(I) complex, but the coordination of the borane substituent changed, as it was now bound in an  $\eta^3$ -BCC fashion, also binding the *ortho*-carbon atom of the mesityl ring. Whereas a previously synthesized phenyl analogue (<sup>Ph</sup>DPB<sup>Ph</sup>)Ni(THF) did not show any activity towards H<sub>2</sub>, (<sup>Mes</sup>DPB<sup>Ph</sup>)Ni showed facile heterolytic activation of the substrate at room temperature, in C<sub>6</sub>D<sub>6</sub>. The hydrogen-bound complex was identified as the hydrido-borohydrido species (<sup>Mes</sup>DPB<sup>Ph</sup>)( $\mu$ -H)NiH, as shown in Figure 14, and was found to be in a 5:1 equilibrium with (<sup>Mes</sup>DPB<sup>Ph</sup>)Ni. Similar activity was found when the iron-CO analogue (<sup>Ph</sup>DPB<sup>Ph</sup>)Fe(CO)<sub>2</sub> was exposed to 1 atm of H<sub>2</sub>, forming (<sup>Ph</sup>DPB<sup>Ph</sup>-H)Fe(H)(CO)<sub>2</sub>, in which the hemilabile  $\eta^3$ -BCC interaction participated and hydrogen was added in a heterolytic manner.<sup>[82]</sup>

The catalytic possibilities of (<sup>Mes</sup>DPB<sup>Ph</sup>)Ni were investigated by addition of styrene under a H<sub>2</sub> atmosphere, after which the hydrogenated product ethyl benzene was formed directly. The reaction was monitored by <sup>1</sup>H NMR spectroscopy, showing that the starting complexes were again present in an equilibrium with H<sub>2</sub> after full consumption of the substrate, showing that the catalyst could be recovered after catalysis.<sup>[81]</sup> Further exploration of (<sup>Mes</sup>DPB<sup>Ph</sup>)Ni in catalytic reactions showed that it is an efficient catalyst for the hydrosilylation of *para*-substituted benzaldehydes with diphenylsilane, *via* the formation of a borohydrido-Ni-silyl species in which SiHPh<sub>2</sub> is bound to nickel and the hydride is inserted in the B-Ni bond.<sup>[83]</sup> Synthesis of the phenyl substituted P<sup>i</sup>Pr<sub>2</sub> analogue (<sup>Ph</sup>DPB<sup>iPr</sup>)Ni showed reactivity toward H<sub>2</sub> as well.<sup>[84]</sup> The introduction of the more electron-rich isopropyl substituent in combination with the less bulky phenyl ring on boron tuned the geometric and electronic environment such that the observation of the hydrogen adduct was possible. This unusual Ni-(H<sub>2</sub>) complex

subsequently reacted to form a similar hydrido-borohydrido species, forming  $(^{\text{Ph}}\text{DPB}^{\text{Pr}})(\mu\text{-H})\text{NiH}$ .

Similar binding modes for the DPB scaffold also play a role in iron-mediated dinitrogen functionalization. The dinitrogen-bridged di-iron complex  $(^{\text{Ph}}\text{DPB}^{\text{Pr}})\text{Fe}(\mu\text{-1,2N}_2)\text{Fe}(\text{PhDPB}^{\text{Pr}})^{[85]}$  could be functionalized by addition of 1,2-bis(chlorodimethylsilyl)ethane (bse) and 2.1 equivalents of Na/Hg under 1 atm of  $\text{N}_2$ , forming  $(^{\text{Ph}}\text{DPB}^{\text{Pr}})\text{Fe}(\text{N}_2\text{bse})$ . This new complex formed an  $\eta^3(\text{B,C,C})$ -interaction with the iron center and the phenyl substituted borane tether. Activation of phenylsilane was performed by hydrosilylation of the Fe–N bond, placing  $\text{SiH}_2\text{Ph}$  to  $\text{N}\alpha$  and H to B. Similar reactivity was found for the Co analogue  $(^{\text{Ph}}\text{DPB}^{\text{Pr}})\text{Co}(\text{N}_2)$ , and the substrate scope was extended with both, the iron and cobalt nitrogen bound complexes.<sup>[86]</sup>

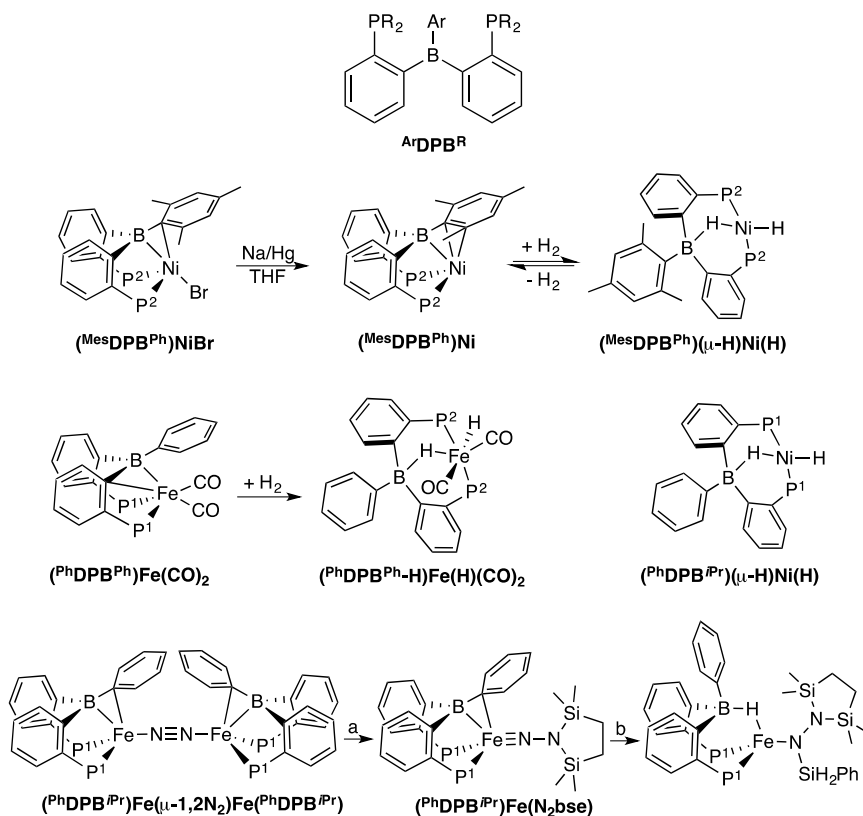


**Figure 14.** Selected DPB complexes. P = P<sup>1</sup> or P<sup>2</sup>; P<sup>1</sup> = *i*Pr, P<sup>2</sup> = Ph; R = Ph or *i*Pr; Ar = Mes or Ph; a = 1,2-bis(chlorodimethylsilyl)ethane, 2.1 equiv Na/Hg, 1 atm of  $\text{N}_2$ , b =  $\text{PhSiH}_3$ .

Stephan and co-workers developed ruthenium-based systems containing the  $^{\text{Ph}}\text{DPB}^{\text{Ph}}$  ligand.<sup>[87]</sup> The ligand was bound to Ru *via* both phosphorus atoms and an interaction with the phenyl substituent on the borane, forming a positively charged complex with

a  $B(C_6F_5)_4$  counterion, i.e.  $[(^{Ph}DPB^{Ph})RuCl]B(C_6F_5)_4$ . The complex showed reactivity upon addition of  $PCy_3$ , binding the phosphorus atom to the interacting phenyl ring on its *ortho*-position, resulting in the cyclohexadienyl (chd) containing Ru-complex  $(^{chd}DPB^{Ph})Ru(PCy_3)Cl]B(C_6F_5)_4$ . A subsequent reaction was observed upon exposure to  $H_2$ , activating it in a heterolytic fashion and cleaving the  $C_{Ar}-PCy_3$  bond. The resulting neutral cyclohexadienyl complex was found to be present in two isomers, with an *ortho* or a *para* addition at the arene ring.  $[(^{Ph}DPB^{Ph})RuCl]B(C_6F_5)_4$  was explored in the hydrogenation of imines, which were shown to proceed at room temperature under high pressures of  $H_2$  (102 atm, 1-10 mol% cat, 83-99% yield). The proposed mechanism proceeds *via* the previously synthesized complex  $(^{chd}DPB^{Ph})RuCl$ , both the *ortho* or a *para* form. This is consistent with an FLP-type (FLP = frustrated Lewis pair) hydrogenation in which the complex and the substrate act as an FLP to split  $H_2$ . The cleaved hydrogen is subsequently delivered to the formed iminium cation (Figure 15).

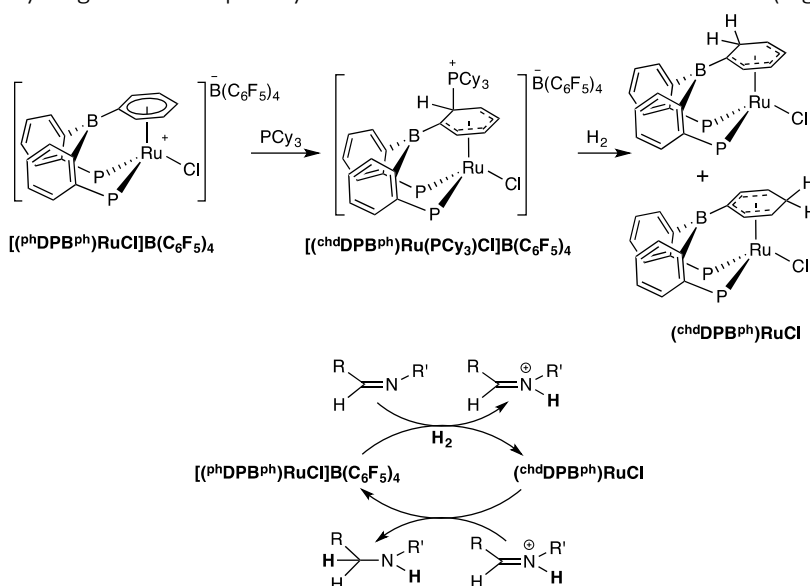


**Figure 15.** (DPB)Ru structures and its mechanism for the hydrogenation of imines. P =  $Ph_2$ ; R = Ph, R' =  $t$ Bu or Ph.

These examples show the versatility that incorporation of borane ligands can bring to the coordination chemistry *via* their extended  $\pi$ -system, leading to various coordination modes making them excellent adaptive ligands. The resulting complexes are shown to be active toward small molecule activation *via* a heterolytic pathway transiently accepting hydrides either at the boron site or at a remote carbon site of the conjugated aromatic ring as demonstrated in the last example.



## 1.4 $\pi$ -Bound C=E bonds

In comparison with olefins, the C=E (E = O or N) bond of carbonyls and imines becomes both polar and electron deficient because of the high electronegativity of the element E. Hence, the backdonation interaction is expected to play a dominant role in the description of  $\pi$ -bound C=E bonds. In addition, the presence of lone pairs on the heteroelement may open up reactive pathways that are not accessible to C=C bonds.

Polar C=E bonds can bind to the metal center in either an  $\eta^1(\text{E})$  or  $\eta^2(\text{C,E})$ -fashion, the former being by far the most common mode. Here situations are discussed in which the latter ( $\pi$ -coordination) is favored. The incorporation of a carbonyl will be discussed first, followed by the incorporation of imine and iminium moieties.

### 1.4.1 Carbonyl complexes

Carbonyl groups (i.e. aldehydes and ketones) are known to bind to a metal center in two distinct ways, i.e.  $\eta^1(\text{O})$  to electrophilic metals, by donation of the oxygen lone pair to the metal center, and  $\eta^2(\text{C,O})$  to electron-rich metals. The latter case is stabilized by  $\pi$ -backdonation of the metal to the ligand, creating a stronger M–L bond and a weakening of the C=O bond, in line with the binding mode of alkene systems. The C=O interaction can be described by two resonance extremes; the side-on bound extreme and the metallaoxacycle extreme (Figure 16). Cooperative behavior in such systems can be envisioned arising from the labile (C=O)–M bond, creating the possibility of a hemilabile system. Activation of a small molecule can proceed *via* heterolytic activation, adding part of the substrate to the oxygen of the ligand backbone and part to the metal center, provided that the carbonyl moiety has an  $\eta^2(\text{C,O})$  interaction with the metal center. In general, this interaction is scarcely found compared to the  $\eta^1(\text{O})$  bound structure, but it is found more commonly for electron rich systems which can efficiently back donate.<sup>[39]</sup>

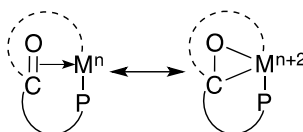


**Figure 16.** Resonance extremes of an  $\eta^2$ -bound ketone-metal interaction, left: the side-on adduct, right: the metallaoxo-cycle in which the oxidation state is raised by 2.

An early example of a pincer-type ligand incorporating an  $\eta^2$ -coordinating ketone was developed in the group of Milstein. The synthesis and characterization of an iridium complex containing a quinone-based ligand was reported.<sup>[88]</sup> The ligand was designed with phosphorus groups attached at the *ortho* positions to bind the metal center in a multidentate fashion. Upon synthesis of a cationic complex, a bond between the

iridium center and the phosphorus groups was obtained, as well as an interaction with the *ipso* C=O group, establishing the first stable phenoxonium complex (Figure 17a). The C=O moiety was bound *via* an  $\eta^2$ -coordination to the metal, resulting in a stabilized cationic ligand. It was shown that the positive charge was mainly delocalized over the aromatic ring. An X-ray single crystal structure was obtained for the acetonitrile bound PCOP-complex (Figure 17b). The bond angles inside the ring were found to be close to  $120^\circ$ , of which it was concluded that the system is best described as an Ir(I) complex with a C=O double-bond coordination compared to the Ir(III) three-centered metalaoxa-cycle structure.<sup>[88]</sup>

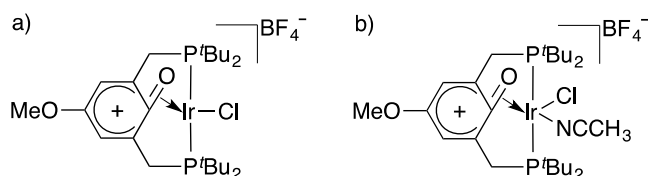


**Figure 17.** a) The pincer-type quinone based iridium complex and b) the acetonitrile bound analogue of which an X-ray single crystal structure was obtained.

A somewhat analogous structure was obtained by Piers and coworkers<sup>[89]</sup> from the reaction of a pincer type iridium  $PC_{sp^2}P$  with  $N_2O$  to form an iridaepoxide complex. The C=O moiety was formed by exposure of the carbene chloride complex to  $N_2O$ , by addition of an oxygen atom to the Ir=C bond, cleanly synthesizing the iridium complex containing the  $\eta^2$ -coordinated C=O moiety (Figure 18). The iridaepoxide shows a moderate upfield shift at  $\delta$  65 ppm in  $^{13}C$  NMR. X-ray crystal structure analysis showed a C–O distance of 1.350(7) Å, which is in between a C–O double and single bond, i.e.  $\sim 1.21$  Å and  $\sim 1.45$  Å. An Ir–O distance of 2.034(4) Å was found and an Ir–C distance of 2.080(6) Å, both in the range of a single bond.

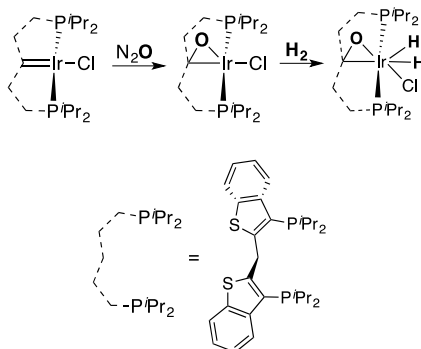


**Figure 18.** Schematic representation of the pincer type iridium  $PC_{sp^2}P$  iridium complex and its reaction with  $N_2O$ , forming the iridaepoxide complex, and the following reaction with  $H_2$  (top) and the schematic and chemical representation of the ligand (bottom).

Hydrogen binds to the iridium center upon exposure of the iridaepoxide to 1 atm H<sub>2</sub> at room temperature, from which H<sub>2</sub>O is subsequently eliminated. The mechanism of this formal hydrogenation of N<sub>2</sub>O was investigated in detail, in which it was proposed that this elimination occurs *via* migration of a proton to the oxygen atom, forming an alcohol group on the carbene carbon atom and a hydride on the iridium center, as shown in Figure 19a.<sup>[90]</sup> This step can either be seen as a reductive elimination/oxidative addition mechanism when starting from the iridaepoxide extreme, or as a 1,2-insertion/ $\beta$ -elimination when starting from the  $\eta^2$ -coordinated C=O extreme (Figure 19b). In a next step the alcohol group migrates to iridium and H<sub>2</sub>O is eliminated.<sup>[90]</sup> In this proposed mechanism the metal-ligand system operates in a truly cooperative fashion, storing part of the activated small molecule on the ligand backbone.

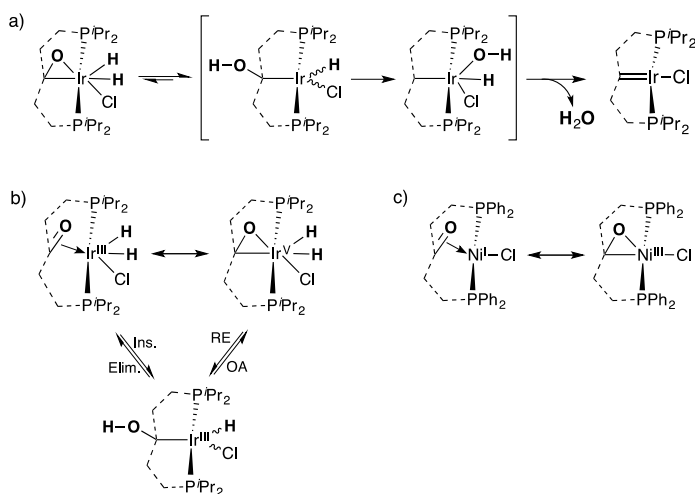


**Figure 19.** a) The iridaepoxide complex with one equivalent of H<sub>2</sub> added and the following H<sub>2</sub>O elimination pathway. The ligand is represented schematically as in Figure 18. b) Resonance structures of the hydrogen bound iridium complex and the visualization of the proton migration, starting from either Ir(III) or Ir(V) as described by Piers.<sup>[90]</sup> c) Resonance structures for the (Phdpbp)NiCl complex as described by Moret (*vide infra*).<sup>[91]</sup>

A more direct synthetic access to supported metallaepoxide structures is provided by the 2,2'-bis(diphenylphosphine)benzophenone (<sup>Ph</sup>dpbp) ligand.<sup>[91]</sup> The use of <sup>Ph</sup>dpbp as a chiral ligand was first explored in the group of Ding, where Ru(II)-based Noyori-type systems were developed to perform hydrogenation reactions. The benzophenone backbone was found to induce enantioselectivity in the catalytic hydrogenation of aromatic systems, in which the coordination of the C=O moiety is believed to be the key feature to obtain high yields and selectivity.<sup>[92]</sup> Our group further explored the chemistry by coordination of <sup>Ph</sup>dpbp to nickel in the oxidation states of 0, 1 and 2 (Figure 20, Chapter 2). It was found that the ligand ketone moiety does not bind to the metallic

center in the high-spin Ni(II) complex  $(\text{Phdpbb})\text{NiCl}_2$  (Ni–C: 3.4031(12) Å, Ni–O: 3.1012(10) Å), but this interaction was induced by reduction of the complex. The synthesis of  $(\text{Phdpbb})\text{Ni(I)Cl}$  and  $(\text{Phdpbb})\text{Ni(O)PPh}_3$  both lead to an  $\eta^2(\text{C,O})$  interaction, leading to shorter bond distances between the ketone moiety and the metallic center (Ni–C: 2.006(2) Å, Ni–O: 1.9740(15) Å for Ni(I) and Ni–C: 2.001(2) Å, Ni–O: 2.0091(14) Å for Ni(O)). Next to this, the C=O bond was elongated from 1.213(3) Å in the Ni(II) structure to 1.310(2) Å in the Ni(I) and 1.330(3) Å in the Ni(O) structure, showing significant  $\pi$ -backdonation from the metal to the C=O moiety in the latter two cases (Figure 21). NBO analysis of a DFT-computed electron density revealed an increased negative charge on the C=O fragment of  $-0.5e$  and  $-0.6e$  upon binding to Ni(I)Cl and Ni(O)PPh<sub>3</sub>, respectively. This additionally supports the predominantly electron accepting nature of the ketone moiety, which can be seen to function as a hemilabile acceptor ligand.<sup>[91]</sup>

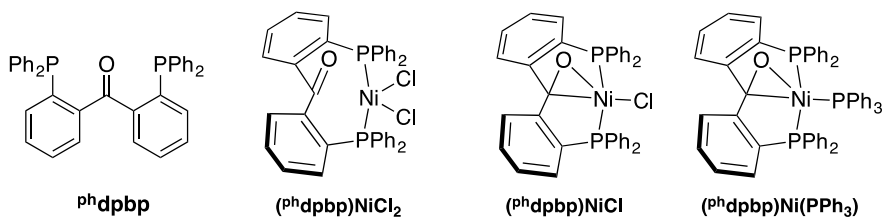


**Figure 20.** Left-to-right: Diphosphine-ketone ligand 2,2'-bis(diphenylphosphino)-benzophenone ( $\text{Phdpbb}$ ), and the metal complexes  $(\text{Phdpbb})\text{NiCl}_2$ ,  $(\text{Phdpbb})\text{NiCl}$  and  $(\text{Phdpbb})\text{Ni}(\text{PPh}_3)$ .

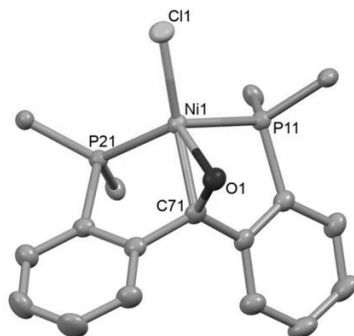


**Figure 21.** Crystal structure of  $(\text{Phdpbb})\text{NiCl}$  showing the  $\eta^2(\text{C,O})$  interaction with the nickel center, phenyl groups on the phosphorus atoms are omitted for clarity except for the bound carbon atom.

In a related study, Ruhland and co-workers explored the use of bisphosphinite ligands for the activation of unstrained  $\text{C}(\text{sp}^2)\text{--C}(\text{sp}^2)$  bonds. Coordination of the bisphosphinite ligand ( $^{\text{iPr}}\text{Prdpobb}$ , Figure 22) to nickel,<sup>[93]</sup> rhodium<sup>[94]</sup> or iridium<sup>[95]</sup> resulted in quantitative oxidative addition of the  $\text{PhC--CO}$  bond, breaking the ligand backbone. This reaction is proposed to proceed *via* an  $\eta^2(\text{C,O})$  interaction of the ketone moiety. Such pathways

were not observed when using  $^{\text{Ph}}\text{dpbb}$  as the ligand, suggesting that the tether length is of importance to the stability of  $\eta^2(\text{C},\text{O})$  complexes.

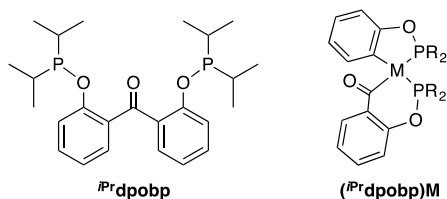


**Figure 22.** Bisphosphite ligand  $^{\text{iPr}}\text{dpobb}$  and the metal complexes. M = Ni, Rh, Ir; R = *i*Pr.

Coordination of a phosphine-tethered aldehyde ligand was explored in the group of Yeh. The bidentate P,O-chelating ligand *o*-(diphenylphosphine)benzaldehyde (PCHO) in combination with group 6 metals Mo<sup>[96]</sup> and W<sup>[97]</sup> was described. A complex with an octahedral geometry around the metal center was synthesized in both cases, binding two PCHO ligands and two CO ligands (Figure 23a). The aldehyde moieties were shown to bind to the metal center in an  $\eta^2$ -fashion by elongation of the aldehyde C=O bonds upon complexation due to  $\pi$ -backbonding to the empty  $\pi^*$ -orbital of this fragment (Mo, C–O: 1.335(4) Å and 1.323(4) Å; W, C–O: 1.338(5) Å and 1.357(5) Å). A distinctive shift of the furan proton was observed in <sup>1</sup>H NMR, from  $\delta$  10.50 ppm in the free PCHO ligand to  $\delta$  5.38 ppm in case of Mo and  $\delta$  5.12 ppm in case of W. The phosphorus signal was shown to shift from  $\delta$  –11.37 ppm in the free PCHO ligand to  $\delta$  18.04 ppm for Mo and  $\delta$  10.03 ppm for W. The reactivity of the molybdenum complex **Mo(PCHO)<sub>2</sub>(CO)<sub>2</sub>** with C<sub>60</sub> was explored: the formed molybdenum complex still contained two CO ligands next to C<sub>60</sub>, the latter being bound in an  $\eta^2$ -fashion through a 6:6-ring junction. Furthermore, the two bound PCHO ligands unexpectedly reacted, forming a *trans*-stilbene type ligand, bound *via* the carbon–carbon double bond in the backbone as well as the phosphorus ligands, resulting in **Mo(PCH=CHP)(CO)<sub>2</sub>(C<sub>60</sub>)** (Figure 23b). This binding is similar to the *trans*-stilbene type ligands shown in section 2.1 (*vide supra*). Analysis by single crystal X-ray diffraction showed an  $\eta^2$ -bound C=C moiety with a bond length of 1.418(7) Å, which is in the range of the olefinic C–C bonds of the described *trans*-stilbene type ligands that were found to be between 1.40 Å and 1.44 Å.<sup>[96]</sup>

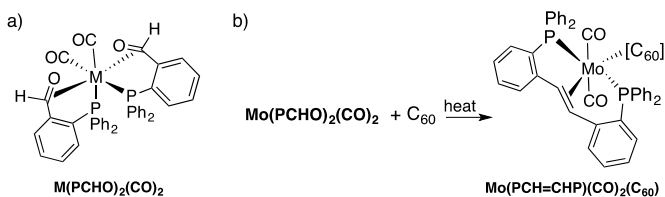


**Figure 23.** a) Octahedral complexes **M(PCHO)<sub>2</sub>(CO)<sub>2</sub>**, M = Mo or W, PCHO = *o*-(diphenylphosphine)benzaldehyde. b) Activity study of **Mo(PCHO)<sub>2</sub>(CO)<sub>2</sub>** with C<sub>60</sub>, resulting in the *trans*-stilbene complex **Mo(PCH=CHP)(CO)<sub>2</sub>(C<sub>60</sub>)**.

### 1.4.2 Imine complexes

Imines are ubiquitous as ligands for transition metals, forming  $\sigma$  dative bonds by donation of one of the lone pairs of the nitrogen atom. Because this binding mode is generally preferred,  $\pi$ -complexes of C=N bonds are rare (Figure 24). Recent examples where this binding mode is accessed upon formal deactivation of the N-centered lone pair either by coordination to another metal or by substitution to generate an iminium cation are discussed here.

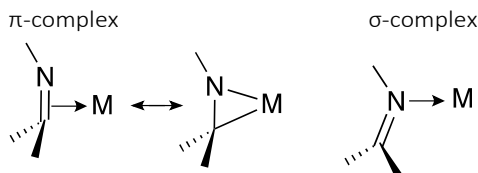


**Figure 24.** Left: Schematic representation of the two resonance extremes of an imine  $\pi$ -complex, right: representation of the imine  $\sigma$ -complex.

A rhodium based amido-bridged dinuclear complexes was synthesized in the group of de Bruin,  $[\text{Rh}(\text{nbd})_2(\mu\text{-bpa})]\text{Cl}$  (nbd = norbornadiene, bpa = bis(2-picoly)amine).<sup>[98]</sup> The complex was shown to be susceptible to deprotonation by  $\text{KO}^t\text{Bu}$ , resulting in the complex  $\text{Rh}(\text{nbd})_2(\mu\text{-bpi})$ , where the doubly deprotonated bis(2-picoly)amine ( $\text{PyCH}_2\text{NHCH}_2\text{Py}$ , bpa) ligand is transformed to a neutral  $\text{PyCH}=\text{N}-\text{CH}_2\text{Py}$  (bpi) ligand containing an imine functionality (Figure 25a). The two complexes are related by acid-base chemistry, as the backward reaction is possible by protonation with  $\text{NHEt}_3\text{Cl}$ . Both the C and N atom of the deprotonated complex have a trigonal geometry, suggesting the formation of a  $\pi$ -coordinating imine C=N fragment (Figure 25b). Next to this, the C–N distance was found to be shorter upon comparison to the protonated complex, i.e. 1.415(4) Å versus 1.482(6) Å, respectively. In agreement with further analysis, this complex was described as a mixed valence  $\text{Rh}(-1,1)$  complex. The complex reacted rapidly with oxygen in benzene, leading to new, mononuclear complexes.<sup>[98]</sup> Analogues to this rhodium complex, the synthesis of another group 9 binuclear complex was explored using iridium (Figure 25c).<sup>[99]</sup> An X-ray crystal structure of the cationic complex  $[\text{Ir}(\text{nbd})_2(\mu\text{-bpi})]\text{PF}_6$  was obtained, showing a similar complex as the rhodium analogue. The rather unusual bridging  $\pi$ -coordination was again obtained, which was described as the first example of a  $\pi$ -bound imine moiety for iridium. Both of the iridium centers in the complex bind to the imine moiety, of which one adopts a  $\sigma$ -coordination to the imine nitrogen atom, activating the imine for  $\eta^2$ -coordination to the other iridium center. Next to this, both iridium centers also bear a cod ligand. The  $\eta^2$ -bound imine was shown to gain substantial  $\pi$ -backdonation, as the C–N bond has a length of 1.407(3) Å which is substantially longer compared to  $\sigma$ -coordinated imines to iridium that have

a typical length of  $\sim 1.30$  Å.<sup>[99]</sup> As a result it can be concluded that both resonance extremes play a role in binding, i.e. the side-on bound Ir(I) extreme and the Ir(III) irida-za-cyclopropane extreme (Figure 25d). The iridium complex was shown to be an active pre-catalyst for water oxidation after treatment with cerium ammonium nitrate ( $\text{Ce}^{\text{IV}}$ ) as the oxidant.<sup>[99]</sup> The research using the bpi ligand was extended to the use of mixed metal systems. Complexes with Rh–Ir<sup>[100]</sup> and Pd–Ir<sup>[101]</sup> were synthesized, which both still contained the  $\eta^2$ -bound imine moiety.

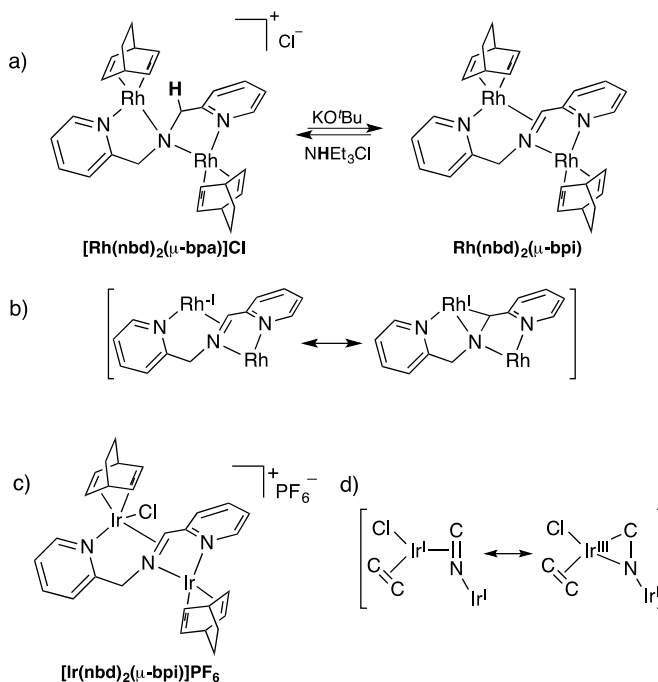


**Figure 25.** a) Rh-based complexes and their acid-base chemistry. b) Resonance extremes of the Rh-imine bound structure. c) Structure of the cationic Ir-based complex. d) Resonance extremes of the Ir-imine bound structure. Figure adapted from de Bruin.<sup>[98,99]</sup>

Other rhodium complexes with an  $\eta^2$ -bound  $\text{N}=\text{C}$  double bond have been synthesized from a bulky  $\text{trop}_2\text{NMe}$  ligand ( $\text{trop} = 5\text{H-dibenzo}[a,d]\text{cyclohepten-5-yl}$ ).<sup>[102,103]</sup> They were formed in multiple steps, starting from  $\text{trop}_2\text{NMe}$ ,  $\text{Rh}(\mu_2\text{-Cl})_2(\text{cod})_2$  and  $\text{PPh}_3$ , resulting in  $\text{Rh}(\text{trop}_2\text{NMe})(\text{PPh}_3)$  which was further reacted with  $\text{AgOTf}$  to yield the positively charged complex  $[\text{Rh}(\text{trop}_2\text{NMe})(\text{PPh}_3)]\text{OTf}$ . The methyl group was subsequently deprotonated with  $\text{KO}^t\text{Bu}$  to form an interaction between  $\text{C}_{\text{Me}}$  and Rh, forming an unsaturated  $\text{C}=\text{N}$  ligand ( $\text{Rh}(\text{trop}_2\text{N}=\text{C})(\text{PPh}_3)$ ) (Figure 26a,b). The binding of this moiety can either be considered as a rhodaazacyclopropane or as the  $\eta^2$ -side-on bound  $(\text{C}=\text{N})\text{-M}$  complex (Figure 26c). The  $\text{N}-\text{CH}_2$  distance is  $1.446(5)$  Å, which is significantly shorter compared to the  $\text{N}-\text{CH}_3$  which was found to be  $1.505(7)$  Å, but on

the other hand longer than other C=N bonds in iminium ions (1.274-1.301 Å). The rhodaazacyclopropane description has an energetically low-lying  $\pi^*$ -orbital of the N-C bond, and so  $\pi$ -backdonation to the ligand is strong. For these reasons in combination with further analysis by NMR, the metallacycle description is the most accurate for this complex. The properties of  $\text{Rh}(\text{trop}_2\text{N}=\text{C})(\text{PPh}_3)$  were explored with cyclic voltammetry in a THF solution, in which the complex could be oxidized. The  $\text{Rh}(\text{trop}_2\text{N}=\text{C})(\text{PPh}_3)^+$  complex was stable enough to be analyzed by EPR spectroscopy, from which it was shown that the structural features of the starting complex were retained, obtaining a rhodaazacyclopropyl radical cation. In analogy to the neutral complex, this complex is also best described as a RhNC metallacycle (Figure 26c), showing the possibility of this ligand to stabilize multiple oxidation states with a single geometry.<sup>[103]</sup>

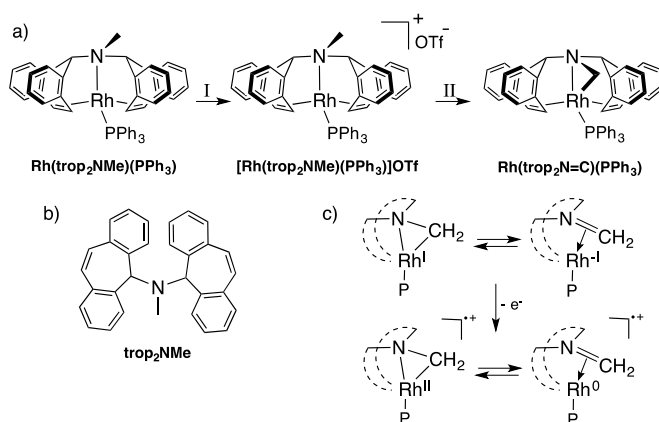


**Figure 26.** a) Synthesis of Rh-based complexes, I = AgOTf ; II = KO<sup>t</sup>Bu. b) The ligand  $\text{trop}_2\text{NMe}$ . c) Binding modes of  $\text{Rh}(\text{trop}_2\text{N}=\text{C})(\text{PPh}_3)$  and  $\text{Rh}(\text{trop}_2\text{N}=\text{C})(\text{PPh}_3)^+$ , the rhodaazacyclopropane and the  $\eta^2$ -side-on bound (C=N)-M complex.

## 1.5 Conclusions

The inclusion of  $\pi$ -coordinating ligands in organometallic complexes is a versatile tool to induce metal-ligand cooperativity. The recent advances described here illustrate how the reactivity of metal-bound  $\pi$ -systems can be controlled by ligand design. In particular, the incorporation of a variety of tethers to connect the  $\pi$ -coordinating moiety and additional donor groups, mainly based on coordinating P-donors, exerts a strong influence on its coordination mode and reactivity. In the arene based chemistry, the tether length can favor or disfavor coordination of the aromatic  $\pi$ -system: the long, flexible tether in  $(\text{P}^{\text{h}}\text{PArP})\text{Rh}$  complexes combined with steric encumbrance turns a strong  $\eta^6$ -arene ligand into a hemilabile moiety. Conversely, the rigid *ortho*-phenylene



tethers in terphenyl-based ligands impose a close proximity between an aromatic moiety and group 10 metals.

The use of rigid tethers also stabilize unusual coordination modes of certain  $\pi$ -systems, such as the side-on coordination of the C=O moiety in Milstein's quinone based iridium pincer complexes. Similarly, the *ortho*-phenylene tethers in ketone-based pincer ligands favor the  $\eta^2(\text{CO})$  binding mode over the  $\eta^1(\text{O})$ , resulting in hemilabile-acceptor behavior in  $(^{\text{Ph}}\text{dppb})\text{NiL}$  complexes. Another striking example of tether-imposed binding mode is the unusual coordination mode of the pyridine moiety in  $\text{Ni}(\text{PPyP})$  complexes: the anchoring of the phosphorus groups on the meta positions leads to the nickel center coordinating a C=C bond of the aromatic ring, whereas a pyridine ring usually coordinates *via* its nitrogen atom lone pair. Due to this binding mode, an electron deficient aromatic ring could be generated *via* coordination of Lewis-acidic borane ligand to the lone pair on the pyridine nitrogen atom, leading to enhanced hydride affinity and allowing for bifunctional activation of silanes and boranes.

This last example also illustrates how reactivity at  $\pi$ -ligands can be tuned by electronic effects. Related reactivity was observed upon introduction of electron-deficient borane substituents. Interaction of arylborane moieties with reduced metal centers often involves both the boron atom and the aromatic system in  $\eta^2(\text{BC})$  or  $\eta^3(\text{BCC})$  coordination modes, as featured in the chemistry of diphosphine-borane (DPB) ligands. Cooperative reactivity of DPB complexes usually involves the boron center functioning as a hydride acceptor, allowing for the activation of a range of small molecules by iron, cobalt, and nickel compounds. Remarkably, a high hydride affinity at the boron-substituted aromatic ring has also been observed in ruthenium chemistry of the  $^{\text{Ph}}\text{DPB}^{\text{Ph}}$  ligand: a hydride can be incorporated on the carbon-backbone of the ligand, allowing the  $\eta^6$ -bound arene moiety in  $[(^{\text{Ph}}\text{DPB}^{\text{Ph}})\text{RuCl}]^+$  to function as a hydride acceptor in frustrated Lewis pair chemistry.

Metal-ligand cooperation is a versatile tool in current efforts to transition from precious to base metals in catalysis. The recent advances discussed herein highlight the incorporation of tethered  $\pi$ -ligands as a promising strategy for the design of new and tuneable cooperative systems, hopefully stimulating further development of this class of compounds for base metal catalysis.

## 1.6 References

- [1] J. I. van der Vlugt, *Eur. J. Inorg. Chem.*, **2012**, 363–375.
- [2] J. R. Khusnutdinova, D. Milstein, *Angew. Chem. Int. Ed.*, **2015**, *54*, 12236–12273.
- [3] P. J. Chirik and K. Wieghardt, *Science*, **2010**, *327*, 794–795.
- [4] J. C. Jeffrey, T. B. Rauchfuss, *Inorg. Chem.*, **1979**, *18*(10) 2658–2666.
- [5] P. Braunstein, F. Naud, *Angew. Chem. Int. Ed.*, **2001**, *40*, 680–699.

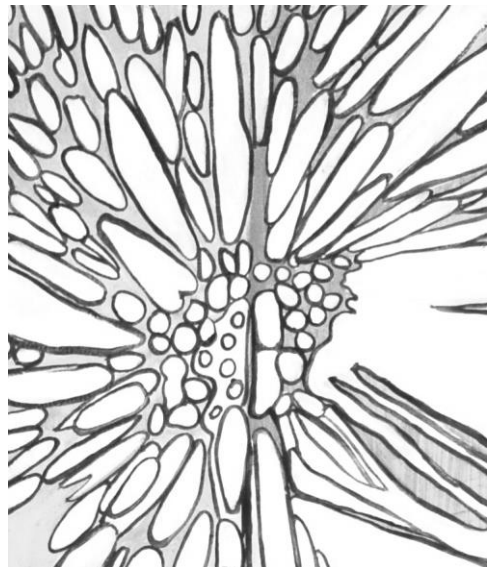
- [6] W. I. Dzik, J. I. van der Vlugt, J. N. H. Reek, B. de Bruin, *Angew. Chem. Int. Ed.*, **2011**, *50*, 3356–3358.
- [7] O.R. Luca and R.H. Crabtree, *Chem. Soc. Rev.*, **2013**, *42*, 1440–1459.
- [8] P. J. Chirik, *Inorg. Chem.*, **2011**, *50*, 9737–9740.
- [9] T. W. Myers, L. A. Berben, *J. Am. Chem. Soc.*, **2011**, *133*, 11865–11867.
- [10] T. W. Myers, L. A. Berben, *J. Am. Chem. Soc.*, **2013**, *135*, 9988–9990.
- [11] R. Noyori, *Angew. Chem. Int. Ed.*, **2002**, *41*, 2008–2022.
- [12] E. Balaraman, C. Gunanathan, J. Zhang, L. J. W. Shimon, D. Milstein, *Nat. Chem.*, **2011**, *3*, 609–614.
- [13] S. P. Semproni, C. Milsmann, P. J. Chirik, *J. Am. Chem. Soc.*, **2014**, *136*, 9211–9224.
- [14] R. Langer, G. Leitius, Y. Ben-David, D. Milstein, *Angew. Chem. Int. Ed.*, **2011**, *50*, 2120–2124.
- [15] Y. Shvo, D. Czarkie, Y. Rahamim, *J. Am. Chem. Soc.*, **1986**, *108*, 7400–7402.
- [16] J. Pearson, R. J. Shively, Jr., R. A. Dubbert, *Organometallics*, **1992**, *11*, 4096–4104.
- [17] H.-J. Knölker, E. Baum, R. Klauss, *Tetrahedron Lett.*, **1995**, *36*, 7647–7650.
- [18] C. P. Casey, H. Guan, *J. Am. Chem. Soc.*, **2007**, *129*, 5816–5817.
- [19] B. L. Conley, M. K. Pennington-Boggio, E. Boz, T. J. Williams, *Chem. Rev.*, **2010**, *110*, 2294–2312.
- [20] I. Bauer, H.-J. Knölker, *Chem. Rev.*, **2015**, *115*, 3170–3387.
- [21] P. E. Sues, K. Z. Demmans, R. H. Morris, *Dalton Trans.*, **2014**, *43*, 7650–7667.
- [22] S. Chakraborty, P. O. Lagaditis, M. Förster, E. A. Bielinski, N. Hazari, M. C. Holthausen, W. D. Jones, S. Schneider, *ACS Catal.*, **2014**, *4*, 3994–4003.
- [23] R. Langer, M. A. Iron, L. Konstantinovski, Y. Diskin-Posner, G. Leitius, Y. Ben-David, D. Milstein, *Chem. Eur. J.*, **2012**, *18*, 7196–7209.
- [24] N. Gorgas, B. Stöger, L. F. Veiros, E. Pittenauer, G. Allmaier, K. Kirchner, *Organometallics*, **2014**, *33*, 6905–6914.
- [25] S. Chakraborty, H. Dai, P. Bhattacharya, N. T. Fairweather, M. S. Gibson, J. A. Krause, H. Guan, *J. Am. Chem. Soc.*, **2014**, *136*, 7869–7872.
- [26] J. I. van der Vlugt, J. N. H. Reek, *Angew. Chem. Int. Ed.*, **2009**, *48*, 8832–8846.
- [27] S. Schneider, J. Meiners, B. Askevold, *Eur. J. Inorg. Chem.*, **2012**, 412–429.
- [28] C. Gunanathan, D. Milstein, *Acc. Chem. Res.*, **2011**, *44*(8), 588–602.
- [29] V. Lyaskovskyy and B. de Bruin, *ACS Catal.*, **2012**, *2*, 270–279.
- [30] M. Asay, D. Morales-Morales, *Dalton Trans.*, **2015**, *44*, 17432–17447.
- [31] G. van Koten, D. Milstein, *Topics in Organometallic Chemistry*, Organometallic Pincer Chemistry, Springer, **2013**.
- [32] A. M. Tondreau, C. C. Hojilla Atienza, K. J. Weller, S. A. Nye, K. M. Lewis, J. G. P. Delis, P. J. Chirik, *Science*, **2012**, *335*(6068), 567–570.
- [33] D. Morales-Morales, C. M. Jensen, *The Chemistry of Pincer Compounds*, Elsevier Science, Amsterdam, **2007**.
- [34] K. J. Szabó, O. F. Wendt, *Pincer and Pincer-Type Complexes*, Wiley-VCH, Weinheim, **2014**.
- [35] M. Albrecht, G. van Koten, *Angew. Chem. Int. Ed.*, **2001**, *40*, 3750–3781.
- [36] M. E. van der Boom, D. Milstein, *Chem. Rev.*, **2003**, *103*, 1759–1792.
- [37] M. W. O'Reilly, A. S. Veige, *Chem. Soc. Rev.*, **2014**, *43*, 6325–6369.
- [38] W. C. Zeise, *Poggendorffs Ann. Phys.*, **1827**, *9*, 632–633.

- [39] R. H. Crabtree, *The organometallic chemistry of the transition metals*, Fifth edition, Wiley, New Haven, **2009**.
- [40] M. A. Bennett, P. W. Clark, *J. Organomet. Chem.*, **1976**, *100*, 367–381.
- [41] M. A. Bennett, R. N. Johnson, I. B. Tomkins, *J. Organomet. Chem.*, **1976**, *118*, 205–232.
- [42] W. Baratta, E. Herdtweck, P. Martinuzzi, P. Rigo, *Organometallics*, **2001**, *20*, 305–308.
- [43] B. J. Barrett, V. M. Iluc, *Organometallics*, **2014**, *33*, 2565–2574.
- [44] B. J. Barrett, V. M. Iluc, *Inorg. Chem.*, **2014**, *53*, 7248–7259.
- [45] C. C. Comanescu, M. Vyushkova, V. M. Iluc, *Chem. Sci.*, **2015**, *6*, 4570–4579.
- [46] A. V. Polukeev, R. Marcos, M. S. G. Ahlquist, O. F. Wendt, *Chem. Sci.*, **2015**, *6*, 2060–2067.
- [47] a) A. Friedrich, R. Ghosh, R. Kolb, E. Herdtweck, S. Schneider, *Organometallics*, **2009**, *28*, 708–718; b) C. Bianchini, E. Farnetti, M. Graziani, G. Nardin, A. Vacca, F. Zanobini, *J. Am. Chem. Soc.*, **1990**, *112*, 9190–9197.
- [48] A. V. Polukeev, O. F. Wendt, *Organometallics*, **2015**, *34*, 4262–4271.
- [49] K. J. Jonasson, A. V. Polukeev, R. Marcos, M. S. G. Ahlquist, O. F. Wendt, *Angew. Chem. Int. Ed.*, **2015**, *54*, 9372–9375.
- [50] L. Zhang, T. Yan, Y-F Han, F. E. Hahn, G-X Jin, *Dalton Trans.*, **2015**, *44*, 8797–8800.
- [51] K. Okamoto, Y. Omoto, H. Sano, K. Ohe, *Dalton Trans.*, **2012**, *41*, 10926–10929.
- [52] F. M. Dixon, J. R. Farrell, P. E. Doan, A. Williamson, D. A. Weinberger, C. A. Mirkin, C. Stern, C. D. Incarvito, L. M. Liable-Sands, L. N. Zakharov, A. L. Rheingold, *Organometallics*, **2002**, *21*, 3091–3093.
- [53] F. M. Dixon, M. S. Masar III, P. E. Doan, J. R. Farrell, F. P. Arnold Jr., C. A. Mirkin, C. D. Incarvito, L. N. Zakharov, A. L. Rheingold, *Inorg. Chem.*, **2003**, *42*(10), 3245–3255.
- [54] R. C. Smith, J. D. Protasiewicz, *Organometallics*, **2004**, *23*, 4215–4222.
- [55] B. P. Morgan, R. C. Smith, *J. Organomet. Chem.*, **2008**, *693*, 11–16.
- [56] K. T. Horak, A. Velian, M. W. Day, T. Agapie, *Chem. Commun.*, **2014**, *50*, 4427–4429.
- [57] K. T. Horak, S. Lin, J. Rittle, T. Agapie, *Organometallics*, **2015**, *34*, 4429–4432.
- [58] J. T. Henthorn, S. Lin, T. Agapie, *J. Am. Chem. Soc.*, **2015**, *137*, 1458–1464.
- [59] K. T. Horak, T. Agapie, *J. Am. Chem. Soc.*, **2016**, *138*, 3443–3452.
- [60] J. A. Buss, T. Agapie, *Nature*, **2016**, *529*, 72–75.
- [61] A. Velian, S. Lin, A. J. M. Miller, M. W. Day, T. Agapie, *J. Am. Chem. Soc.*, **2010**, *132*, 6296–6297.
- [62] S. Lin, M. W. Day, T. Agapie, *J. Am. Chem. Soc.*, **2011**, *133*, 3828–3831.
- [63] K. T. Horak, D. G. VanderVelde, T. Agapie, *Organometallics*, **2015**, *34*, 4753–4765.
- [64] G. A. Edouard, P. Kelley, D. E. Herbert, T. Agapie, *Organometallics*, **2015**, *34*, 5254–5277.
- [65] M. L. H. Green, *J. Organomet. Chem.*, **1995**, *500*, 127–148.
- [66] D. J. H. Emslie, B. E. Cowie, S. R. Oakley, N. L. Huk, H. A. Jemkins, L. E. Harrington, J. F. Britten, *Dalton Trans.*, **2012**, *41*, 3523–3535.
- [67] A. F. Hill, G. R. Owen, A. J. P. White, D. J. Williams, *Angew. Chem. Int. Ed.*, **1999**, *38*(18), 2759–2761.
- [68] G. Bouhadir, D. Bourissou, *Chem. Soc. Rev.*, **2016**, *45*, 1065–1079.
- [69] A. Amgoune, D. Bourissou, *Chem. Commun.*, **2011**, *47*, 859–871.
- [70] H. Braunschweig, R. D. Dewhurst, *Dalton Trans.*, **2011**, *40*, 549–558.
- [71] I. Kuzu, I. Krummenacher, J. Meyer, F. Armbruster, F. Breher, *Dalton Trans.*, **2008**, *43*, 5836–5865.

- [72] D. J. H. Emslie, B. E. Cowie, K. B. Kolpin, *Dalton Trans.*, **2012**, 41, 1101–1117.
- [73] R. Malacea, F. Chahdoura, M. Devillard, N. Saffon, M. Gómez, D. Bourissou, *Adv. Synth. Catal.*, **2013**, 355, 2274–2284.
- [74] R. Malacea, N. Saffon, M. Gómez, D. Bourissou, *Chem. Comm.*, **2011**, 47, 8163–8165.
- [75] B. E. Cowie, D. J. H. Emslie, *Chem. Eur. J.*, **2014**, 20, 16899–16912.
- [76] B. E. Cowie, D. J. H. Emslie, *Organometallics*, **2013**, 32, 7297–7305.
- [77] B. E. Cowie, D. J. H. Emslie, *Organometallics*, **2015**, 34, 4093–4101.
- [78] S. Bontemps, H. Gornitzka, G. Bouhadir, K. Miqueu, D. Bourissou, *Angew. Chem. Int. Ed.*, **2006**, 45, 1611–1614.
- [79] M. Sircoglou, S. Bontemps, M. Mercy, K. Miqueu, S. Ladeira, N. Saffon, L. Maron, G. Bouhadir, D. Bourissou, *Inorg. Chem.*, **2010**, 49(9), 3983–3990.
- [80] W. -C. Shih, W. Gu, M. C. MacInnis, S. D. Timpa, N. Bhuvanesh, J. Zhou, O. V. Ozerov, *J. Am. Chem. Soc.*, **2016**, 138, 2086–2089.
- [81] W. H. Harman, J. C. Peters, *J. Am. Chem. Soc.*, **2012**, 134, 5080–8082.
- [82] D. L. M. Suess, J. C. Peters, *J. Am. Chem. Soc.*, **2013**, 135, 12580–12583.
- [83] S. N. MacMillan, W. H. Harman, J. C. Peters, *Chem. Sci.*, **2014**, 5, 590–597.
- [84] W. H. Harman, T. -P. Lin, J. C. Peters, *Angew. Chem. Int. Ed.*, **2014**, 53, 1081–1086.
- [85] D. L. M. Suess, J. C. Peters, *J. Am. Chem. Soc.*, **2013**, 135, 4938–4941.
- [86] M. A. Nesbit, D. L. M. Suess, J. C. Peters, *Organometallics*, **2015**, 34(19), 4741–4752.
- [87] M. P. Boone, D. W. Stephan, *J. Am. Chem. Soc.*, **2013**, 135, 8508–8511.
- [88] A. Vignalok, B. Rybtchinski, Y. Gozin, T. S. Koblenz, Y. Ben-David, H. Rozenberg, D. Milstein, *J. Am. Chem. Soc.*, **2003**, 125, 15692–15693.
- [89] L. E. Doyle, W. E. Piers, J. Borau-Garcia, *J. Am. Chem. Soc.*, **2015**, 137, 2187–2190.
- [90] L. E. Doyle, W. E. Piers, J. Borau-Garcia, M. J. Sgro, D. M. Spasyuk, *Chem. Sci.*, **2016**, 7, 921–931.
- [91] Chapter 2 of this thesis: B. W. H. Saes, D. G. A. Verhoeven, M. Lutz, R. J. M. Klein Gebbink, M.-E. Moret, *Organometallics*, **2015**, 34, 2710–2713.
- [92] Q. Jing, C. A. Sandoval, Z. Wang, K. Ding, *Eur. J. Org. Chem.*, **2006**, 3606–3616.
- [93] K. Ruhland, A. Obenhuber, S. D. Hoffman, *Organometallics*, **2008**, 27, 3482–3495.
- [94] A. Obenhuber, K. Ruhland, *Organometallics*, **2011**, 30, 4039–4051.
- [95] A. Obenhuber, K. Ruhland, *Organometallics*, **2011**, 30, 171–186.
- [96] C.-S. Chen, C.-S. Lin, W.-Y. Yeh, *J. Organomet. Chem.*, **2011**, 696, 1474–1478.
- [97] W.-Y. Yeh, C.-S. Lin, *Organometallics*, **2004**, 23, 917–920.
- [98] C. Tejel, M. A. Ciriano, M. Pilar del Rio, F. J. van den Bruele, D. G. H. Hetterscheid, N. Tschlis i Spithas, B. de Bruin, *J. Am. Chem. Soc.*, **2008**, 130, 5844–5845.
- [99] W. I. Dzik, S. E. Calvo, J. N. H. Reek, M. Lutz, M. A. Ciriano, C. Tejel, D. G. H. Hetterscheid, B. de Bruin, *Organometallics*, **2011**, 30, 372–374.
- [100] C. Tejel, L. Asensio, M. P. del Río, B. de Bruin, J. A. López, M. A. Ciriano, *Eur. J. Inorg. Chem.*, **2012**, 512–519.
- [101] C. Tejel, L. Asensio, M. P. del Río, B. de Bruin, J. A. López, M. A. Ciriano, *Angew. Chem. Int. Ed.*, **2011**, 50, 8839–8843.
- [102] T. Büttner, F. Breher, H. Grützmacher, *Chem. Commun.*, **2004**, 2820–2821.
- [103] P. Maire, A. Sreekanth, T. Büttner, J. Harmer, I. Gromov, H. Rügger, F. Breher, A. Schweiger, H. Grützmacher, *Angew. Chem. Int. Ed.*, **2006**, 45, 3265–3269.



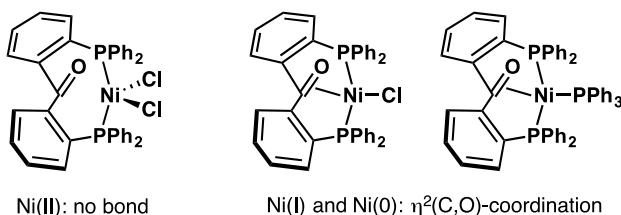
*Since we cannot change reality,  
Let us change the eyes which see reality.*  
- Nikos Kazantzakis



# | Chapter 2 |

## Coordination of a Diphosphine-Ketone Ligand to Ni(0), Ni(I), and Ni(II): Reduction-Induced Coordination

**Abstract** Coordination chemistry of the diphosphine-ketone ligand 2,2'-bis(diphenylphosphino)benzophenone ( $^{\text{Ph}}\text{dppb}$ ) with nickel is reported. The ketone moiety does not bind to Ni(II) in complex  $(^{\text{Ph}}\text{dppb})\text{NiCl}_2$ , whereas reduction to Ni(I) or Ni(0) induces  $\eta^2(\text{C},\text{O})$  coordination of the ketone to form pseudotetrahedral complexes  $(^{\text{Ph}}\text{dppb})\text{NiCl}$  and  $(^{\text{Ph}}\text{dppb})\text{Ni}(\text{PPh}_3)$ . DFT calculations indicate that the metal-ketone bond is dominated by  $\pi$ -backdonation; hence,  $^{\text{Ph}}\text{dppb}$  functions as a hemilabile acceptor ligand in this series of complexes.



---

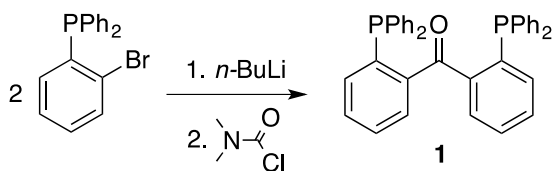
Published as: B. W. H. Saes, D. G. A. Verhoeven, M. Lutz, R. J. M. Klein Gebbink, M. -E. Moret, *Organometallics*, **2015**, *34*, 2710–2713.

## 2.1 Introduction

The development of greener and less expensive chemical processes motivates a widespread investigation of complexes of first-row transition metals as potential homogeneous catalysts to replace or, better, improve on traditional systems that are widely based on noble metals.<sup>[1]</sup> Progress in this area has been intimately related to the development of tailored ligands: cooperative ligands<sup>[2]</sup> that actively participate in chemical reactions – e.g. by accepting and releasing electrons,<sup>[3]</sup> protons,<sup>[4]</sup> or hydride equivalents<sup>[5]</sup> – and hemilabile ligands<sup>[6]</sup> that facilitate reaction steps by adapting their coordination mode to the electronic structure of the metal center along the reaction coordinate. In particular, multidentate ligands containing a Lewis-acidic moiety tethered to one or more chelating arms have recently been subjected to intense scrutiny<sup>[7]</sup> and were found to facilitate several catalytic reactions such as hydrogenation<sup>[5]</sup> (bifunctional H<sub>2</sub>-activation) and N<sub>2</sub> reduction<sup>[8]</sup> (hemilabile behavior).

Ketones are known to form relatively weak coordination bonds in two distinct modes:  $\eta^1(\text{O})$  with electrophilic metals<sup>[9]</sup> and  $\eta^2(\text{C},\text{O})$  with electron-rich metals.<sup>[10]</sup> Because of the electronegativity of oxygen, the latter binding mode, described by the Dewar-Chatt-Duncanson model, is often dominated by  $\pi$ -backbonding: for example, the formation of complexes of type  $(\text{Et}_3\text{P})_2\text{Ni}(\eta^2\text{-benzophenone})$  from  $(\text{Et}_3\text{P})_4\text{Ni}$  and substituted benzophenones is strongly accelerated by electron-withdrawing substituents.<sup>[10a]</sup> Therefore, it was reasoned that a ketone moiety tethered to strongly chelating arms would be of interest as a hemilabile, pincer-type ligand featuring a strong  $\pi$ -acceptor in the central position.<sup>[11]</sup> The ligand 2,2'-bis(diphenylphosphino)benzophenone<sup>[12]</sup> (<sup>Ph</sup>dpbp (**1**), Scheme 1) has been applied as a co-ligand for chirality transfer in rhodium<sup>[13]</sup> and ruthenium<sup>[14]</sup> hydrogenation catalysts, but to our knowledge has not been used in first-row transition metal chemistry.

In this chapter the coordination chemistry of the <sup>Ph</sup>dpbp ligand to nickel in three different oxidation states is reported, showing that it can act as a wide bite angle bidentate ligand for Ni(II) and adopts a pincer-like geometry in Ni(I) and Ni(0) complexes, in which the ketone moiety is coordinated in an  $\eta^2$  fashion dominated by  $\pi$ -backdonation.



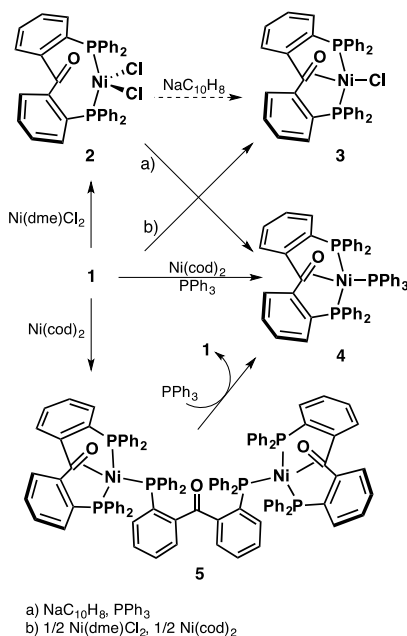
**Scheme 1.** Synthesis of the <sup>Ph</sup>dpbp ligand.



## 2.2 Results and Discussion

Improving on Ding's original 5-step synthesis,<sup>[12]</sup> ligand <sup>Ph</sup>dppb (**1**) was synthesized in 84% yield from *o*-bromo(diphenylphosphino)benzene<sup>[15]</sup> by lithiation with *n*-BuLi followed by reaction with 0.5 equivalents *N,N*-dimethylchloroformamide (Scheme 1). Reaction of **1** with (dme)NiCl<sub>2</sub> (dme = 1,2-dimethoxyethane) in dichloromethane afforded 83% of the 1:1 complex **2** as brown crystals (Scheme 2). Broad <sup>1</sup>H NMR resonances ranging from  $\delta$  -6.6 to 20.7 ppm and a solution effective magnetic moment ( $\mu_{\text{eff}}$ ) of 2.8  $\mu_{\text{B}}$  indicate a paramagnetic *S* = 1 state consistent with a high spin Ni(II) center. Complex **2** displays an intense IR band at 1634 cm<sup>-1</sup>, only slightly shifted from the C=O band in the free ligand **1** (1661 cm<sup>-1</sup>), suggesting at most a weak interaction of the C=O moiety with the metal.

Crystallization of **2** from CH<sub>2</sub>Cl<sub>2</sub> resulted in two crystal forms, which were both analyzed by X-ray crystal structure determinations. The results for the solvent-free **2** are discussed here (Figure 1). For the results of **2**·CH<sub>2</sub>Cl<sub>2</sub>, see Appendix B. The Ni–C (3.4031(12) Å) and Ni–O (3.1012(10) Å) distances are large enough to exclude coordination of the carbonyl moiety but nevertheless shorter than the sum of van der Waals radii<sup>[16]</sup> (Ni–C: 4.17 Å; Ni–O: 3.90 Å), which is likely imposed by the rigidity of the *o*-phenylene linkers but may result in a weak interaction. Hence, the coordination geometry is best described as distorted tetrahedral with a P–Ni–P bite angle of 112.996(13)° and a large Cl–Ni–Cl angle (133.302(14)°). Similar distortions have been observed in NiCl<sub>2</sub> complexes of other diphosphine ligands with large bite angles and ascribed to lone-pair repulsion between Cl atoms.<sup>[17a]</sup>



**Scheme 2.** Coordination of the <sup>Ph</sup>dppb ligand to Ni(0), Ni(I), and Ni(II).

The nickel(I) complex **3** was accessed *via* comproportionation of (dme)NiCl<sub>2</sub> and Ni(cod)<sub>2</sub> in the presence of ligand **1** (Scheme 2). Complex **3** was also observed by NMR following direct reduction of **2** with sodium naphthalide but could not be isolated from the reaction mixture. Its crystal structure<sup>[18]</sup> (Figure 1) reveals a mononuclear, four-coordinate complex in which the ketone unit is coordinated to the nickel in an  $\eta^2(\text{C},\text{O})$  fashion (Ni–C: 2.006(2) Å, Ni–O: 1.9740(15) Å). Significant  $\pi$ -backdonation into the C=O fragment is evidenced by an elongated C=O bond (1.310(2) Å vs 1.213(3) Å in **1**<sup>[12]</sup>) and the pyramidalization of the C71 atom, which displays a sum of valence angles of 354.1(3)°. The overall coordination geometry is best described as slightly distorted tetrahedral, in line with known tris(phosphine)Ni(I)–X (X=I, Br, Cl) complexes.<sup>[19]</sup> To our knowledge, **3** is the first example of a structurally characterized  $\eta^2(\text{C},\text{O})$ -ketone complex of Ni(I). The  $\eta^1(\text{O})$  binding mode is known in the Ni(I) complex [(nacnac)Ni(O=CPh<sub>2</sub>)] (nacnac = HC[CMenC<sub>6</sub>H<sub>3</sub>(*i*Pr)<sub>2</sub>]<sub>2</sub>),<sup>[20]</sup> which displays a much shorter C–O distance (1.239(7) Å) indicating a lower extent of  $\pi$ -backdonation than in **3**. The preference for the  $\eta^2(\text{C},\text{O})$  mode in **3** can be attributed to i) a more electron rich Ni(I) center and ii) geometrical constraints imposed by the rigid *o*-phenylene linkers.

Samples of **3** – even after multiple recrystallizations – contain a diamagnetic component evidenced by aromatic <sup>1</sup>H NMR resonances between  $\delta$  6.5 and 8 ppm (next to the expected broad, paramagnetically shifted spectrum) and a single <sup>31</sup>P resonance at  $\delta$  30.6 ppm, which was tentatively ascribed to a Ni–Ni bonded species (Appendix B, Figure B5).<sup>[21,22]</sup> The IR spectrum of **3** displays no absorption corresponding to an unbound ketone, but exhibits two absorptions at 1331 and 1340 cm<sup>-1</sup> that do not appear in the spectrum of the free ligand and are assigned to the bound C=O moiety (See Appendix B2). More insight in the electronic structure of compound **3** was obtained by EPR spectroscopy and DFT calculations.<sup>[23]</sup> The room-temperature EPR spectrum of **3** (Figure 2) displays a broad doublet ( $A_{\text{iso}}(^{31}\text{P}) = 380$  MHz) centered at  $g = 2.177$ , consistent with a metal-centered radical with superhyperfine coupling to one of the <sup>31</sup>P nuclei. A spectrum recorded at 100 K in frozen toluene (Appendix B3, Figure B2-3) displays a complex pattern that can be adequately simulated as a rhombic signal ( $g_x = 2.325$ ,  $g_y = 2.175$ ,  $g_z = 2.026$ ) with anisotropic hyperfine coupling to two inequivalent <sup>31</sup>P nuclei ( $A_1(^{31}\text{P}) = [360, 300, 500]$  MHz,  $A_2(^{31}\text{P}) = [210, 100, 95]$  MHz). The spin density obtained from DFT at the B3LYP/6-31G\*\* level (Figure 2) suggests that the inequivalency of the two <sup>31</sup>P nuclei both at 100K and at RT – where only one hyperfine coupling is resolved – can be ascribed to delocalization of the unpaired electron on a single P atom: NBO<sup>[24,25]</sup> analysis of the spin density ascribes a natural spin density (NSD) of 1.026 to Ni and of respectively 0.094 and 0.004 to the two phosphorus atoms, supporting the predominant metalloradical character of **3**. Negative NSDs on the ketone C (–0.12) and O (–0.04) atoms suggest that a charge-transfer configuration (Ni(II) + ketyl radical anion) might contribute to the overall electronic structure of **3**.

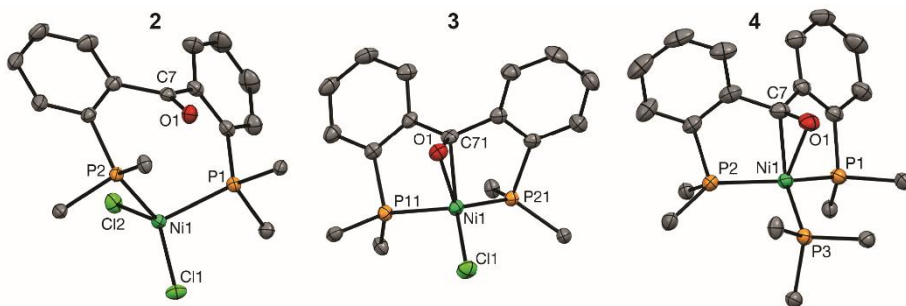


**Figure 1.** Molecular structures of compounds **2**, **3**, and **4** in the crystal (50% probability level), determined by single crystal X-ray structure determination. For clarity, only the *ipso* C-atoms of phosphorus-bound phenyl groups are represented. Only one of the two independent molecules of **3** is represented, and an Et<sub>2</sub>O molecule in the solid-state structure of **4** is omitted.

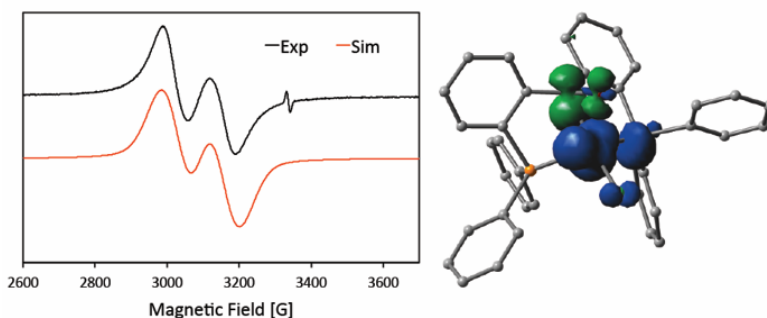


**Figure 2.** Left: Experimental (black) and simulated (red) room temperature X-band EPR spectrum of **3**. Simulation parameters:  $g = 2.177$ ,  $A_{iso}(^{31}\text{P}) = 380$  Hz. Right: Spin-density of **3** calculated at the B3LYP/6-31G\*\* level.

To study its coordination to Ni(0) centers, ligand **1** was treated with one equivalent Ni(cod)<sub>2</sub> to afford a brown solid that is formulated as the ligand:metal 3:2 complex **5** (Scheme 2) on basis of NMR data. The <sup>31</sup>P NMR spectrum of **5** at room temperature consists of three broad peaks that sharpen upon heating to 100 °C, becoming three mutually coupled doublet of doublets at  $\delta$  44.4, 21.3, and 5.6 ppm. The <sup>1</sup>H NMR spectrum of **5** exhibits a complex set of aromatic signals ranging from  $\delta$  8.8 to 6.2 ppm and no additional one that would suggest the presence of other organic ligands. The simplest structure that is consistent with this data is a symmetrical dinuclear complex in which a central <sup>Ph</sup>dpbp ligand bridges two Ni(0) centers chelated by an additional <sup>Ph</sup>dpbp ligand each (Scheme 2). This structural model is further corroborated by bands at 1679 and 1310 cm<sup>-1</sup> in the IR spectrum of **5** corresponding to the unbound and bound C=O units, respectively.

When a solution of **5** in toluene-*d*<sub>7</sub> was treated with excess PPh<sub>3</sub> in an NMR tube, two equivalents of the mononuclear complex **4** formed with concomitant release of one equivalent of the free ligand **1** (Scheme 2). Complex **4** could also be synthesized as a brown

solid from the reaction of **1**, Ni(cod)<sub>2</sub>, and PPh<sub>3</sub>, or by direct reduction of **2** with 2.2 equivalents sodium naphthalide in the presence of PPh<sub>3</sub>. Its <sup>31</sup>P NMR spectrum consists of a triplet at δ 38.2 ppm (<sup>2</sup>J<sub>PP</sub> = 25 Hz) and a doublet at δ 17.9 ppm in a 1:2 integral ratio, indicating that the two <sup>31</sup>P nuclei from the Ph<sub>2</sub>dpbp ligand are equivalent on the <sup>1</sup>H NMR timescale, in contrast with compound **5**. This can be explained by the less sterically congested structure of **4**, which allows for rapid exchange of the P-atoms (see Appendix B4 for an extended discussion). The η<sup>2</sup>(C,O)-coordinated ketone is characterized by a doublet (<sup>2</sup>J<sub>P,C</sub> = 14 Hz) of triplets (<sup>2</sup>J<sub>P,C</sub> = 9 Hz) at δ 120.4 ppm in the <sup>13</sup>C NMR spectrum and an IR absorption at 1309 cm<sup>-1</sup>.

The X-ray crystal structure of **4** (Figure 1) reveals a pseudotetrahedral environment of the metal similar to that found in **3**, albeit with a significantly larger P–Ni–P angle (120.65(2)° vs 107.57(2)°). The C=O bond (1.330(3) Å) is somewhat more elongated than that in **3**, consistent with stronger π-backdonation from Ni(0). The Ni–C (2.001(2) Å) and Ni–O (2.0091(14) Å) distances are longer than in three-coordinate (R<sub>3</sub>P)<sub>2</sub>Ni(benzophenone) complexes (Ni–C: 1.97–1.99 Å; Ni–O: 1.84–1.87 Å),<sup>[10]</sup> which might be due to more steric congestion.

**Table 1.** Wiberg Bond Indices (WBI) and natural charges (q) from densities calculated at the B3LYP/6-31+G\*\* level.

Compound	<b>1</b>	<b>2</b>	<b>3</b>	<b>4</b>
WBI (C–O)	1.75	1.67	1.30	1.23
WBI (Ni–O)	–	<0.01	0.33	0.30
WBI (Ni–C)	–	<0.01	0.46	0.50
q(C)	0.58	0.56	0.18	0.12
q(O)	–0.54	–0.55	–0.69	–0.73
q(C) + q(O)	0.04	0.01	–0.51	–0.61

More insight into the bonding of the carbonyl fragment to Ni was obtained from NBO<sup>[24,25]</sup> analysis performed on ligand **1** and complexes **2**, **3**, and **4** (Table 1). Coordination of the Ph<sub>2</sub>dpbp ligands through its P atoms in **2** induces a slight decrease of the C–O Wiberg bond index (WBI), consistent with the observed shift of the corresponding IR band from 1661 to 1634 cm<sup>-1</sup>; however, the orbital interaction between the Ni center and the C=O moiety is minimal, with Ni–C and Ni–O WBIs below 0.01. In contrast, the C–O WBI decreases upon binding from 1.75 in the free ligand **1** to 1.30 in **3** and 1.23 in **4**. Interestingly, the Ni–O WBIs in **3** (0.33) and **4** (0.30) are lower than the corresponding Ni–C WBIs (0.46 in **3**, 0.50 in **4**), suggesting that backdonation into the π\*(C–O) orbital (which has a larger coefficient on C) contributes more to the bonding than donation from the π(C–O) orbital. The primarily acceptor character of the C=O moiety is additionally corroborated by a decrease of the total charge of the C–O fragment by 0.55 and 0.65 e<sup>-</sup> upon coordination to Ni(I) in **3** and to Ni(0) in

4, respectively. In accordance, NBO analysis performed on the Ni(0) complex **4** characterizes the (Ni–C–O) triangle as engaging in three-centers four-electrons bonding.

## 2.3 Conclusions

In conclusion, the coordination chemistry of *o*-phenylene-bridged diphosphine ketone (<sup>Ph</sup>dpbp) ligand **1** with nickel was studied, showing that the central ketone moiety in **1** can act as hemilabile moiety. In the Ni(II) complex **2**, the <sup>Ph</sup>dpbp ligand acts as a flexible, wide bite angle diphosphine ligand<sup>[17]</sup> and the ketone moiety is not bound to the metal. Moving to more reduced Ni(I) and Ni(0) complexes induces coordination of the ketone so that the <sup>Ph</sup>dpbp ligand acts as a tridentate, pincer-like ligand. Consequences of this acceptor-hemilabile behavior in small molecule activation and catalysis are currently under investigation.

## 2.4 Experimental

### 2.4.1 General working procedures

All reagents were purchased from commercial sources and used as received unless stated otherwise. Dichloromethane (CH<sub>2</sub>Cl<sub>2</sub>), triethylamine (Et<sub>3</sub>N), *N*-isopropylidimethylamine (*i*-PrEt<sub>2</sub>N) and *N,N*-dimethylformamide (DMF) were degassed by bubbling N<sub>2</sub> through the liquid for at least 30 minutes and subsequently stored over molecular sieves. Deuterated benzene (C<sub>6</sub>D<sub>6</sub>) and deuterated toluene (C<sub>7</sub>D<sub>8</sub>) were degassed using four freeze-thaw-pump cycles and subsequently stored over molecular sieves. Tetrahydrofuran (THF) was distilled over sodium/benzophenone before use, degassed by bubbling N<sub>2</sub> through it and stored over molecular sieves. Dry diethylether (Et<sub>2</sub>O) and toluene (C<sub>7</sub>H<sub>8</sub>) were acquired from a MBRAUN MB SPS-80 solvent purification system and used without further purification.

<sup>1</sup>H, <sup>13</sup>C and <sup>31</sup>P NMR spectra (respectively 400, 100 and 161 MHz) were recorded on an Agilent MRF400 spectrometer at 25 °C. <sup>1</sup>H and <sup>13</sup>C NMR chemical shifts are reported in ppm relative to TMS using the residual solvent resonance as internal standard. <sup>31</sup>P NMR chemical shifts are reported in ppm relative to 85% aqueous H<sub>3</sub>PO<sub>4</sub>. Infrared spectra were recorded using a Perkin Elmer Spectrum One FT-IR spectrometer equipped with a general liquid cell accessory. For air-sensitive complexes, KBr-IR was used. KBr was pre-dried in the oven for at least 72 hours at 140 °C and stored under inert atmosphere. UV-Vis spectra were measured using a Lambda 35 UV-Vis spectrometer. The UV-Vis samples were prepared under N<sub>2</sub> atmosphere and sealed with a Teflon cap after which the spectra were recorded directly. Toluene (C<sub>7</sub>H<sub>8</sub>) was used as solvent for all spectra to generate solutions with compound/complex concentrations of ~50 μM. EPR analyses were carried out by dissolving several milligrams of substrate in an appropriate solvent under inert conditions followed by filtration of the sample. The sample was transferred to a quartz EPR tube and spectra were recorded on a Bruker EMX Plus 6000 Gauss machine with ER 041 XG X-Band Microwave Bridge. Compounds of which elemental analysis is reported were either recrystallized or precipitated and dried under high vacuum overnight before submission and analysis was performed by the Mikroanalytisches Laboratorium Kolbe, Mülheim

an der Ruhr, Germany. Details on X-ray crystal structure determination and selected spectra are given in Appendix B.

### 2.4.2 DFT calculations

DFT results were obtained using the Gaussian 09 software package,<sup>[23]</sup> using the B3LYP (Becke, three-parameter, Lee-Yang-Parr) functional and the 6-31g(d,p) basis set on all atoms. For EPR calculations, IGLO III basis sets were obtained from the EMSL basis set exchange.<sup>[26]</sup> The structures were optimized without any symmetry restraints. Frequency analyses were performed on all calculations. DFT calculation-derived pictures have been generated using the GaussView 5.0.8. software. For NBO calculations, the NBO6 program up to the NLMO basis set was used.<sup>[25]</sup>

### 2.4.3 Synthesis

***o*-Bromophenyldiphenylphosphine:** Modification on a literature procedure by Chou *et al.*<sup>[27]</sup> Dry Et<sub>3</sub>N (3.1 mL, 22 mmol), Pd(PPh<sub>3</sub>)<sub>4</sub> (100.2 mg, 0.09 mmol), *o*-bromiodobenzene (2 mL, 15.4 mmol), diphenylphosphine (2.85 mL, 15.4 mmol) and toluene (40 mL) were combined under N<sub>2</sub> atmosphere giving an orange solution. After the mixture had been heated to 80 °C for 12 hours, the deep red organic layer was washed with brine (2 x 20 mL). The aqueous phase was washed twice with Et<sub>2</sub>O and the organic layers were combined. The solvent was evaporated on the rotary evaporator. Cold MeOH (3 x 4 mL) was used to wash the crude product. The product was dried vacuum and isolated as a pale-yellow powder (3.0 g, 8.8 mmol, 57%). <sup>1</sup>H NMR (C<sub>6</sub>D<sub>6</sub>): δ<sub>H</sub> 7.29 (m, 5H), 6.98, (m, 6H), 6.83 (dt, 1H, *J* = 7.8 Hz, *J* = 2.2 Hz), 6.70 (dt, 1H, *J* = 7.4 Hz, *J* = 1.2 Hz), 6.61 (dt, 1H, *J* = 7.8 Hz, *J* = 2.0 Hz) ppm. <sup>31</sup>P NMR (C<sub>6</sub>D<sub>6</sub>): δ<sub>P</sub> -4.83 ppm. ATR-IR v: 3049, 1554, 1475, 1423, 1248, 1094, 1014, 750, 742, 693 cm<sup>-1</sup>.

**2,2'-bis(diphenylphosphino)benzophenone (P<sup>h</sup>dpbp, **1**):** *o*-Bromophenyldiphenylphosphine (3.732 g, 10.9 mmol) was suspended in Et<sub>2</sub>O (40 mL). The yellow suspension was cooled to -50°C using an acetone ice bath. *n*-BuLi (1.6 M in hexane, 11.5 mmol, 7.18 mL) was added drop wise while stirring. In 30 minutes, the reaction mixture was heated up to room temperature and directly cooled again to -50°C, after which a solution of *N,N*-dimethylcarbamoylchloride in 15 mL Et<sub>2</sub>O (588 mg, 5.5 mmol) was added drop wise over 5-10 minutes. During the addition, the temperature of the bath was kept between -30 °C and -40 °C, after which the suspension stirred overnight, allowing the mixture to heat up to room temperature. The reaction was then cooled down again and treated at 0 °C with 2.5 M NH<sub>4</sub>Cl solution in water (30 mL, 4.00 g, 90 mmol NH<sub>4</sub>Cl) turning the suspension yellow. The product was isolated by extraction with Et<sub>2</sub>O, obtaining it as a yellow powder (2.5 g, 4.54 mmol, 84%). <sup>1</sup>H NMR (C<sub>6</sub>D<sub>6</sub>): δ<sub>H</sub> 7.33 (t, 4H, *J* = 7.4 Hz), 7.32 (t, 4H, *J* = 7.0 Hz), 7.21 (t, 2H, *J* = 7.4 Hz), 7.20 (t, 2H, *J* = 7.0 Hz), 7.00 (m, 14H), 6.84 (td, 2H, *J* = 7.8 Hz), 6.74 (td, 1H, *J* = 7.4 Hz) ppm. <sup>13</sup>C NMR (C<sub>6</sub>D<sub>6</sub>): δ<sub>C</sub> 196.8 (t, *J* = 3.1 Hz, C=O), 144.2, 144.0, 139.7 (d, *J* = 2.3 Hz), 139.5 (d, *J* = 3.1 Hz), 138.3 (t, *J* = 3.1 Hz), 138.2 (t, *J* = 3.8 Hz), 134.7, 133.9 (d, *J* = 21.4 Hz), 130.6 (t, *J* = 3.1 Hz), 130.4, 128.2, 127.7 ppm. <sup>31</sup>P NMR (C<sub>6</sub>D<sub>6</sub>): δ<sub>P</sub> -8.3 ppm. ATR-IR v: 3049, 2962, 2915, 1661, 1582, 1479, 1434, 1296, 1087, 1026, 929, 744, 692, 498 cm<sup>-1</sup>.

**(P<sup>h</sup>dpbp)NiCl<sub>2</sub> (**2**):** NiCl<sub>2</sub>(DME) (101.4 mg, 0.46 mmol) and 2,2'-bis(diphenylphosphino)benzophenone (**1**, 260.4 mg, 0.47 mmol) were mixed in a vial in the glovebox at room temperature. CH<sub>2</sub>Cl<sub>2</sub> (2 mL) was

added and the obtained solution was stirred for 1 h. From this solution, the product was precipitated as a dark brown material with hexane, followed by filtration to isolate and extraction with  $\text{CH}_2\text{Cl}_2$ . The product was obtained after drying the solids in vacuum, resulting in **2** as a brown powder (259 mg, 0.38 mmol, 83%).  $^1\text{H}$  NMR ( $\text{CD}_2\text{Cl}_2$ ):  $\delta_{\text{H}}$  20.67 (s, sharp), 19.38 (s, broad), 9.25 (s, sharp), 7.37 (s, sharp), 5.88 (s, sharp), 5.01 (s, sharp), -0.47 (s, sharp), -6.63 (s, broad) ppm.  $^1\text{H}$  NMR Evans Method ( $\text{CD}_2\text{Cl}_2$ ):  $\mu_{\text{eff}}$ : 2.8. FT-IR (KBr-Pellet)  $\nu$ : 3394, 3058, 1963, 1634, 1579, 1560, 1482, 1455, 1435, 1294, 1185, 1163, 1132, 1094, 1029, 998, 932, 805, 753, 744, 693, 641, 529, 504  $\text{cm}^{-1}$  Anal: calcd for  $\text{C}_{37}\text{H}_{28}\text{Cl}_2\text{NiOP}_2$ : C 65.34, H 4.15; found: C 65.21, H 4.19.

**Reduction of  $(^{\text{Ph}}\text{dppb})\text{NiCl}_2$  (**2**) with sodium naphthalide:** Naphthalene (4.7 mg, 0.037 mmol) was dissolved in THF (1 mL) in the glovebox at room temperature. A lump of sodium was added and the resulting dark green mixture was stirred for 3 h. **2** (19.3 mg, 0.028 mmol) was dissolved in THF (1.5 mL) in a separate vial and cooled to  $-78$  °C using the cold well with a dry ice/acetone mixture. The sodium naphthalide mixture was decanted and added dropwise in 15 min to the suspension of **2** and the resulting dark green mixture was stirred at  $-78$  °C for 1.25 h and after that stirred overnight at room temperature, resulting in a dark yellow to brown turbid solution. The solvent was removed in vacuum and the residue was extracted in  $\text{C}_6\text{D}_6$  and analyzed by  $^1\text{H}$  and  $^{31}\text{P}$  NMR. The  $^1\text{H}$  NMR spectrum exhibited the paramagnetically shifted resonances of  $(^{\text{Ph}}\text{dppb})\text{NiCl}$  (**3**) together with a complex mixture of diamagnetic species from which **3** could not be separated.

**$(^{\text{Ph}}\text{dppb})\text{NiCl}$  (**3**):**  $\text{Ni}(\text{COD})_2$  (25.0 mg, 0.09 mmol),  $\text{NiCl}_2(\text{DME})$  (20.0 mg, 0.09 mmol) and 2,2'-bis(diphenylphosphino)benzophenone (**1**, 100 mg, 0.18 mmol) were combined in a vial in the glovebox at room temperature. THF (3 mL) was added and the brown solution was stirred for 45 min. The mixture was filtered and the residue was washed with hexane (3 x 0.3 mL) and dried under vacuum. Hexane (5 mL) was added to the filtrate to initiate further precipitation of the product from the solvent, resulting in a suspension that was kept in the freezer for 3 days. The obtained solids were collected by filtration, dried in vacuum and combined with the first solid fraction. The product was obtained as a dark brown powder (45 mg, 0.07 mmol, 38%).  $^1\text{H}$  NMR ( $d_8$ -THF, 400 MHz):  $\delta_{\text{H}}$  16.32 (s, broad), 14.41 (s, broad), 12.71 (s, broad), 7.25 (m, sharp, diamagnetic impurity), -0.36 (s, broad), -3.00 (s, broad) ppm.  $^{31}\text{P}$  NMR ( $d_8$ -THF, 161 MHz):  $\delta$  30.6 (diamagnetic impurity) ppm. FT-IR (KBr pellet)  $\nu$ : 3421, 3053, 2361, 2342, 1651, 1482, 1459, 1435, 1340, 1332, 1298, 1262, 1240, 1098, 1028, 919, 778, 746, 693, 520, 505  $\text{cm}^{-1}$ . Due to difficulties with the storage of the obtained product, no elemental analysis data was obtained.

**$(^{\text{Ph}}\text{dppb})\text{Ni}(\text{PPh}_3)$  (**4**):**  $\text{PPh}_3$  (120.9 mg, 0.46 mmol), 2,2'-bis(diphenylphosphino)benzophenone (**1**, 250.0 mg, 0.45 mmol) and  $\text{Ni}(\text{COD})_2$  (124.9 mg, 0.45 mmol) were combined in a vial in the glovebox at room temperature and  $\text{Et}_2\text{O}$  (3 mL) was added. The obtained suspension immediately turned brown. After 45 min of stirring, the solid was separated from the liquid, the product was extracted with THF and concentrated in vacuum to obtain **4** as a brown powder (284 mg, 0.33 mmol, 72%).  $^1\text{H}$  NMR ( $\text{C}_6\text{D}_6$ ):  $\delta_{\text{H}}$  7.84 (d, 2H,  $J = 7.8$  Hz), 7.59 (t, 6H,  $J = 8.2$  Hz), 7.21-7.31 (m, broad, 10H,  $J = 19.2$  Hz), 6.98 (t, 3H,  $J = 7.4$ ), 6.85-6.95 (m, 7H), 6.77-6.85 (m, 11H), 6.72 (t, 4H,  $J = 7.4$  Hz) ppm.  $^{13}\text{C}$  NMR ( $\text{C}_6\text{D}_6$ ):  $\delta_{\text{C}}$  154.6 (dd,  $J = 19.1$  Hz,  $J = 16.0$  Hz), 141.6 (dt,  $J = 8.4$  Hz,  $J = 16.8$  Hz), 137.9 (t,  $J = 14.5$  Hz), 137.0 (dt,  $J = 29.8$  Hz,  $J = 4.6$  Hz), 136.2 (t,  $J = 11.4$  Hz), 133.8 (d,  $J = 13.7$  Hz), 133.4 (t,  $J = 7.6$  Hz), 132.3 (t,  $J = 6.1$  Hz), 132.0, 128.5-127 (m), 126.5, 120.4 (dt,  $J_{\text{dt}} = 13.7$  Hz,  $J_{\text{t}} = 9.2$  Hz) ppm.  $^{31}\text{P}$  NMR ( $\text{C}_6\text{D}_6$ ):  $\delta_{\text{P}}$  38.2 (t,  $J = 25$  Hz,

$\text{PPh}_3$ ), 17.9 (d,  $J = 25$  Hz) ppm. FT-IR (KBr pellet)  $\nu$ : 3447, 3052, 2347, 1585, 1480, 1459, 1434, 1309, 1262, 1092, 1027, 914, 777, 740, 695, 660, 625, 517  $\text{cm}^{-1}$ . Due to difficulties with the storage of the obtained product, no elemental analysis data was obtained.

**Alternative synthesis of  $(\text{Phdpbp})\text{Ni}(\text{PPh}_3)$  (**4**):** Naphthalene (8.6 mg, 0.067 mmol) was dissolved in THF (2 mL) in the glovebox at room temperature. A lump of sodium was added and the resulting dark green mixture was stirred for 3 h. **2** (20.5 mg, 0.030 mmol) and  $\text{PPh}_3$  (7.8 mg, 0.030 mmol) were dissolved in THF (2 mL) in a separate vial and cooled to  $-78$  °C using the cold well with a dry ice/acetone mixture. The sodium naphthalide mixture was decanted and added dropwise in 20 min to the suspension of **2** and the resulting dark green mixture was stirred at  $-78$  °C for 1 h and after that stirred overnight at room temperature, resulting in a dark yellow to brown turbid solution. The solvents were removed *in vacuo*. A few drops of THF were added to the obtained dark yellow to brown solids so that all the solids were dissolved, after which hexane (3 mL) was added. The mixture was decanted, the solids were washed using hexane (2 x 3 mL) and dried in vacuum to obtain **4** as a brown powder (20.1 mg, 0.023 mmol, 77%). The  $^1\text{H}$  NMR and  $^{31}\text{P}$  NMR spectra match those obtained above.

**$\text{Ni}_2(\text{Phdpbp})_3$  (**5**):**  $\text{Ni}(\text{COD})_2$  (26.3 mg, 0.096 mmol) and 2,2'-bis(diphenylphosphino)benzophenone (**1**, 78.8 mg, 0.143 mmol) were combined in a vial under inert atmosphere.  $\text{Et}_2\text{O}$  (3 mL) was added and the dark brown suspension was stirred for 15 min. The suspension was filtered and the light brown solid phase was washed with  $\text{Et}_2\text{O}$  (3 mL). Toluene (4 mL) was used to extract the product and the resulting brown solution was concentrated and dried under vacuum, to yield **5** as a light brown powder (54 mg, 0.03 mmol, 65%).  $^1\text{H}$  NMR ( $\text{C}_6\text{D}_6$ ):  $\delta_{\text{H}}$  8.78 (s, 2H, broad), 7.79 (d, 2H,  $J = 7.0$  Hz), 7.57 (m, 6H), 7.24 (m, 8H), 7.07-6.68 (m, broad, 52H), 6.54 (m, 8H), 6.34 (t, 4H,  $J = 7.0$  Hz), 6.18 (d, 2H,  $J = 7.4$  Hz) ppm.  $^{31}\text{P}$  NMR ( $\text{C}_6\text{D}_6$ , 300 K):  $\delta_{\text{P}}$  44.06 (dd,  $J = 36.9$  Hz,  $J = 22.2$  Hz, Ni-P), 22.93 (d, broad,  $J = 36.9$  Hz, **1-PNiP-1**), 11.22 (d, broad,  $J = 35.6$  Hz, **1-PNiP-1**) ppm.  $^{31}\text{P}$  NMR ( $\text{C}_7\text{D}_8$ , 373 K):  $\delta_{\text{P}}$  44.4 (dd,  $J = 28$  Hz,  $J = 31$  Hz, Ni-P), 21.3 (dd,  $J = 28$  Hz,  $J = 62$  Hz, **1-PNiP-1**), 5.6 (dd, 2P,  $J = 31$  Hz,  $J = 62$  Hz, **1-PNiP-1**) ppm. FT-IR (KBr pellet)  $\nu$ : 3436, 3051, 1679, 1585, 1481, 1459, 1433, 1261, 1184, 1157, 1092, 1027, 921, 802, 775, 739, 694, 658, 626, 514  $\text{cm}^{-1}$ . Due to difficulties with the storage of the obtained product, no elemental analysis data was obtained.

**Reaction of **5** with triphenylphosphine:**  $\text{Ni}_2(\text{Phdpbp})_3$  (**5**, 5.7 mg, 3.22  $\mu\text{mol}$ ) and  $\text{PPh}_3$  (3.4 mg, 12.96  $\mu\text{mol}$ ) were combined in the glovebox and dissolved in  $\text{C}_7\text{H}_8$  at room temperature. In situ NMR showed full conversion to **3**, generation of 1 equivalent of **1** with regard to the amount of **5** and an excess of  $\text{PPh}_3$ .

## 2.5 References

- [1] R. M. Bullock, Ed. *Catalysis Without Precious Metals*; Wiley-VCH: Weinheim, **2010**.
- [2] J. I. van der Vlugt, *Eur. J. Inorg. Chem.*, **2012**, 363.
- [3] (a) P. J. Chirik, K. Wieghardt, *Science*, **2010**, 327, 794. (b) W. I. Dzik, J. I. van der Vlugt, J. N. H. Reek, B. de Bruin, *Angew. Chem. Int. Ed.*, **2011**, 50, 3356.



- [4] (a) R. Langer, Y. Diskin-Posner, G. Leitus, L. J. W. Shimon, Y. Ben-David, D. Milstein, *Angew. Chem. Int. Ed.*, **2011**, *50*, 9948. (b) S. Schneider, J. Meiners, B. Askevold, *Eur. J. Inorg. Chem.*, **2011**, *2012*, 412.
- [5] W. H. Harman, J. C. Peters, *J. Am. Chem. Soc.*, **2012**, *134*, 5080.
- [6] (a) J. C. Jeffrey, T. B. Rauchfuss, *Inorg. Chem.*, **1979**, *18*, 2658. (b) P. Braunstein, F. Naud, *Angew. Chem. Int. Ed.*, **2001**, *40*, 680.
- [7] (a) A. Amgoune, D. Bourissou, *Chem. Commun.*, **2010**, *47*, 859. (b) H. Braunschweig, R. D. Dewhurst, A. Schneider, *Chem. Rev.*, **2010**, *110*, 3924.
- [8] (a) J. S. Anderson, J. Rittle, J. C. Peters, *Nature*, **2013**, *501*, 84. (b) M.-E. Moret, J. C. Peters, *J. Am. Chem. Soc.*, **2011**, *133*, 18118.
- [9] (a) J. M. Malinoski, M. Brookhart, *Organometallics*, **2003**, *22*, 5324. (b) H. A. Kalamarides, S. Iyer, J. Lipian, L. F. Rhodes, C. Day, *Organometallics*, **2000**, *19*, 3983. (c) A. M. Oertel, V. Ritleng, A. Busiah, L. F. Veiros, M. J. Chetcuti, *Organometallics*, **2011**, *30*, 6495.
- [10] (a) T. T. Tsou, J. C. Huffman, J. K. Kochi, *Inorg. Chem.*, **1979**, *18*, 2311. (b) D. J. Mindiola, R. Waterman, D. M. Jenkins, G. L. Hillhouse, *Inorg. Chim. Acta*, **2003**, *345*, 299.
- [11] Related ligands involving weaker  $\pi$ -acceptor olefin and arene units in the central position have been recently introduced: (a) B. J. Barrett, V. M. Iluc, *Organometallics*, **2014**, *33*, 2565. (b) B. J. Barrett, V. M. Iluc, *Inorg. Chem.* **2014**, *53*, 7248. (c) D. E. Herbert, N. C. Lara, T. Agapie, *Chem. Eur. J.*, **2013**, *19*, 16453. (d) S. Lin, M. W. Day, T. Agapie, *J. Am. Chem. Soc.*, **2011**, *133*, 3828.
- [12] Q. Jing, C. A. Sandoval, Z. Wang, K. Ding, *Eur. J. Org. Chem.*, **2006**, 3606.
- [13] K. Mikami, K. Wakabayashi, Y. Yusa, K. Aikawa, *Chem. Commun.*, **2006**, 2365.
- [14] K. Mikami, K. Wakabayashi, K. Aikawa, *Org. Lett.*, **2006**, *8*, 1517.
- [15] F. Zhang, L. Wang, S. -H. Chang, K. -L. Huang, Y. Chi, W. -Y. Hung, C. -M. Chen, G. -H. Lee, P. -T. Chou, *Dalton Trans.*, **2013**, *42*, 7111
- [16] S. Alvarez, *Dalton Trans.*, **2013**, *42*, 8617.
- [17] (a) W. Goertz, W. Keim, D. Vogt, U. Englert, M. D. K. Boele, L. A. van der Veen, P. C. J. Kamer, P. W. N. M. van Leeuwen, *Dalton Trans.*, **1998**, 2981 (b) S. -M. Kuang, D. G. Cuttell, D. R. McMillin, P. E. Fanwick, R. A. Walton, *Inorg. Chem.*, **2002**, *41*, 3313. (c) E. E. Marlier, S. J. Tereniak, K. Ding, J. E. Mulliken, C. C. Lu, *Inorg. Chem.*, **2011**, *50*, 9290.
- [18] The asymmetric unit of **3** contains two independent molecules displaying the same coordination geometry. For simplicity, the metrics of only one of them are discussed in the text.
- [19] Representative Phosphine-Ni(I) complexes: (a) D. J. Mindiola, G. L. Hillhouse, *J. Am. Chem. Soc.*, **2001**, *123*, 4623. (b) P. Dapporto, G. Fallani, L. Sacconi, *Inorg. Chem.*, **1974**, *13*, 2847. (c) C. Mealli, P. Dapporto, V. Sriyungwat, T. A. Albright, *Acta Crystallogr. Sect. C Cryst. Struct. Commun.*, **1983**, *39*, 995.
- [20] G. Bai, P. Wei, D. W. Stephan, *Organometallics*, **2005**, *24*, 5901.
- [21] (a) A. Velian, S. Lin, A. J. M. Miller, M. W. Day, T. Agapie, *J. Am. Chem. Soc.*, **2010**, *132*, 6296. (b) N. Grüger, H. Wadepohl, L. H. Gade, *Dalton Trans.*, **2012**, *41*, 14028.
- [22] The fraction of diamagnetic material appears not to depend on the concentration of the sample as expected for a simple monomer-dimer equilibrium, suggesting a more complex process.
- [23] All calculations were performed with Gaussian 09, Revision D.01, M. J. Frish, G. W. Trucks, H. B. Schlegel, G. E. Scuseria, M. A. Robb, J. R. Cheeseman, G. Scalmani, V. Barone, B. Mennucci, G. A. Petersson, H. Nakatsuji, M. Caricato, X. Li, H. P. Hratchian, A. F. Izmaylov, J. Bloino, G. Zheng, J. L. Sonnenberg, M. Hada, M. Ehara, K. Toyota, R. Fukuda, J. Hasegawa, M. Ishida, T. Nakajima, Y.

- Honda, O. Kitao, H. Nakai, T. Vreven, J. A. Montgomery, Jr., J. E. Peralta, F. Ogliaro, M. Bearpark, J. J. Heyd, E. Brothers, K. N. Kudin, V. N. Staroverov, R. Kobayashi, J. Normand, K. Raghavachari, A. Rendell, J. C. Burant, S. S. Iyengar, J. Tomasi, M. Cossi, N. Rega, J. M. Millam, M. Klene, J. E. Knox, J. B. Cross, V. Bakken, C. Amado, J. Jaramillo, R. Gomperts, R. E. Stratmann, O. Yazyev, A. J. Austin, R. Cammi, C. Pomelli, J. W. Ochterski, R. L. Martin, K. Morokuma, V. G. Zakrzewski, G. A. Voth, P. Salvador, J. J. Dannenberg, S. Dapprich, A. D. Daniels, Ö. Farkas, J. B. Foresman, J. V. Ortiz, J. Cioslowski, D. J. Fox, "Gaussian 09 Revision A.02".
- [24] F. Weinhold, C. R. Landis, Valency and Bonding: A Natural Bond Orbital Donor-Acceptor Perspective; Cambridge University Press: New York, **2005**.
- [25] NBO analyses performed with NBO 6.0. E. D. Glendening, J. K. Badenhoop, A. E. Reed, J. E. Carpenter, J. A. Bohmann, C. M. Morales, C. R. Landis, and F. Weinhold (Theoretical Chemistry Institute, University of Wisconsin, Madison, WI, 2013); <http://nbo6.chem.wisc.edu/>.
- [26] <https://bse.pnl.gov/bse/portal>, The Role of Databases in Support of Computational Chemistry Calculations, D. Feller, *J. Comp. Chem.*, **1996**, *17*(13), 1571, Basis Set Exchange: A Community Database for Computational Sciences K. L. Schuchardt, B. T. Didier, T. Elsethagen, L. Sun, V. Gurumoorthi, J. Chase, J. Li, T. L. Windus, *J. Chem. Inf. Model.*, **2007**, *47*(3), 1045, doi:10.1021/ci600510j. Website last visited on 9/10/2014.
- [27] F. Zhang, L. Wang, S. H. Chang, K. L. Huang, Y. Chi, W. Y. Hung, C. M. Chen, G. H. Lee, P. T. Chou, *Dalton Trans.*, **2013**, *42*, 7111.



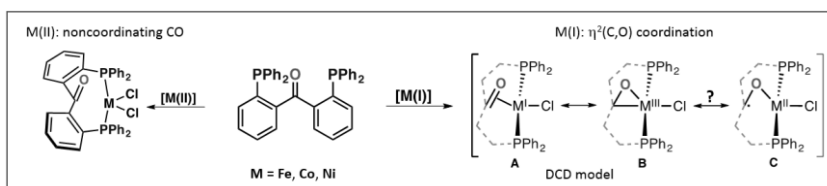
*Imagination will often carry us to worlds that never were.  
But without it we go nowhere.*  
- Carl Sagan



# Chapter 3

## Periodic Trends in the Binding of a Phosphine–Tethered Ketone Ligand to Fe, Co, Ni, and Cu

**Abstract**  $\pi$ -Coordinating ligands are commonly found in intermediate structures in homogeneous catalysis, and are gaining interest as supporting ligands for the development of cooperative catalysts. Herein, the binding of the ketone group – a strongly accepting  $\pi$ -ligand – to mid-to-late metals of the first transition series is systematically investigated. To this end, the coordination of 2,2'-bis(diphenylphosphino)benzophenone ( $\text{P}^{\text{h}}\text{dppb}$ ), featuring a ketone moiety flanked by two strongly binding P-donor groups, to Fe, Co, Ni and Cu is explored. The ketone moiety does not bind to the metal in M(II) complexes, whereas M(I) complexes (Fe, Co, Ni) adopt an  $\eta^2(\text{C},\text{O})$ -coordination. A structural and computational investigation of periodic trends in this series was performed. These data suggest that the coordination of the ketone to M(I) can mostly be described by the resonance extremes of the Dewar-Chatt-Duncanson model, i.e. the  $\pi$ -complex and the metallaoxacycle extreme, with a possible minor contribution of a ketyl radical resonance structure in the case of the iron complex.

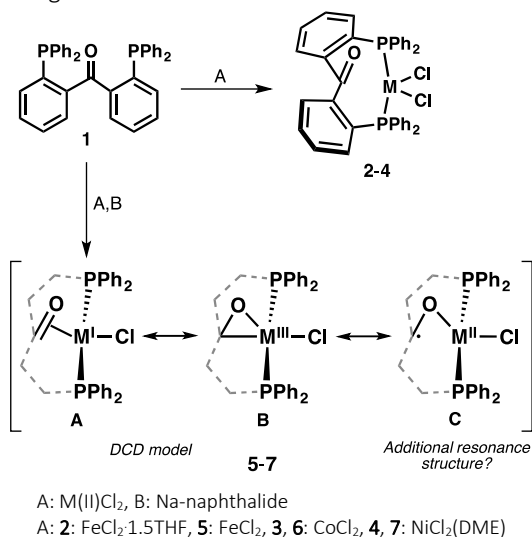


Published as: D. G. A. Verhoeven, M. A. C. van Wiggen, J. Kwakernaak, M. Lutz, R. J. M. Klein Gebbink, and M.-E. Moret, *Chem. Eur. J.*, **2017**, DOI: 10.1002/chem.201703254.

### 3.1 Introduction

The coordination of  $\pi$ -ligands is of paramount importance in organometallic chemistry and transition metal catalysis.  $\pi$ -Complexes of carbon-carbon and carbon-heteroatom multiple bonds are reactive intermediates in a large number of catalytic reactions including hydrogenations, hydrofunctionalizations, oligo- and polymerizations.<sup>[1-3]</sup> In addition, incorporation of such moieties in multidentate ligand architectures is a promising approach to cooperative ligand design.<sup>[4]</sup>

The polarity of the carbon-oxygen double bonds of aldehydes and ketones sets them apart amongst  $\pi$ -binding ligands. The C=O bond can bind to transition metals *via* either an  $\eta^1(\text{O})$ -interaction based on  $\sigma$ -donation, allowed by the presence of oxygen-centered lone-pairs, or *via* a  $\pi$ -coordinating  $\eta^2(\text{C,O})$ -interaction. The latter, less common binding mode has been proposed in intermediate structures for Cu-catalyzed addition of Grignard reagents,<sup>[5,6]</sup> Ru catalyzed hydrogenation reactions,<sup>[7,8]</sup> and oxidative addition of arylketone C–C bonds<sup>[9-11]</sup>. In particular, Piers and co-workers recently reported a remarkable oxygen atom transfer from  $\text{N}_2\text{O}$  to an  $\text{Ir}=\text{C}$  double bond to yield an iridaepoxide complex that serves as a motif was described as intermediate between an  $\eta^2$  ketone complex ( $\text{Ir}^{\text{III}}$ ) and an iridaepoxide ( $\text{Ir}^{\text{V}}$ ) structure.<sup>[13,14]</sup> Seeking a direct access to ketone  $\pi$ -complexes of first-row transition metals (Chapter 1), the coordination chemistry of the diphosphine-ketone ligand 2,2'-bis(diphenylphosphino)benzophenone<sup>[8]</sup> ( $\text{Ph}_2\text{dbpp}$ , **1**) with nickel (Chapter 2, Scheme 1) was recently explored.<sup>[15]</sup> The ketone moiety does not bind to the  $\text{Ni}(\text{II})\text{Cl}_2$  fragment but binds in an  $\eta^2(\text{C,O})$ -fashion upon reduction of the nickel center from  $\text{Ni}(\text{II})$  to  $\text{Ni}(\text{I})$  or  $\text{Ni}(\text{0})$ , hence acting as a hemilabile acceptor ligand.



**Scheme 1.** Synthesis of base metal complexes 2-7. Bottom:  $\text{M}(\text{I})$  complexes, resonance structures: the side-on bound extreme **A** ( $\text{M}^{\text{I}}$ ), the metalla-oxo-cycle extreme **B** ( $\text{M}^{\text{III}}$ ) of the DCD model, and the additional ketone-radical extreme **C** ( $[\text{M}^{\text{II}}]$ ).

Side-on binding is generally favored by electron-rich metal centers and can be described by the Dewar-Chatt-Duncanson (DCD) model for  $\pi$ -coordinating ligands: the bond is established by electron donation from a filled  $\pi$ -orbital ( $\sigma$ -donation) and, simultaneously, donation of  $d$  electrons from the metal to the  $\pi$ -antibonding orbital ( $\pi$ -backbonding).<sup>[16,17]</sup> The latter process is expected to dominate the binding of the C=O moiety because the high electronegativity of the oxygen atom lowers both the  $\pi$  and  $\pi^*$  orbitals, resulting in net charge transfer from the metal to the ligand upon binding. In addition, the larger C-coefficient of the accepting  $\pi^*(\text{C}-\text{O})$  orbital should result in a strengthening of the M–C bond as backdonation increases.<sup>[18]</sup> The DCD model can also be expressed in terms of two resonance structures: the  $\pi$ -complex (Scheme 1 **A**) and the metallaoxacycle (Scheme 1 **B**) extreme, leading to ambiguity in the complexes' oxidation state ( $\text{M}^n$  or  $\text{M}^{n+2}$ ).

This Chapter describes the systematic study of the coordination of the ketone moiety in  $\text{Ph}^{\text{d}}\text{pbp}$  to mid-to-late metals of the first transition series: Fe, Co, Ni and Cu. The rigid phenylene linkers and the strong phosphine donor groups in the  $\text{Ph}^{\text{d}}\text{pbp}$  ligand are suitable for  $\eta^2(\text{C},\text{O})$ -coordination of the ketone but disfavor  $\eta^1(\text{O})$ -coordination, making this ligand an ideal platform to study the former mode in details. Indeed, the ketone group in  $\text{Ph}^{\text{d}}\text{pbp}$  is not bound in complexes of the  $\text{M}(\text{II})\text{Cl}_2$  fragments ( $\text{M} = \text{Fe}, \text{Co}, \text{Ni}$ ), as evidenced by M–C and M–O distances above 3 Å, even though some evidence for a weak residual interaction arises from C–O bond distances and the corresponding IR absorption frequencies. In contrast,  $\eta^2(\text{C},\text{O})$ -coordination is observed with the more reduced  $\text{M}(\text{I})\text{Cl}$  fragment ( $\text{M} = \text{Fe}, \text{Co}, \text{Ni}$ ), resulting in high-spin pseudotetrahedral  $(\text{Ph}^{\text{d}}\text{pbp})\text{MCl}$  complexes. Structural and computational analysis of the series indicates that increased charge transfer to the ketone moiety from Ni to Fe correlates with stronger M–O bonding and weaker M–C bonding. Whereas the  $\eta^2(\text{C},\text{O})$ -coordination of the ketone is mostly described by the covalent DCD model, the observed trend appears to be in disagreement with the large C-coefficient of the accepting  $\pi^*(\text{C}-\text{O})$  orbital in this model. A possible way to resolve this apparent discrepancy is the consideration of a minor contribution of a third resonance structure (Scheme 1C) arising from the interaction of a ketyl radical anion with a high-spin  $\text{M}(\text{II})$  center.

## 3.2 Results and Discussion

### 3.2.2 $\text{M}(\text{II})\text{Cl}_2$ complexes

The coordination chemistry of  $\text{Ph}^{\text{d}}\text{pbp}$  (**1**) with Fe(II) and Co(II) was investigated: reaction with  $\text{FeCl}_2 \cdot 1.5\text{THF}$  or  $\text{CoCl}_2$  in THF followed by precipitation with hexanes afforded the high spin complexes  $(\text{Ph}^{\text{d}}\text{pbp})\text{FeCl}_2$  (**2**) and  $(\text{Ph}^{\text{d}}\text{pbp})\text{CoCl}_2$  (**3**), respectively (Figure 1).  $^1\text{H}$  NMR signals ranging from  $\delta -1.4$  to 14.1 ppm for **2** and  $\delta -3.7$  to 18.7 ppm for **3** indicate the formation of paramagnetic complexes. The high spin state ( $S = 3/2$ ) of cobalt in complex **3** is additionally confirmed by an effective magnetic moment ( $\mu_{\text{eff}}$ ) of 4.1  $\mu_{\text{B}}$  (Evans' method).<sup>[19]</sup> Single crystal

X-ray structure determinations of **2** and **3** reveal that both exhibit a distorted tetrahedral geometry around the M(II) center without coordination of the C=O moiety, analogously to the previously reported (<sup>Ph</sup>dppb)NiCl<sub>2</sub> complex (**4**).<sup>[15]</sup>

A systematic study of the series of compounds **2-4** provides further insight into the interaction between the unbound C=O fragment and the metal. Even though the C=O moiety is not bound, a consistent trend is observed in the C=O bond lengths of the three complexes: starting from 1.213(3) Å in the free ligand,<sup>[8]</sup> the C–O distance gradually increases to 1.2288(16) Å upon complexation to more electron-rich metallic centers (Fe<sup>II</sup>, Co<sup>II</sup> and Ni<sup>II</sup>) (Table 1). A similar trend was found for the bands in ATR-IR spectroscopy: the C=O band of the free ligand is observed at 1661 cm<sup>-1</sup>, and shifts towards lower energy upon complexation to Fe (1651 cm<sup>-1</sup>), Co (1647 cm<sup>-1</sup>) and Ni (1634 cm<sup>-1</sup>).<sup>[15]</sup>

Both of these trends suggest that the C=O bond is increasingly, although slightly, weakened upon complexation of <sup>Ph</sup>dppb to Fe, Co, and Ni. A first hypothesis to explain this trend could be that the decreasing size of the metal ion would result in a gradual conformational change around the C=O. However, the absence of a systematic trend in the P–M–P angle argues against this interpretation. Hence, an electronic metal–ketone interaction is likely present either: a) through space *via* residual orbital overlap or b) through bonds *via* inductive effects. This question is further addressed on the basis of structural consideration and DFT calculations at the B3LYP/TZVP level of theory (Table 2). First, the sum-of-angles around the central C=O carbon atom of complexes **2** to **4** remains close to 360° throughout the series (**2**: 359.99°, **3**: 359.44°, **4**: 359.64°), indicating negligible rehybridization. In addition, M–O and M–C Wiberg bond indices (WBI) consistently below 0.01 indicate the absence of significant covalent bonding. The C–O bond index is in all cases close to the value for the free ligand (1.7-1.8 e), indicating that this bond retains its double bond character. In agreement, the calculated natural charge on the ketone fragment (q<sub>C+O</sub>) hardly deviates from that of the free ligand. Finally, an atoms in molecules analysis<sup>[20]</sup> does not identify a bonding pathway between the ketone moiety and the metal center. Considered collectively, these calculated data rule out a covalent bonding interaction between the metal and the ketone moiety. Hence, the observed trend in the C=O bond length and IR absorption frequency is tentatively ascribed to through-bond inductive effects, the ketone moiety being maintained in proximity of the metal by the rigid phenylene linkers. Next, it is investigated whether coordination can be induced by either halide abstraction (making the metal more electrophilic) or reduction (making the metal more electron-rich).



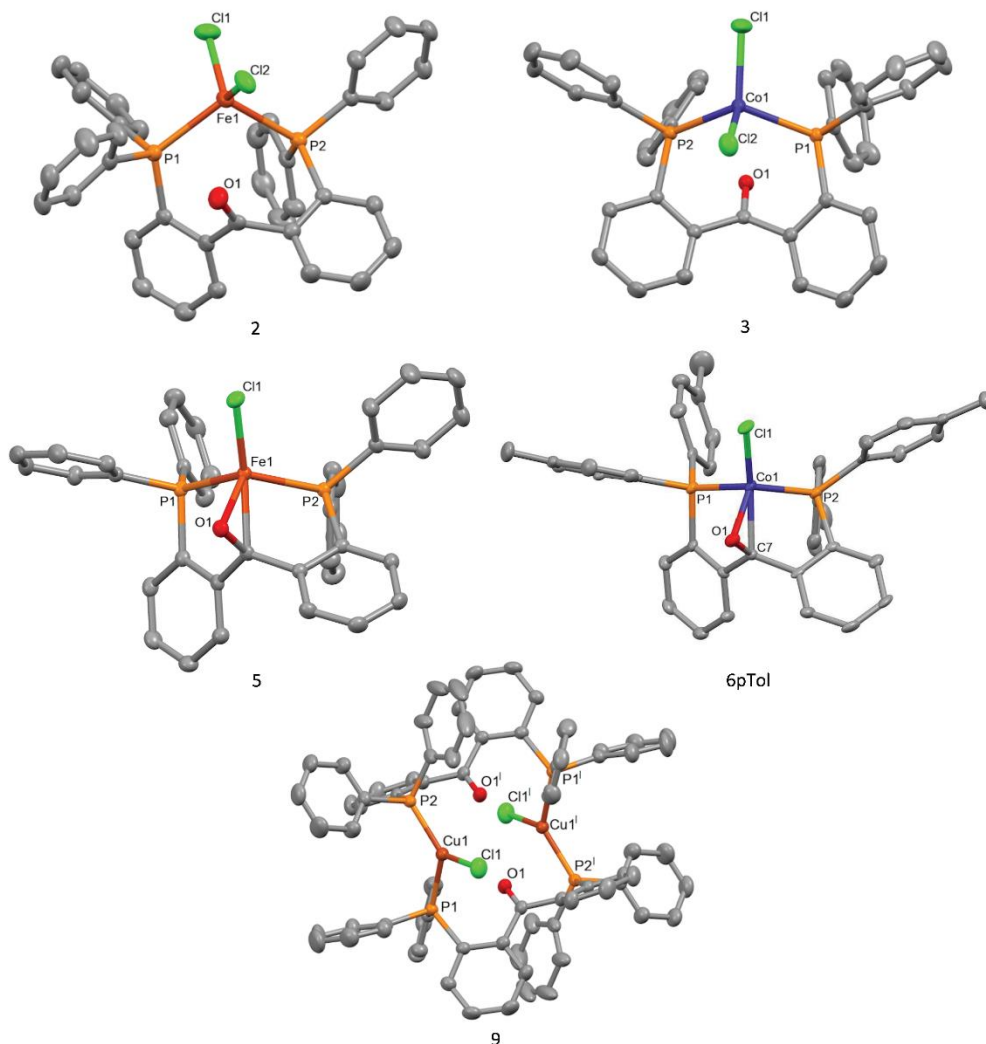


**Figure 1.** X-ray crystal structures of  $(^{Ph}dbbp)FeCl_2$  (**2**),  $(^{Ph}dbbp)CoCl_2$  (**3**),  $(^{Ph}dbbp)FeCl$  (**5**),  $(^{pTol}dbbp)CoCl$  (**6pTol**) and  $[(^{Ph}dbbp)CuCl]_2$  (**9**). Co-crystallized solvent molecules (**2**: toluene, **3**: THF, **5**: toluene) and hydrogen atoms are omitted for clarity, ellipsoids are shown at 50% probability level. Selected distances (Å) and angles ( $^{\circ}$ ): **2**: Fe1–O1: 2.9414(17), Fe1–C7: 3.353(7), Fe1–P1: 2.4918(7), Fe1–P2: 2.5055(6), Fe1–Cl1: 2.2355(7), Fe1–Cl2: 2.2487(7), P1–Fe1–P2: 105.32(2). Dihedral angle: 65.18(11). **3**: Co1–O1: 2.9255(13), Co1–C7: 3.2896(18), Co1–P1: 2.3908(5), Co1–P2: 2.4059(5), Co1–Cl1: 2.1980(6), Co1–Cl2: 2.2238(5), P1–Co1–P2: 116.676(18). Dihedral angle: 36.16(9). **5**: Fe1–O1: 1.9072(8), Fe1–C7: 2.0881(12), C7–O1: 1.3296(14), Fe1–P1: 2.3992(3), Fe1–P2: 2.3559(3), Fe1–Cl1: 2.2328(3), P1–Fe1–P2: 106.350(12). **6pTol**: Co1–O1: 1.947(3), Co1–C7: 2.071(5), C7–O1: 1.307(6), Co1–P1: 2.2908(14), Co1–P2: 2.3013(15), Co1–Cl1: 2.2072(15), P1–Co1–P2: 109.62(6). **9**: Structure contains a centro-symmetric point. Cu1–O1: 2.9953(11), Cu1–O1': 3.0529(12), Cu1–P1: 2.2488(4), Cu1–P2': 2.2077(4), Cu1–Cl1: 2.2145(5), C7–O1: 1.2218(19), P1–Cu1–P2': 126.495(17). Symmetry code  $i$ : 1-x, 1-y, 1-z.

**Table 1.** Selected bond distances (Å), angles (°), and IR frequencies (cm<sup>-1</sup>) for **1** and (Phdppb)M(II) complexes.

	C=O	O--M	PMP angle	IR freq C=O
Phdppb ( <b>1</b> )	1.213(3) <sup>[8]</sup>	-	-	1661
(Phdppb)FeCl <sub>2</sub> ( <b>2</b> )	1.218(3)	2.9414(17)	105.32(2)	1651
(Phdppb)CoCl <sub>2</sub> ( <b>3</b> )	1.227(2)	2.9255(13)	116.676(18)	1647
(Phdppb)NiCl <sub>2</sub> ( <b>4</b> ) <sup>[15,21]</sup>	1.2288(16)	3.1012(10)	112.996(13)	1634

**Table 2.** Wiberg bond indices (WBI), natural charges (q) and natural spin densities (NSD) from calculated densities at the B3LYP/TZVP level for the ligand and the M(II) complexes.

	Phdppb, <b>1</b>	Fe(II), <b>2</b>	Co(II), <b>3</b>	Ni(II), <b>4</b>
WBI(C–O)	1.78	1.80	1.71	1.71
WBI(M–O)	-	<0.01	<0.01	<0.01
WBI(M–C)	-	<0.01	<0.01	<0.01
q(C)	0.56	0.54	0.54	0.54
q(O)	-0.52	-0.48	-0.53	-0.53
q(C+O)	0.04	0.06	0.01	0.02
NSD(M)	-	3.61	2.56	1.51

### 3.2.2 Halide abstraction

The abstraction of a halide ligand is a common strategy to induce binding of a hemilabile moiety,<sup>[22-25]</sup> as was recently demonstrated by Iluc for the central olefin of diphosphine substituted *trans*-stilbene ligands.<sup>[23]</sup> To probe whether coordination of the C=O moiety could be facilitated in the same way, halide abstraction from the nickel complex (Phdppb)NiCl<sub>2</sub> (**4**) was investigated. Compound **4** and NaB(Ar<sup>F</sup>)<sub>4</sub> (Ar<sup>F</sup> = 3,5-bis(trifluoromethyl)phenyl) were mixed in Et<sub>2</sub>O and stirred overnight. Subsequent precipitation of the product from Et<sub>2</sub>O/hexanes, followed by extraction with Et<sub>2</sub>O resulted in the diamagnetic Ni(II) complex **8**. The <sup>1</sup>H NMR spectrum of **8** shows sharp aromatic signals ranging from δ 6 to 8 ppm, and 4 broadened aromatic peaks (Appendix C2). Analysis by <sup>13</sup>C NMR shows the presence of the carbonyl-moiety as a triplet signal at δ 206.8 ppm (<sup>3</sup>J<sub>CP</sub> = 2.9 Hz). This was further confirmed by ATR-IR analysis, as a band is visible at 1525 cm<sup>-1</sup>, both indicating that an η<sup>2</sup>(C,O)-interaction

is not present. The shift of the C=O vibration of  $-109\text{ cm}^{-1}$  in IR spectroscopy is relatively large and is expected to be caused by an  $\eta^1(\text{O})$ -interaction to nickel.<sup>[26]</sup> Next to this, the  $^{31}\text{P}$  NMR spectrum contains two singlet signals, at  $\delta$  5.6 and 36.4 ppm, consistent with the presence of an unbound phosphine ( $\delta$  5.6 ppm) and a metal-coordinated phosphine ( $\delta$  36.4 ppm)<sup>[27]</sup>. 2D NMR analysis by  $^1\text{H}$ - $^{31}\text{P}$  HMBC NMR and  $^1\text{H}$ - $^1\text{H}$  zTOCSY are consistent with these results (Figure A7). Together, these findings suggest that the diphosphine-ketone ligand binds in a chelating  $\kappa^2(\text{P},\text{O})$ -fashion. This structural motif has been previously documented in, for example, the synthesis of nickel complexes for ethylene oligomerization and polymerization reactions, using 2-(diphenylphosphine)benzoic acid, or its methyl ester analogue, as chelating  $\kappa^2(\text{P},\text{O})$ -ligands.<sup>[26-31]</sup> The  $\text{B}(\text{Ar}^{\text{F}})_4$  counter ion was found in  $^{11}\text{B}$  and  $^{19}\text{F}$  NMR at  $\delta$   $-6.6$  and  $-62.9$  ppm, respectively.<sup>[23]</sup> Furthermore, the atom composition of the complex was confirmed by elemental analysis. Combining the collected data suggests the synthesis of a dimeric structure in which two monomers are bound *via* two bridging chloride atoms in the form  $[\text{Ni}(\text{Ph}^{\text{d}}\text{dbp})(\mu\text{-Cl})_2\text{B}(\text{Ar}^{\text{F}})_4]_2$  (**8**) (Figure 2),<sup>[32,33]</sup> analogous to the  $[\text{Ni}(\text{dtpbe})(\mu\text{-Cl})_2\text{B}(\text{Ar}^{\text{F}})_4]_2$  (dtpbe = 1,2-bis(di-*tert*-butylphosphino)-ethane) complex as reported by Hew-Hawkins and coworkers.<sup>[34]</sup> Compound **8** eluded structural characterization by X-ray crystallography, and the proposed structure was investigated by DFT calculations at the B3LYP/6-31G\*\* level of theory (Figure 2). These calculations predict a frequency shift of  $-129\text{ cm}^{-1}$  between compound **4** and **8**, in line with the observed shift of  $-109\text{ cm}^{-1}$ . Comparison of the dimeric structure with a possible monomer showed an energy difference of 41 kcal/mol, favoring the dimeric structure with the incorporated  $\eta^1(\text{O})$  binding mode. Similar experiments were performed with Fe(II) and Co(II) complexes **2** and **3**, but unfortunately led to intractable mixtures of products.

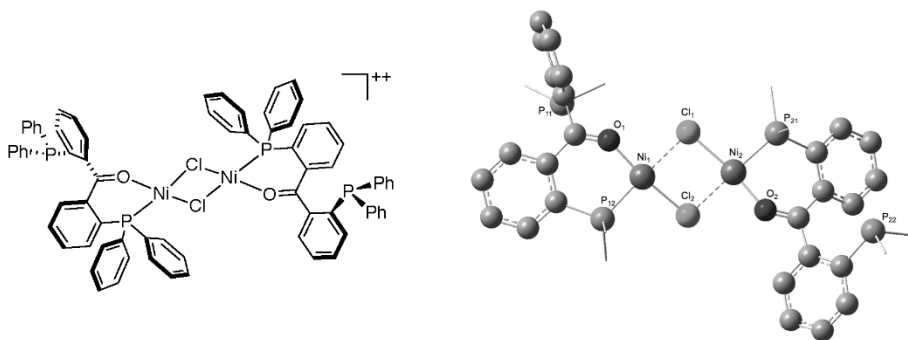


**Figure 2.** Structure of the dimeric  $\text{Ni}(\text{II})^+$  complex (**8**). Left: schematic representation. Right: the structure as calculated with DFT at the B3LYP/6-31G\*\* level of theory, all hydrogen atoms and the phenyl substituents on the phosphorus atom were omitted for clarity.

### 3.2.3 $M(\text{I})\text{Cl}$ complexes

As  $\pi$ -coordination is generally favored by more electron rich metal centers, the ability of the ketone moiety of the  $\text{Ph}^{\text{d}}\text{dbp}$  ligands to undergo  $\eta^2(\text{C},\text{O})$ -coordination to the metals in reduced

oxidation states is investigated. A series of complexes analogues to the previously reported (<sup>Ph</sup>dpbbp)NiCl is presented herein, involving Fe, Co and Cu, which allows for elucidation of the trends.

A reduced iron complex was obtained upon addition of sodium naphthalide to a solution of **2** generated *in situ* from FeCl<sub>2</sub> and <sup>Ph</sup>dpbbp in THF. The product (<sup>Ph</sup>dpbbp)FeCl (**5**) was isolated after precipitation from the mixture using hexanes. Analysis by NMR showed a paramagnetic species with signals ranging from δ -33.9 to 51.9 ppm in <sup>1</sup>H NMR, and no signal in the corresponding <sup>31</sup>P NMR.<sup>[35]</sup> Analysis by ATR-IR spectroscopy shows the disappearance of the C=O band at 1651 cm<sup>-1</sup> (Appendix C3). As in the case of the Ni(I) analogue (<sup>Ph</sup>dpbbp)NiCl,<sup>[15]</sup> the band most likely shifts to lower energies, but exact assignment is hampered by the presence of a large number of signals in the fingerprint region of the IR spectrum. The structure of **5** was determined by single crystal X-ray structure determination, which showed a distorted tetrahedral geometry around the iron center (Figure 1, Table 3), binding both phosphine arms, a chloride and the ketone moiety. The C=O bond length elongates from 1.218(3) in **2** to 1.3296(14) in **5**, indicating the presence of backdonation from Fe to the ketone moiety. This compound is, to the best of our knowledge, the first structurally characterized η<sup>2</sup>(C,O)-bound Fe(I) complex. EPR measurements conducted in toluene at 100 K of **5** show signals at g = 1.97, 3.13 and 4.99, which is typical for a high spin Fe(I) species with S = 3/2 (E/D = 0.16) (Appendix C5). A similar EPR spectrum was obtained by Harman and coworker, for a high spin TpFe(I)-N<sub>2</sub> species (Tp = tripyrazolylborate) with signals at g<sub>eff</sub> = 4.0 and 2.0, which was also assigned as an Fe(I) species.<sup>[36]</sup> Reduction of cobalt complex **3** was performed similarly and resulted in a paramagnetic species (**6**) as shown by its <sup>1</sup>H NMR spectrum with signals ranging from δ -12 to 32 ppm, and no signal in the corresponding <sup>31</sup>P NMR spectrum. The obtained IR spectrum is consistent with the before mentioned Fe(I) and Ni(I) complexes: the intense C=O band, located at 1647 cm<sup>-1</sup> in **3**, shifted to a lower value, and a fingerprint region analogous to **5** and **7** is observed. Magnetic susceptibility measurement using Evans method resulted in a μ<sub>eff</sub> of 3.16 μ<sub>B</sub> (n = 2), consistent with a high-spin Co(I) complex (S = 1). Crystals suitable for X-ray diffraction could not be obtained for complex **6** but from the closely related analogue **6pTol** (Figure 1, bottom), whose structure confirms the η<sup>2</sup>(C,O)-coordination of the ketone moiety.

**Table 3.** Selected bond distances (Å), angles (°) for **5**, **6pTol** and **7**.

	C=O	M-O	M-C	PMP angle
( <sup>Ph</sup> dpbbp)FeCl, <b>5</b>	1.3296(14)	1.9072(8)	2.0881(12)	106.350(12)
( <sup>pTol</sup> dpbbp)CoCl, <b>6pTol</b>	1.307(6)	1.947(3)	2.071(5)	109.62(6)
( <sup>Ph</sup> dpbbp)NiCl, <b>7</b> <sup>[15]</sup>	1.310(2)	1.9740(15)	2.006(2)	107.57(2)

Moving further to the right of the transition series, complexation with copper(I) was investigated. A reaction of CuCl with <sup>Ph</sup>dpbbp in MeCN did not afford the analogous η<sup>2</sup>(C,O)

complex, but instead resulted in a dimeric copper complex  $[(^{\text{Ph}}\text{dppb})\text{CuCl}]_2$  (**9**). X-ray crystal structure determination (Figure 1) reveals that complex **9** consists of two Cu atoms with a trigonal planar geometry, bridged by the two diphosphine ligands, which contribute each one P atom to the coordination environment of each metal. The structure contains an inversion center, resulting in two different Cu–O distances of 2.9953(11) and 3.0529(12) Å, and a C=O bond length of 1.2218(19) Å indicating the absence of  $\pi$ -coordination. This is confirmed by ATR-IR spectroscopy, as a single intense C=O band is visible at 1643  $\text{cm}^{-1}$ . To understand why the Cu(I) complex adopts a different coordination geometry from the previously described ketone-bound complexes **5** to **7**, DFT calculations were performed on the putative monomeric Cu(I) complex  $(^{\text{Ph}}\text{dppb})\text{CuCl}$  at the B3LYP/TZVP level of theory (Table 4). Interestingly, it exhibits a bidentate binding mode analogous to that observed in compounds **2-4**, in which the C=O moiety is not bound to the metal. Consequently, M–O and M–C WBIs below 0.01 are obtained, and the C–O WBI (1.79) as well as the corresponding NBO charge ( $q(\text{C}+\text{O}) = +0.06 \text{ e}$ ) are close to those of the free ligand. The fact that a  $\pi$ -coordinating structure is less favored for Cu is in line with the experimental observation dimeric structure **9**. This is likely a consequence of d-orbital contraction along the transition series making  $\pi$ -backdonation less efficient for Cu(I) in accord with the description of the C=O moiety as a mostly electron-accepting ligand.

### 3.2.4 Discussion on the $\eta^2(\text{C},\text{O})$ binding mode of the ketone moiety

Complexes **5-7** constitute a unique series of  $\eta^2(\text{C},\text{O})$  complexes with paramagnetic, first row transition metals, and provides an opportunity to investigate periodic trends in  $\pi$ -bonding. First, the degree of activation of the C–O bond, as indicated by elongation of the C–O bond with respect to the free ligand (1.213(3) Å), is approximately the same for Ni (1.310(2) Å) and Co (1.307(6) Å) and somewhat higher for Fe (1.3296(14) Å). This is consistent with an increasing degree of  $\pi$ -backdonation as the metal becomes less electronegative from Ni (1.91) to Fe (1.83). More strikingly, the ratio between the M–C and M–O bonds changes significantly along the series: the M–C bond shortens going from Fe to Ni (**5**: 2.0881(12) Å, **7**: 2.006 Å), while the M–O distance increases (**5**: 1.9072(8) Å, **7**: 1.974(3) Å).

In complement of the above experimental data, DFT calculations were performed on compounds **5-7**. The optimized geometries for the  $\eta^2(\text{C},\text{O})$  complexes **5-7** adequately reproduce the experimental data (Appendix C4). The charge transfer increases from Ni to Fe, with the highest amount of charge transfer at iron complex **5**, as seen in the total natural charge ( $q(\text{C}+\text{O})$ ) on the C=O fragment (**5**: –0.45, **6**: –0.35 and **7**: –0.32). This is additionally supported by an increase in the C–O WBI from Fe to Ni (**5**: 1.31, **6**: 1.40 and **7**: 1.46), in accord with the corresponding trend in C–O bond elongation. The M–C WBI is constant at 0.33 in complexes **5** to **7**, whereas the M–O WBI significantly decreases from 0.38 for **5** to 0.24 for **7**. In other words, the M–O bond becomes comparatively stronger as the extent of charge transfer to the C=O fragment increases.

**Table 4.** Wiberg bond indices (WBI), natural charges (q) and natural spin densities (NSD) from calculated densities at the B3LYP/TZVP level for the ligand and the M(I) complexes.

	Phdpbp <b>1</b>	Fe(I) <b>5</b>	Co(I) <b>6</b>	Ni(I) <b>7</b>	Cu(I)
WBI(C–O)	1.78	1.31	1.40	1.46	1.79
WBI(M–O)	-	0.38	0.31	0.24	<0.01
WBI(M–C)	-	0.33	0.33	0.33	<0.01
q(C)	0.56	0.21	0.27	0.29	0.55
q(O)	-0.52	-0.66	-0.62	-0.61	-0.49
q(C+O)	0.04	-0.45	-0.35	-0.32	0.06
NSD(M)	-	3.21	2.01	0.99	-
NSD(CO)	-	-0.34	-0.23	-0.14	-

More light is shed on the bonding situation by Atoms In Molecule (AIM) analyses of **5**, **6** and **7** (Figure 3). The Ni complex **7** displays bond paths for both the M–C and the C–O interaction, with a corresponding ring critical point (RCP) close to equidistant from both bond critical points (BCP).<sup>[37]</sup> In contrast, no M–C bond path – and consequently no RCP – is found in the Fe complex **5**. The Co complex **6** exhibits an intermediate situation in which the RCP is close to the M–C BCP, without complete merging.

Taken together, the above computational and experimental data consistently indicate that moving from Ni(I) to Fe(I) results in 1) a higher degree of charge transfer to the C=O moiety and 2) an increase in the M–O contribution and a concomitant decrease in the M–C contribution to the bonding. These two trends may appear difficult to reconcile with the DCD model: as the degree of  $\pi$ -backdonation increases, one would expect the M–C bond to *shorten* because the accepting  $\pi^*(\text{C}=\text{O})$  orbital has a larger coefficient on the carbon atom.<sup>[18]</sup> Therefore, a minor contribution of a third, ketyl radical resonance structure is proposed (Scheme 1C) which can be described as the interaction of a ketyl radical anion strongly coupled to a high-spin M(II) center.<sup>[38]</sup> An increasing, but small contribution of resonance structure C to the overall bonding from Ni to Fe is consistent with both the higher activation of the C–O bond and the decrease in M–C bonding complemented with a stronger, ionic M–O bonding with the more electropositive metal.

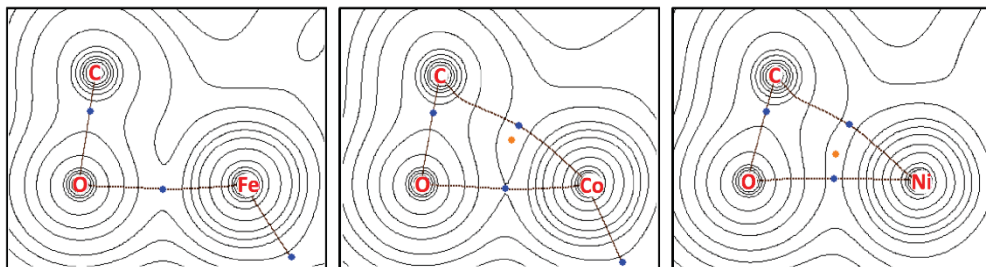


**Figure 3.** Electron density plots of the atoms in molecules calculations from 5, 6 and 7 (top-to-bottom). Bond critical points are given in blue, ring critical point are given in orange.

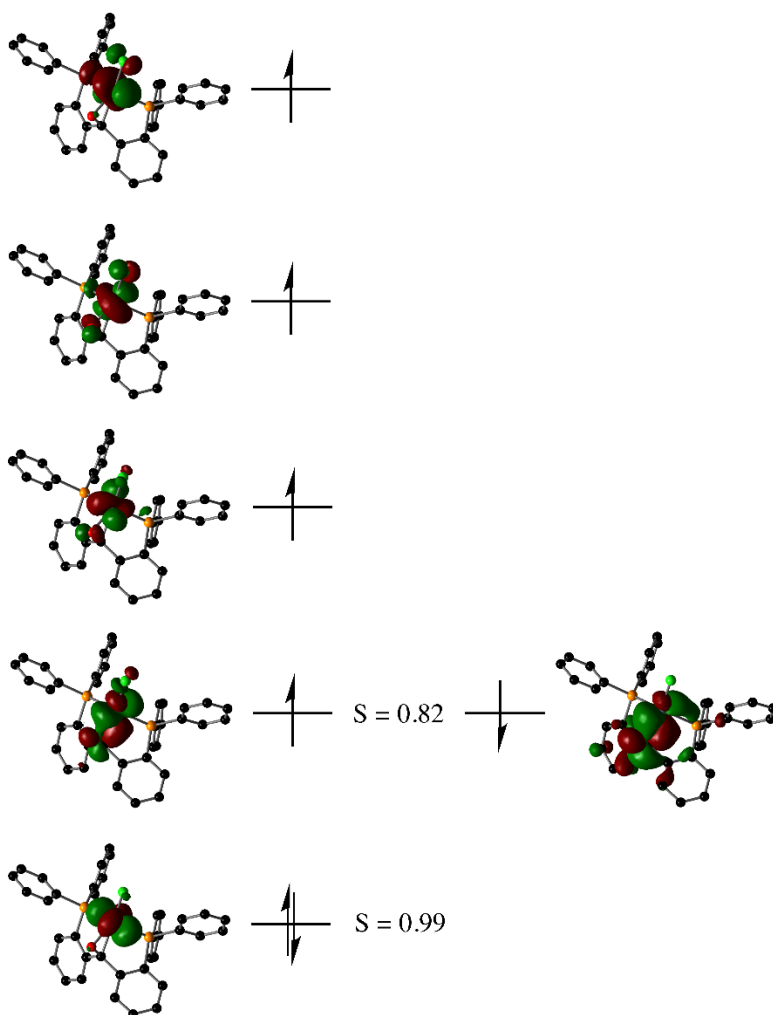


**Figure 4.** Qualitative molecular orbital diagram of 5.

Some extent of spin separation is also observed in the qualitative molecular orbital diagrams calculated for compounds **5** (Figure 4), **6**, and **7**. Of the five MOs of *d* parentage found for the Fe(I) complex **5**, three are singly occupied and one is doubly occupied ( $\alpha/\beta$  overlap:  $S = 0.99$ ). The last MO displays some spin separation, i.e. the  $\alpha$  and  $\beta$  spin-orbitals overlap to a lesser extent: while it can be described in both cases as a bonding combination of a *d*-orbital with the accepting  $\pi^*(\text{C}=\text{O})$  orbital, the  $\beta$  spin-orbitals displays a somewhat higher ligand character. The observed overlap integral ( $S = 0.82$ ) is too large for the spin-separated resonance structure C (Scheme 1) to be considered the best description of **5**, and suggests only a minor contribution of the ketyl radical resonance structure. In agreement with other observations (*vide supra*), this lower degree of orbital overlap is observed in the Fe(I) complex **5** and much less in the Co(I) ( $S=0.92$ ) and Ni(I) complex ( $S = 0.97$ ), for which the contribution of resonance structure C is close to negligible. This interpretation is also consistent with the decreasing amount of calculated  $\beta$ -spin density from 0.34 e in **5** to 0.14 e in **7** (Table 4, NSD(CO)).

Spin-separated electronic structures are widely accepted to be a good representation of reduced complexes featuring redox non-innocent  $\sigma$ -ligands such as imines and pyridines, which can accept an electron in a remote  $\pi^*$  orbital.<sup>[1, 39-44]</sup> Such structures typically display low overlap integrals ( $S < 0.5$ ) between the relevant  $\alpha$  and  $\beta$  orbitals. In contrast, the overlap integrals are much higher for the series of complexes described herein, consistent with mostly covalent DCD bonding with a minor contribution of the ketyl radical resonance structure in the case of Fe.

### 3.3 Conclusions

The coordination chemistry of the diphosphine-ketone ligand  $\text{Ph}_2\text{dpbp}$  with first-row transition metals ( $M = \text{Fe, Co, Ni, Cu}$ ) in the +II and +I formal oxidation state was investigated. The  $\text{C}=\text{O}$  moiety can adopt several binding modes, i.e. nonbound in the  $M(\text{II})$  ( $M = \text{Fe, Co, Ni}$ ) and  $\text{Cu}(\text{I})$  complexes,  $\eta^1(\text{O})$  in the  $\text{Ni}(\text{II})^+$  cation, and  $\eta^2(\text{C},\text{O})$  in the  $M(\text{I})$  complexes ( $M = \text{Fe, Co, Ni}$ ). The latter structures can be described as intermediate between a  $\pi$ -complex and a metallaepoxide according to the Dewar-Chatt-Duncanson model. Geometric changes in the  $M(\text{I})$  complexes were observed to follow a periodic trend, i.e. lengthening of the  $M-\text{C}$  bond and concomitant shortening of the  $M-\text{O}$  bond, accompanied by a slight increase of the  $\text{C}=\text{O}$  bond length, from Ni to Fe. This somewhat unexpected trend suggests a minor contribution of the ketyl radical resonance structure  $(\text{C}=\text{O})^{\bullet-}-M(\text{II})$  to the bonding in the case of Fe, which is corroborated by DFT calculations. These results contribute to a better understanding of the binding of  $\pi$ -ligands to high-spin, first-row transition metal centers and will be of use for the design and mechanistic understanding of catalytic cycles involving such species.



## 3.4 Experimental Section

### 3.4.1 General considerations

All reagents were purchased from commercial sources and used as received unless stated otherwise. All reactions were performed in a N<sub>2</sub> glovebox and at room temperature unless stated otherwise. Deuterated benzene (C<sub>6</sub>D<sub>6</sub>) and deuterated dichloromethane (CD<sub>2</sub>Cl<sub>2</sub>) were degassed using the freeze-thaw-pump method (4x) and subsequently stored over molecular sieves. Dichloromethane (CH<sub>2</sub>Cl<sub>2</sub>) was distilled over calciumhydride and tetrahydrofuran (THF) was distilled over sodium/benzophenone before use, both were degassed by bubbling N<sub>2</sub> through it for 30 minutes and stored over molecular sieves. Dry diethylether (Et<sub>2</sub>O), hexanes, acetonitrile (MeCN) and toluene (C<sub>7</sub>H<sub>8</sub>) were acquired from a MBRAUN MB SPS-80 solvent purification system and further dried over molecular sieves before use. MeCN was filtered over alumina prior to use. NaBARF<sub>4</sub> was purchased and further dried under high vacuum for 3 days at 50°C. CuCl was dried following standard procedures.<sup>[45]</sup> <sup>Ph</sup>dbbp and (<sup>Ph</sup>dbbp)NiCl<sub>2</sub> were synthesized following literature procedures.<sup>[15]</sup>

<sup>1</sup>H, <sup>11</sup>B, <sup>13</sup>C, <sup>19</sup>F and <sup>31</sup>P NMR spectra (respectively 400, 128, 100, 376 and 161 MHz) were recorded on an Agilent MRF400 (<sup>1</sup>H, <sup>13</sup>C, <sup>31</sup>P) or a Varian AS400 spectrometer (<sup>1</sup>H, <sup>11</sup>B, <sup>13</sup>C, <sup>19</sup>F, <sup>31</sup>P) at 25 °C. <sup>1</sup>H and <sup>13</sup>C NMR chemical shifts are reported in ppm relative to TMS using the residual solvent resonance as internal standard. <sup>11</sup>B NMR chemical shifts are reported in ppm and externally referenced to BF<sub>3</sub>OEt<sub>2</sub>, <sup>31</sup>P NMR chemical shifts are externally referenced to 85% aqueous H<sub>3</sub>PO<sub>4</sub> and <sup>19</sup>F NMR chemical shifts are externally referenced to CFCl<sub>3</sub>. Infrared spectra were recorded using a Perkin Elmer Spectrum One FT-IR spectrometer equipped with a general liquid cell accessory under a N<sub>2</sub> flow. UV-Vis spectra were measured using a Lambda 35 UV-Vis spectrometer. The UV-Vis samples were prepared under a N<sub>2</sub> atmosphere and sealed with a Teflon cap after which the spectra were recorded directly. EPR analyses were carried out by dissolving several milligrams of the compound in an appropriate solvent under inert conditions followed by filtration of the sample to ensure no solids were present. EPR spectra were recorded on a Bruker EMX Plus 6000 Gauss machine with ER 041 XG X-Band Microwave Bridge. ESI-MS spectra were recorded on a Walters LCT Premier XE KE317 Micromass Technologies spectrometer. Compounds of which elemental analysis is reported were either recrystallized or precipitated and dried under high vacuum overnight before submission. Compounds of which elemental analysis is reported were either recrystallized or precipitated and dried under high vacuum overnight before submission and analysis was performed by the Mikroanalytisches Laboratorium Kolbe, Mülheim an der Ruhr, Germany. Details on X-ray crystal structure determination and selected spectra are given in Appendix C.

### 3.4.2 DFT

DFT calculations were performed using the Gaussian 09 software package<sup>[46]</sup> using the B3LYP (Becke, three-parameter, Lee-Yang-Parr) functional and the TZVP basis set on all atoms, except for the calculations of **9**, which were performed with the B3LYP functional and the 6-31G\*\* basis set. The structures were optimized without any symmetry restraints. Frequency analyses were performed on all calculations to verify that the obtained stationary points are in fact minima. For qualitative MO diagrams, the canonical orbitals were biorthogonalized to maximize alignment of electron pairs. For NBO calculations, the NBO6 program up to the NLMO basis set was used.<sup>[47]</sup> Atoms in molecules

calculations<sup>[20]</sup> were performed and corresponding pictures were generated using the Multiwfn program.<sup>[48]</sup>

### 3.4.3 Synthesis

***Ph*<sup>o</sup>*dpbp***: *o*-bromophenyl-di-*p*-tolyl-phosphine (4.93 g, 13.4 mmol) was suspended in Et<sub>2</sub>O (30 mL). The light-yellow suspension was cooled to -50 °C using an acetone ice bath. *n*-BuLi (1.6 M in hexane, 16 mmol, 10 mL) was added drop wise while stirring, resulting in a rapid color change from yellow to brown. Within 30 min, the reaction mixture was allowed to warm up to room temperature and was directly cooled down again to -50 °C, after which a solution of *N,N*-dimethylcarbamoylchloride (0.61 mL, 6.5 mmol) in Et<sub>2</sub>O (15 mL) was added drop wise over 20 minutes. During the addition, the temperature of the bath was kept between -35 °C and -45 °C, after which the suspension stirred overnight, allowing the mixture to warm up to room temperature. The reaction was then cooled down again and treated at 0 °C with 2.5 M NH<sub>4</sub>Cl solution in water (38 mL, 4.5 g, 85 mmol NH<sub>4</sub>Cl) turning the suspension orange-yellow. The product was isolated by washing with Et<sub>2</sub>O and dried with MgSO<sub>4</sub> and solvents were evaporated. The obtained sticky-yellow compound was washed with MeOH, resulting in the product as a yellow powder after solvent removal (2.41 g, 4.0 mmol, 61%). <sup>1</sup>H NMR (C<sub>6</sub>D<sub>6</sub>): δ<sub>H</sub> 7.37 (t, *J* = 7.6 Hz, 8H), 7.37 (m, 2H), 7.31 (dd, *J* = 7.7, 2.4 Hz, 2H), 6.95 (td, *J* = 7.5, 1.1 Hz, 2H), 6.91 (d, *J* = 7.7 Hz, 8H), 6.83 (td, *J* = 7.5, 1 Hz, 2H), 2.03 (s, 12H) ppm. <sup>31</sup>P NMR (C<sub>6</sub>D<sub>6</sub>): δ<sub>P</sub> -9.77 ppm. <sup>13</sup>C NMR (CDCl<sub>3</sub>): δ<sub>C</sub> 197.35 (t, *J*<sub>CP</sub> = 3 Hz), 144.64 (dd, *J*<sub>CP</sub> = 24.4, 1 Hz), 140.68 (*J*<sub>CP</sub> = 26.1, 2.2 Hz), 138.21, 135.56 (dt, *J*<sub>CP</sub> = 3, 11 Hz), 135.00, 134.45 (m), 131.03 (t, *J*<sub>CP</sub> = 3.3 Hz), 130.66, 129.48 (m), 128.00, 21.21 ppm. ATR-IR ν: 3012, 2956, 2920, 2863, 1910, 1738, 1664, 1598, 1495, 1446, 1395, 1296, 1271, 1243, 1185, 1090, 1018, 928, 805, 747, 637, 507 cm<sup>-1</sup>. ESI-MS (MeCN AgNO<sub>3</sub>/H<sub>2</sub>O) *m/z*: [2M+Ag]<sup>+</sup>: 1319.3529, calc: 1319.3534. Elemental analysis: calcd: C 81.17, H 5.98, found: C 80.84, H 6.05.

**(*Ph*<sup>o</sup>*dpbp*)FeCl<sub>2</sub> (2)**: FeCl<sub>2</sub>·1.5THF (38.1 mg, 0.162 mmol) was suspended in CH<sub>2</sub>Cl<sub>2</sub> (2 mL) in a vial in the glovebox at room temperature. *Ph*<sup>o</sup>*dpbp* (89.2 mg, 0.162 mmol) was dissolved in CH<sub>2</sub>Cl<sub>2</sub> (2 mL) in a separate vial. After stirring both mixtures for 10 min, the ligand solution was added to the Fe precursor, resulting in a yellow suspension, which turned to yellow/brown after 10 min. The mixture was stirred overnight, after which all volatiles were removed in vacuum. The obtained solids were precipitated from THF/hexanes (1:4) and isolated *via* filtration. The product was extracted using THF and dried in vacuum, after which **2** was obtained as a pale brownish-yellow solid (95.7 g, 0.141 mmol, 87%). <sup>1</sup>H NMR (CD<sub>2</sub>Cl<sub>2</sub>): δ<sub>H</sub> 30.85, 16.04, 14.17, 12.51, 8.32, 7.36, 6.50, 3.90, 2.84, 1.92, 1.25, 0.85, 0.09, -1.31, -5.74 ppm. ATR-IR ν: 3055, 1650, 1584, 1561, 1482, 1435, 1302, 1283, 1095, 930, 747, 691, 635, 495 cm<sup>-1</sup>. ESI-MS (THF) *m/z*: [M-X]<sup>+</sup>: 641.0737, calc: 641.0654. UV-Vis: λ<sub>max</sub>: 400 nm. Elemental analysis: calcd: C 65.61, H 4.17, found: C 64.96, H 4.07.

**(*Ph*<sup>o</sup>*dpbp*)CoCl<sub>2</sub> (3)**: CoCl<sub>2</sub> (23.9 mg, 0.184 mmol) was suspended in Et<sub>2</sub>O (1 mL) in a vial in the glovebox at room temperature. *Ph*<sup>o</sup>*dpbp* (100.8 mg, 0.183 mmol) was dissolved in Et<sub>2</sub>O (6 mL) in a separate vial. After stirring both mixtures for 10 min, the ligand suspension was added to the Co precursor. Mixing resulted in a green suspension. The mixture was stirred overnight, after which all volatiles were removed in vacuum. The obtained solids were precipitated from THF/hexanes (1:3) and isolated *via* filtration. The product was extracted using THF and dried in vacuum, after which **3** was obtained as a green solid (103 mg, 0.152 mmol, 83%). <sup>1</sup>H NMR (CD<sub>2</sub>Cl<sub>2</sub>): δ<sub>H</sub> 18.68, 13.71, 11.76 (minor), 10.13, 8.00, 7.31, 7.22, 7.12,

1.26 (minor), 0.94, 0.08, -0.56, -3.73 (broad) ppm. ATR-IR v: 3051, 1647, 1482, 1435, 1284, 1254, 1166, 1126, 1095, 930, 769, 748, 740, 634, 522, 511, 497, 471  $\text{cm}^{-1}$ . ESI-MS (MeCN) m/z:  $[\text{M}-\text{Cl}]^+$ : 644.0635, calc: 644.0636,  $[\text{M}-\text{Cl}+\text{MeCN}]^+$ : 685.0905, calc: 685.0901. UV-Vis:  $\lambda_{\text{max}}$ : 648, 737 nm. Elemental analysis: calcd: C 65.31, H 4.15, found: C 64.87, H 4.03.

**(Phdpbp)FeCl (5):** Naphthalene (141.2 mg, 1.1 mmol) was dissolved in THF (20 mL) in the glovebox at room temperature. A lump of  $\text{Na}^0$  was added and the mixture was stirred for 3 h, after which a dark green solution was obtained.  $\text{FeCl}_2$  (115.3 mg, 0.909 mmol) was suspended in THF (8 mL) in a separate vial and Phdpbp (500.2 mg, 0.908 mmol) was dissolved in again a different vial in THF (12 mL). The  $\text{FeCl}_2$  suspension was cooled to  $-78^\circ\text{C}$  and stirred for 10 min, after which the dissolved ligand was added and the resulting mixture was stirred for 15 min. The naphthalide solution was filtered and added to the cooled mixture in 15 min. This final mixture was stirred further for 1 h at  $-78^\circ\text{C}$  and for 18 h at room temperature, after which it was concentrated in vacuum to a total volume of 10 mL. A brown precipitate was obtained after the addition of hexanes (50 mL), which was collected by filtration. The product was extracted using THF and dried in vacuum, resulting in pure **5** (0.566 g, 0.882 mmol, 97%).  $^1\text{H}$  NMR ( $\text{CD}_2\text{Cl}_2$ ):  $\delta_{\text{H}}$  52.08, 33.93, 11.87, 11.12, 3.83, 0.30, -1.30, -5.74, -6.38, -13.24, -33.76 ppm. ATR-IR v: 2962, 1725, 1658, 1584, 1480, 1435, 1262, 1117, 1099, 1003, 928, 817, 742, 692, 542, 502  $\text{cm}^{-1}$ . UV-Vis:  $\lambda_{\text{max}}$ : 480 nm.

**(Phdpbp)CoCl (6):** Naphthalene (27.9 mg, 0.218 mmol) was dissolved in THF (2 mL) in the glovebox at room temperature. A lump of  $\text{Na}^0$  was added and the mixture was stirred for 3 h, after which a dark green solution was obtained.  $\text{CoCl}_2$  (23.7 mg, 0.182 mmol) was suspended in THF (1 mL) in a vial and Phdpbp (100.1 mg, 0.182 mmol) was dissolved in THF (3 mL) in a separate vial. Both mixtures were stirred for 10 min, after which the ligand was added to the Co suspension. The resulting mixture was cooled to  $-78^\circ\text{C}$  and stirred for 45 min. The naphthalide solution was filtered and added to the cooled mixture in 45 min. This final mixture was stirred further for 1.5 h at  $-78^\circ\text{C}$  and for 18 h at room temperature, after which the mixture was concentrated in vacuum to  $\sim 1.5$  mL. Hexane was added (5 mL) and the solids were collected by filtration. The product was extracted with THF and dried in vacuum, resulting in **6** as a brown solid (74.5 mg, 0.109 mmol, 60%).  $^1\text{H}$  NMR ( $\text{C}_6\text{D}_6$ ):  $\delta_{\text{H}}$  20.38, 14.24, 13.68, 3.57, 1.41, 1.25, 0.89, 0.06, -1.42, -2.37, -6.59, -8.10, -9.49, -16.73 ppm. ATR-IR v: 3054, 1585, 1481, 1460, 1435, 1241, 1160, 1133, 1096, 1069, 1027, 998, 918, 878, 847, 776, 743, 691, 657, 623, 581, 543, 517, 501, 480  $\text{cm}^{-1}$ . UV-Vis:  $\lambda_{\text{max}}$ : 448, 530, 660 nm.

**(p<sup>Tol</sup>dpbp)CoCl (6pTol):** synthesis was performed *via* an analogous procedure to **6**, with a yield of 86% (300.3 mg, 0.43 mmol).  $^1\text{H}$  NMR ( $\text{C}_6\text{D}_6$ ):  $\delta_{\text{H}}$  31.59, 20.00, 17.64, 14.34, 13.54, 9.21, -0.06, -0.98 (broad), -6.07, -7.97, -16.38 ppm. ATR-IR v: 2919, 2863, 1599, 1498, 1434, 1397, 1258, 1241, 1189, 1096, 1019, 917, 803, 777, 693, 626, 510  $\text{cm}^{-1}$ . UV-Vis:  $\lambda_{\text{max}}$ : 525 nm. Elemental analysis: calcd: C 70.24, H 5.18, found: C 70.00, H 5.37.

**[Ni(Phdpbp)( $\mu$ -Cl)]<sub>2</sub>(B(Ar<sup>F</sup>)<sub>4</sub>)<sub>2</sub> (8):** (Phdpbp)NiCl<sub>2</sub> was suspended in Et<sub>2</sub>O (0.5 mL) in a vial in the glovebox. NaB(Ar<sup>F</sup>)<sub>4</sub> was also suspended in Et<sub>2</sub>O (2 mL) and transferred to the [Ni] mixture. The final mixture was stirred overnight at room temperature, after which all solvents were removed in vacuum. Subsequently, Et<sub>2</sub>O (1 mL) and hexanes (3 mL) were added and the formed precipitation was filtered and washed with hexanes (3 x 1 mL). The product was extracted using Et<sub>2</sub>O (3 mL), after which the solvents were removed

in vacuum and **9** was obtained as a brown powder (89%, 31.5 mg, 0.0104 mmol).  $^1\text{H}$  NMR ( $\text{CD}_2\text{Cl}_2$ ):  $\delta_{\text{H}}$  8.04 (t,  $J = 7.6$  Hz), 7.93 (t,  $J = 7.6$  Hz), 7.80 (d,  $J = 7.4$  Hz), 7.77 (d,  $J = 5.0$  Hz), 7.73 (m, broad,  $\text{BAR}^{\text{F}_4}$ ), 7.62 (q) 7.58 (d,  $J = 7.6$  Hz), 7.56 (s,  $\text{BAR}^{\text{F}_4}$ ), 7.49 (t,  $J = 7.7$  Hz), 7.43 (t,  $J = 7.6$  Hz), 7.37 (m), 7.25 (t,  $J = 7.7$  Hz + s, broad, 1H), 7.14 (t,  $J = 7.6$  Hz), 7.07 (t,  $J = 7.7$  Hz), 6.95 (t,  $J = 7.9$  Hz), 6.89 (s, broad, 1H), 6.33 (d, 1H,  $J = 7.9$  Hz), 6.04 (s, broad, 1H) ppm.  $^{13}\text{C}$  NMR ( $\text{CD}_2\text{Cl}_2$ ):  $\delta_{\text{C}}$  206.83 (t,  $J_{\text{CP}} = 2.9$  Hz), 162.14 (q,  $J_{\text{CB}} = 49.2$  Hz), 140.94 (t,  $J = 5.7$  Hz), 140.28 (t,  $J = 3.6$  Hz), 138.26 (t,  $J = 18.8$  Hz), 137.47 (t,  $J = 3.2$  Hz), 137.01 (t,  $J = 4.0$  Hz), 136.68 (q,  $J = 4.0$  Hz), 136.47 (t,  $J = 5.1$  Hz), 135.90 (s), 135.48 (t,  $J = 5.1$  Hz), 135.20 (s), 134.83 (s), 134.50 (s), 133.94 (s), 133.74 (t,  $J = 5.8$  Hz), 132.80 (s), 132.06 (s), 130.34 (t,  $J = 5.7$  Hz), 130.01 (s), 129.59 (t,  $J = 4.9$  Hz), 129.42 (q,  $J = 2.8$  Hz), 129.10 (m), 128.87 (t,  $J = 4.9$  Hz), 128.60 (s), 128.39 (s), 127.46 (t,  $J = 25.6$  Hz), 126.34 (s), 120.93 (s), 120.29 (s), 119.77 (s), 118.73 (s), 117.89 (septet,  $J = 3.9$  Hz), 103.36 (s), 66.20 (s) ppm.  $^{31}\text{P}$  NMR ( $\text{CD}_2\text{Cl}_2$ ):  $\delta_{\text{P}}$  36.38, 5.58 ppm.  $^{11}\text{B}$  NMR ( $\text{CD}_2\text{Cl}_2$ ):  $\delta_{\text{B}}$  -6.64 ppm.  $^{19}\text{F}$  NMR ( $\text{CD}_2\text{Cl}_2$ ):  $\delta_{\text{F}}$  -62.86 ppm. ATR-IR v: 1610, 1571, 1525, 1439, 1354, 1273, 1115, 886, 839, 744, 712, 681, 474  $\text{cm}^{-1}$ . Elemental analysis: calcd: C 54.96, H 2.67; found: C 54.70, H 2.72. ESI-MS (MeCN) m/z:  $[\text{M-NiCl}]^+$  (monomer): 643.0549, calc: 643.0657.

**$[(\text{Phdpbp})\text{CuCl}]_2$  (**9**):** Anhydrous CuCl (8.7 mg, 0.088 mmol) was dissolved in MeCN (0.5 mL) in a vial in the glovebox at room temperature.  $\text{Phdpbp}$  (48.4 mg, 0.092 mmol) was dissolved in MeCN (10 mL) in a separate vial. After stirring both mixtures for 10 min, the dissolved CuCl was slowly added to the ligand, after which the mixture was directly filtered over a pipet filter into a new vial. The mixture was left standing for 48 h after which orange/brown crystals were formed. The MeCN was removed by decantation, after which the crystals were washed with MeCN (2 x 1 mL) and all residual solvents were removed in vacuum, resulting in **8** as crystalline material (35 mg, 0.027 mmol, 61%).  $^1\text{H}$  NMR ( $\text{CD}_2\text{Cl}_2$ ):  $\delta_{\text{H}}$  7.40, 7.34, 7.02, 1.98, 1.28, 0.87, 0.43 ppm.  $^{31}\text{P}$  NMR ( $\text{CD}_2\text{Cl}_2$ ):  $\delta_{\text{P}}$  -12.19 ppm. ATR-IR v: 3049, 1643, 1584, 1561, 1479, 1435, 1300, 1266, 1254, 1167, 1125, 1094, 929, 744, 694, 639, 525, 493  $\text{cm}^{-1}$ . Elemental analysis: calcd: C 68.42, H 4.35; found: C 69.12, H 4.32. ESI-MS (MeCN) m/z:  $[\text{M-Cl}]^+$ : 1263.1427, calc: 1263.1510;  $[\text{M-CuCl-Cl+MeCN}]^+$  (monomer): 654.1066, calc: 654.1177. UV-Vis:  $\lambda_{\text{max}}$ : 400, 890 nm.

### 3.5 References and notes

- [1] P. J. Chirik, *Angew. Chem. Int. Ed.*, **2017**, *56*, DOI: 10.1002/anie.201611959.
- [2] B. Marciniak, H. Maciejewski, C. Pietraszuk, P. Pawluc, *Hydrosilylation: A Comprehensive Review on Recent Advances*, Springer, **2009**.
- [3] E. P. Kundig, *Transition Metal Arene  $\pi$ -Complexes in Organic Synthesis and Catalysis*, Springer-Verlag Berlin Heidelberg, **2004**.
- [4] Chapter 1 of this thesis: D. G. A. Verhoeven, M. -E. Moret, *Dalton Trans.*, **2016**, *45*, 15762–15778.
- [5] S. H. Bertz, R. A. Hardin, T. J. Heavey, C. A. Ogle, *Angew. Chem. Int. Ed.*, **2013**, *52*, 10250–10252.
- [6] A. V. R. Madduri, S. R. Harutyunyan, A. J. Minnaard, *Angew. Chem. Int. Ed.*, **2012**, *51*, 3164–3167.
- [7] K. Mikami, K. Wakabayashi, K. Aikawa, *Org. Lett.* **2006** 1517–1519.
- [8] Q. Jing, C. A. Sandoval, Z. Wang, K. Ding, *Eur. J. Org. Chem.*, **2006**, *8(8)*, 3606–3616.
- [9] K. Ruhland, A. Obenhuber, S. D. Hoffman, *Organometallics*, **2008**, *27*, 3482–3495.
- [10] A. Obenhuber, K. Ruhland, *Organometallics*, **2011**, *30*, 4039–4051.
- [11] A. Obenhuber, K. Ruhland, *Organometallics*, **2011**, *30*, 171–186.

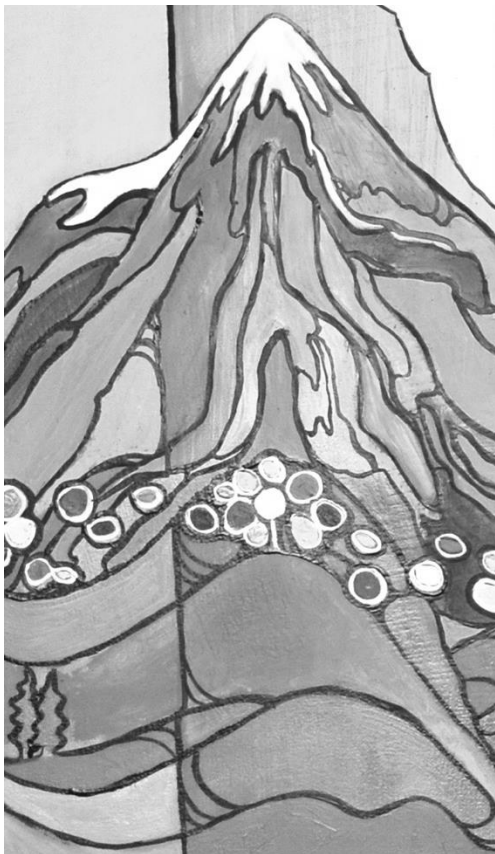
- [12] L. E. Doyle, W. E. Piers, J. Borau-García, *J. Am. Chem. Soc.*, **2015**, *137*, 2187–2190.
- [13] L. E. Doyle, W. E. Piers, J. Borau-García, M. J. Sgro, D. M. Spasyuk, *Chem. Sci.*, **2016**, *7*, 921–931.
- [14] L. E. Doyle, W. E. Piers, D. W. Bi, *Dalton Trans.*, **2017**, DOI: 10.1039/c7dt00563f.
- [15] Chapter 2 of this thesis: B. W. H. Saes, D. G. A. Verhoeven, M. Lutz, R. J. M. Klein Gebbink, M. -E. Moret, *Organometallics*, **2015**, *34*, 2710–2713.
- [16] G. J. Kubas, *J. Organomet. Chem.*, **2001**, *635*, 37–68.
- [17] R. H. Crabtree, *The organometallic chemistry of the transition metals*, Sixth edition, John Wiley & Sons, Inc., Hoboken, New Jersey, **2014**.
- [18] T. A. Albright, R. Hoffmann, J. C. Thibeault, D. L. Thorn, *J. Am. Chem. Soc.*, **1979**, *101*(14), 3801–3812.
- [19] The magnetic susceptibility by Evans method could not be determined for **2** due to solubility issues.
- [20] R. F. W. Bader, *Chem. Rev.*, **1991**, *91*, 893–928.
- [21] As described in reference [15], the crystals grown of compound **4** were in two forms: **4** and **4·CH<sub>2</sub>Cl<sub>2</sub>**. This lead to slight changes in the mentioned distances between the two compounds, of which **4** is presented in Table 1. The values for **4·CH<sub>2</sub>Cl<sub>2</sub>** are the following: C=O 1.223(4) Å, O–M 3.092(2) Å, PMP angle 113.76(3)°.
- [22] J. I. van der Vlugt, E. A. Pidko, D. Vogt, M. Lutz, A. L. Spek, A. Meetsma, *Inorg. Chem.*, **2008**, *47*(11), 4442–4444.
- [23] B. J. Barrett, V. M. Iluc, *Inorg. Chem.*, **2014**, *53*, 7248–7259.
- [24] D. L. Coombs, S. Aldridge, C. Jones, D. J. Willock, *J. Am. Chem. Soc.*, **2003**, *125*, 6356–6357.
- [25] N. R. Bunn, S. Aldrige, D. L. Kays, N. D. Coombs, A. Rossin, D. J. Willock, J. K. Day, C. Jones, L.-I. Ooi, *Organometallics*, **2005**, *24*, 5891–5900.
- [26] M. C. Bonnet, F. Dahan, A. Ecke, W. Keim, R. P. Schulz, I. Tkatchenko, *Chem. Commun.*, **1994**, 615–616.
- [27] B. T. Rasley, M. Rapta, R. J. Kulawiec, *Organometallics*, **1996**, *15*, 2852–2854.
- [28] C. P. Butts, J. Crosby, G. C. Lloyd-Jones, S. C. Stephen, *Chem. Commun.*, **1999**, 1707–1708.
- [29] G. Sánchez, J. García, D. Meseguer, J. L. Serrano, L. García, J. Pérez, G. López, *Dalton Trans.*, **2003**, 4709–4717.
- [30] G. Sánchez, J. García, J. J. Ayllón, J. L. Serrano, L. García, J. Pérez, G. López, *Polyhedron*, **2007**, *26*, 2911–2918.
- [31] Z. J. A. Komon, G. C. Bazan, C. Fang, X. Bu, *Inorg. Chim. Acta*, **2003**, *345*, 95–102.
- [32] M. -T. Chen, W. -Y. Lee, T. -L. Tsai, L. -C. Liang, *Organometallics*, **2014**, *33*, 5852–5862.
- [33] D. J. Mindiola, R. Waterman, D. M. Jenkins, G. L. Hillhouse, *Inorg. Chim. Acta*, **2003**, *345*, 299–308.
- [34] Y. Ganushevich, V. Miluykov, D. Yakhrov, O. Sinyashin, P. Lönnecke, E. Hey-Hawkins, *Inorg. Chim. Acta*, **2011**, *376*, 118–122.
- [35] Attempts were made to perform spin multiplicity measurements following Evans method, but failed due to the low solubility of **5**.
- [36] A. McSkimming, W. H. Harman, *J. Am. Chem. Soc.*, **2015**, *137*, 8940–8943.
- [37] G. Frenking, S. Shaik, *The Chemical Bond*, Wiley-VCH, **2014**, Chapter 8: The QTAIM Perspective of Chemical Bonding, P. L. A. Popelier, 271–308. A bond critical point (BCP) is a saddle point in the electron density map at which the electron density decreases in two perpendicular directions and increases in the third direction. The bond path between two atoms is the path of maximal

electron density that connects the BCP to the corresponding atoms. A ring critical point (RCP) describes the presence of a ring-structure in the electron density map. It is also a saddle point in the electron density map: the electron density rises in two perpendicular directions and decreases in one.

- [38] J. F. Berry, *Chem. Eur. J.*, **2010**, *16*, 2719–2724.
- [39] A. C. Bowman, C. Milsman, C. C. Hojilla Atienza, E. Lobkovsky, K. Wieghardt, P. J. Chirik, *J. Am. Chem. Soc.*, **2010**, *132*, 1676–1684.
- [40] P. J. Chirik, K. Wieghardt, *Science*, **2010**, *327*, 794–795.
- [41] B. de Bruin, E. Bill, E. Bothe, T. Weyhermuller, K. Wieghardt, *Inorg. Chem.*, **2000**, *39*, 2936–2947.
- [42] D. G. H. Hetterscheid, J. Kaiser, E. Reijerse, T. P. J. Peters, S. Thewissen, A. N. J. Blok, J. M. M. Smits, R. de Gelder, B. de Bruin, *J. Am. Chem. Soc.*, **2005**, *127*, 1895–1905.
- [43] D. G. H. Hetterscheid, M. Bens, B. de Bruin, *Dalton Trans.*, **2005**, 979–984.
- [44] S. K. Russell, J. M. Hoyt, S. C. Bart, C. Milsman, S. C. E. Stieber, S. P. Semproni, S. DeBeer, P. J. Chirik, *Chem. Sci.*, **2014**, *5*, 1168–1174.
- [45] W. L. F. Armarego, C. L. L. Chai, *Purification of Laboratory Chemicals*, **2009**, Elsevier Inc., p. 470.
- [46] M. J. Frish, G. W. Trucks, H. B. Schlegel, G. E. Scuseria, M. A. Robb, J. R. Cheeseman, G. Scalmani, V. Barone, B. Mennucci, G. A. Petersson, H. Nakatsuji, M. Caricato, X. Li, H. P. Hratchian, A. F. Izmaylov, J. Bloino, G. Zheng, J. L. Sonnenberg, M. Hada, M. Ehara, K. Toyota, R. Fukuda, J. Hasegawa, M. Ishida, T. Nakajima, Y. Honda, O. Kitao, H. Nakai, T. Vreven, J. A. Montgomery, Jr., J. E. Peralta, F. Ogliaro, M. Bearpark, J. J. Heyd, E. Brothers, K. N. Kudin, V. N. Staroverov, R. Kobayashi, J. Normand, K. Raghavachari, A. Rendell, J. C. Burant, S. S. Iyengar, J. Tomasi, M. Cossi, N. Rega, J. M. Millam, M. Klene, J. E. Knox, J. B. Cross, V. Bakken, C. Amado, J. Jaramillo, R. Gomperts, R. E. Stratmann, O. Yazyev, A. J. Austin, R. Cammi, C. Pomelli, J. W. Ochterski, R. L. Martin, K. Morokuma, V. G. Zakrzewski, G. A. Voth, P. Salvador, J. J. Dannenberg, S. Dapprich, A. D. Daniels, Ö. Farkas, J. B. Foresman, J. V. Ortiz, J. Cioslowski, D. J. Fox, "Gaussian 09 Revision A.02".
- [47] NBO 6.0. E. D. Glendening, J. K. Badenhoop, A. E. Reed, J. E. Carpenter, J. A. Bohmann, C. M. Morales, C. R. Landis, and F. Weinhold, Theoretical Chemistry Institute, University of Wisconsin, Madison, WI, 2013, <http://nbo6.chem.wisc.edu/>
- [48] T. Lu, F. Chen, *J. Comput. Chem.*, **2012**, *33*, 580–592.



*Of course, you have to be in balance,  
But don't be in equilibrium*  
- B. Feringa





# | Chapter 4 |

## Cobalt-Catalyzed Hydrosilylation of Olefins and Ketones

**Abstract** The hydrosilylation of unsaturated compounds homogeneously catalyzed by cobalt complexes has gained considerable attention in the last years, aiming at substituting precious metal based catalysts. In this study, the catalytic activity of Co(II) and Co(I) complexes of the  $p^{Tol}$ dpbp ligand is demonstrated in the hydrosilylation of 1-octene with phenylsilane. The Co(I) complex is a better precatalyst for the mentioned reaction under mild conditions, at 1 mol% catalyst, 1 h, room temperature, and without solvent, yielding 84% of octylphenylsilane. Investigation of the substrate scope shows lower performance of the catalyst in styrene hydrosilylation, but excellent results with allylbenzene (84%) and acetophenone (>99%). This catalytic study contributes to the field of Co-catalyzed hydrosilylation reactions, and shows a first example of catalysis employing the dpbp ligand in combination with a base metal.

---

D. G. A. Verhoeven, J. Kwakernaak, M. A. C. van Wiggeren, M. Lutz, R. J. M. Klein Gebbink, M. -E. Moret, *to be submitted*.

## 4.1 Introduction

The hydrosilylation of unsaturated compounds catalyzed by cobalt complexes has received significant attention in recent years.<sup>[1,2]</sup> This reaction is highly important in the silicon industry as it is used in the synthesis of silicon polymers, oils and resins, as well as in the production of organosilicon reagents for fine chemicals. Generally, extremely active and selective Pt-based homogeneous catalysts, such as Speier's or Karstedt's catalysts,<sup>[3-5]</sup> are used but the ongoing quest for more sustainable processes leads to interest in employing base metals iron,<sup>[6-8]</sup> cobalt and nickel<sup>[9-12]</sup>. While hydrosilylation catalyzed by the low-valent Co(0) complex  $\text{Co}_2(\text{CO})_8$  was reported as early as 1965 by Chalk and Harrod,<sup>[13-16]</sup> the number of cobalt catalysts increased explosively in recent years. The scope for the unsaturated substrate is versatile, including alkene,<sup>[1,17-24]</sup> alkyne<sup>[25-27]</sup> and carbonyl<sup>[28]</sup> groups. Additionally, a number of different silanes can be used. Much research is performed with phenylsilane, but also other silanes can be employed, such as diphenylsilane,<sup>[21]</sup> alkyl silanes,<sup>[17]</sup> and alkoxy silanes.<sup>[21,29]</sup> Prominent examples for hydrosilylation (Figure 1) of alkenes with phenylsilane are the  $\beta$ -diketiminate cobalt complexes reported by Holland,<sup>[19]</sup> the phosphine-iminopyridine cobalt complexes used by Huang<sup>[22]</sup> and the bis(carbene)cobalt-dinitrogen complex by Fout.<sup>[21]</sup> A carbonyl hydrosilylation is for example reported by the group of Peters, using diphosphine-borane cobalt-dinitrogen complexes.<sup>[28]</sup> The first step in the catalytic cycle of hydrosilylation reactions is commonly the oxidative addition of the silane substrate, forming metal-hydrides.<sup>[13]</sup> To assist this two-electron step on cobalt – a first row transition metal which has the tendency to undergo one-electron steps – the incorporation of cooperative ligands can be of interest.<sup>[28,30,31]</sup>

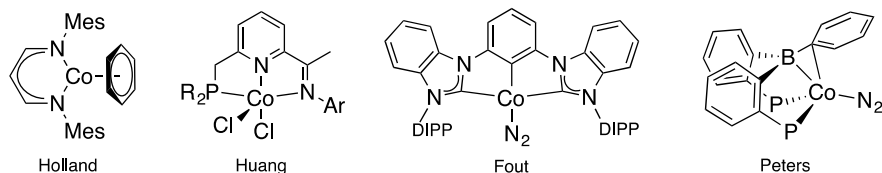


**Figure 1.** Examples of Co-catalysts for hydrosilylation reactions. P in most right structure:  $\text{P}^i\text{Pr}_2$ .

Our group is interested in the use of the diphosphine ketone ligand  $^{\text{Ph}}\text{dppb}$  (**1<sup>Ph</sup>**, Figure 2). Its coordination to the base metals Fe, Co, Ni and Cu is described (Chapter 2 and 3 of this thesis). Especially, exploration of the cobalt complexes in hydrosilylation reactions is of interest, given the recent success in the field.  $(^{\text{Ph}}\text{dppb})\text{CoCl}_2$  (**2<sup>Ph</sup>**) and  $(^{\text{Ph}}\text{dppb})\text{CoCl}$  (**3<sup>Ph</sup>**) were developed in Chapter 3, showing hemilabile behavior of the ketone moiety upon changing the oxidation state from Co(II) to Co(I), resulting in an  $\eta^2(\text{C},\text{O})$ -coordination in the latter complex (Figure 2). The hemilability of the ligand in combination with the low oxidation state of particularly the Co(I) complex makes for a good candidate in hydrosilylation reactions, to enable reactivity and electronic changes on the metal center. Herein, the catalytic activity of

these Co(I) and Co(II) complexes is described. The diphosphine ketone ligand  $^R\text{d}^{\text{Ph}}\text{bbp}$  is employed, equipped with *para*-tolylphosphine functionalities to improve solubility of the complexes, instead of the previously reported phenyl substituents.

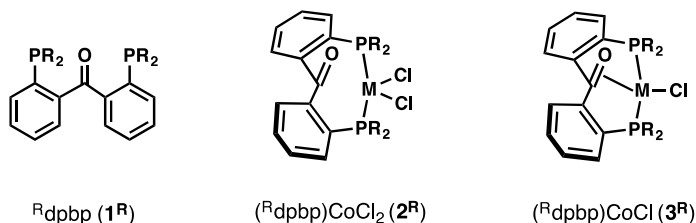
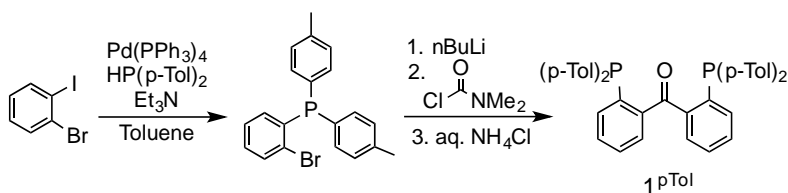


**Figure 2.** Structures of  $^R\text{d}^{\text{Ph}}\text{bbp}$  (left),  $(^R\text{d}^{\text{Ph}}\text{bbp})\text{CoCl}_2$  (middle) and  $(^R\text{d}^{\text{Ph}}\text{bbp})\text{CoCl}$  (right).  $1^{\text{Ph}}$ ,  $2^{\text{Ph}}$ ,  $3^{\text{Ph}}$ : R = Ph;  $1^{p\text{Tol}}$ ,  $2^{p\text{Tol}}$ ,  $3^{p\text{Tol}}$ : R = *p*-tolyl.

## 4.2 Results and Discussion

### 4.2.1 Synthesis of Co complexes

The synthesis of Co(I) complex  $(^{\text{Ph}}\text{d}^{\text{Ph}}\text{bbp})\text{CoCl}$  ( $3^{\text{Ph}}$ ) was described previously (Chapter 3 of this thesis).<sup>[30]</sup> An initial experiment with  $3^{\text{Ph}}$  in the hydrosilylation reaction of 1-octene with phenylsilane showed promising results: applying a high catalyst loading of 10 mol% in  $\text{C}_6\text{D}_6$  in a Young-type NMR tube resulted in full conversion of the substrates and formation of octylphenylsilane as the major product in 30 min. However, the low solubility of the precatalyst resulted in a turbid mixture during catalysis. To improve solubility, the phenyl groups of  $^{\text{Ph}}\text{d}^{\text{Ph}}\text{bbp}$  were replaced by *p*-tolyl groups, with the additional benefit of providing a convenient handle for NMR analysis of the complex. The ligand  $^{p\text{Tol}}\text{d}^{\text{Ph}}\text{bbp}$  ( $1^{p\text{Tol}}$ ) was synthesized in two steps similarly to its phenyl substituted analogue, *via* first a Pd-catalyzed cross coupling reaction to yield the *o*-bromo-substituted phenyldi-*p*-tolylphosphine precursor which was subsequently used in a double nucleophilic substitution reaction on dimethylcarbonylchloride, resulting in the diphosphine-ketone ligand (Scheme 1).<sup>[32]</sup>



**Scheme 1.** Synthesis of  $1^{p\text{Tol}}$ .

A Co(II) complex was formed by addition of  $^{p\text{Tol}}\text{d}^{\text{Ph}}\text{bbp}$  to  $\text{CoCl}_2$  in  $\text{CH}_2\text{Cl}_2$  resulting in  $(^{p\text{Tol}}\text{d}^{\text{Ph}}\text{bbp})\text{CoCl}_2$  ( $2^{p\text{Tol}}$ ) after workup. The  $^1\text{H}$  NMR spectrum shows the formation of a species

with signals from  $\delta$  18 to  $-2$  ppm, and no peak was observed in the corresponding  $^{31}\text{P}$  NMR spectrum, indicating the formation of a paramagnetic species. A distorted tetrahedral cobalt center is observed in the crystal structure of  $2^{p\text{Tol}}$  with the two phosphine tethers of the ligand coordinated to the metal center, next to two chloride ligands (Figure 3, left). The P–Co–P angle is  $115.734(16)^\circ$ , akin to  $2^{\text{Ph}}$  (Table 1). The ketone moiety of the ligand backbone has a C=O bond distance of  $1.2262(19)$  Å and Co–C and Co–O distances of  $3.3599(15)$  Å and  $3.0474(13)$  Å, respectively, and is not coordinated to cobalt. Reduction of the Co(II) complex with sodium naphthalide in THF results in the Co(I) complex  $(^{p\text{Tol}}\text{dppb})\text{CoCl}$  ( $3^{p\text{Tol}}$ ) after precipitation from the mixture with hexanes, followed by extraction of the product with THF and evaporation of the solvents.  $^1\text{H}$  NMR analysis indicates once more the formation of a paramagnetic species with signals from  $\delta$  33 to  $-17$  ppm. Distinctive signals for the *p*-tolyl methyl groups are present at  $\delta$  9.24 and 17.67 ppm, identified by integration and comparison to  $3^{\text{Ph}}$ , and the magnetic moment of the complex as measured by Evans method ( $\mu_{\text{eff}} = 2.8$ ) indicates a spin state of  $S = 1$ . Whereas the phenyl-substituted analogue  $3^{\text{Ph}}$  was reluctant to crystallization (Chapter 3), slow vapor diffusion of toluene/hexanes with  $3^{p\text{Tol}}$  resulted in single crystals suitable for XRD analysis. The crystal structure of  $3^{p\text{Tol}}$  reveals a tetrahedral geometry around Co with  $^{p\text{Tol}}\text{dppb}$  bound in a  $\kappa^4(\text{P,P,C,O})$ -fashion, including an  $\eta^2(\text{C,O})$ -coordination of the ketone, and coordination of both phosphine groups (Figure 3, right). Next to this, a chloride is bound to cobalt. The C–O bond is elongated due to  $\pi$ -backdonation in the  $\pi^*$  antibonding orbital of the ketone moiety from  $1.2262(19)$  Å in  $2^{p\text{Tol}}$  to  $1.307(6)$  Å in  $3^{p\text{Tol}}$ . This is similar to the elongation as found in the Fe(I) and Ni(I) complexes (C–O bond distance for Fe(II):  $1.218(3)$ , Fe(I):  $1.3296(14)$ , Ni(II):  $1.2288(16)$  and Ni(I):  $1.310(2)$  Å).<sup>[30]</sup>

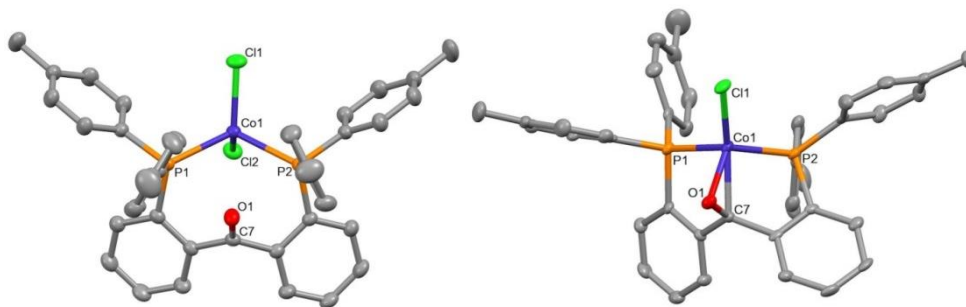


**Figure 3.** XRD structures of  $2^{p\text{Tol}}$  (left) and  $3^{p\text{Tol}}$  (right). Hydrogen atoms are omitted for clarity and the ellipsoids are shown at 50% probability level. In  $2^{p\text{Tol}}$ : the co-crystallized THF molecule was omitted for clarity.

**Table 1.** Crystal structure comparison of the cobalt complexes. Selected distances (Å) and angles (°).

	Co–O1	Co–C7	C7–O1	P1–Co–P2	Dihedral angle*	IR C=O (cm <sup>-1</sup> )
<b>2<sup>Ph</sup></b>	2.9255(13)	3.2896(18)	1.227(2)	116.676(18)	36.16(9)	1647
<b>2<sup>pTol</sup></b>	3.0474(13)	3.3599(15)	1.2262(19)	115.734(16)	34.03(8)	1663
<b>3<sup>pTol</sup></b>	1.947(3)	2.071(5)	1.307(6)	109.62(6)	64.2(2)	~1300

\* The dihedral angle is calculated between the two phenyl rings connected to the carbonyl group.

### 4.2.2 Hydrosilylation reactions

The reactivity of Co(I) complex **3<sup>pTol</sup>** with phenylsilane was explored. Addition of 3 eq of PhSiH<sub>3</sub> to **3<sup>pTol</sup>** in C<sub>6</sub>D<sub>6</sub> leads to an exothermic reaction, resulting in a mixture of species. The <sup>1</sup>H NMR spectrum shows a diamagnetic spectrum containing three broad signals around δ – 12 ppm, of which one exhibits apparent triplet multiplicity, consistent with the presence of one or more diamagnetic Co(I)-hydride species (Appendix D, Figure D5-6).<sup>[33,34]</sup> Attempts to perform further analyses were unsuccessful due to the high reactivity of the obtained Co–H species, therefore the structure has not been elucidated. Nevertheless, the high reactivity prompted for further investigation on catalytic hydrosilylation by **3<sup>pTol</sup>**.

Pre-catalyst **3<sup>pTol</sup>** is active in the hydrosilylation reaction of 1-octene with phenylsilane, resulting in 98% conversion of both substrates with 84% octylphenylsilane as product (Table 2, Entry 1). Initial optimization lead to the following standard conditions: 1 mol% **3<sup>pTol</sup>**, a reaction time of 1 h at room temperature under neat conditions. The catalyst exhibits full selectivity toward the anti-Markovnikov, i.e. linear, product, as shown by APT <sup>13</sup>C NMR after its isolation. Only a single signal containing the opposite phasing is observed in the aliphatic region of the <sup>13</sup>C NMR spectrum, corresponding to the single CH<sub>3</sub> group in the resulting product (Figure 4). Furthermore, analyses by <sup>1</sup>H NMR and GC(MS) confirmed the presence of a single product isomer.

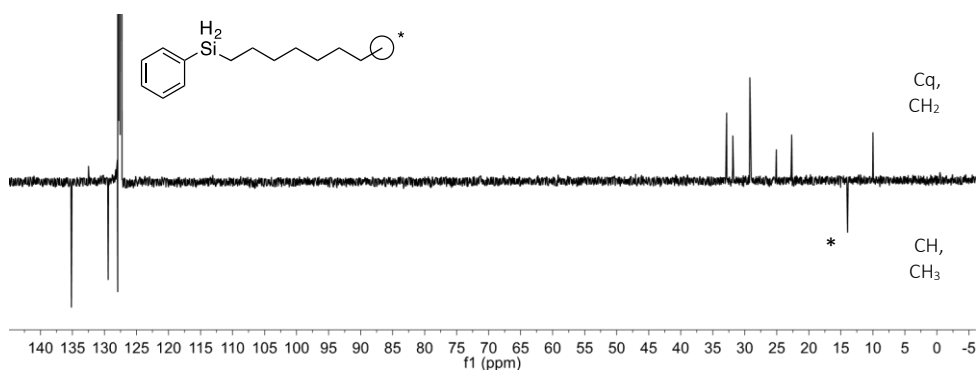
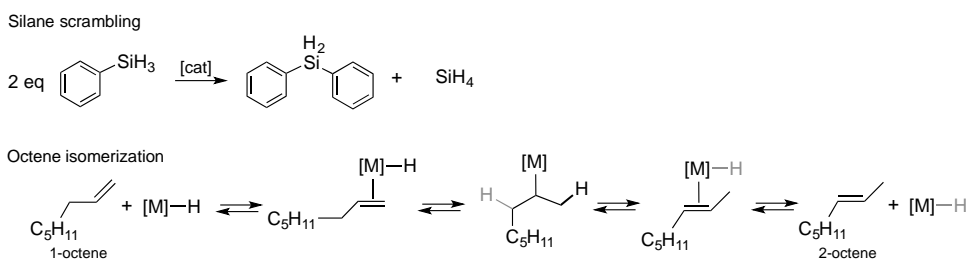


**Figure 4.** APT <sup>13</sup>C NMR spectrum after hydrosilylation of 1-octene with PhSiH<sub>3</sub> by **3<sup>pTol</sup>** forming octylphenylsilane, containing one signal (\*) with the opposite phasing in the aliphatic region.

Analysis was performed by GC-MS and NMR for product characterization and GC for quantitative analysis. Besides remaining starting materials and formed product, three main side-products are observed.  $\text{Ph}_2\text{SiH}_2$  is formed with a yield of 5%, which is explained by a scrambling reaction of  $\text{PhSiH}_3$  (Scheme 1). Besides GC and GC-MS analyses,  $\text{Ph}_2\text{SiH}_2$  was also characterized using NMR techniques. The  $\text{SiH}_2$  moiety gives rise to a distinctive peak in  $^1\text{H}$  NMR at  $\delta$  5.04 ppm ( $J_{\text{HSi}} = 198$  Hz) and in  $^{29}\text{Si}$  NMR a peak is observed at  $\delta$   $-33.75$  ppm, which were confirmed to belong to  $\text{Ph}_2\text{SiH}_2$  by comparison to an authentic sample. Completing the stoichiometry in this reaction would result in the formation of one equivalent of  $\text{SiH}_4$ , which however could not be detected directly, presumably due to its high volatility. To account for the incorporated silane in this byproduct, it is assumed that the amount is equal to the amount of  $\text{Ph}_2\text{SiH}_2$ . This silane scrambling is a known side-reaction in hydrosilylation reactions<sup>[35-37]</sup> and it hampers product formation as it converts  $\text{PhSiH}_3$  to less reactive side-products. A slight excess of 1.1 equivalents of  $\text{PhSiH}_3$  was therefore used to maximize the yield of hydrosilylation reactions.

Furthermore, formation of octane (2%) was observed, which can tentatively be explained by a reduction of the double bond, and formation of 2- and 3-octene (both 3%) is observed. These latter products likely originate from isomerization of the carbon-carbon double bond of 1-octene, which may proceed via a separate catalytic cycle, catalyzed by  $\mathbf{3}^{\text{pTol}}$ . A test reaction for the conditions of isomerization was performed. 1-Octene was mixed with 1 mol% of  $\mathbf{3}^{\text{pTol}}$  and stirred for 4 h at room temperature, which did not lead to any side-product formation. To proceed, the reaction likely needs a hydride source, i.e.  $\text{PhSiH}_3$ , to form the active  $\text{Co-H}$  catalyst (Scheme 2). The  $\text{Co-H}$  catalyzed reaction is assumed to follow a mechanism as proposed by Cramer in 1966,<sup>[38]</sup> in which the double bond of 1-octene initially coordinates in an  $\eta^2$ -fashion to  $\text{Co}$ , followed by addition of the hydride to  $\text{C}_\alpha$ . Next, the hydride positioned at  $\text{C}_\gamma$  is added to  $\text{Co}$ , and the substrate dissociates from the metal resulting in 2-octene and the  $\text{Co-H}$  catalyst (Scheme 2).



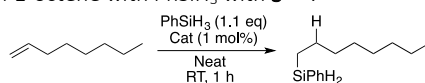
**Scheme 2.** Observed side-products and possible side-reaction pathways.

With the benchmark hydrosilylation of 1-octene with phenylsilane established, a number of control experiments were performed to validate the need of the pre-catalyst. Experiments without the addition of a catalyst showed no conversion of the substrates and no product

formation (Table 2, Entry 2). Using 1 mol% of  $\text{CoCl}_2$  as catalyst without addition of a co-ligand leads to low conversion of the substrates, i.e. 4% conversion of 1-octene and 16% conversion of phenylsilane, but no formation of the product was observed. Conversion of the substrates is attributed to ongoing heterogeneous processes (Table 2, Entry 3), as a result of the poor solubility of  $\text{CoCl}_2$  in organic solvents. Addition of  $\text{PPh}_3$  in combination with  $\text{CoCl}_2$  again lead to low conversion of 1-octene (3%), but high conversion of phenylsilane was obtained (95%) (Table 2, Entry 4). The products of 1-octene conversion were analyzed as the isomerization (3%) and hydrogenation (traces) products. The product of phenylsilane conversion is unknown, but it is likely that a minor fraction was used in the formation of hydride species, as these are needed for the 1-octene based side reactions (*vide supra*).

Comparison of Co(II) complex  $\mathbf{2}^{pTol}$  to Co(I) complex  $\mathbf{3}^{pTol}$  shows lower conversion of the substrates when using  $\mathbf{2}^{pTol}$ : 42% for 1-octene and 60% for phenylsilane with a lower selectivity toward octylphenylsilane, resulting in a yield of 32% (Table 2, Entry 5). Low amounts of the 1-octene based side products were obtained and no silane scrambling was observed. The higher yield when using  $\mathbf{3}^{pTol}$  could be explained by the reduced Co center, the  $\eta^2(\text{CO})$ -coordination of the ligand, or a combination of these two. It is also plausible that the same active species is generated, albeit less efficiently, via reduction of the Co(II) complex by the silane. Comparison of  $\mathbf{3}^{pTol}$  to its phenyl substituted analogue  $\mathbf{3}^{Ph}$  shows a somewhat lower product yield of 75% caused by lower solubility of  $\mathbf{3}^{Ph}$  as performing the reaction in THF results in 86% yield (Table 2, Entry 6-7, respectively).

**Table 2.** The hydrosilylation of 1-octene with  $\text{PhSiH}_3$  with  $\mathbf{3}^{pTol}$ .



	Catalyst	Conversion Silane	Conversion Alkene	Product Yield	Isomerization 1-octene	Octane	$\text{Ph}_2\text{SiH}_2$ <sup>[A]</sup>
1	$\mathbf{3}^{pTol}$	98	98	84	6	2	5
2	No cat	-	-	-	-	-	-
3	$\text{CoCl}_2$	16	4	-	-	-	-
4	$\text{CoCl}_2 + \text{PPh}_3$	95	3	-	3	Traces	-
5	$\mathbf{2}^{pTol}$	60	42	32	4	1	-
6	$\mathbf{3}^{Ph}$	99	98	75	5	2	3
7	$\mathbf{3}^{Ph} + \text{THF}$	99	99	86	6	1	3

All amounts are all given in percentage. Conversion is determined by GC (for more info, see Appendix D). <sup>[A]</sup> Amount of  $\text{SiH}_4$  is considered equimolar to  $\text{Ph}_2\text{SiH}_2$ .

### 4.2.3 Substrate scope

Extending the alkene substrate scope, styrene was explored in a hydrosilylation reaction with  $\text{PhSiH}_3$  catalyzed by  $\mathbf{3}^{\text{PTol}}$ . The reaction conditions were slightly changed to enhance product formation, to an extended reaction time of 4 h, and THF was used as the solvent instead of neat conditions. The hydrosilylation of styrene proceeded to a low yield of 7% (Table 3, Entry 1). Product determination by GC-MS,  $^1\text{H}$  NMR,  $^{13}\text{C}$  NMR and 2D  $^1\text{H}$ - $^1\text{H}$  COSY NMR (Appendix D, Figure D1-3), and subsequent quantitative analysis by GC showed the formation of both the Markovnikov and anti-Markovnikov product with respective yields of 3% and 4%. Formation of the Markovnikov and anti-Markovnikov products is commonly observed when using styrene.<sup>[7,39]</sup> The catalytic selectivity of styrene hydrosilylation with  $\mathbf{3}^{\text{PTol}}$  is significantly lower, as a styrene conversion of 17% and a silane conversion of 31% is obtained after 4 h. Besides silane scrambling, a number of unidentified byproducts were observed in small quantities. Increasing the reaction time to 24 h did not improve the reaction significantly, as only the conversion improved poorly and larger amount of byproduct diphenylsilane was obtained (Table 3, Entry 2). Low conversion of styrene is presumably due to delocalization of the double bond along the complete molecule as a consequence of the extended conjugated  $\pi$ -system, resulting in a less reactive C=C bond. Therefore, the hydrosilylation of allylbenzene was explored next, to investigate the difference upon changing to an elongated chain between the olefin and phenyl ring. Reaction of 4 h in THF resulted in 96% conversion of allylbenzene, 97% conversion of phenylsilane and a product yield of 84%, with full selectivity toward the anti-Markovnikov product over the possible Markovnikov product formation (Table 3, Entry 3; Appendix D, Figure D4). Diphenylsilane was again obtained as a byproduct (4%). The significantly higher product yield in comparison to the hydrosilylation reaction of styrene shows that the extra  $\text{CH}_2$  group in the substrate makes for a great difference in reactivity, explained by the lesser extent of the conjugated  $\pi$ -system of allylbenzene.

The activity of  $\mathbf{3}^{\text{PTol}}$  with a ketone was explored in the hydrosilylation of acetophenone. This is generally known to be a more reactive substrate, due to the polarized nature of the carbon-oxygen double bond. The reaction of acetophenone with phenylsilane at RT for 4 h in THF catalyzed by 1 mol%  $\mathbf{3}^{\text{PTol}}$ , lead to an excellent yield of the hydrosilylated product phenyl(1-phenylethoxy)silane (>99%) (Table 3, Entry 4). The product was quantified by GC and GC-MS analyses after acidification, forming the alcohol species 1-phenylethanol.



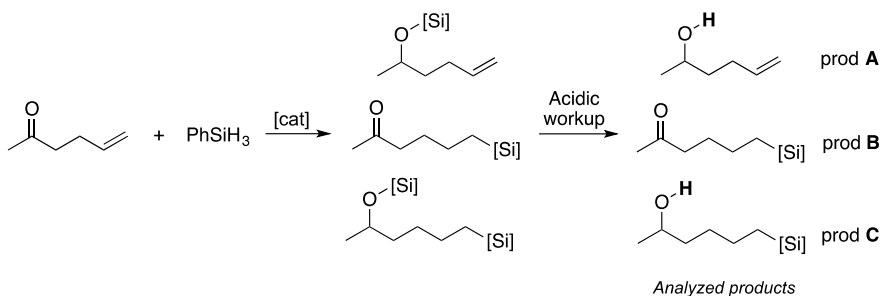
**Table 3.** Substrate scope of the hydrosilylation reactions with **3<sup>pTol</sup>**.

	Time	Substrate	Conversion Silane	Conversion Substrate	Product Yield	Ph <sub>2</sub> SiH <sub>2</sub> <sup>[A]</sup>
1	4 h	Styrene	31	17	7 (3:4) <sup>[B]</sup>	5
2	24 h	Styrene	39	20	7 (3:4) <sup>[B]</sup>	7
3	4 h	Allylbenzene	97	96	84	4
4	4 h	Acetophenone	92	>99	>99 <sup>[C]</sup>	4

All amounts are all given in percentage. Conversion is determined by GC (see Appendix D). <sup>[A]</sup> Amount of SiH<sub>4</sub> is considered equimolar to Ph<sub>2</sub>SiH<sub>2</sub>. <sup>[B]</sup> Markovnikov:anti-Markovnikov product, ratio determined by NMR and GC. <sup>[C]</sup> Analysis of 1-phenylethanol.

#### 4.2.4 Chemoselectivity

Combining both an olefinic and ketone functionality in one substrate gives insight in possible chemoselectivity of the catalyst, for which the hydrosilylation of 5-hexen-2-one with PhSiH<sub>3</sub> was performed. After the reaction, an acidic workup was performed before analysis by GC. Addition of 2.1 equivalents of silane results in full conversion of both the olefin and ketone functionality after 24 h (Figure 5, product **C**), showing the catalysts capability of double addition on one substrate. Addition of a limiting amount of silane, i.e. 1 equivalent, is more indicative of the catalysts behavior regarding chemoselectivity. After reaction for 4 h the substrates did not yet reach full conversion and GC analysis showed, next to 5-hexen-2-one and PhSiH<sub>3</sub>, the three products of hydrosilylation (Figure 5) on a) the ketone, b) the olefin, c) both the ketone and olefin, in a 1:1:1 ratio, forming products **A**, **B** and **C**, respectively. Hence, the catalyst does not discriminate between a terminal olefin and a ketone under the chosen conditions, and the second addition seems to have a higher rate as this is obtained in similar ratio.

**Figure 5.** Products of the chemoselectivity experiment. Acidic workup was applied before analysis.

#### 4.2.5 Discussion of the mechanism

Cobalt-catalyzed hydrosilylation is a growing field with a number of highly efficient catalysts reported in recent years. The Co-catalyzed hydrosilylation reactions reported by Holland,<sup>[19]</sup> Huang<sup>[22]</sup> and Fout<sup>[21]</sup> (*vide supra*, Figure 1) are proposed to follow the Chalk-Harrod mechanism, in agreement with an in-depth investigation on mechanistic aspects, using a Co-bound phosphine substituted 2-iminopyridine ligand, as published by Rauchfuss, van Gastel and co-workers.<sup>[40]</sup> A rare example in which the specific role of a cooperative ligand is determined was shown by Peters and co-workers with a diphosphine-borane cobalt-dinitrogen complex (Figure 1, right), where the silane substrate is activated between the metal and the ligand backbone by addition of  $-\text{SiHPh}_2$  to Co and insertion of the hydride into the Co–B bond.<sup>[28]</sup>

The role – if any – of the ketone moiety in cobalt catalysts presented herein cannot be established with certainty from the data at hand. It could exhibit hemilabile behavior upon changing the oxidation state of the metal center (Chapter 3). It could also be envisioned that the ketone moiety reversibly accepts a hydride under catalytic conditions in analogy to the borane in Peters' catalyst, or that it undergoes hydrosilylation to generate the catalytically active species, analogously to the Ni-imine complexes described in Chapter 6. Investigations of the reaction of the Co-precatalyst with phenylsilane suggest activation by formation of Co–H species, consistent with the Chalk-Harrod mechanism.<sup>[13]</sup> However, the exact nature of these species is unclear, and further investigations would be required to address details of the mechanism.

### 4.3 Conclusions

The investigated cobalt complexes equipped with a diphosphine-ketone ligand ( $^R\text{dpbp}$ ) are active catalysts in hydrosilylation reactions with phenylsilane, showing a first example of catalysis with this family of complexes. Both,  $2^{\text{PTol}}$  and  $3^{\text{PTol}}$  are active in the hydrosilylation of 1-octene with phenylsilane, but  $3^{\text{PTol}}$  is superior. The Co(I) catalyst proceeds under very mild conditions of 1 h, room temperature and without the need of a solvent, resulting in 84% of octylphenylsilane. Extending the scope of the alkene substrate was performed to a small extent, showing that the hydrosilylation of styrene leads to a low yield, whereas full conversion was reached using allylbenzene. The hydrosilylation of a polar double bond was shown to be the most facile reaction, with full substrate conversion and high selectivity for the product with >99% yield. The observed high catalytic reactivity combined with excellent product selectivity adds to the quickly developing field of Co-catalyzed hydrosilylation reactions. Further investigation of the mechanism would be of interest for the development of a better understanding of possible metal-ligand cooperativity, as well as exploration of the substrate scope.

## 4.4 Experimental section

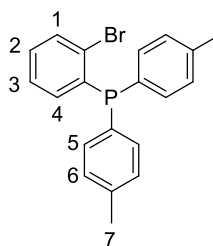
### 4.4.1 General considerations

Unless stated otherwise, all reagents were purchased from commercial sources and used as received. Reactions are performed in a N<sub>2</sub>-filled glovebox at room temperature with dry, degassed solvents. Deuterated benzene (C<sub>6</sub>D<sub>6</sub>) and deuterated dichloromethane (CD<sub>2</sub>Cl<sub>2</sub>) were degassed using the freeze-thaw-pump method (4x) and subsequently stored over molecular sieves. Dry diethylether, toluene and hexane were taken from an MB SPS-800 solvent purification set-up and degassed by bubbling N<sub>2</sub> through the solvent for 30 min and were further dried overnight over molecular sieves. CH<sub>2</sub>Cl<sub>2</sub> was distilled over CaH<sub>2</sub> and tetrahydrofuran (THF) was distilled over sodium/benzophenone before use, both were degassed by bubbling N<sub>2</sub> through it for 30 min and stored over molecular sieves. THF, ether or petroleum ether (40-60 °C) used for column chromatography and calibration curve preparation were wet solvents of technical purity. Diphenylphosphine, Pd(PPh<sub>3</sub>)<sub>4</sub>, CoCl<sub>2</sub>, metallic sodium and naphthalene were placed in the glovebox without additional purification. *o*-Bromiodobenzene, Et<sub>3</sub>N and all substrates were degassed by bubbling N<sub>2</sub> for 30 min and dried over molecular sieves before use in the glovebox.

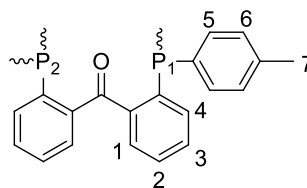
<sup>1</sup>H, <sup>13</sup>C, <sup>29</sup>Si and <sup>31</sup>P NMR spectra (respectively 400, 100, 80 and 161 MHz) were recorded on an Agilent MRF400 or a Varian AS400 spectrometer at 25 °C. <sup>1</sup>H and <sup>13</sup>C NMR chemical shifts are reported in ppm relative to TMS using the residual solvent resonance as internal standard. <sup>31</sup>P NMR chemical shifts are externally referenced to 85% aqueous H<sub>3</sub>PO<sub>4</sub> and <sup>29</sup>Si NMR chemical shifts are externally referenced to TMS. Infrared spectra were recorded using a Perkin Elmer Spectrum One FT-IR spectrometer equipped with a N<sub>2</sub> flow over the crystal. UV-Vis spectra were measured using a Lambda 35 UV-Vis spectrometer. The UV-Vis samples were prepared under a N<sub>2</sub> atmosphere and sealed with a Teflon cap after which the spectra were recorded directly. ESI-MS spectra were recorded on a Walters LCT Premier XE KE317 Micromass Technologies spectrometer. Compounds of which elemental analysis is reported were either recrystallized or precipitated and dried under high vacuum overnight before submission and analysis was performed by the Mikroanalytisches Laboratorium Kolbe, Mülheim an der Ruhr, Germany. Gas chromatography mass spectrometry was carried out on a PerkinElmer Clarus 680 Gas Chromatograph with a PE Elite 5MS 15 m x 0.25 mm x 0.25 μm column, connected to a PerkinElmer Clarus SQ 8 T Mass Spectrometer. Gas chromatography was carried out on a PerkinElmer Clarus 500 Gas chromatograph with an Alltech Econocap™ ec TM 30.0 m x 0.32 mm ID x 0.25 μm, 5% phenyl and 95% methylpolysiloxane column. In general method 1 was used: 50 °C for 3 min, 40 °C/min increase for 5.75 min to reach 280 °C, 280 °C for 3 min (total 11.75 min). For analysis of reactions using 5-hexen-2-one, method 2 was used: 50 °C for 3 min, 5 °C/min increase for 46 min to reach 280 °C, 280 °C for 3 min (total 52 min). Compounds of which elemental analysis is reported were either recrystallized or precipitated and dried under high vacuum overnight before submission and analysis was performed by the Mikroanalytisches Laboratorium Kolbe, Mülheim an der Ruhr, Germany. Details on X-ray crystal structure determination and selected spectra are given in Appendix D.

#### 4.4.2 Synthesis

***o*-Bromophenyl-di-*p*-tolylphosphine:**<sup>[41]</sup> *o*-Bromiodobenzene (6 mL, 46.7 mmol) was dissolved in toluene (10 mL) in a Schlenk tube under N<sub>2</sub> atmosphere. In consecutive order, a mixture of di-*p*-tolylphosphine (10.1 g, 46.7 mmol) in toluene (15 mL), dry Et<sub>3</sub>N (10 mL, 70.1 mmol) and Pd(PPh<sub>3</sub>)<sub>4</sub> (296 mg, 0.26 mmol) in toluene (20 mL) were added resulting in a yellow solution. The mixture was heated to 80 °C for 12 h, after which the deep brown mixture was washed with brine (2 x 65 mL). The aqueous phase was extracted with Et<sub>2</sub>O (2 x 75 mL, 4 x 35 mL). The combined organic layers were dried with MgSO<sub>4</sub>, filtered and the solvent was evaporated. Cold MeOH (3 x 15 mL) was used to wash the crude product. The product was dried in vacuum and isolated as an off-white powder (14.7 g, 39.7 mmol, 85%). <sup>1</sup>H NMR (C<sub>6</sub>D<sub>6</sub>): δ<sub>H</sub> 7.34 (ddd, <sup>3</sup>J<sub>HH</sub> = 7.9, <sup>3</sup>J<sub>HP</sub> = 3.6 Hz, <sup>4</sup>J<sub>HH</sub> = 1.2 Hz, 1H, H4), 7.29 (t, <sup>3</sup>J<sub>HH</sub> = 7.8 Hz, <sup>3</sup>J<sub>HP</sub> = 7.8 Hz, <sup>4</sup>J<sub>HH</sub> = 1.7 Hz, 4H, H5), 6.93 (dt, <sup>3</sup>J<sub>HH</sub> = 7.7 Hz, <sup>3</sup>J<sub>HP</sub> 2.1 Hz, <sup>4</sup>J<sub>HH</sub> = 2.1 Hz, 1H, H1), 6.87 (d, <sup>3</sup>J<sub>HH</sub> = 7.7 Hz, 4H, H6), 6.76 (td, <sup>3</sup>J<sub>HH</sub> = 7.5 Hz, <sup>4</sup>J<sub>HH</sub> = 1.2 Hz, 1H, H3), 6.64 (td, <sup>3</sup>J<sub>HH</sub> = 7.7 Hz, <sup>4</sup>J<sub>HH</sub> = 1.7 Hz, 1H, H2), 1.97 (s, 6H, 7) ppm. <sup>13</sup>C NMR (C<sub>6</sub>D<sub>6</sub>): δ<sub>C</sub> 138.61, 134.43, 134.25, 134.05, 132.94 (d, J = 2.2 Hz), 129.69, 129.48, 129.41, 127.05, 20.78 ppm. <sup>31</sup>P NMR (C<sub>6</sub>D<sub>6</sub>): δ<sub>P</sub> -6.31 ppm.



***p*<sup>Tol</sup>dppb (1<sup>pTol</sup>):** *o*-Bromophenyl-di-*p*-tolyl-phosphine (4.93 g, 13.4 mmol) was suspended in Et<sub>2</sub>O (30 mL). The light-yellow suspension was cooled to -50 °C using an acetone dry ice bath. *n*-BuLi (1.6 M in hexane, 16 mmol, 10 mL) was added drop wise while stirring, resulting in a rapid color change from yellow to brown. Within 30 min, the reaction mixture was allowed to warm up to room temperature and was directly cooled down again to -50 °C, after which a solution of N,N-dimethylcarbamoylchloride (0.61 mL, 6.5 mmol) in Et<sub>2</sub>O (15 mL) was added drop wise over 20 minutes.



During addition, the temperature of the bath was kept between -35 °C and -45 °C, after which the suspension was stirred overnight allowing the mixture to warm up to room temperature. The reaction was cooled down again and treated at 0 °C with a degassed 2.5 M NH<sub>4</sub>Cl solution in water (38 mL, 4.5 g, 85 mmol NH<sub>4</sub>Cl) turning the suspension orange-yellow. The product was extracted with Et<sub>2</sub>O and dried with MgSO<sub>4</sub> and solvents were evaporated. The obtained yellow compound was washed with MeOH, resulting in the product as a yellow powder after solvent removal (2.41 g, 4.0 mmol, 61%). <sup>1</sup>H NMR (C<sub>6</sub>D<sub>6</sub>): δ<sub>H</sub> 7.37 (t, J = 7.6 Hz, 8H, H5), 7.37 (m, 2H, H4), 7.31 (dd, J = 7.7, 2.4 Hz, 2H, H1), 6.95 (td, J = 7.5, 1.1 Hz, 2H, H2/3), 6.91 (d, J = 7.7 Hz, 8H, H6), 6.83 (td, J = 7.5, 1 Hz, 2H, H3/2), 2.03 (s, 12H, H7) ppm. <sup>13</sup>C NMR (CDCl<sub>3</sub>): δ<sub>C</sub> 197.35 (t, J = 3 Hz, C=O), 144.64 (dd, J = 24.4, 1 Hz, Cq<sup>Ar</sup>), 140.68 (J = 26.1, 2.2 Hz, Cq<sup>Ar</sup>), 138.21 (Cq<sup>Ar</sup>), 135.56 (dt, J = 3, 11 Hz, Cq<sup>Ar</sup>), 135.00 (CH<sup>Ar</sup>), 134.45 (m, CH<sup>Ar</sup>), 131.03 (t, J = 3.3 Hz, CH<sup>Ar</sup>), 130.66 (CH<sup>Ar</sup>), 129.48 (m, CH<sup>Ar</sup>), 128.00 (CH<sup>Ar</sup>), 21.21 (-CH<sub>3</sub>) ppm. <sup>31</sup>P NMR (C<sub>6</sub>D<sub>6</sub>): δ<sub>P</sub> -9.77 ppm. ATR-IR ν: 3012, 2956, 2920, 2863, 1910, 1738, 1664, 1598, 1495, 1446, 1395, 1296, 1271, 1243, 1185, 1090, 1018, 928, 805, 747, 637, 507 cm<sup>-1</sup>. ESI-MS (MeCN AgNO<sub>3</sub>/H<sub>2</sub>O) m/z: [2M+Ag]<sup>+</sup>: 1319.3529, calc: 1319.3534. Elemental analysis: calcd: C 81.17, H 5.98, found: C 80.84, H 6.05.

***p*<sup>Tol</sup>dppb)CoCl<sub>2</sub> (2<sup>pTol</sup>):** *p*<sup>Tol</sup>dppb (101.0 mg, 0.17 mmol) and CoCl<sub>2</sub> (65.0 mg, 0.16 mmol) were suspended in CH<sub>2</sub>Cl<sub>2</sub> (5 mL) and stirred for 17 h, resulting in a green solution. The product was precipitated from CH<sub>2</sub>Cl<sub>2</sub>/hexane, collected via filtration, extracted using CH<sub>2</sub>Cl<sub>2</sub> and dried in vacuum resulting in a green powder (88.2 mg, 0.12 mmol, 72%). <sup>1</sup>H NMR (CD<sub>2</sub>Cl<sub>2</sub>): δ<sub>H</sub> 18.82, 13.63, 11.77, 9.99, 7.88, 0.54, 0.10, -

0.55 ppm. ATR-IR v: 1634, 1499, 1286, 1096, 805. Solution cell IR (THF,  $\text{cm}^{-1}$ ): 1662, 1598 (weak)  $\text{cm}^{-1}$ . ESI-MS m/z:  $[\text{M}-\text{Cl}]^+$  obs. 700.1297, calcd. 700.1262. UV-Vis ( $\text{CH}_2\text{Cl}_2$ )  $\lambda_{\text{max}}$ , nm: 603, 650, 734, 760. Elemental Analysis: calcd: C 66.02, H 5.42, found: C 66.86, H 4.93.

**( $p^{\text{Tol}}$ dpbp)CoCl ( $3^{p^{\text{Tol}}}$ ):** Naphthalene (79.9 mg, 0.62 mmol) was dissolved in THF (4 mL). A lump of  $\text{Na}^0$  was added and the mixture was stirred for 3 h, after which a dark green solution was obtained.  $\text{CoCl}_2$  (65.0 mg, 0.50 mmol) and  $p^{\text{Tol}}$ dpbp (300.6 mg, 0.49 mmol) were suspended in THF (25 mL) and cooled to  $-78^\circ\text{C}$ . The naphthalide solution was filtered and added to the cooled Co-mixture. This final mixture was stirred further for 1 h at  $-78^\circ\text{C}$  and for 18 h at room temperature, after which it was concentrated in vacuum to  $\sim 1.5$  mL. Hexane was added (5 mL) and the precipitated solids were collected by filtration. The product was extracted with THF and dried in vacuum, resulting in ( $p^{\text{Tol}}$ dpbp)CoCl as a brown powder with a yield of 86% (300.3 mg, 0.43 mmol).  $^1\text{H}$  NMR ( $\text{C}_6\text{D}_6$ ):  $\delta_{\text{H}}$  31.59, 20.00, 17.64 (s, 3H,  $-Me$ ), 14.34, 13.54, 9.21 (s, 3H,  $-Me$ ),  $-0.06$ ,  $-0.98$  (broad),  $-6.07$ ,  $-7.97$ ,  $-16.38$  ppm. ATR-IR v: 2919, 2863, 1599, 1498, 1434, 1397, 1258, 1241, 1189, 1096, 1019, 917, 803, 777, 693, 626, 510  $\text{cm}^{-1}$ . UV-Vis:  $\lambda_{\text{max}}$ : 525 nm. Elemental analysis: calcd: C 70.24, H 5.18, found: C 70.00, H 5.37.

#### 4.4.3 Catalysis

All catalytic reactions were performed *in duplo* and given values are the average of the two runs, unless stated otherwise. Conversion and yield were determined by GC analysis, for which calibration curves were prepared for all substrates and products. The yields of product arising from 1-octene isomerization were determined using the calibration curve for 1-octene. Next to the characterized and quantified products, a number of small signals (GC area  $>1\%$ ) were generally obtained in GC analysis. These products could not be identified, and are therefore not described in the analysis. Analysis of the hydrosilylation products of styrene and allylbenzene are given in Appendix D.

**Hydrosilylation method 1** (Table 2): In a glovebox, catalyst (0.01 mmol) was added to a 6 mL vial. 1-Octene (0.160 mL, 1.0 mmol) was added. Addition of  $\text{PhSiH}_3$  (0.135 mL, 1.1 mmol) while stirring caused bubbling of the mixture, and resulted in a clear brown solution after 1 minute. The solution was stirred for 1 h at room temperature and then taken out of the glovebox, where it was opened in air. The mixture was filtered over a plug of silica ( $\sim 1$  cm) using THF as eluent (total amount of mixture: 25 mL) to remove cobalt. From this a GC-MS sample was taken. For GC analysis, 1 mL of the prepared solution was added to 2.5 mL of a mesitylene (Mes) solution (internal standard, 0.017 M Mes solution: 102.4 mg Mes in 50 mL THF) and THF was added to a total volume of 10 mL.

**Hydrosilylation method 2** (Table 3, Entry 1-3): In a glovebox,  $3^{p^{\text{Tol}}}$  (7.0 mg, 0.01 mmol) was dissolved in THF (1 mL) resulting in a clear brown solution. A mixture of two substrates was added with a syringe while stirring. The solution was stirred for 4 h at room temperature and then taken out of the glovebox and opened in air. The mixture was filtered over a silica plug ( $\sim 1$  cm) using THF as eluent (total amount of mixture: 25 mL) to remove cobalt. From this a GC-MS sample was taken. For GC analysis, 1 mL of the prepared solution was added to 2.5 mL of a mesitylene (Mes) solution (internal standard, 0.017 M Mes solution: 102.4 mg Mes in 50 mL THF) and THF was added to a total volume of 10 mL.

**Hydrosilylation method 3** (Table 3, Entry 4; chemoselectivity experiment): In a glovebox, **3<sup>pTol</sup>** (7.0 mg, 0.01 mmol) was added to a small vial and dissolved in THF (1 mL) resulting in a clear brown solution. A mixture of two substrates was added with a syringe while stirring. The solution was stirred for 4 h at room temperature and taken out of the glovebox and opened in air. The reaction mixture was transferred to a separation funnel using Et<sub>2</sub>O and quenched with a HCl solution (2.5 mL, 10%) to form the alcohol product. The aqueous layer was removed, and the organic layer was washed with H<sub>2</sub>O (0.2 mL). The aqueous layer was washed Et<sub>2</sub>O (3 x 2 mL). The Et<sub>2</sub>O fractions were filtered over a silica plug (~1 cm, total volume after Et<sub>2</sub>O addition: 25 mL). For GC analysis, 1 mL of the prepared solution was added to 2.5 mL of a mesitylene (Mes) solution (internal standard, 0.017 M Mes solution: 102.4 mg Mes in 50 mL THF) and THF was added to a total volume of 10 mL. For NMR analysis, the solvent and precursors were evaporated in vacuum resulting in a turbid white liquid.

**Isolation of octylphenylsilane:** In a nitrogen-filled glovebox, **3<sup>pTol</sup>** (21.0 mg, 0.03 mmol) was dissolved in THF (1 mL). 1-Octene (0.470 mL, 3.0 mmol) and PhSiH<sub>3</sub> (0.405 mL, 3.3 mmol) were subsequently added, and bubbling occurred upon addition of the latter. The clear brown solution was stirred for 4 h and taken out of the glovebox. Air was bubbled through the solution for 20 min to quench the catalyst, turning the solution green. Cobalt was removed by filtration over a silica plug (~1 cm) with petroleum ether. The product was isolated by column chromatography using petroleum ether as the eluent. Evaporation of the solvents in vacuum resulted in a turbid white liquid (319 mg, 1.45 mmol, 48%). <sup>1</sup>H NMR (C<sub>6</sub>D<sub>6</sub>): δ 7.52-7.43 (m, 3H, Ar-H), 7.18-7.01 (m, 2H, Ar-H), 4.48 (t, <sup>3</sup>J<sub>HH</sub> = 3.7 Hz, <sup>2</sup>J<sub>H<sub>Si</sub></sub> = 190.99 Hz, 2H, Si-H<sub>2</sub>), 1.47-1.37 (m, 2H, -CH<sub>2</sub>), 1.33-1.13 (m, 10H, -CH<sub>2</sub>), 0.94-0.87 (t, <sup>3</sup>J<sub>HH</sub> = 6.9 Hz, 3H, -CH<sub>3</sub>), 0.87-0.79 (m, 2H, -CH<sub>2</sub>) ppm. <sup>13</sup>C NMR (C<sub>6</sub>D<sub>6</sub>): δ 135.59 (Ar-CH), 132.91 (Ar-CH), 129.85 (Ar-CH), 128.36 (Ar-CH), 33.25 (octyl), 32.29 (octyl), 29.64 (octyl), 25.50 (octyl), 23.09 (octyl), 14.38 (-CH<sub>3</sub>), 10.41 (SiH<sub>2</sub>-CH<sub>2</sub>) ppm. INEPT <sup>29</sup>Si-NMR (C<sub>6</sub>D<sub>6</sub>): δ -31.03 ppm. GC-MS: Octylphenylsilane: t: 15.91, m/z: [M-C<sub>6</sub>H<sub>6</sub>]<sup>+</sup> obs. 142.2, calcd: 142.1. GC: Octylphenylsilane t: 3.63.

**Silane activation:** In a glovebox, **3<sup>pTol</sup>** (21.0 mg, 0.03 mmol) was dissolved in C<sub>6</sub>D<sub>6</sub> (0.4 mL) and stirred. PhSiH<sub>3</sub> (15.6 mg, 0.14 mmol) was added to a second vial and diluted with C<sub>6</sub>D<sub>6</sub> (1 mL). 0.6 mL of the PhSiH<sub>3</sub> solution (0.09 mmol) was added to the solution of **3<sup>pTol</sup>** and the mixture was stirred for 15 min, after which it was filtered into a Young-type NMR tube. <sup>1</sup>H NMR (C<sub>6</sub>D<sub>6</sub>): δ -11.98 (m, hydride), <sup>31</sup>P NMR (C<sub>6</sub>D<sub>6</sub>): δ<sub>p</sub> broad signals: 74, 70, 64, 60. Sharp signals: -16.08, -16.19, -16.37, -17.32, -17.64 ppm. Spectra are shown in Appendix D, Figure D5 and D6.

## 4.5 References and notes

- [1] J. Sun, L. Deng, *ACS Catal.*, **2016**, *6*, 290–300.
- [2] X. Du, Z. Huang, *ACS Catal.*, **2017**, *7*, 1227–1243.
- [3] J. L. Speier, J. A. Webster, G. H. Barnes, *J. Am. Chem. Soc.*, **1957**, *79*, 974–979.
- [4] B. D. Karstedt, General Electric Company., U.S. Patent US3775452A, **1973**.
- [5] X. Du, Z. Huang, *ACS Catal.*, **2017**, *7*, 1227–1243.
- [6] R. Langer, Y. Diskin-Posner, G. Leitnus, L. J. W. Shimon, Y. Ben-David, D. Milstein, *Angew. Chem. Int. Ed.*, **2011**, *50*(42), 9948–9952.

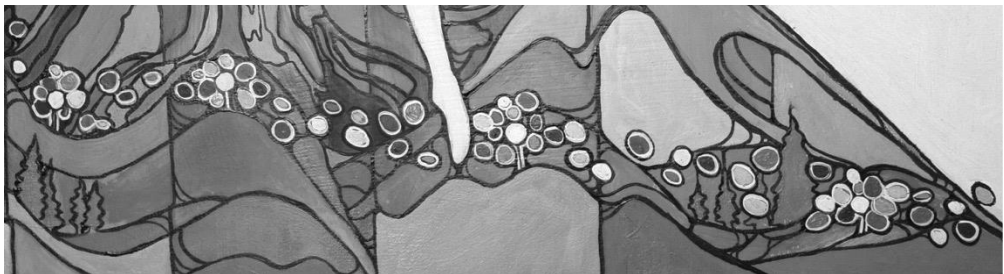
- [7] A. M. Tondreau, C. C. H. Atienza, K. J. Weller, S. A. Nye, K. M. Lewis, J. G. P. Delis, P. J. Chirik, *Science*, **2012**, 335(6068), 567–570.
- [8] X. Du, Y. Zhang, D. Peng, Z. Huang, *Angew. Chem. Int. Ed.*, **2016**, 55, 6671–6675.
- [9] T. J. Steiman, C. J. Uyeda, *J. Am. Chem. Soc.*, **2015**, 5(4), 2081–2084.
- [10] I. Buslov, J. Becouse, S. Mazza, M. Montandon-Clerc, X. Hu, *Angew. Chem. Int. Ed.*, **2015**, 54(48), 14523–14526.
- [11] I. Buslov, S. C. Keller, X. Hu, *Org. Lett.*, **2016**, 18(8), 1928–1931.
- [12] I. Pappas, S. Treacy, P. J. Chirik, *ACS Catal.*, **2016**, 55(40), 12295–12299.
- [13] A. J. Chalk, J. F. Harrod, *J. Am. Chem. Soc.*, **1965**, 87, 1133–1135.
- [14] M. A. Schroeder, M. A. Wrighton, *J. Organomet. Chem.*, **1977**, 128(3), 345–358.
- [15] S. Sakaki, N. Mizoe, M. Sugimoto, *Organometallics*, **1998**, 7333, 2510–2523.
- [16] A. K. Roy, R. B. Taylor, *J. Am. Chem. Soc.*, **2002**, 124(32), 9510–9524.
- [17] M. Brookhart, B. E. Grant, *J. Am. Chem. Soc.*, **1993**, 115, 2151–2156.
- [18] Z. Mo, Y. Liu, L. Deng, *Angew. Chem. Int. Ed.*, **2013**, 52, 10845–10849.
- [19] C. Chen, M. B. Hecht, A. Kavara, W. W. Brennessel, B. Q. Mercado, D. J. Weix, P. L. Holland, *J. Am. Chem. Soc.*, **2015**, 137, 13244–13247.
- [20] C. H. Schuster, T. Diao, I. Pappas, P. J. Chirik, *ACS Catal.*, **2016**, 6, 2632–2636.
- [21] A. D. Ibrahim, S. W. Entsminger, L. Zhu, A. R. Fout, *ACS Catal.*, **2016**, 6, 3589–3593.
- [22] X. Du, Y. Zhang, D. Peng, Z. Huang, *Angew. Chem. Int. Ed.*, **2016**, 55, 6671–6675.
- [23] D. Noda, A. Tahara, Y. Sunada, H. Nagashima, *J. Am. Chem. Soc.*, **2016**, 138, 2480–2483.
- [24] A. Gorczynski, M. Zaraneek, S. Witomska, A. Bocian, A. R. Stefankiewicz, M. Kubicki, V. Patroniak, P. Pawluc, *Catal. Commun.*, **2016**, 78, 71–74.
- [25] J. Guo, X. Shen, Z. Lu, *Angew. Chem. Int. Ed.*, **2017**, 56, 615–618.
- [26] L. Yong, K. Kirleis, H. Butenschon, *Adv. Synth. Catal.*, **2006**, 348, 833–836.
- [27] Z. Mo, J. Xiao, Y. Gao, L. Deng, *J. Am. Chem. Soc.*, **2014**, 136, 17414–17417.
- [28] M. A. Nesbit, D. J. M. Suess, J. C. Peters, *Organometallics*, **2015**, 34(19) 4741–4752.
- [29] Y. Liu, L. Deng, *J. Am. Chem. Soc.*, **2017**, 139(5), 1798–1801.
- [30] Chapter 3 of this thesis: D. G. A. Verhoeven, M. A. C. van Wiggen, J. Kwakernaak, M. Lutz, R. J. M. Klein Gebbink, M.-E. Moret, *Chem. Eur. J.*, **2017**, DOI: 10.1002/chem.201703254.
- [31] Chapter 1 of this thesis: D. G. A. Verhoeven, M. -E. Moret, *Dalton Trans.*, **2016**, 45, 15762–15778.
- [32] Chapter 2 of this thesis: B. W. H. Saes, D. G. A. Verhoeven, M. Lutz, R. J. M. Klein Gebbink, M. -E. Moret, *Organometallics*, **2015**, 34, 2710–2713.
- [33] The <sup>31</sup>P NMR shows a few very weak signals around δ –15 ppm, which are attributed to ligand decomposition, and broad features around δ 45 and 60 ppm.
- [34] a) S. P. Semproni, C. Milsman, P. J. Chirik, *J. Am. Chem. Soc.*, **2014**, 136, 9211–9224. b) M. L. Scheuermann, S. P. Semproni, I. Pappas, P. J. Chirik, *Inorg. Chem.*, **2014**, 53, 9463–9465.
- [35] Y. Nakjima, S. Shimada, *RSC Adv.*, **2015**, 5(26), 20603–20616.
- [36] M. Itoh, K. Inoue, J. I. Ishikawa, K. Iwata, *J. Organomet. Chem.*, **2001**, 629(1–2), 1–6.
- [37] B. Becker, R. J. P. Corriu, C. Guerin, B. J. L. Henner, *J. Organomet. Chem.*, **1989**, 369(2), 147–154.
- [38] a) T. C. Morrill, C. A. D'Souza, *Organometallics*, **2003**, 22, 1626–1629. b) R. Cramer, *J. Am. Chem. Soc.*, **1966**, 88, 2272–2282. c) T. J. Mooibroek, E. C. M. Wenker, W. Smit, I. Mutikainen, M. Lutz, E. Bouwman, *Inorg. Chem.*, **2013**, 52, 8190–8201.
- [39] J. W. Sprengers, M. de Greef, M. A. Duin, C. J. Elsevier, *Eur. J. Inorg. Chem.*, **2003**, 3811–3819.

- [40] W.-Y. Chu, R. Gilbert-Wilson, T. B. Rauchfuss, M. van Gastel, F. Neese, *Organometallics*, **2016**, 35(17), 2900–2914.
- [41] Q. Shen, J. F. Hartwig, *J. Am. Chem. Soc.*, **2007**, 129, 7734–7735.





*The reasonable man adapts oneself to the world,  
The unreasonable one persists in trying to adapt the world to oneself.  
Therefore all progress depends on the unreasonable one.*  
- Malcolm Gladwell



# | Chapter 5 |

## Nickel Complexes of Diphosphine-Tethered Imine Ligands

**Abstract** The coordination chemistry of chelating ligands with a diphosphine imine framework (PCNP) to nickel is investigated. Imine moieties can bind to metal centers in either an  $\eta^1(\text{N})$ -fashion *via*  $\sigma$ -donation of the lone pair, or in an  $\eta^2(\text{C,N})$ -fashion *via*  $\pi$ -coordination, of which the first form is much more common. The imine functionality of this diphosphine chelating ligand binds in an  $\eta^1(\text{N})$ -fashion in a Ni(II) complex. The uncommon  $\eta^2(\text{C,N})$ -interaction is obtained in Ni(0) complexes in the presence of a  $\text{PPh}_3$  co-ligand. Increasing the bulk on the diphosphine linkers in the Ni(0) complexes, by substituting phenyl for *o*-tolyl groups, leads to a distinct binding mode in which only one of the phosphine tethers is coordinated. In the absence of a co-ligand, a mixture of two different dimeric Ni(0) complexes is formed. In one of them, the imine adopts an uncommon  $\eta^1(\text{N})\eta^2(\text{C,N})$  bridging mode of the ligand to nickel, while the second one may involve reactivity on the ligand by the formation of a new C–C bond by reductive coupling. This is supported by the isolation and structural characterization of a crystalline bis-CO derivative.

---

D. G. A. Verhoeven, H. A. Negenman, M. Lutz, M. -E. Moret, *to be submitted*.

## 5.1 Introduction

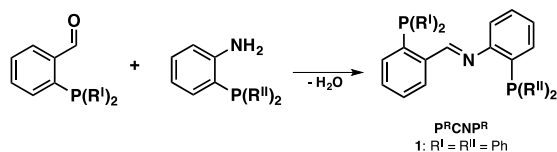
In light of the ongoing interest in the substitution of precious metals by earth abundant metals in catalysis, the development of systems displaying metal-ligand cooperativity is flourishing.<sup>[1-4]</sup> Ligands with versatile binding modes facilitating hemilabile or adaptive behavior, or with the possibility of stabilizing multielectron redox processes, are of interest for incorporation in base metal catalysts.

Imine functionalities are prevalent as ligands in organometallic chemistry, which is reflected in their numerous applications in homogeneous catalysis.<sup>[5,6]</sup> Examples are the NNN-pincer Fe and Co complexes as reported by Chirik and co-workers active in alkene polymerization and cycloaddition reactions,<sup>[7]</sup> dinuclear Ni complexes as published by Uyeda that catalyze hydrosilylation reactions,<sup>[6]</sup> or diphosphine imine complexes, reported by several groups, for olefin polymerization and oligomerization.<sup>[8-11]</sup> Generally, the imine nitrogen atom is reported to bind the metal center *via* its lone pair in an  $\eta^1(\text{N})$ -fashion, forming a  $\sigma$  dative bond. A second, and far less common, possibility is formation of  $\pi$ -complexes *via* an  $\eta^2(\text{C,N})$ -coordination of the imine. This latter binding mode follows the Dewar-Chatt-Duncanson (DCD) model for coordination of  $\pi$ -ligands, i.e. the side-on bound and the metallo-aza-cycle extreme. Limited examples of an  $\eta^2(\text{C,N})$ -bound benzophenone-imine to Ni(0) are reported,<sup>[12]</sup> as well as a recently published bimetallic Ni complex with a chelating NNN-bis(imino)pyridine ligand.<sup>[13]</sup> Monometallic complexes with a chelating ligand with an  $\eta^2(\text{C,N})$ -coordinating imine functionality based on precious metals Pd, Rh and Ir are described as well.<sup>[14-19]</sup> Imine ligands bound in an  $\eta^2(\text{C,N})$ -fashion are of interest as the binding mode can adjust upon reactivity, possibly stabilizing metal complexes and enhancing catalyst reactivity and selectivity.

Here, the versatile binding of an imine ligand, bridged between two *ortho*-diphosphine substituted phenyl rings, to nickel is explored. The design of the ligand allows for a chelated binding structure *via* the phosphine arms to the metal center. Synthesis of the diphosphine-imine ligand P<sup>Ph</sup>CNP<sup>Ph</sup> (**1**, Scheme 1) and its complexation to Co(II)<sup>[8,9]</sup>, Ni(II)<sup>[8,10]</sup> and Pd(II)<sup>[9,10]</sup> with the imine backbone bound in an  $\eta^1(\text{N})$ -fashion has been reported previously by other groups, mainly for the use in olefin oligomerization and polymerization reactions. In this contribution, the coordination chemistry of the PCNP ligand to nickel is investigated, showing that the imine moiety is able to adopt a variety of coordination modes (end-on, side-on, bridging), changing upon varying the oxidation state from Ni(II) to Ni(0), and upon the addition of steric bulk on the phosphine tethers. Of particular interest is the observation of a reductive C–C coupling reaction in dimeric complexes, in which a Ni(0)Ni(0) core is oxidized to Ni(II)Ni(0).

## 5.2 Results and discussion

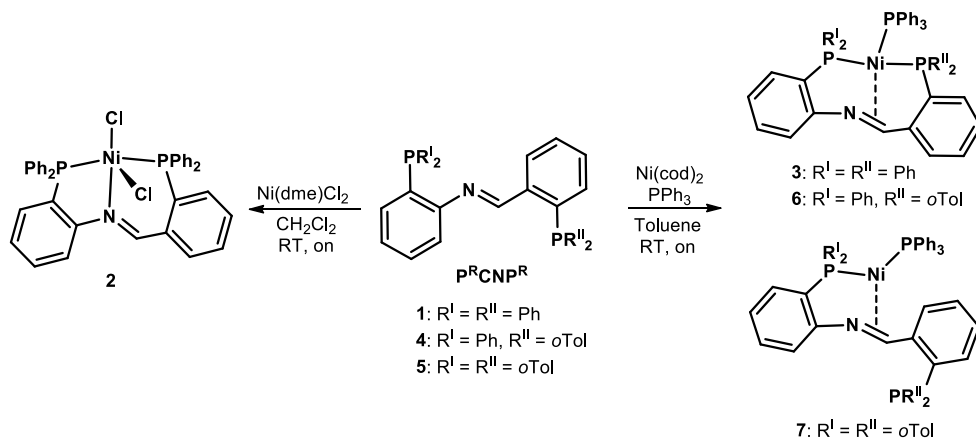
The diphosphine-imine ligand  $P^{Ph}CNP^{Ph}$  (**1**) was readily synthesized *via* an imine condensation of the diphenylphosphine substituted aldehyde and amine compounds (Scheme 1).<sup>[20,21]</sup> A Ni(II) complex was synthesized from a mixture of  $NiCl_2(DME)$  and  $P^{Ph}CNP^{Ph}$  in  $CH_2Cl_2$ , resulting in  $Ni(P^{Ph}CNP^{Ph})Cl_2$  (**2**) after isolation *via* precipitation from THF/hexanes and extraction of the product (Scheme 2).<sup>[8]</sup> Analysis by  $^1H$  NMR spectroscopy at room temperature showed the formation of a paramagnetic species, with broad aromatic peaks in the region of  $\delta$  6 to 9 ppm, and one largely shifted broad peak at  $\delta$  35.1 ppm. Upon lowering the temperature to  $-80$  °C, the peaks sharpen, and the peak at  $\delta$  35.1 ppm shifts to  $\delta$  8.9 ppm, suggesting a spin transition from probably a high spin tetrahedral structure at room temperature – where one chloride ligand is dissociated in solution – to a diamagnetic low spin square planar structure at low temperature (Appendix E, Figure E2-3). X-ray crystal structure determination of crystals grown by slow vapor diffusion of hexanes into  $CH_2Cl_2$  showed that **2** has a strongly distorted square pyramidal geometry around nickel (Figure 1). The  $P^{Ph}CNP^{Ph}$  ligand is bound *via* both phosphorus tethers, and the imine moiety in an  $\eta^1(N)$ -fashion. The  $P^{Ph}CNP^{Ph}$  ligand is disordered by a  $180^\circ$  rotation about the imine bond in a ratio 0.550(6):0.450(6) (Appendix E1). Next to this, two chloride ligands are bound, of which the apical Ni–Cl bond is strongly elongated to 2.6545(6) Å, *versus* 2.1889(5) Å for the in-plane chloride atom. Hence, the geometry can be seen as derived from a cationic square-planar Ni(II) complex weakly interacting with a  $Cl^-$  counterion. This is similar to the dibromide analogue of **2**, as published by Sun and co-workers, with Ni–Br bond lengths of 2.3222(11) Å for the in plane Br and 2.7754(11) Å for the apical Ni–Br bond.<sup>[8]</sup> Furthermore Ni–P and Ni–N distances are similar for the Cl and Br analogue (**2**: Ni1–N1A: 1.963(3), Ni1–P1A: 2.1892(6), Ni1–P2A: 2.1837(6) Å (Table 1). **2Br**<sup>[8]</sup>: Ni–N: 1.956(6), Ni–P(N-side): 2.154(2), Ni–P(C-side): 2.1972(19) Å). The torsion angle for C–N=C–C is  $175.4(6)^\circ$ , indicating a slightly distorted flat configuration of the ligand backbone (close to  $180^\circ$ ) and the largely  $sp^2$  character of the imine-carbon atom.



**Scheme 1.** Synthesis of  $P^{R^I}CNP^{R^{II}}$  ligand **1**.

An  $\eta^2(C,N)$ -coordination mode of the imine moiety was accessed by synthesis of a Ni(0) complex. Reaction of ligand **1** with  $Ni(cod)_2$  in the presence of  $PPh_3$  as co-ligand in THF afforded the Ni(0) complex  $Ni(P^{Ph}CNP^{Ph})(PPh_3)$  (**3**) as a dark red solid after precipitation from THF/hexanes. Analysis by NMR displays a diamagnetic species with three signals in the  $^{31}P$  NMR: a sharp doublet at  $\delta$  29.5 ppm and two broad signals at  $\delta$  6.3 and 44.1 ppm. The

broadening is possibly caused by the presence of a small amount of coprecipitated free  $\text{PPh}_3$ , causing the spectrum to broaden by exchange of the co-ligand. The  $^{31}\text{P}$  NMR signals sharpen both at  $-50^\circ\text{C}$  and  $50^\circ\text{C}$  (Appendix E, Figure E4). The sharp low-temperature spectrum shows the splitting pattern and coupling constants for complex **3**, from which it is evident that the three signals couple together ( $\delta$  46.80 (d,  $J_{\text{PP}} = 41$  Hz), 30.00 (d,  $J_{\text{PP}} = 28$  Hz), 4.16 (dd,  $J_{\text{PP}} = 28, 41$  Hz) ppm). Free  $\text{PPh}_3$  is not observed in this spectrum, which is probably due to its low concentration. The free imine is no longer present in **3**, as the distinctive imine-CH peak in the  $^1\text{H}$  NMR spectrum at  $\delta$  9.32 ppm in **1** is not observed, nor is the C=N band in IR analysis.<sup>[22]</sup>  $^1\text{H}$ - $^{13}\text{C}$  HMQC 2D NMR shows a cross peak for a signal at  $\delta$  84 ppm in  $^{13}\text{C}$  NMR and  $\delta$  6 ppm in  $^1\text{H}$  NMR, which is assigned to the imine-CH (Appendix E, Figure E5). The considerable shift of the  $^{13}\text{C}$  NMR signal towards high field is indicative of a strong rehybridization towards  $\text{sp}^3$ , i.e. a substantial metallacycle character of the M-C-N moiety. It is, however, somewhat smaller than that observed in tricoordinate aldimine complexes of the (dippe)Ni fragment (dippe = bis(diisopropylphosphino)ethane),<sup>[12d]</sup> in which this signal is found at c.a.  $\delta$  60 ppm. This difference likely arises from more efficient  $\pi$ -backdonation from the (Ni-P)  $\sigma$ -antibonding in plane d-orbital in tricoordinate complexes. Crystals suitable for X-ray diffraction were grown by slow vapor diffusion of hexanes into a THF mixture of **3**, and the crystal structure showed a distorted tetrahedral geometry around the nickel center (Figure 1). The Ni(0) center is bound to **1** in a  $\kappa^4(\text{P},\text{P},\text{C},\text{N})$ -fashion with an  $\eta^2(\text{C},\text{N})$ -coordination of the imine backbone, and to the  $\text{PPh}_3$  co-ligand. The C-N distance of the imine moiety is clearly larger, being 1.364(5) Å in **3** compared to 1.294(5) Å for the Ni(II) complex **2**, as a result of  $\pi$ -backdonation to the anti-bonding  $\pi^*$  orbital of the imine C=N bond.



Scheme 2. Overview of the ligands and Ni-complexes.

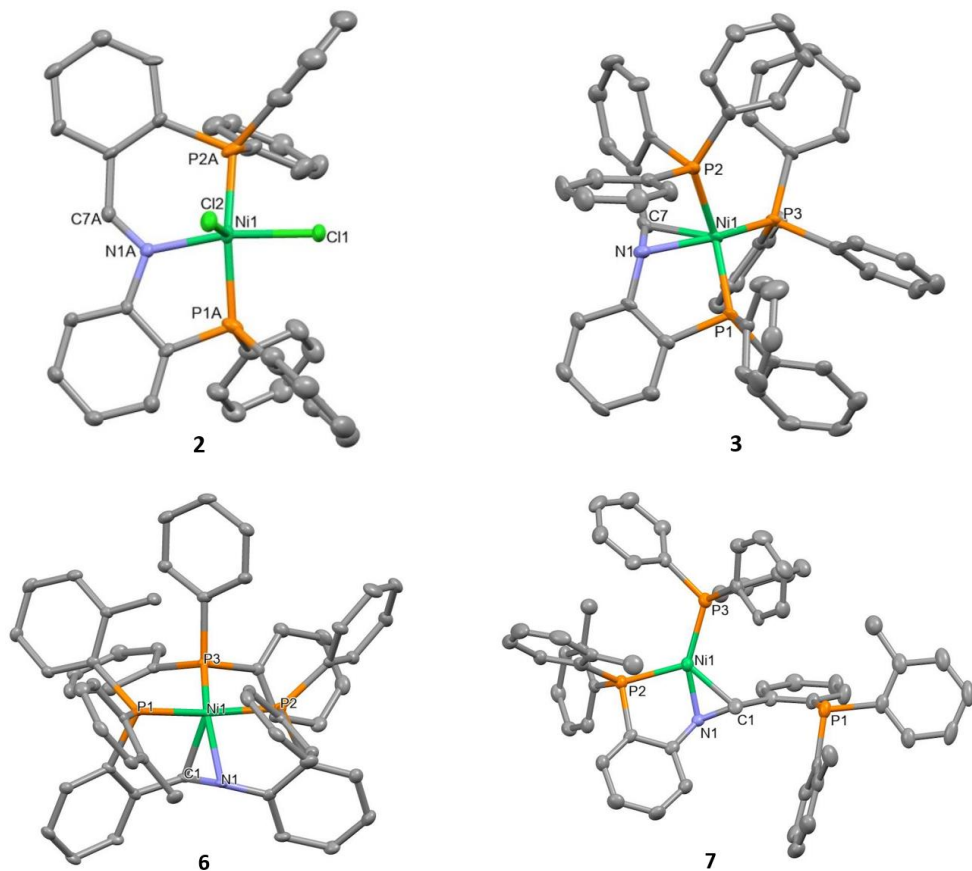


**Figure 1.** Molecular structures of **2**, **3**, **6** and **7** in the crystal. Displacement ellipsoids are drawn at the 50% probability level. Co-crystallized solvent molecules and hydrogen atoms omitted for clarity: **2**: 0.5 Et<sub>2</sub>O and 0.5 CH<sub>2</sub>Cl<sub>2</sub>; **7**: THF. Selected distances (Å) and angles (°): **2**: only the major disorder component of the structure is shown here. Ni1–N1A: 1.963(3), Ni1–C7A: 2.913(4), N1A–C7A: 1.294(5), Ni1–P1A: 2.1892(6), Ni1–P2A: 2.1837(6), Ni1–Cl1: 2.1889(5), Ni1–Cl2: 2.6545(6), P1A–Ni1–P2A: 153.13(3), Cl1–Ni1–N1A: 169.69(10). **3**: Ni1–N1: 1.943(3), Ni1–C7: 2.075(4), N1–C7: 1.364(5), Ni1–P1: 2.1888(11), Ni1–P2: 2.3234(11), Ni1–P3: 2.1761(11), P1–Ni1–P2: 121.89(4). **6**: Ni1–N1: 1.969(2), Ni1–C1: 2.031(3), N1–C1: 1.358(4), Ni1–P1: 2.2996(8), Ni1–P2: 2.2189(8), Ni1–P3: 2.1904(9). **7**: Ni1–N1: 1.864(3), Ni1–C1: 2.044(4), N1–C1: 1.368(4), Ni1–P1: 4.8493(12), Ni1–P2: 2.2048(11), Ni1–P3: 2.1475(12).

### 5.2.2 Ligand variation

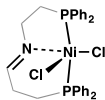
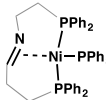
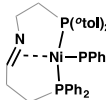
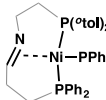
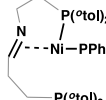
The design of the ligand allows for facile incorporation of different substituents on phosphorus, forming even mixed ligands, as the building blocks of the imine condensation can be adjusted. The influence of additional bulk on the P<sup>R</sup>CNP<sup>R</sup> ligand was explored by the synthesis of the *o*-tolyl substituted ligands (Scheme 2). The ligands P<sup>Ph</sup>CNP<sup>*o*Tol</sup> (**4**) and *po*<sup>Tol</sup>CNP<sup>*o*Tol</sup> (**5**) were synthesized accordingly, and subsequent complexation *via* a reaction of

the ligand with Ni(cod)<sub>2</sub> and PPh<sub>3</sub> in toluene afforded Ni(0) complexes Ni(P<sup>Ph</sup>CNP<sup>oTol</sup>)(PPh<sub>3</sub>) (**6**) and Ni(P<sup>oTol</sup>CNP<sup>oTol</sup>)(PPh<sub>3</sub>) (**7**), respectively, after precipitation with hexanes and isolation of the solids. Complex **6** gives rise to three broad signals in <sup>31</sup>P NMR at δ 36, 29 and 1 ppm, all in the region of nickel bound phosphorus compounds. The broad signals suggest fluxionality in the complex, which is assumed to be caused by the increased bulk. <sup>1</sup>H NMR indicates a shift of the imine-CH moiety as the distinctive imine-proton (δ 9.33 ppm in **4**) is no longer present.

The X-ray crystal structure on single crystals grown from vapor diffusion of hexane into THF showed a tetrahedral configuration around the nickel center, bound to PPh<sub>3</sub>, and **4** in a κ<sup>4</sup>(P,P,C,N)-fashion with an η<sup>2</sup>(C,N)-coordination of the imine backbone (Figure 1). The imine C–N distance is 1.358(4) Å, which is similar to that in complex **3** (Table 1). Likewise, the Ni–P distances closely resemble the analogues distances of complex **3**.

The addition of even more bulk, i.e. tetra-*ortho*-tolyl substituted PCNP ligand **5** and its nickel complex **7**, results in decoordination of one of the phosphine arms: the <sup>31</sup>P NMR of **7** shows again three signals, but in this case one peak appears as a broad singlet at δ –28 ppm, indicating a non-coordinated phosphorus atom. The remaining two signals – also broad singlets – are at δ 11 and 40 ppm, consistent with coordination to Ni. Single crystal X-ray structure determination confirms this interpretation: nickel is bound to the ligand in a κ<sup>3</sup>(P,C,N)-fashion with an η<sup>2</sup>(C,N)-coordination of the imine moiety (Figure 1). Next to this, PPh<sub>3</sub> is bound and the carbon-side phosphine of the PCNP ligand is dissociated. The imine C–N bond length is 1.368(4) Å for **7**, which is comparable to the elongation of the imine backbone in **3** and **6**, indicating a similar degree of π-backbonding despite the lower coordination number. The Ni–N bond distance of 1.864(3) Å is however shorter compared to **3** and **6**, which is likely caused by the lesser amount of geometric strain due to the detachment of the second phosphine arm. The torsion angle C–N=C–C for **3**, **6** and **7** are similar, with 151.4(3)° for **3**, 147.0(3)° for **6**, and 145.8(3)° for **7**. These angles differ from an sp<sup>2</sup> (180°) and an sp<sup>3</sup> (120°), consistent with an intermediate hybridization, with a slightly higher degree of sp<sup>3</sup> character for **7**.

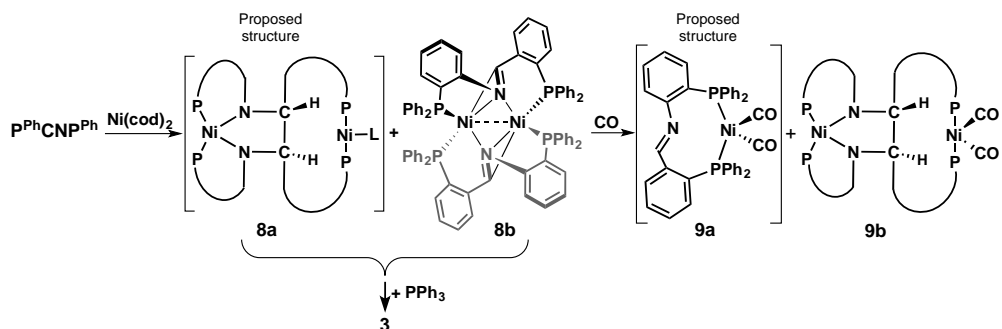
**Table 1.** Selected bond distances (Å) and angles (°) in the X-ray crystal structures. **2a** is the major and **2b** the minor disorder component of complex **2**.

					
	<b>2a</b>	<b>2b</b>	<b>3</b>	<b>6</b>	<b>7</b>
C–N	1.294(5)	1.287(6)	1.364(5)	1.358(4)	1.368(4)
Ni–C	2.913(4)	2.886(4)	2.075(4)	2.031(3)	2.044(4)
Ni–N	1.963(3)	1.968(4)	1.943(3)	1.969(2)	1.864(3)
Torsion angle	175.4(6)	–179.0(7)	151.4(3)	147.0(3)	145.8(3)
C–C–N–C					



### 5.2.3 Dimeric complexes

A reaction of **1** and Ni(cod)<sub>2</sub> in toluene without the addition of a co-ligand results in a mixture of two species, major species **8a** and minor species **8b** (Scheme 3). A workup was performed by precipitation of the products upon addition of hexanes to a THF solution, removing the majority of cod in the filtrate, followed by extraction of the solids in THF and evaporation of the solvent in vacuum and remaining cod by high vacuum.<sup>[23]</sup> The mixture mainly consists of **8a** allowing for its spectroscopic characterization, which shows the absence of a free imine moiety, as the imine-hydrogen peak is shifted in <sup>1</sup>H NMR and the according band in the IR spectrum at 1621 cm<sup>-1</sup> is not observed.<sup>[22]</sup> Four signals are observed in <sup>31</sup>P NMR, two doublets at δ 35.4 and -7.9 ppm (*J*<sub>PP</sub> = 9 and *J*<sub>PP</sub> = 70 Hz) and two double-doublets at δ 35.5 and 22.9 ppm (*J*<sub>PP</sub> = 2, 70 and *J*<sub>PP</sub> = 2, 9 Hz). This indicates that the four non-equivalent phosphorus atoms belong to a single product, which is likely to be caused by a dimeric nature of **8a**. Next to **8a**, the minor species **8b** is consistently present in a ratio of approximately 4:1, which shows two doublet signals in the <sup>31</sup>P NMR at δ 1.1 and 38.3 ppm (*J*<sub>PP</sub> = 43 Hz). To establish the overall composition of the mixture, one equivalent of PPh<sub>3</sub> with respect to nickel was added. Quantitative conversion of **8a/8b** into **3** was observed, confirming the overall composition of [Ni(P<sup>Ph</sup>CNP<sup>Ph</sup>)]<sub>2n</sub> (Scheme 3).



**Scheme 3.** Synthesis of dimeric complexes derived from **1**. P = PPh<sub>2</sub>, L is a solvent molecule.

Diffusion of hexanes into a THF solution afforded crystals suitable for X-ray diffraction, although only a minor fraction of the material crystallized. The crystalline material was covered by precipitation of a second compound, making quantitative isolation not possible. Nevertheless, a crystal could be harvested from the mixture for X-ray diffraction. The obtained crystal structure presents a dimeric species with two ligands and two nickel centers, identified as **8b** (Figure 2): even though no crystallographic symmetry is found, the overall structure of **8b** possesses an approximate two-fold rotation axis perpendicular to the Ni–Ni axis, which suggests that its <sup>31</sup>P NMR spectrum should display only two signals. Each imine moiety acts as a bridge, binding side-on to one metal and end-on to the other, with the two P-donor sites of one ligand binding each to a different Ni center. The structure has a

rather short Ni–Ni distance of 2.5595(3) Å which is likely sterically enforced due to the geometrical arrangement of the ligands. An electronic Ni–Ni interaction is unlikely because both centers are formally  $d^{10}$  metals. The C=N bond distances in **8b** are 1.347(6) Å and 1.361(6) Å, both in line with the discussed monomeric Ni(0) complexes, and so the additional  $\sigma(N)$ -interaction does not seem to contribute to a more activated imine.

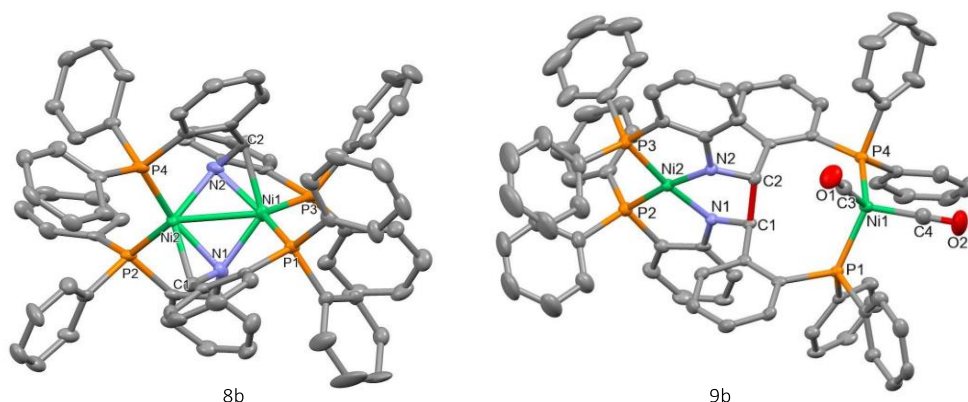


**Figure 2.** Molecular structures of **8b** and **9b** in the crystal. Displacement ellipsoids are drawn at the 50% probability level and hydrogen atoms omitted for clarity. Selected distances (Å) and angles (°): **8b**: N1–C1: 1.347(6), N2–C2: 1.361(6), N1–Ni1: 2.033(4), N1–Ni2: 1.992(4), N2–Ni1: 2.004(4), N2–Ni2: 2.031(4), Ni1–Ni2: 2.5595(9), Ni1–C2: 2.063(5), Ni2–C1: 2.046(5). **9b**: Formed C1–C2 bond is shown in red. C1–C2: 1.550(4), N1–C1: 1.448(4), N2–C2: 1.460(4), Ni2–P2: 2.1545(10), Ni2–P3: 2.1529(10), Ni2–N1: 1.884(3), Ni2–N2: 1.884(3), Ni1–P1: 2.2228(9), Ni1–P4: 2.2269(9), Ni1–C3: 1.765(4), Ni1–C4: 1.774(4).

The somewhat unusual  $\mu\text{-}\eta^1(N)\eta^2(C,N)$  binding mode observed in **8b** has been previously reported by de Bruin and co-workers in dinuclear rhodium(I) complexes formed by deprotonation of the  $\alpha\text{-CH}_2$  group of a bridging dipicolylamine (dpa) ligand (Chapter 1, Figure 25).<sup>[14]</sup> Subsequent work by the same group has afforded a number of related (hetero)bimetallic compounds featuring the same binding mode, which could also be accessed directly from the imine analogue of the ligand (dpi).<sup>[16–18]</sup> Very recently, a similar  $\text{Co}_2(\text{imine})_2$  core was observed by Rauchfuss and co-workers in the dimer  $[\text{CoMe}(\text{Ph}_2\text{PC}^2\text{N}^{\text{H}}\text{py})]_2$ , where  $\text{Ph}_2\text{PC}^2\text{N}^{\text{H}}\text{py}$  is a tridentate pyridine-imine-phosphine (pyCNP) ligand, differing from the PCNP framework by substitution of the second *o*-diphosphine-phenylene linker by a pyridine group.<sup>[24]</sup> Notably, the Co–Co distance of c.a. 2.9 Å is considerably longer than the Ni–Ni distance of 2.5595(9) Å in **8b**, which is likely a result of the different local coordination geometry: 5-coordinate, trigonal bipyramidal (TBP) for  $\text{Co}^{\text{I}}$  vs. tetracoordinate, tetrahedral for  $\text{Ni}^{\text{0}}$ .

The signals of **8b** in  $^{31}\text{P}$  NMR were shown to increase in time, in several days in a  $\text{C}_6\text{D}_6$  solution, and therefore the species likely formed in larger amount during crystallization. Attempts to harvest the grown crystals for NMR analysis lead to mixtures of **8a** and **8b** (about 1:1), showing the increasing presence of the minor species after crystallization.

The chemical nature of major dimeric species **8a** could not be fully elucidated. Further analysis of the mixture shows the presence of two distinctive signals in the  $^1\text{H}$  NMR at  $\delta$  4.58 and 5.49 ppm that belong to the major species **8a**, besides numerous aromatic signals. Even though the low solubility of the compound leads to a low quality  $^{13}\text{C}$  NMR spectrum, the  $^1\text{H}$ - $^{13}\text{C}$  HMQC NMR shows clear cross peaks with  $^{13}\text{C}$  NMR signals at  $\delta$  78.7 and 86.90 ppm, respectively, which are both shown to be CH signals, according to APT  $^{13}\text{C}$  NMR analysis (Figure 3; Appendix E, Figure E6-7). A possible explanation is the incorporation of a new C–C bond in the species. The absence of a large  $^3J_{\text{HH}}$  between these two signals would then be due to a constrained H–C–C–H dihedral angle in the low-coupling Karplus region.<sup>[25]</sup> Upon arrangement of two imine bonds in close proximity to each other, possibly in the form of a dimer, the imine-carbon atoms can undergo a coupling reaction in which two electrons from a metal center are transferred to the ligand, forming a new carbon-carbon bond (Scheme 3). A similar reaction was reported by Rauchfuss and coworkers,<sup>[26]</sup> where the coupling of two imine moieties from diphenylphosphino-2-benzimine ligands bound to iron(0) undergo a coupling reaction upon addition of ferrocene, analogous to a pinacol coupling observed on iron(0) in their earlier research.<sup>[27-29]</sup> However, it should be noted that a single molecule with two inequivalent  $\eta^2(\text{C},\text{N})$ -coordinating imine moieties cannot be excluded on the basis of the obtained data, since a shift around  $\delta$  5 ppm in  $^1\text{H}$  NMR and  $\delta$  80 ppm  $^{13}\text{C}$  NMR could also correspond to such a structure.<sup>[12d]</sup>

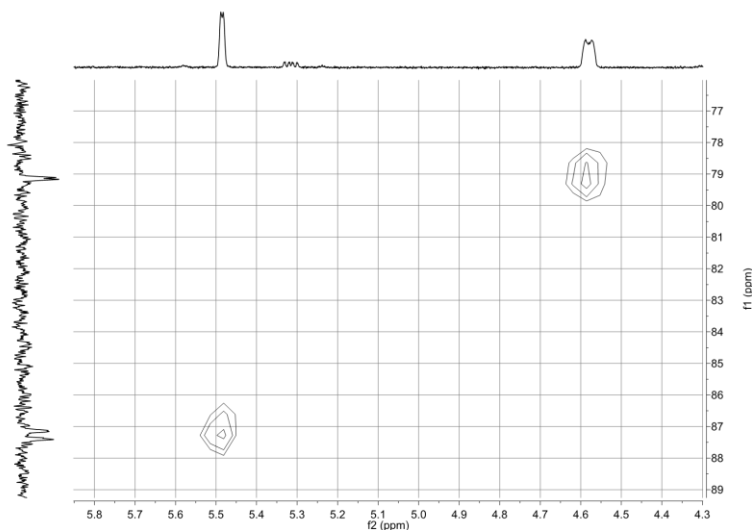


Figure 3. 2D  $^1\text{H}$ - $^{13}\text{C}$  ASAPHMQC NMR spectrum ( $\text{C}_6\text{D}_6$ ) of **8a/8b** (zoom).

Evidence supporting the structure containing a new C–C bond arises from the reactivity of the **8a/8b** mixture with CO. A solution of **8a/8b** in  $\text{C}_6\text{D}_6$  was exposed to CO (1 atm), after which the mixture was monitored in situ by NMR spectroscopy.  $^{31}\text{P}$  NMR data shows the formation of two species: major species **9a** with two doublet signals at  $\delta$  33.0 and 16.2 ppm ( $J_{\text{PP}} = 11$  Hz) and minor species **9b** with two singlet signals at  $\delta$  39.8 and 22.1 ppm

(approximate ratio of 3.3:1) (Appendix E, Figure E8). Crystallization by slow vapor diffusion of hexanes into a benzene mixture resulted in single crystals of the minor product **9b** (Figure 2, Scheme 3). The X-ray crystal structure shows a dimeric, mixed valence Ni(0)Ni(II) complex with two added equivalents of CO both bound to the Ni(0) center. The Ni(II) center is surrounded by two neutral phosphine ligands and two anionic amido ( $R_2N^-$ ) ligands, an uncommon coordination environment that was also observed in the Ni(II) complex of the  $P_2N_2$  ligand *N,N'*-bis[2-(diphenylphosphino)phenyl]propane-1,3-diamine published by Duckworth, McPartlin and co-workers.<sup>[29]</sup> Compared to Ni(II) complex **2**, the Ni–N bonds are rather short, 1.963(3) Å in **2** (major disorder component) and 1.884(3) Å and 1.884(3) Å in **9b**, originating from the strong  $\pi$ -donating nature of the nitrogen-ligands. Noteworthy, the C–H hydrogen bound to C2 in the formed C–C bond has a rather short distance below 3 Å to the Ni(0) center. This is, however, attributed to the rigid geometry of the structure rather than a chemical interaction.

The crystals of **9b** could be isolated from the **9a/9b** mixture and were analyzed by NMR.  $^{31}P$  NMR analysis indeed shows the signals earlier attributed to **9b**, without presence of other species, and the  $^1H$  NMR spectrum shows a number of aromatic signals located in the range of  $\delta$  5.94 to 10.09 ppm. The large shift of the aromatic signals was confirmed by  $^1H$ - $^{13}C$  HMQC 2D NMR analysis, as coupling signals are observed for these peaks with the aromatic region of the  $^{13}C$  NMR spectrum. The exception is a broad singlet signal at  $\delta$  6.18 ppm, which has a coupling signal in the  $^{13}C$  NMR spectrum at  $\delta$  70.35 ppm and is identified as the amido–CH functionality of the formed C–C bond. Furthermore, 2D  $^1H$ - $^{31}P$  HMBC NMR analysis shows a coupling with both phosphorus substituents of this proton (Appendix E, Figure E9). The IR spectrum of the crystals contains two signals for the CO bands at 1938 and 1999  $cm^{-1}$ . Complex **9b** contains two Ni-centers, in two oxidation states, i.e. the Ni(0) and Ni(II) center. The formal oxidation state of the Ni(0) center is unchanged, starting from the Ni(0) precursor Ni(cod)<sub>2</sub>. The Ni(II) center, on the other hand, was formed *via* an intramolecular redox process, by transfer of its electrons to the formed C–C bond originating from the imine moieties (Scheme 3).

The isolated compound **9b** is however not the major species in the reaction mixture. The majority of the material (**9a**) shows two intense CO signals in the IR spectrum at 1929 and 1991  $cm^{-1}$ , slightly shifted from the CO signals in **9b**, and NMR analysis shows the presence of aromatic signals in the  $^1H$  and  $^{13}C$  NMR spectra. In addition, the  $^1H$ - $^{13}C$  HMQC 2D NMR spectrum shows a coupling signal for a peak at  $\delta$  7.8 ppm in  $^1H$  NMR and  $\delta$  155 ppm in  $^{13}C$  NMR consistent with a non-coordinating imine-CH, which suggests the monomeric structure depicted in Scheme 3 for compound **9a**. More complex, possibly oligomeric structures can however not be fully excluded.

Combining the obtained data of compounds **8a**, **8b** and **9a**, **9b** suggests that the CO ligands act here as a trapping agent for the structure with the C–C bond, **8a**, making its isolation possible. In the case of **8a**, solvent molecules such as THF are likely coordinating to the Ni(0) center, which upon dissolution in benzene could be replaced by a benzene

molecule.<sup>[33]</sup> Isolation is facilitated by replacing loosely bound solvents for stronger binding CO ligands, resulting in **9b**. The higher apparent symmetry of **9b** (two <sup>31</sup>P NMR signals) with respect to **9a** (four <sup>31</sup>P NMR signals) may be due to higher fluxionality of the Ni(0) center in **9b**. The formation of the inter ligand C–C bond by a two-electron transfer from the metal to the ligand resulting in **8a** and **9b** shows the possibility of the PCNP ligand to engage into ligand-centered redox processes, possibly opening new venues for cooperative processes besides the versatile binding as observed in complexes **2**, **3**, **6** and **7**. Interestingly, the fact that the mixture **8a/8b** can be quantitatively converted to the imine complex **3** by addition of PPh<sub>3</sub> suggests that C–C bond formation may be reversible. These properties make Ni(PCNP)-complexes potentially interesting candidates for cooperative activation of substrates and subsequent catalysis. Further reactivity of these complexes is investigated in Chapter 6.

### 5.3 Conclusions

The coordination chemistry of chelating diphosphine-imine P<sup>R</sup>CNP<sup>R</sup> ligands to nickel was studied. The potential adaptive behavior of the phenyl-substituted ligand is exemplified in its coordination to Ni(II) and Ni(0): the imine moiety binds in an η<sup>1</sup>(N) fashion to Ni(II) and in an η<sup>2</sup>(C,N) fashion to the more electron-rich Ni(0). The addition of steric bulk to the P<sup>R</sup>CNP<sup>R</sup> framework in the form of *o*-tolyl substituents on the phosphorus atoms affords mixed-ligand complex **6**, where both phosphine tethers of the P<sup>*o*Tol</sup>CNP<sup>Ph</sup> ligand are bound to nickel, and tetra-*o*-tolyl ligand complex **7**, where one phosphine arm is dissociated from the metal center. When no co-ligand is used in the synthesis of the Ni(0) complex with the P<sup>Ph</sup>CNP<sup>Ph</sup> ligand, a mixture of dimeric structures is obtained, with a) an η<sup>1</sup>(N)η<sup>2</sup>(C,N)-coordination of the two imine ligands to both Ni centers as shown by its X-ray crystal structure, or b) a complex in which the imine functionalities seem to undergo a coupling reaction forming a new C–C bond. Addition of CO to the mixture leads to the isolation of a derivative of the C–C bound complex. The current study provides detailed insight into the coordination of η<sup>2</sup>(C,N)-bonding imine ligands to nickel, which are becoming prolific tools in the field of metal-ligand cooperativity. The observed adaptive behavior of the ligand upon different oxidation states and the redox-activity of the dimeric species make these complexes highly interesting for investigation toward their cooperative reactivity and catalytic activity (see Chapter 6).

### 5.4 Experimental section

#### 5.4.1 General considerations

All reagents were purchased from commercial sources and used as received unless stated otherwise. All reactions were performed in a N<sub>2</sub> glovebox and at room temperature unless stated otherwise.

Deuterated benzene (C<sub>6</sub>D<sub>6</sub>) and deuterated dichloromethane (CD<sub>2</sub>Cl<sub>2</sub>) were degassed using the freeze-thaw-pump method (4x) and subsequently stored over molecular sieves. Dichloromethane (CH<sub>2</sub>Cl<sub>2</sub>) was distilled over calciumhydride and tetrahydrofuran (THF) was distilled over sodium/benzophenone before use, both were degassed by bubbling N<sub>2</sub> through it for 30 minutes and stored over molecular sieves. Dry diethylether (Et<sub>2</sub>O), hexanes, acetonitrile (MeCN) and toluene were acquired from a MBRAUN MB SPS-80 solvent purification system and further dried over molecular sieves before use. MeCN was filtered over alumina prior to use. 2-Diphenylphosphanyl-benzaldehyde<sup>[32-34]</sup> and 2-diphenylphosphinoaniline<sup>[35]</sup> were synthesized according to literature procedures.

<sup>1</sup>H, <sup>13</sup>C and <sup>31</sup>P NMR spectra (respectively 400, 100 and 161 MHz) were recorded on an Agilent MRF400 or a Varian AS400 spectrometer at 25 °C. <sup>1</sup>H and <sup>13</sup>C NMR chemical shifts are reported in ppm relative to TMS using the residual solvent resonance as internal standard. <sup>31</sup>P NMR chemical shifts are reported in ppm and externally referenced to 85% aqueous H<sub>3</sub>PO<sub>4</sub>. Infrared spectra were recorded using a Perkin Elmer Spectrum One FT-IR spectrometer equipped with a general liquid cell accessory under a N<sub>2</sub> flow. ESI-MS spectra were recorded on a Walters LCT Premier XE KE317 Micromass Technologies spectrometer. Compounds of which elemental analysis is reported were either recrystallized or precipitated and dried under high vacuum overnight before submission and analysis was performed by the Mikroanalytisches Laboratorium Kolbe, Mülheim an der Ruhr, Germany. Details on X-ray crystal structure determination and selected spectra are given in Appendix E.

### 5.4.2 Synthesis

**2-Ph<sub>2</sub>PC<sub>6</sub>H<sub>4</sub>N=C(H)C<sub>6</sub>H<sub>4</sub>PPh<sub>2</sub> (P<sup>Ph</sup>CNP<sup>Ph</sup>, **1**):** Adapted from a literature procedure.<sup>[36]</sup> 2-Diphenylphosphanyl-benzaldehyde (6.0 g, 0.021 mol), 2-diphenylphosphinoaniline (5.73 g, 0.021 mol) and *p*-toluene sulfonic acid (0.11 g, 0.58 mmol) were dissolved in toluene (500 mL) in a 3-necked round-bottom flask under an N<sub>2</sub> atmosphere. A Dean-Stark trap was attached and the collecting end was filled with molecular sieves (4 Å). The brown solution was heated to reflux for 17 h, after which all solvents were evaporated. The product was precipitated from a CH<sub>2</sub>Cl<sub>2</sub>/MeOH mixture, after which the solids were collected and washed with MeOH until the supernatant was colorless. Drying of the yellow solid resulted in the product with a yield of 60% (6.94 g, 0.013 mol). <sup>1</sup>H NMR: δ<sub>H</sub> 9.32 (d, *J* = 5.9 Hz, 1H, -N=CH-), 8.39 (dd, *J* = 3.7, 3.9 Hz, 1H, Ar-H), 7.45 (t, *J* = 7 Hz, 4H, Ar-H), 7.28 (m, 4H, Ar-H), 6.93-7.02 (m, 16H, Ar-H), 6.82-6.89 (m, 2H, Ar-H), 6.58 (dd, *J* = 3.4, 4.9 Hz, 1H, Ar-H) ppm. <sup>13</sup>C NMR: 158.15 (dd, *J*<sub>CP</sub> = 2.0, 24.0 Hz), 155.04 (d, *J*<sub>CP</sub> = 18.1 Hz), 140.09 (d, *J*<sub>CP</sub> = 17.55 Hz), 138.67 (d, *J*<sub>CP</sub> = 19.3 Hz), 138.16 (d, *J*<sub>CP</sub> = 13.7 Hz), 136.89 (d, *J*<sub>CP</sub> = 11.1 Hz), 134.5 (dd, *J*<sub>CP</sub> = 2.6, 18.2 Hz), 133.63 (d, *J*<sub>CP</sub> = 13.8 Hz), 133.29 (d, *J*<sub>CP</sub> = 33.4 Hz), 131.15, 130.09, 129.29, 129.12, 129.01 (d, *J*<sub>CP</sub> = 7.0 Hz), 128.70, 128.63, 126.29, 117.50 ppm. <sup>31</sup>P NMR: -13.5, -14.9 ppm. IR cm<sup>-1</sup>: 3054, 1621, 1561, 1465, 1432, 1358, 1309, 1263, 1189, 1157, 1090, 1069, 1026, 999, 751, 738, 695, 499, 409 ppm. ESI-MS (MeCN/formic acid) *m/z*: [M+H]<sup>+</sup> calcd: 550.1854, Found: 550.1780.

**Ni(PCNP)Cl<sub>2</sub> (**2**):** P<sup>Ph</sup>CNP<sup>Ph</sup> (**1**) (499 mg, 0.908 mmol) was dissolved in CH<sub>2</sub>Cl<sub>2</sub> (2 mL). A solution of NiCl<sub>2</sub>(DME) (199.9 mg, 0.910 mmol) in CH<sub>2</sub>Cl<sub>2</sub> (8 mL) was added, after which the color of the mixture turned from a bright yellow suspension to a yellow/brown solution. The mixture was stirred for 3h 15min, after which all solvents were removed in vacuum. The remaining solids were dissolved in a minimum amount of THF, and addition of hexanes caused precipitation. The solids were filtered off and collected *via* filtration with CH<sub>2</sub>Cl<sub>2</sub>. The product was obtained as a brown solid after evaporation of all

solvents with a yield of 94.6% (0.584 g, 0.860 mmol).  $^1\text{H}$  NMR ( $\text{CD}_2\text{Cl}_2$ ):  $\delta_{\text{H}}$  35.09, 8.63, 8.22, 7.94, 7.88, 7.76, 7.10, 7.01, 6.91, 6.75, 6.28 ppm.  $^{31}\text{P}$  and  $^{13}\text{C}$  NMR: no signal detected. ESI-MS ( $\text{MeCN}$ )  $[\text{M}-\text{Cl}]^+$   $m/z$ : calcd: 642.0817, found: 642.0851. IR  $\text{cm}^{-1}$ : 3051, 1585, 1572, 1223, 1481, 1434, 1309, 1280, 1182, 1155, 1096, 1067, 998, 766, 747, 729, 691, 575, 521, 501. Crystals for Xray analysis grown from  $\text{CH}_2\text{Cl}_2/\text{hexanes}$ . Elemental analysis, calcd: C 65.43, H 4.30, N 2.06, found: C 65.29, H 4.52, N 2.04.

**$\text{Ni}(\text{P}^{\text{Ph}}\text{CNP}^{\text{Ph}})(\text{PPh}_3)$  (3):**  $\text{P}^{\text{Ph}}\text{CNP}^{\text{Ph}}$  (1) (200 mg, 0.364 mmol),  $\text{PPh}_3$  (95.4 mg, 0.364 mmol) and  $\text{Ni}(\text{COD})_2$  (100.1 mg, 0.364 mmol) were combined in a vial and  $\text{Et}_2\text{O}$  (9 mL) was added, resulting in a yellow-brown turbid mixture. The mixture was stirred for 5 h, in which the color changed to red-brown, after which the solvent was evaporated. THF (2 mL) was added to the solids, followed by addition of hexanes (6 mL) to precipitate the product as a red-brown solid, which was isolated *via* filtration and collected using THF. After evaporation of all solvents, 5 was obtained with a yield of 94% (299.3 mg, 0.344 mmol).  $^1\text{H}$  NMR ( $\text{C}_6\text{D}_6$ ) due to extended overlap between the signals and with the solvent, integrals could not be assigned:  $\delta_{\text{H}}$  7.79 (m, Ar-H), 7.49 (t,  $J = 8$  Hz, Ar-H), 7.39 (s, broad, Ar-H), 7.35-7.19 (m, Ar-H), 7.08-6.61 (m, Ar-H), 6.00 (t,  $J = 5$  Hz, Ar-H) ppm.  $^{13}\text{C}$  NMR ( $\text{C}_6\text{D}_6$ ): (note: precise assignment of signals hampered due to quality of the spectrum)  $\delta_{\text{C}}$  137.9, 137.5, 133.6, 133.5, 133.4, 133.2, 133.1, 132.9, 132.4, 132.2, 132.0, 129.4, 128.2, 127.0, 125.1, 124.7, 120.4, 120.0, 99.6, 83.8 ppm.  $^{31}\text{P}$  NMR ( $\text{C}_6\text{D}_6$ ,  $25^\circ\text{C}$ ):  $\delta_{\text{P}}$  44.1, 29.5, 6.1 ppm.  $^{31}\text{P}$  NMR ( $\text{C}_6\text{D}_6$ ,  $-50^\circ\text{C}$ ):  $\delta_{\text{P}}$  46.80 (d,  $^2J_{\text{PP}} = 41$  Hz), 30.00 (d,  $^2J_{\text{PP}} = 28$  Hz), 4.16 (d,  $^2J_{\text{PP}} = 28$ , 41 Hz) ppm. IR  $\text{cm}^{-1}$ : 3050, 1574, 1554, 1477, 1455, 1432, 1398, 1313, 1179, 1152, 1113, 1089, 1027, 815, 739, 693, 502, 436, 417. Crystals for Xray analysis grown from THF/hexanes. Compound is too sensitive for transportation for elemental analysis.

**2-Di-*o*-tolyl-phosphinoaniline:** Triethylamine (0.25 mL, 1.79 mmol) was added to a solution of 2-iodoaniline (375 mg, 1.71 mmol) and di-*o*-tolyl-phosphine (365 mg, 1.70 mmol) in MeCN (9 mL), to which subsequently a suspension of  $\text{Pd}(\text{PPh}_3)_4$  (20.4 mg, 0.018 mmol) in  $\text{H}_2\text{O}/\text{MeCN}$  (12 mL, 1:2 ratio) was added. The pale orange mixture was refluxed for 64 h, after which all solvents were evaporated. Degassed  $\text{CH}_2\text{Cl}_2$  (10 mL) was added and the organic layer was washed with degassed  $\text{H}_2\text{O}$  (3 x 10 mL), collected and the solvents were evaporated. The pale brown solid was washed with cold, degassed MeOH (3 x 4 mL) and dried in vacuum, resulting in the product as an off-white to pink solid with a yield of 87% (452.1 mg, 1.48 mmol).  $^1\text{H}$  NMR ( $\text{C}_6\text{D}_6$ ):  $\delta_{\text{H}}$  7.14 (m, 2H, Ar-H), 7.08-6.89 (m, 8H, Ar-H), 6.57, (t,  $J = 7$  Hz, Ar-H), 6.32 (t,  $J = 7$  Hz, Ar-H), 3.73 (s, 2H,  $-\text{NH}_2$ ), 2.39 (s, 6H,  $-\text{CH}_3$ ) ppm.  $^{13}\text{C}$  NMR ( $\text{C}_6\text{D}_6$ ):  $\delta_{\text{C}}$  151.10 (d,  $J_{\text{CP}} = 21$  Hz), 142.80 (d,  $J_{\text{CP}} = 27$  Hz), 135.11 (d,  $J_{\text{CP}} = 2$  Hz), 134.19 (d,  $J_{\text{CP}} = 8$  Hz), 133.26, 130.74, 130.58 (d,  $J_{\text{CP}} = 4$  Hz), 129.13, 126.65, 117.10 (d,  $J_{\text{CP}} = 6$  Hz), 115.32 (d,  $J_{\text{CP}} = 3$  Hz), 21.32 (d,  $J_{\text{CP}} = 20$  Hz) ppm.  $^{31}\text{P}$  NMR ( $\text{C}_6\text{D}_6$ ):  $\delta_{\text{P}}$  -36.56 ppm. IR  $\text{cm}^{-1}$ : 3457, 3344, 3055, 3005, 1613, 1599, 1475, 1439, 1304, 1245, 1161, 1081, 1033, 799, 746, 717, 556, 517, 456. Elemental analysis: calcd: C 78.67, H 6.60, N 4.59; found: C 78.86, H 6.77, N 4.57. ESI-MS ( $\text{MeCN}/\text{formic acid}$ )  $m/z$ : calcd: 306.1412, found: 306.1478.

**2-Di-*o*-tolyl-phosphinobenzaldehyde:** The compound is reported in literature,<sup>[34]</sup> but an adapted synthesis method was used. 2-Bromobenzaldehyde (3.00 mL, 0.476 g, 25.7 mmol), di-*o*-tolyl-phosphine (5.51 g, 25.7 mmol) and  $\text{Pd}(\text{PPh}_3)_4$  (16.2 mg, 0.014 mmol) were dissolved in toluene (90 mL), to which triethylamine (3.60 mL, 2.60 g, 25.8 mmol) was added. The orange suspension was refluxed for 8 h, after which the mixture was filtered, and washed with subsequently  $\text{NH}_4\text{Cl}$  (3 x 50 mL) and brine (1 x 50 mL). The solvents were removed in vacuum and the remaining solids were washed with cold degassed

MeOH (3 x 40 mL) and dried in vacuum, resulting in the product as an off-white solid to brown with a yield of 93% (7.65 g, 24.0 mmol).  $^1\text{H}$  NMR ( $\text{C}_6\text{D}_6$ ):  $\delta_{\text{H}}$  10.61 (d,  $J = 6$  Hz, 1H,  $\text{CH}=\text{O}$ ), 7.77 (ddd,  $J = 1, 3, 4$  Hz, 1H,  $\text{Ar}-\text{H}$ ), 7.06-6.84 (m, 11 H,  $\text{Ar}-\text{H}$ ), 2.34 (s, 6H,  $-\text{CH}_3$ ) ppm.  $^{13}\text{C}$  NMR ( $\text{C}_6\text{D}_6$ ):  $\delta_{\text{C}}$  190.62 (d,  $J_{\text{CP}} = 22$  Hz), 143.02 (d,  $J_{\text{CP}} = 27$  Hz), 140.02 (d,  $J_{\text{CP}} = 26$  Hz), 139.61 (d,  $J_{\text{CP}} = 16$  Hz), 135.03 (d,  $J_{\text{CP}} = 11$  Hz), 134.17, 133.77, 133.54, 130.67 (d,  $J_{\text{CP}} = 5$  Hz), 130.66, 129.42, 129.02, 126.75, 21.35 (d,  $J_{\text{CP}} = 23$  Hz) ppm.  $^{31}\text{P}$  NMR ( $\text{C}_6\text{D}_6$ ):  $\delta_{\text{P}}$  -28.54 ppm. IR  $\text{cm}^{-1}$ : 3054, 2963, 2908, 2824, 1693, 1584, 1449, 1391, 1290, 1261, 1199, 1116, 1034, 843, 823, 800, 746, 716, 556, 528, 507, 481.

**P<sup>Ph</sup>CNP<sup>oTol</sup> (4):** The whole procedure was performed under inert conditions and with dry and degassed solvents. 2-Di-*o*-tolyl-phosphanyl-benzaldehyde (4.00 g, 0.013 mol), 2-diphenylphosphinoaniline (3.48 g, 0.013 mol) and *p*-toluene sulfonic acid (60 mg, 0.32 mmol) were dissolved in toluene (110 mL) in a 3-necked round-bottom flask under an  $\text{N}_2$  atmosphere. A Dean-Stark trap was attached and the tap was filled with molecular sieves (3 Å). The clear yellow-brown solution was heated to reflux for 17 h and the color changed to red/yellow-brown, after which all solvents were evaporated.  $\text{CH}_2\text{Cl}_2$  was added (20 mL) and subsequently MeOH was added (20 mL) and the mixture was cooled in an ice bath for 20 min to precipitate the crude product. The solids were washed with MeOH until the supernatant was colorless and the solids were dried in vacuum resulting in **4** as a yellow powder with a yield of 47% (3.43 g, 5.94 mmol).  $^1\text{H}$  NMR ( $\text{C}_6\text{D}_6$ ):  $\delta_{\text{H}}$  9.33 (d,  $J = 6.0$  Hz, 1H,  $-\text{N}=\text{CH}-$ ), 8.43 (ddd,  $J = 7.9, 4.1, 1.3$  Hz, 1H,  $\text{Ar}-\text{H}$ ), 7.46-7.42 (m, 4H,  $\text{Ar}-\text{H}$ ), 7.06-6.93 (m, 16H,  $\text{Ar}-\text{H}$ ), 6.87-6.80 (m, 4H,  $\text{Ar}-\text{H}$ ), 6.59 (ddd,  $J = 7.9, 4.4, 1.2$  Hz, 1H,  $\text{Ar}-\text{H}$ ), 2.34 (s, 6H,  $-\text{CH}_3$ ) ppm.  $^{13}\text{C}$  NMR ( $\text{C}_6\text{D}_6$ ):  $\delta_{\text{C}}$  158.08 (dd,  $J_{\text{CP}} = 2, 28$  Hz), 155.13 (d,  $J_{\text{CP}} = 18$  Hz), 142.76 (d,  $J_{\text{CP}} = 25$  Hz), 140.49 (d,  $J_{\text{CP}} = 17$  Hz), 138.14 (d,  $J_{\text{CP}} = 12$  Hz), 137.21 (d,  $J_{\text{CP}} = 19$  Hz), 134.79, 134.61 (d,  $J_{\text{CP}} = 21$  Hz), 133.95, 133.74, 133.59 (d,  $J_{\text{CP}} = 13$  Hz), 133.10, 131.34, 130.59 (d,  $J_{\text{CP}} = 4$  Hz), 130.09, 129.39, 129.33, 128.68, 128.60, 128.41 (d,  $J_{\text{CP}} = 4$  Hz), 126.84, 126.25, 117.47 (d,  $J_{\text{CP}} = 2$  Hz), 21.39 (d,  $J_{\text{CP}} = 22$  Hz) ppm.  $^{31}\text{P}$  NMR ( $\text{C}_6\text{D}_6$ ):  $\delta_{\text{P}}$  -13.49, -31.62 ppm. IR  $\text{cm}^{-1}$ : 3048, 3004, 2965, 2941, 2912, 2875, 1698, 1627, 1618, 1561, 1466, 1431, 1357, 1265, 1191, 1118, 1093, 1068, 1024, 861, 766, 747, 740, 695, 555, 503, 457. ESI-MS (MeCN/formic acid)  $m/z$ : calcd: 578.2167, found: 578.2456. Elemental analysis: calcd: C 81.09, H 5.76, N 2.42; found: C 80.68, H 5.89, N 2.41.

**P<sup>oTol</sup>CNP<sup>oTol</sup> (5):** The same method was used as for **4** with adjusted amounts: 2-di-*o*-tolyl-phosphanyl-benzaldehyde (0.258 g, 0.810 mmol), 2-di-*o*-tolyl-phosphinoaniline (0.252 g, 0.825 mmol), *p*-toluene sulfonic acid (8 mg, 0.042 mmol) and toluene (20 mL). After the procedure **5** was obtained as an off-white/yellow powder with a yield of 81.5% (0.400 g, 0.66 mmol).  $^1\text{H}$  NMR ( $\text{C}_6\text{D}_6$ ):  $\delta_{\text{H}}$  9.32 (d,  $J = 5.9$  Hz, 1H,  $-\text{N}=\text{CH}-$ ), 8.38 (m, 1H,  $\text{Ar}-\text{H}$ ), 6.79-7.10 (m, 22H,  $\text{Ar}-\text{H}$ ), 6.59 (dd,  $J = 2.9, 4.6$  Hz, 1H,  $\text{Ar}-\text{H}$ ), 2.51 (s, 6H,  $-\text{CH}_3$ ), 2.33 (s, 6H,  $-\text{CH}_3$ ) ppm.  $^{13}\text{C}$  NMR ( $\text{C}_6\text{D}_6$ ):  $\delta_{\text{C}}$  158.12 (dd,  $J_{\text{CP}} = 2, 27$  Hz), 155.72 (d,  $J_{\text{CP}} = 19$  Hz), 142.92 (d,  $J_{\text{CP}} = 26$  Hz), 142.79 (d,  $J_{\text{CP}} = 27$  Hz), 140.59 (d,  $J_{\text{CP}} = 18$  Hz), 137.35 (d,  $J_{\text{CP}} = 18$  Hz), 135.96 (d,  $J_{\text{CP}} = 13$  Hz), 134.79 (d,  $J_{\text{CP}} = 10$  Hz), 134.15, 133.96, 133.52 (d,  $J_{\text{CP}} = 46$  Hz), 131.63 (d,  $J_{\text{CP}} = 12$  Hz), 131.28, 130.58 (d,  $J_{\text{CP}} = 4.6$  Hz), 130.29 (d,  $J_{\text{CP}} = 4.4$  Hz), 130.16, 129.30 (d,  $J_{\text{CP}} = 6$  Hz), 129.31, 128.81, 128.35, 126.82, 126.47, 126.31, 125.70, 21.61-21.28 (21.61, 21.49, 21.38, 21.28: 4 signals, 2 x d, assignment unknown) ppm.  $^{31}\text{P}$  NMR ( $\text{C}_6\text{D}_6$ ):  $\delta_{\text{P}}$  -30.28, -31.56 ppm. IR  $\text{cm}^{-1}$ : 3057, 2967, 2934, 2864, 1625, 1586, 1564, 1464, 1380, 1356, 1264, 1129, 1033, 800, 750, 733, 717, 555, 485, 453. ESI-MS (MeCN/formic acid)  $m/z$ :  $[\text{M}]^+$  calcd: 606.2479, found: 606.2273. Elemental analysis: calcd: C 81.30, H 6.16, N 2.31; found: C 80.91, H 6.36, N 2.17.



**Ni(P<sup>Ph</sup>CNP<sup>oTol</sup>)(PPh<sub>3</sub>) (6):** P<sup>Ph</sup>CNP<sup>oTol</sup> (**4**) (252.4 mg, 0.437 mmol), PPh<sub>3</sub> (115.8 mg, 0.441 mmol) and Ni(cod)<sub>2</sub> (120.5 mg, 0.438 mmol) were combined in a vial and THF (5 mL) was added, resulting in a red/brown solution. The mixture was stirred overnight, after which the mixture was concentrated to ~2 mL. Hexanes (6 mL) were added and the vial was placed at -35 °C for 1 h. The solids were isolated by filtration and collected by dissolution in toluene. After evaporation of all solvents, **6** was obtained with a yield of 90% (352.1 mg, 0.392 mmol). Single crystals for XRD analysis were grown by slow vapor diffusion of hexanes into THF. <sup>1</sup>H NMR (C<sub>6</sub>D<sub>6</sub>): δ<sub>H</sub> 7.77 (t, *J* = 9 Hz, 2H, Ar-*H*), 7.40 (s, broad, Ar-*H*), 7.30 (t, *J* = 6 Hz, Ar-*H*), 7.24 (m, Ar-*H*), 7.13-6.86 (m, Ar-*H*), 6.79-6.68 (m, Ar-*H*), 5.88 (t, *J* = 7 Hz, 1H, Ar-*H*), 2.54 (s, 3H, *o*Tol-Me), 1.88 (s, 3H, *o*Tol-Me) ppm. <sup>13</sup>C NMR (C<sub>6</sub>D<sub>6</sub>): δ<sub>C</sub> 166.83 (dd, *J*<sub>CP</sub> = 4, 28 Hz), 153.86 (d, *J*<sub>CP</sub> = 33 Hz), 142.06, 141.95, 138.41, 138.15, 137.87, 137.52, 137.28, 136.24, 136.09, 135.50, 133.97 (d, *J*<sub>CP</sub> = 13 Hz), 133.50 (d, *J*<sub>CP</sub> = 14 Hz), 132.95, 132.95 (d, *J*<sub>CP</sub> = 11 Hz), 131.83 (m), 131.49 (d, *J*<sub>CP</sub> = 4 Hz), 130.16, 129.34, 126.24, 126.03 (dd, *J*<sub>CP</sub> = 4, 11 Hz), 125.74 (m), 125.15 (d, *J*<sub>CP</sub> = 4 Hz), 120.27 (d, *J*<sub>CP</sub> = 5 Hz), 119.11 (broad), 22.98, 22.91 ppm. <sup>31</sup>P NMR (C<sub>6</sub>D<sub>6</sub>): δ<sub>P</sub> 36.02, 28.79, 1.09 ppm. IR cm<sup>-1</sup>: 3047, 1585, 1570, 1453, 1433, 1387, 1297, 1089, 1026, 818, 740, 693, 514, 484, 460, 407. Crystals for Xray analysis grown from THF/hexanes. Elemental analysis: calcd: C 76.19, H 5.38, N 1.56; found: C 75.99, H 5.57, N 1.46.

**Ni(P<sup>oTol</sup>CNP<sup>oTol</sup>)(PPh<sub>3</sub>) (7):** P<sup>oTol</sup>CNP<sup>oTol</sup> (**5**) (40.0 mg, 0.066 mmol), PPh<sub>3</sub> (17.3 mg, 0.066 mmol) and Ni(cod)<sub>2</sub> (18.2 mg, 0.066 mmol) were combined in a vial and THF (5 mL) was added, resulting in a red/brown solution. The mixture was stirred overnight, after which the mixture was concentrated to ~1.5 mL. Hexanes (8 mL) was added and the vial was placed at -35 °C for 2 h. The solids were isolated by filtration, washed with hexanes (3 x 2 mL) and collected by dissolution in toluene. After evaporation of all solvents, **7** was obtained with a yield of 94% (57.5 mg, 0.062 mmol). Single crystals for XRD analysis were grown by slow vapor diffusion of hexanes into THF. <sup>1</sup>H NMR (C<sub>6</sub>D<sub>6</sub>): δ<sub>H</sub> 7.73 (broad singlet, 2H, Ar-*H*), 7.41 (broad singlet, 6H, Ar-*H*), 7.20 (broad singlet, 1H, Ar-*H*), 7.12-6.72 (m, 30H, Ar-*H*), 6.45 (t, *J* = 7 Hz, 1H, imine-*CH* (or Ar-*H*)), 6.17 (broad singlet, 1H, Ar-*H* (or imine-*CH*)), 5.81 (dd, *J* = 3, 8 Hz, 1H, Ar-*H* (or imine-*CH*)), 2.48 (broad singlet, 6H, *o*Tol-Me) 2.43 (broad singlet, 3H, *o*Tol-Me), 1.76 (broad singlet, 3H, *o*Tol-Me) ppm. <sup>13</sup>C NMR (C<sub>6</sub>D<sub>6</sub>): δ<sub>C</sub> 165.23 (broad), 149.68 (broad), 143.32, 143.03, 142.76, 141.91, 141.79, 135.86, 135.50, 134.12 (d, *J*<sub>CP</sub> = 14 Hz), 133.87, 133.40, 132.98, 131.91, 131.28, 130.79, 130.34, 130.05, 129.11, 128.69, 126.68, 126.35, 126.04, 125.93, 123.47, 120.16, 117.71, 23.07, 21.70, 21.48, 21.12 ppm. <sup>31</sup>P NMR (C<sub>6</sub>D<sub>6</sub>): δ<sub>P</sub> 39.90, 10.80, -27.72 ppm. IR cm<sup>-1</sup>: 3052, 2969, 2924, 2854, 1952, 1919, 1811, 1669, 1573, 1454, 1435, 1392, 1309, 1260, 1202, 1159, 1118, 1093, 1026, 803, 748, 716, 695, 572, 521, 487, 460. Crystals for Xray analysis grown from THF/hexanes. Compound is too sensitive for transportation for elemental analysis.

**[Ni(P<sup>Ph</sup>CNP<sup>Ph</sup>)]<sub>2</sub> (8):** P<sup>Ph</sup>CNP<sup>Ph</sup> (**1**) (150.2 mg, 0.273 mmol) was suspended in toluene (2 mL). In a second vial, Ni(COD)<sub>2</sub> (74.9 mg, 0.272 mmol) was suspended in toluene (6 mL) and transferred to the ligand suspension. The yellow suspension directly changed color to a turbid yellow-brown mixture, and was left to stir for 5 h. All solvent was evaporated and the remaining solids were dissolved in THF (1 mL). The product was precipitated by addition of 8 mL of hexanes, followed by cooling the mixture to -35 °C before the solids were collected by filtration. The solids were collected by dissolution in THF, after which the solvents were evaporated. The mixture was dried under vacuum for 2 nights, after which the product mixture was obtained with a yield of 96% (159.6 mg, 0.131 mol). <sup>1</sup>H NMR (C<sub>6</sub>D<sub>6</sub>) major species **8a**: δ<sub>H</sub> 7.83-7.78 (m, Ar-*H*), 7.66-7.61 (m, Ar-*H*), 7.58-7.53 (m, Ar-*H*), 7.47 (ddd, *J* = 1.3, 3, 4.5 Hz, Ar-

*H*), 7.35-7.30 (m, Ar-*H*), 7.25 (dt, *J* = 2, 8 Hz, Ar-*H*), 7.13-6.44 (m, Ar-*H*), 6.39-6.35 (m, 1H, Ar-*H*), 5.49 (d, *J* = 2 Hz, 1H, CH-CH or imine-CH), 4.58, (d, *J* = 6 Hz, 1H, CH-CH or imine-CH) ppm. Minor species **8b**:  $\delta_{\text{H}}$  7.91 (t, *J* = 8 Hz, Ar-*H*), 7.21 (s, Ar-*H*), 7.19 (s, Ar-*H*), 6.29 (t, *J* = 8 Hz, Ar-*H*), 6.17 (t, *J* = 7 Hz, Ar-*H*), 5.31 (m), 3.88 (s) ppm.  $^{13}\text{C}$  NMR ( $\text{C}_6\text{D}_6$ ) **8a** + **8b**:  $\delta_{\text{C}}$  166.28 (d,  $J_{\text{CP}}$  = 38 Hz), 152.39 (d,  $J_{\text{CP}}$  = 38 Hz), 151.91 (dd,  $J_{\text{CP}}$  = 5, 15 Hz), 143.64 (d,  $J_{\text{CP}}$  = 12 Hz), 143.16 (d,  $J_{\text{CP}}$  = 11 Hz), 140.95, 140.66 (d,  $J_{\text{CP}}$  = 10 Hz), 140.43, 140.16, 139.92, 139.12, 139.04, 138.78, 138.601 (d,  $J_{\text{CP}}$  = 7 Hz), 140.65 (d,  $J_{\text{CP}}$  = 10 Hz), 139.13, 139.04, 138.78, 137.61 (d,  $J_{\text{CP}}$  = 7 Hz), 136.78 (d,  $J_{\text{CP}}$  = 5 Hz), 136.42, 136.16, 135.72, 135.56, 135.08, 134.93, 133.70, 133.61, 133.52, 133.46, 133.39, 133.26, 133.11, 133.01, 132.88, 132.73, 132.63, 132.21, 132.09, 131.56, 130.72, 130.06, 129.39, 129.34, 129.27, 129.13, 128.91, 128.82, 128.69, 128.57, 128.50, 127.53, 127.33, 125.70, 123.54, 121.24, 120.39, 117.32, 87.24 (d,  $J_{\text{CP}}$  = 26 Hz), 79.13 (d,  $J_{\text{CP}}$  = 6 Hz) ppm.  $^{31}\text{P}$  NMR ( $\text{C}_6\text{D}_6$ ) **8a**:  $\delta_{\text{P}}$  35.5 (dd,  $J_{\text{PP}}$  = 2, 70 Hz), 35.4 (d,  $J_{\text{PP}}$  = 9 Hz), 22.9 (dd,  $J_{\text{PP}}$  = 2, 9 Hz), -7.9 (d,  $J_{\text{PP}}$  = 70 Hz); **8b**: 38.32 (d,  $J_{\text{PP}}$  = 43 Hz), 1.05 (d,  $J_{\text{PP}}$  = 43 Hz) ppm. IR  $\text{cm}^{-1}$ : 3048, 2856, 1580, 1568, 1477, 1449, 1431, 1325, 1251, 1202, 1090, 1065, 1026, 919, 850, 735, 693, 497.

**[Ni(P<sup>Ph</sup>CNP<sup>Ph</sup>)]<sub>2</sub>(CO)<sub>2</sub> (**9a** and **9b**):** **8** (8.4 mg, 6.9  $\mu\text{mol}$ , the obtained mixture of **8a** and **8b** was used) was dissolved in  $\text{C}_6\text{D}_6$  (0.6 mL) and transferred to a Young-type NMR tube. The mixture was degassed to remove the  $\text{N}_2$  atmosphere (2 freeze-pump-thaw cycles) and charged with CO (1 atm) upon thawing of the solution. The tube was regularly shaken and the color of the mixture changed overnight from turbid red to clear orange. The progress of the reaction was checked by NMR analysis (Appendix E, Figure E8). The NMR tube was placed back in the glovebox, after which the mixture was filtered and transferred to a small reaction tube. The reaction tube was placed in a vial and hexanes (1 mL) was placed in the vial (crystallization setup) for crystallization to take place. After 2 days, crystals were formed and the liquid phase was removed by decantation. The crystals were washed with hexanes (3 x 1.5 mL), and dried in vacuum for no longer than 5 min, resulting in **9b**. The liquid phase was dried in vacuum as well, resulting in the bulk material **9a**.

**9b: 9b** was isolated as red-brown crystals with a yield of 20.5% (1.8 mg, 1.4  $\mu\text{mol}$ ).  $^1\text{H}$  NMR ( $\text{C}_6\text{D}_6$ ):  $\delta_{\text{H}}$  10.10 (dd, *J* = 4, 8 Hz, 2H, Ar-*H*), 7.91 (t, *J* = 2, 8 Hz, 4H, Ar-*H*), 7.75 (t, *J* = 8 Hz, 4H, Ar-*H*), 7.47 (m, 6H, Ar-*H*), 7.31 (m, 4H, Ar-*H*), 7.12-6.86 (m, 20H, Ar-*H*), 6.79-6.66 (m, 10H, Ar-*H*), 6.58 (t, *J* = 8 Hz, 2H, Ar-*H*), 6.50 (s, broad, 2H, Ar-*H*), 6.18 (t, *J* = 7 Hz, 2H, CH-CH), 5.95 (d, broad, *J* = 9 Hz, 2H, Ar-*H*) ppm.  $^{13}\text{C}$  NMR ( $\text{C}_6\text{D}_6$ ):  $\delta_{\text{C}}$  198.24 (-CO), 150.97, 134.75, 134.69, 134.62, 133.65, 133.59, 133.21, 133.12, 133.07, 132.70, 132.14, 132.07, 131.61, 130.09, 129.96, 129.51, 128.69, 126.53, 113.81, 112.79, 70.35 ppm.  $^{31}\text{P}$  NMR ( $\text{C}_6\text{D}_6$ ):  $\delta_{\text{P}}$  39.81, 22.12 ppm. IR  $\text{cm}^{-1}$ : 3051, 2963, 2922, 2853, 1999, 1938, 1680 (broad), 1578, 1479, 1452, 1435, 1328, 1260, 1095, 1026, 799, 740, 692, 526, 511, 499, 456.

**9a (bulk): 9a** was not isolated and only observed as a mixture together with an unknown byproduct. The mixture is a brown solid. Major signals in  $^1\text{H}$  NMR ( $\text{C}_6\text{D}_6$ ):  $\delta_{\text{H}}$  8.03 (t, *J* = 3 Hz, Ar-*H*), 7.84 (d, *J* = 2 Hz, Ar-*H* or N=CH), 7.62-7.52 (m, Ar-*H*), 7.22 (t, *J* = 8 Hz, Ar-*H*), 7.12 (dt, *J* = 1, 7 Hz, Ar-*H*), 7.01 (d, *J* = 1 Hz, Ar-*H*), 7.00-6.98 (m, Ar-*H*), 6.94-6.89 (m, Ar-*H*), 6.87 (t, *J* = 1 Hz, Ar-*H*), 6.85 (t, *J* = 1 Hz, Ar-*H*), 6.76 (t, *J* = 8 Hz, Ar-*H*), 6.27 (ddd, *J* = 1, 3, 5 Hz, Ar-*H*) ppm. Major signals in  $^{13}\text{C}$  NMR ( $\text{C}_6\text{D}_6$ ):  $\delta_{\text{C}}$  200.24 (dd,  $J_{\text{CP}}$  = 5, 6 Hz, -CO), 156.55, 154.58, 154.43, 139.36 (d,  $J_{\text{CP}}$  = 4 Hz), 139.04 (d,  $J_{\text{CP}}$  = 4 Hz), 138.95 (d,  $J_{\text{CP}}$  = 6 Hz), 138.78 (d,  $J_{\text{CP}}$  = 1 Hz), 138.66 (d,  $J_{\text{CP}}$  = 6 Hz), 138.08 (d,  $J_{\text{CP}}$  = 7 Hz), 134.93 (d,  $J_{\text{CP}}$  = 3 Hz), 133.96, 133.76, 133.62, 133.46, 133.33, 133.27 (d,  $J_{\text{CP}}$  = 5 Hz), 130.98, 130.32 (d,  $J_{\text{CP}}$  = 6 Hz), 129.33, 128.92 (d,  $J_{\text{CP}}$  = 1 Hz), 128.68, 128.58 (d,  $J_{\text{CP}}$  = 1 Hz), 128.50, 128.42, 128.36, 127.40, 127.06, 126.80, 15.85 (d,  $J_{\text{CP}}$  = 4 Hz), 125.70, 117.76 (d,  $J_{\text{CP}}$  = 5 Hz), 110.42 ppm.  $^{31}\text{P}$  NMR ( $\text{C}_6\text{D}_6$ ):  $\delta_{\text{P}}$  33.04 (d,  $J_{\text{PP}}$  = 11 Hz), 16.23 (d,  $J_{\text{PP}}$  = 11 Hz) ppm. Unidentified impurity: 26.32 (d, *J* = 25 Hz), 23.08 (d, *J* = 25 Hz). Major

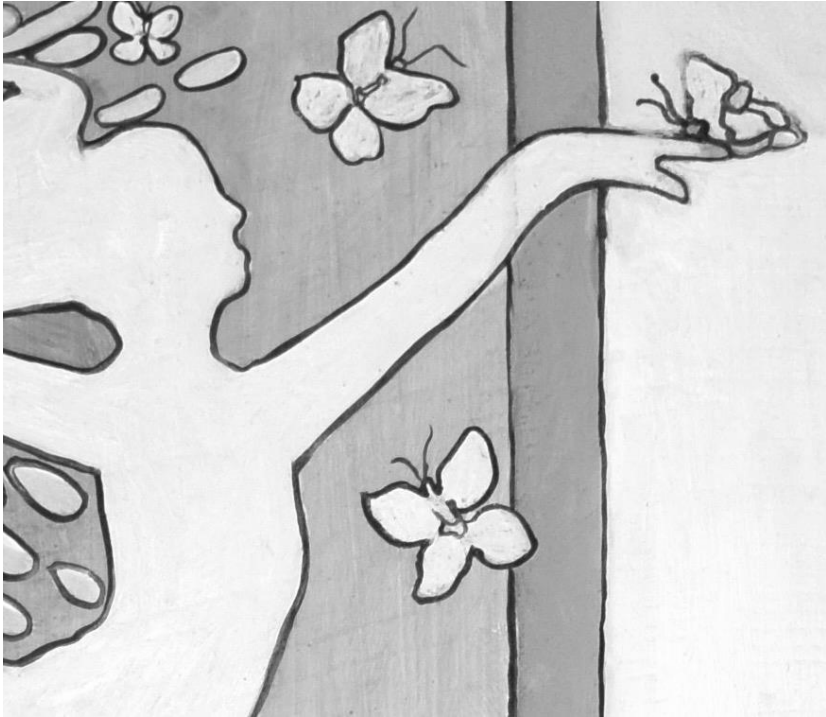
signals in IR  $\text{cm}^{-1}$ : 3054, 3002, 2957, 2925, 2855, 2068, 1991, 1929, 1629, 1578, 1460, 1434, 1266, 1184, 1090, 1028, 884, 766, 744, 695, 508.

## 5.5 References and notes

- [1] J. R. Khusnutdinova and D. Milstein, *Angew. Chem. Int. Ed.*, **2015**, *54*, 12236–12273.
- [2] P. J. Chirik and K. Wieghardt, *Science*, **2010**, *327*, 794–795.
- [3] Chapter 1 of this thesis: D. G. A. Verhoeven, M. -E. Moret, *Dalton Trans.*, **2016**, *45*, 15762–15778.
- [4] J. I. van der Vlugt, *Eur. J. Inorg. Chem.*, **2012**, 363–375.
- [5] F. Fache, E. Schulz, M. L. Tommasino, M. Lemaire, *Chem. Rev.*, **2000**, *100*, 2159–2231.
- [6] Examples are: Salen ligand: a) L. Canali, D. C. Sherrington, *Chem. Soc. Rev.*, **1999**, *28*, 85–93. b) A. W. Kleij, *Eur. J. Inorg. Chem.*, **2009**, 193–205. Morris complexes: c) P. E. Sues, K. Z. Demmans, R. H. Morris, *Dalton Trans.*, **2014**, *43*, 7650–7667. d) S. A. M. Smith, P. O. Lagaditis, A. Lupke, A. J. Lough, R. H. Morris, *Chem. Eur. J.*, **2017**, *23*, 7212–7216. Noyori complex: e) J. -X. Gao, T. Ikariya, R. Noyori, *Organometallics*, **1996**, *15*, 1087–1089. Iminopyrrole ligands: f) F. -B. Han, Y. -L. Zhang, X. -L. Sun, B. -G. Li, Y. -H. Guo, Y. Tang, *Organometallics*, **2008**, *27*, 1924–1928. Pyridine-Imine ligands: g) Z. Chen, K. E. Allen, P. S. White, O. Daugulis, M. Brookhart, *Organometallics*, **2016**, *35*, 1756–1760. h) D. Zhu, I. Thapa, I. Korobkov, S. Gambarotta, P. H. M. Budzelaar, *Inorg. Chem.*, **2011**, 9879–9887. i) E. C. Volpe, P. T. Wolczanski, E. B. Lobkovsky, *Organometallics*, **2010**, *29*, 364–377. Dinuclear Ni-complexes: j) T. J. Steinman, C. Uyeda, *J. Am. Chem. Soc.*, **2015**, *137*, 6104–6110.
- [7] P. J. Chirik, *Angew. Chem. Int. Ed.*, **2017**, *56*, 5170–5181.
- [8] J. Hou, W. -H. Sun, S. Zhang, H. Ma, Y. Deng, X. Lu, *Organometallics*, **2006**, *25*, 236–244.
- [9] L. Chen, P. Ai, J. Gu, S. Jie, B.-G. Li, *J. Orgnomet. Chem.*, **2012**, *716*, 55–61.
- [10] S. Doherty, J. G. Knight, T. H. Scanlan, M. R. J. Elsegood, W. Clegg, *J. Orgnomet. Chem.*, **2002**, *650*, 231–248.
- [11] B. Crociani, S. Antonaroli, P. Paoli, P. Rossi, *Dalton Trans.*, **2012**, *41*, 12490–12500.
- [12] a) H. Hoberg, V. Gotz, C. Kruger, Y. -H. Tsay, *J. Organomet. Chem.*, **1979**, *169*, 209–217. b) R. S. Manan, P. Kilaru, P. Zhao, *J. Am. Chem. Soc.*, **2015**, *137*(19), 6136–6139. c) Y. Hoshimoto, T. Ohata, M. Ohashi, S. Ogoshi, *Chem. Eur. J.*, **2014**, *20*(14), 4105–4110. d) A. L. Iglesias, M. Muñoz-Hernández, J. J. García, *J. Organomet. Chem.*, **2007**, *692*(16), 3498–3507. e) J. Cámpora, I. Matas, P. Palma, E. Álvarez, C. Graiff, A. Tiripicchio, *Organometallics*, **2007**, *26*(15), 3840–3849. f) Z. Weng, S. Teo, L. L. Koh, T. S. A. Hor, *Angew. Chem. Int. Ed.*, **2005**, *44*(46), 7560–7564.
- [13] B. R. Reed, M. Yousif, R. L. Lord, M. McKinnon, J. Rochford, S. Groysman, *Organometallics*, **2017**, *36*, 582–593.
- [14] C. Tejel, M. A. Ciriano, M. Pilar del Rio, F. J. van den Bruele, D. G. H. Hetterscheid, N. Tschlis i Spithas and B. de Bruin, *J. Am. Chem. Soc.*, **2008**, *130*, 5844–5845.
- [15] P. Maire, A. Sreekanth, T. Büttner, J. Harmer, I. Gromov, H. Rüegger, F. Breher, A. Schweiger and H. Grützmacher, *Angew. Chem. Int. Ed.*, **2006**, *45*, 3265–3269.
- [16] W. I. Dzik, S. E. Calvo, J. N. H. Reek, M. Lutz, M. A. Ciriano, C. Tejel, D. G. H. Hetterscheid and B. de Bruin, *Organometallics*, **2011**, *30*, 372–374.

- [17] C. Tejel, L. Asensio, M. P. del Río, B. de Bruin, J. A. López and M. A. Ciriano, *Eur. J. Inorg. Chem.*, **2012**, 512–519.
- [18] C. Tejel, L. Asensio, M. P. del Río, B. de Bruin, J. A. López and M. A. Ciriano, *Angew. Chem. Int. Ed.*, **2011**, *50*, 8839–8843.
- [19] T. Büttner, F. Breher and H. Grützmacher, *Chem. Commun.*, **2004**, 2820–2821.
- [20] E. W. Ainscough, A. M. Brodie, P. D. Buckley, A. K. Burrell, S. M. F. Kennedy, J. M. Waters, *Dalton Trans.*, **2000**, 2663–2671.
- [21] S. Doherty, J. G. Knight, T. H. Scanlan, M. R. J. Elsegood, W. Clegg, *J. Organomet. Chem.*, **2002**, *650*, 231–248.
- [22] The signal likely shifts to a more crowded region and could not be assigned unambiguously.
- [23] Similar experiments with more bulky ligands **4** and **5** lead to unassigned mixtures of products.
- [24] W.-Y. Chu, R. Gilbert-Wilson, T. B. Rauchfuss, M. van Gastel, F. Neese, *Organometallics*, **2016**, *35*(17), 2900–2914.
- [25] A COSY spectrum shows no coupling of these signals. The peaks do not appear as doublets, so if a coupling would be present it would be small. In a C–C bound structure, these protons would be located in vicinal positions. In complex **9** this vicinal angle is determined around 75–80° (determined in XRD of calculated positions and in geom opt structure by DFT), which leads to a very small coupling (0–2 Hz based on the Karplus curve), and so it is likely this is not observed. *Spectroscopic Methods in Organic Chemistry*, M. Hesse, H. Meier, B. Zeeh, Georg Thieme Verlag, Stuttgart, **2008**, p 113.
- [26] W.-Y. Chu, C. P. Richers, E. R. Kahle, T. B. Rauchfuss, *Organometallics*, **2016**, *35*, 2782–2792.
- [27] H. Lei, A. M. Royer, T. B. Rauchfuss, D. Gray, *Organometallics*, **2012**, *31*, 6408–6414.
- [28] Other imine couplings: a) C. Floriani, E. Solari, F. Franceschi, R. Scopelliti, P. Belanzoni, M. Rosi, *Chem. Eur. J.*, **2001**, *7*(14), 3052–3061. b) F. Franceschi, E. Solari, R. Scopelliti, C. Floriani, *Angew. Chem. Int. Ed.*, **2000**, *39*(9), 1685–1987.
- [29] M. K. Cooper, P. A. Duckworth, T. W. Hambley, G. J. Organ, K. Henrick, M. McPartlin, A. Parekh, *J. Chem. Soc., Dalton Trans.*, **1989**, *6*, 1067–1073.
- [30] Other pinacol couplings: a) E. Folkertsma, S. H. Benthem, L. Witteman, C. A. M. R. van Slagmaat, M. Lutz, R. J. M. Klein Gebbink, M. -E. Moret, *Dalton Trans.*, **2017**, *46*(19), 6177–6182. b) Z. Hou, A. Fujita, Y. Zhang, T. Miyano, H. Yamazaki, Y. Wakatsuki, *J. Am. Chem. Soc.*, **1998**, *120*, 754–766.
- [31] a) E. Nicolas, A. Ohleier, F. D’Accriscio, A.-F. Pöcharman, M. Demange, P. Ribagnac, J. Ballester, C. Gosmini, N. Mézailles, *Chem. Eur. J.*, **2015**, *21*, 7690–7694. b) A. N. Desnoyer, E. G. Bowes, B. O. Patrick, J. A. Love, *J. Am. Chem. Soc.*, **2015**, *137*, 12748–12751.
- [32] S. Laue, L. Greiner, J. Wöltinger, A. Liese, *Adv. Synth. Catal.*, **2001**, *343*, 711–720.
- [33] F. Schaufelberger, O. Ramström, *Chem. Eur. J.*, **2015**, *21*, 12735–12740.
- [34] L. B. Schenkel, J. A. Ellman, *Org. Lett.*, **2003**, *5*(4), 545–548.
- [35] J. Okuda, T. Eberle, T. P. Spaniol, V. Piquet-Fauré, *J. Organomet. Chem.*, **1999**, *591*, 127–137.
- [36] S. Doherty, J. G. Knight, T. H. Scanlan, M. R. J. Elsegood, W. Clegg, *J. Organomet. Chem.*, **2002**, *650*, 231–248.





*Like the stars chase the sun over the glowing hills, I will conquer.*  
- Florence L. M. Welch

# | Chapter 6 |

## Nickel Complexes with Diphosphine-Tethered Imine Ligands: Silane Activation, Hydrosilylation and Mechanistic Insights

**Abstract** The reactivity of Ni(0) complexes of chelating diphosphine-imine ligands toward silanes is investigated. The presented complexes activate a Si–H bond of the secondary silane diphenylsilane by hydrosilylation of the imine-backbone, in which a hydride is added to the imine-carbon atom. The resulting *N*-bound silyl group engages in coordination of the Si–H bond to nickel, either *via*  $\eta^2$ (Si,H)-coordination in an 18 electron complex, or *via* oxidative addition of this bond to Ni at 16 electron complexes. The mechanism of this activation is investigated by DFT calculations, suggesting a Ni-mediated mechanism and cooperative activation of the silane. The silane-complexes are active catalysts for the hydrosilylation of 1-octene, resulting in full conversion of the substrates and full selectivity toward the anti-Markovnikov products. Mechanistic investigations by stoichiometric reactions reveal, amongst other, that the Si–N bond can be reversibly cleaved under the catalytic conditions.

---

D. G. A. Verhoeven, M. Lutz, M. -E. Moret, *to be submitted*.

## 6.1 Introduction

Metal-mediated activation of Si–H bonds is often the first step in the homogeneously catalyzed hydrosilylation of alkenes,<sup>[1,2]</sup> where the silane reagent is added over the C=C double bond of the alkene (Figure 1a). Chalk and Harrod proposed the mechanism which is thought to be operative in most cases for metal-catalyzed hydrosilylation reactions (Figure 1c).<sup>[3]</sup> In this mechanism, a Si–H bond is activated and undergoes oxidative addition to a metal center, resulting in a silyl and a hydride ligand. The alkene then coordinates to this metal, followed by migratory insertion into the M–H bond. Reductive elimination closes the cycle, resulting in product formation and regeneration of the catalyst. Most transition-metal catalyzed hydrosilylation reactions are thought to follow the steps of the Chalk-Harrod mechanism, but in some cases isolation of reaction intermediates suggests that the alkene insertion takes place into the M–Si bond instead of the M–H bond, resulting in a modified Chalk-Harrod mechanism (Figure 1c, dotted lines).

The hydrosilylation of unsaturated compounds, amongst which olefins, is of high importance in for example the polymer industry, as it is used in the formation of silicon polymers, oils and resins, and in the fine chemical industry for the production of organosilicon reagents. Whereas hydrosilylation reactions are commonly performed by precious metals such as Pt,<sup>[4-6]</sup> research is now developing toward using first row transition metals<sup>[7-10]</sup> including nickel.<sup>[11-12]</sup> A number of nickel-catalyzed hydrosilylations of olefins are reported.<sup>[13,14]</sup> Key examples for the hydrosilylation of 1-octene with diphenylsilane were shown by Shimada and co-workers in 2015,<sup>[15]</sup> using 0.5 mol% of a (salicylaldiminato)methylnickel catalyst (Figure 1b) at RT for 1 h in MeCN yielding 91% *n*-octyldiphenylsilane, which follows the modified Chalk-Harrod mechanism, and by Hu and coworkers in the same year,<sup>[16]</sup> using 1 mol% of a NNN-pincer Ni(II)OMe complex, at RT for 6 h in THF, resulting in 93% of the same product.

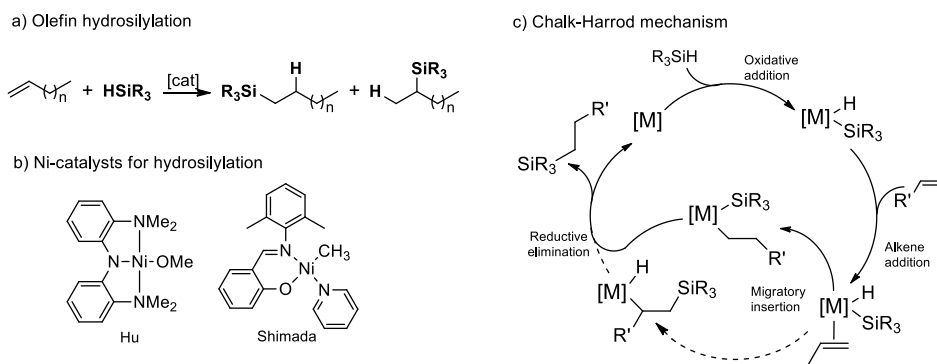


**Figure 1.** Nickel catalyzed hydrosilylation of alkenes. a) Olefin hydrosilylation, b) key examples of hydrosilylation catalysts, c) the Chalk-Harrod mechanism,<sup>[3]</sup> with the modified mechanism shown with dotted lines.



One of the challenges associated with the use of first row transition metals in catalysis is the selective activation of substrates, e.g. by oxidative addition, avoiding often undesired one-electron pathways. Tackling this issue benefits greatly from the development of well-designed ligand systems, assisting in such two-electron steps.<sup>[17,18]</sup> Herein, systems employing metal-ligand cooperativity play an ever-growing role.<sup>[18]</sup> Particularly attractive for element-hydrogen bond activation are  $\pi$ -ligands with the possibility to act as hydride acceptors (Figure 2).<sup>[19,20]</sup> These include the *p*-terphenyl diphenylphosphine nickel(0) complexes introduced by Agapie and co-workers,<sup>[21]</sup> which can undergo hydride shuttling from the metal center to the aromatic ligand backbone, and the diphenylphosphine substituted *trans*-stilbene ligands in a Ni complex as employed by the group of Iluc, which can reversibly transfer a hydride to the metal by oxidative addition of a C-H bond to form a Ni(II) vinyl/hydride complex.<sup>[22]</sup> Moreover, cooperative ligands can assist in the activation of silane substrates, which was for example observed in a nickel system with a diphosphine-pyridine ligand, which activates phenylsilane over a N-C bond in the ring (Figure 2).<sup>[23]</sup> In a related study, the group of Peters showed cooperative activation of diphenylsilane by a tridentate diphosphanylborane-nickel complex, forming a borohydrido-Ni-silyl species in which SiHPh<sub>2</sub> is bound to nickel and the hydride is inserted in the B-Ni bond (Figure 2).<sup>[24]</sup> The latter cooperative Si-H activation is also thought to be involved in catalytic aldehyde hydrosilylation reactions.<sup>[24]</sup>

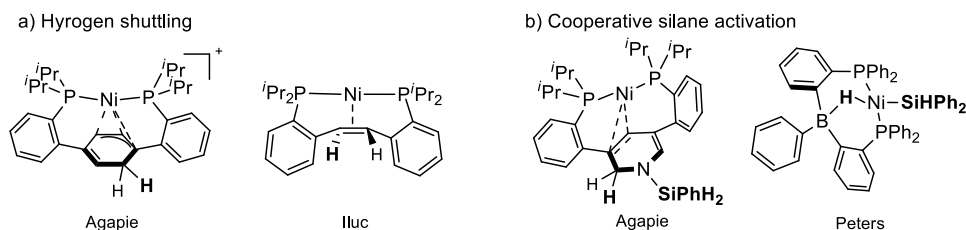
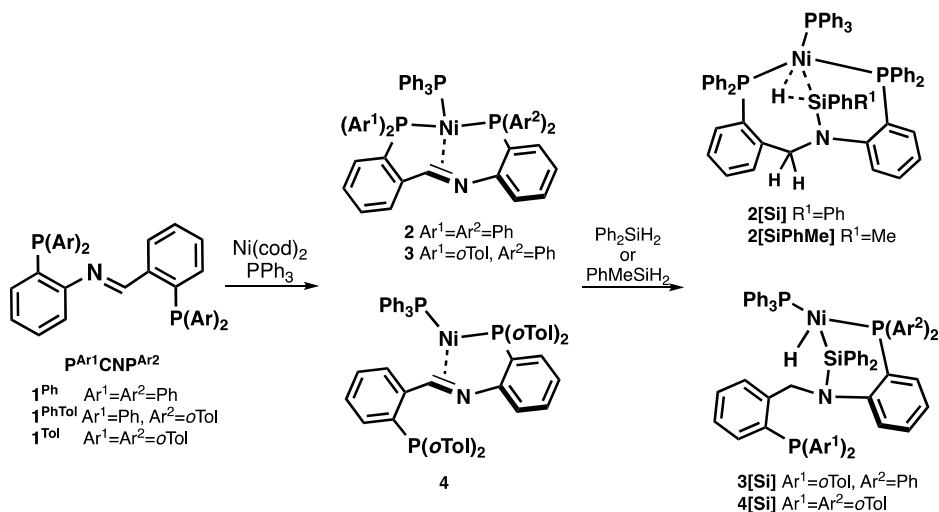


**Figure 2.** Cooperative Ni-systems. a)  $\pi$ -ligands that can reversibly accept a hydride (in bold) from the metal b) Products of cooperative silane activation. Also see Chapter 1, Scheme 4, Figure 11 and 14.

Aiming at developing cooperative  $\pi$ -ligands based on polar C=N bonds, the Ni(0) coordination of a series of ligands consisting of an imine functionality bridged by two *o*-phenylene linkers substituted with phosphine substituents (PCNP) was reported recently by our group (Chapter 5 of this thesis), including the diphenyl, di-*ortho*-tolyl or the mixed phenyl/*o*-tolyl ligands (Scheme 1). The less bulky ligands afforded tetrahedral Ni(0) complexes Ni(P<sup>Ph</sup>CNP<sup>Ph</sup>)PPh<sub>3</sub> (**2**) and Ni(P<sup>Ph</sup>CNP<sup>*o*Tol</sup>)PPh<sub>3</sub> (**3**) with the PCNP ligand bound *via* both phosphine arms and an  $\eta^2$ (C,N)-coordination of the imine moiety. In contrast, the more encumbered ligand P<sup>*o*Tol</sup>CNP<sup>*o*Tol</sup> resulted in the tricoordinate complex **4**, in which the carbon-sided phosphine arm is not bound to nickel due to increased bulk on the ligand.

Herein an investigation of nickel-catalyzed hydrosilylation reactions employing PCNP ligands is presented. Inspired by the use of  $\pi$ -ligands in bifunctional activation of substrates, the reactivity of complexes **2-4** toward diphenylsilane is explored. All complexes activate one equivalent of diphenylsilane, resulting in the formal hydrosilylation of the ligands' C=N backbone accompanied by  $\eta^2$ -coordination or oxidative addition of the remaining Si-H bond (Scheme 1). The resulting complexes are shown to be active precatalysts in the hydrosilylation of 1-octene with diphenylsilane under mild conditions, with a catalyst loading of 1 mol%. The mechanism of this reaction is discussed on the basis of stoichiometric experiments. In particular, silane scrambling *via* reversible Si-N bond cleavage is taking place under the hydrosilylation conditions.



**Scheme 1.** The PCNP ligands, the synthesized Ni(0) complexes **2**, **3** and **4**, and the products of silane activation **2[Si]**, **2[SiPhMe]**, **3[Si]** and **4[Si]**.

## 6.2 Results and discussion

### 6.2.1 Silane activation

In a first experiment, the reaction of **2** with diphenylsilane was investigated. Diphenylsilane was added to a suspension of  $\text{Ni}(\text{P}^{\text{Ph}}\text{CNP}^{\text{Ph}})(\text{PPh}_3)$  (**2**) in benzene resulting in the formation of a single, isolable product **2[Si]** (Scheme 1), identified by multinuclear NMR spectroscopy. In the  $^1\text{H}$  NMR, a single hydridic peak is observed with ddd multiplicity at  $\delta -2.77$  ppm ( $J_{\text{HP}} = 36, 23, 19$  Hz). In a broadband phosphorus decoupled  $^1\text{H}$  NMR spectrum, this signal appears as a singlet peak with  $^{29}\text{Si}$  satellites ( $J_{\text{HSi}} = 109$  Hz), indicating the presence of a Si-H moiety coordinated to nickel(0) in an  $\eta^2$ -fashion (Appendix F, Figure F1-2). Typically, values of about 60–150 Hz<sup>[25]</sup> are found for  $\eta^2$ -Si-H complexes, and smaller coupling constants (10–20 Hz)<sup>[2,26]</sup> are obtained upon oxidative addition of the Si-H bond to nickel, resulting in a Si-Ni-H

complex. Well-characterized  $\sigma$ -coordinating Si–H bonds to nickel are rare, but not unprecedented in literature.<sup>[27-30]</sup>

Next to this, three phosphorus atoms are bound to nickel, as shown by the coupling pattern of the Si–H signal, and the  $^{31}\text{P}$  NMR spectrum which contains three mutually coupled signals at  $\delta$  32.8 (dd,  $J_{\text{PP}} = 3, 17$  Hz), 17.1 (dd,  $J_{\text{PP}} = 17, 45$  Hz) and 7.8 (dd,  $J_{\text{PP}} = 3, 45$  Hz) ppm. The  $^{29}\text{Si}$  NMR spectrum contains one signal at  $\delta$  –6.5 ppm with a ddd coupling pattern, originating from coupling with the three  $^{31}\text{P}$  nuclei ( $J_{\text{SiP}} = 3, 17, 60$  Hz). Moreover, the  $^1\text{H}$  NMR spectrum displays two doublet signals ( $^2J_{\text{HH}} = 15$  Hz) at  $\delta$  4.61 and 5.01 ppm, assigned to the diastereotopic protons of the –CH<sub>2</sub> moiety originating from hydride addition to the imine-carbon **2**. These protons are diastereotopic due to chirality of complex **2[Si]** arising from the stereogenic tetrahedral Ni(0) center. The CH<sub>2</sub> signals in  $^1\text{H}$  NMR show temperature dependent behavior, with coalescence to one broad feature at 70 °C. This could be caused by racemization of the Ni center by reversible dissociation of one of the phosphine tethers to form a planar intermediate. Combining the NMR data leads to the assignment of **2[Si]** as the result of the formal hydrosilylation of the C=N bond, in which the N-bound –SiPh<sub>2</sub>H moiety is coordinated to Ni *via* a  $\sigma$ -bound Si–H bond (Scheme 1).

The IR spectrum of **2[Si]** does not display a signal that can unambiguously be assigned to a hydride vibration and no indicative shift was obtained upon formation and characterization of the deuterium analogue **2[SiD<sub>2</sub>]** (*vide infra*). A likely explanation could be the cyclic character of the Si–H–Ni moiety, as shown by the positions of the  $^{29}\text{Si}$  satellites in  $^1\text{H}$  NMR at 109 Hz, i.e.  $\eta^2$ -coordination of the Si–H bond to Ni. This rigid geometry would hamper vibrational freedom and lowers the intensity of the bands in IR spectroscopy.<sup>[31]</sup>

As anticipated for an imine hydrosilylation reaction, addition of Ph<sub>2</sub>SiD<sub>2</sub> to **2** resulted in the deuterium labelled complex **2[SiD<sub>2</sub>]** with exclusive deuterium incorporation at the Si–H (100%) and CH<sub>2</sub> (50%) positions. Analysis of **2[SiD<sub>2</sub>]** by NMR shows spectra similar to **2[Si]**, but with the incorporation of an extra deuterium coupling in the  $^{31}\text{P}$  NMR spectrum, and the absence of the hydride peak in  $^1\text{H}$  NMR. The  $^2\text{H}$  NMR spectrum shows a broad signal at  $\delta$  –2.6 ppm for Si–D. The geminal –CHD signals are observed as two singlet signals in  $^1\text{H}$  NMR with similar intensity, indicating the random positioning of the deuterium atom over the two diastereotopic sites. This is a result of chemical exchange between these two positions – likely *via* reversible decoordination of the phosphine tethers causing racemization of the nickel center – as was also observed by VT NMR.

In addition, the prochiral silane PhMeSiH<sub>2</sub> also adds cleanly to compound **2** in C<sub>6</sub>D<sub>6</sub>, and forms an equilibrium mixture of two diastereomers (Figure 4). Accordingly, the  $^1\text{H}$  NMR spectrum exhibits two similar sets of signals with a ratio of 3:1, evidently visible at the hydride signals (ddd), where different chemical shifts for the two species are obtained at  $\delta$  –2.52 and –2.84 ppm (Figure 3). The hydride signals become singlets upon broad band phosphorous decoupling, from which the  $J_{\text{HSi}}$  coupling constants were determined at 111 Hz (major) and 102 Hz (minor). Likewise, the  $^{31}\text{P}$  NMR spectrum shows two sets of peaks in a ratio of approximately 3:1, with signals for the major species at  $\delta$  30.28, 17.94 and 10.43

ppm and  $\delta$  33.29, 17.52 and 7.78 ppm for the minor species (Figure 3). This pattern was reflected as well in the  $^{29}\text{Si}$  NMR spectrum ( $\delta$  -3.19 and -8.32 ppm, Figure 3). The two diastereomers of **2[SiPhMe]** are thought to originate from the presence of two tetrahedral stereocenters at Si and Ni, equilibrating *via* racemization of the Ni-center (*vide supra*). In other words, the silicon-bound methyl group can be orientated toward the imine-N or to the imine-C (Figure 4). Optimizing the geometries of the two enantiomers of **2[SiPhMe]** by DFT at the B3LYP/6-31G\*\* level of theory afforded a small Gibbs free energy difference  $\Delta G = 0.02$  kcal/mol, in agreement with the observation of both species at equilibrium.

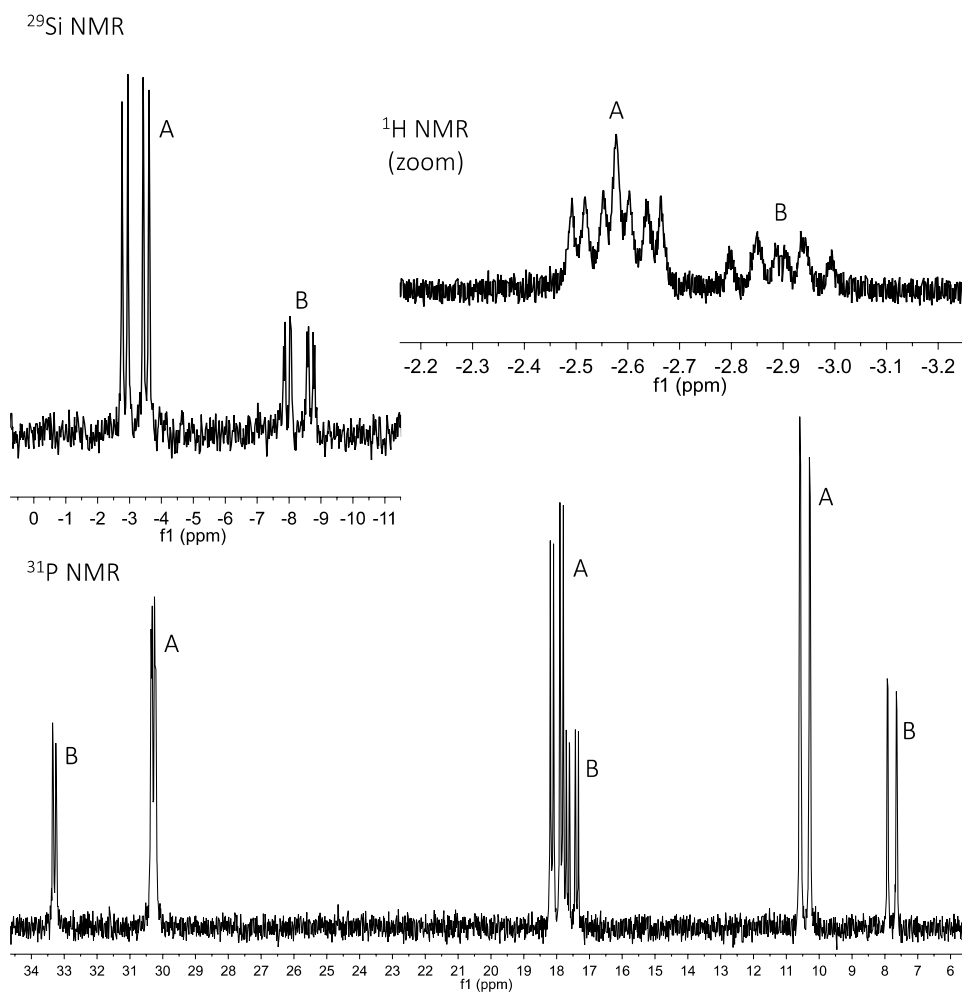


Figure 3. NMR spectra of **2[SiPhMe]**. A: major species, B: minor species.

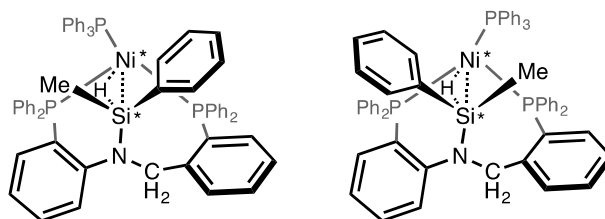


Figure 4. Diastereomers of 2[SiPhMe].

### 6.2.2 Ligand variation

The effect of additional steric bulk on the ligands was studied with *o*-tolyl substituted complexes **3** and **4**. Addition of diphenylsilane to **3** or **4** in C<sub>6</sub>D<sub>6</sub> resulted in both cases in a single species, forming **3[Si]** and **4[Si]**, respectively. NMR analysis of **3[Si]** shows a hydridic signal at  $\delta$  -4.40 ppm (dd,  $J_{HP} = 19, 92$  Hz) in <sup>1</sup>H NMR, and <sup>29</sup>Si satellites are visible upon measuring the broadband phosphorus decoupled <sup>1</sup>H NMR spectrum at  $J_{HSi} = 18$  Hz. In stark contrast with that observed for **2[Si]**, the coupling constant is smaller than typical for  $\eta^2$ -Si-H complexes (~60-150 Hz),<sup>[25]</sup> and is likely to be nickel-mediated in a Ni(II) silyl/hydride compound.<sup>[2]</sup> For **4[Si]**, a similar signal is observed at  $\delta$  -5.53 ppm (dd,  $J_{HP} = 19, 85$  Hz). The observation of the <sup>29</sup>Si satellites corresponding to the hydride signal is complicated due to broadening of all signals, likely due to fluxionality in the structure. Approximate assignment in a broadband phosphorous decoupled <sup>1</sup>H NMR leads to a  $J_{HSi}$  of ~14 Hz. <sup>31</sup>P NMR data of **3[Si]** and **4[Si]** shows in both cases three signals, located at  $\delta$  27, 22 and -32 ppm for **3[Si]** and at  $\delta$  26.0, 4.8 and -31.3 ppm for **4[Si]**, indicating the presence of one unbound and two nickel-bound phosphine moieties. This is consistent with the observed dd coupling pattern of the hydride signals, showing a coupling with only two <sup>31</sup>P nuclei. ATR-IR of **3[Si]** was unreliable due to its high air sensitivity, even in the solid state under a N<sub>2</sub> flow, but analysis of **4[Si]** shows a band at 1862 cm<sup>-1</sup> that was assigned to the Ni-H vibration. Accordingly, this band disappears in the deuterated analogue formed by addition of Ph<sub>2</sub>SiD<sub>2</sub> to **4**, yielding **4[SiD<sub>2</sub>]**. The corresponding M-D band could not be unambiguously identified in the crowded region of the spectrum.

X-ray crystal structure determination on single crystals grown *via* slow vapor diffusion of hexanes into a benzene solution of either **3[Si]** or **4[Si]** confirms the interpretation of the spectroscopic data (Figure 5, bottom). In both complexes a distorted square planar geometry around nickel is observed, bound to a phosphorous atom of the supporting ligand, PPh<sub>3</sub>, and a silyl and hydride originating from the activated Si-H bond. Based on the electron density it was not possible to distinguish P and Si atoms. The assignment was consequently based on spectroscopic data. The hydride could not be located in the difference electron density maps. Similar structures from literature support its allocation,<sup>[1,27,32-24]</sup> such as reports by the group of Radius,<sup>[2,26]</sup> where addition of Ph<sub>2</sub>MeSiH to Ni(*i*Pr<sub>2</sub>Im)<sub>2</sub> (*i*Pr<sub>2</sub>Im = 1,3-di-*isopropyl*-

imidazolin-2-ylidene) was shown, resulting in the hydro silyl complex with distances of Ni–H: 1.462(16) Å, Si–H: 1.979(16) Å and Ni–Si: 2.195(1) Å, which exhibits a  $^2J_{\text{SiH}}$  of 11 Hz.

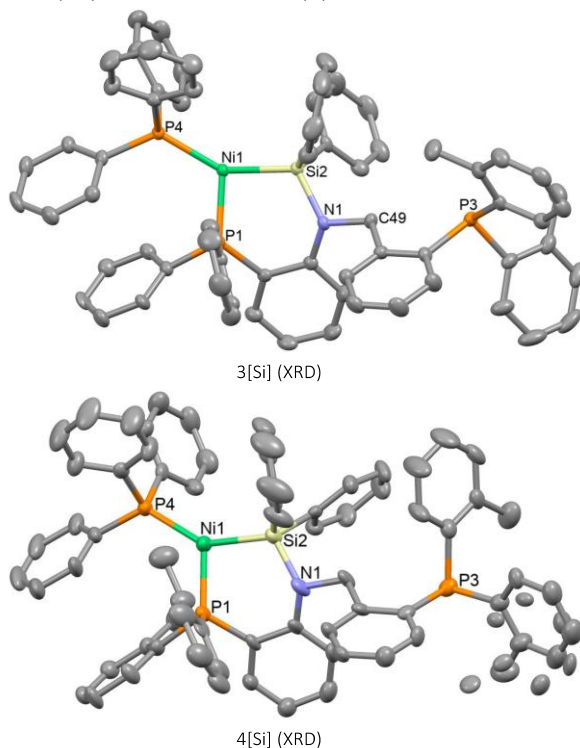


**Figure 5.** X-ray crystal structure **3[Si]** and **4[Si]**, hydrogen atoms omitted for clarity and ellipsoids are shown at 50% probability. Selected bond distances and angles are shown in Table 1.

To get more insight in this bonding situation, geometry optimization calculations by DFT were performed for **2-4** at the B3LYP/6-31G\*\* level of theory (Table 1). For **3** and **4**, the geometry optimizations were performed starting from the X-ray crystal structures. In all complexes, the Ni–H distance is similar (**2**: 1.51 Å, **3**: 1.48 Å, **4**: 1.48 Å). The Si–H distance, however, shows an increase from **2** to **3** and **4**, with calculated values for **2** at 1.71 Å, to 1.98 Å and 1.94 Å for **3** and **4**, respectively. Moreover, the angles around nickel – specifically the  $\angle\text{SiNiH}$  and  $\angle\text{PNiH}$  – indicate the displacement of the hydride atom with respect to the Si–H bond. For **2**, the difference between  $\angle\text{SiNiH}$  and  $\angle\text{PNiH}$  is relatively large, i.e. 49.6° and 87.7°, respectively. These angles are closer in **3** and **4** due to an increase of  $\angle\text{SiNiH}$ : a  $\angle\text{SiNiH}$  of 62.2° and 60.8°, and a  $\angle\text{PNiH}$  of 86.2° and 85.2°, for respectively **3** and **4**, are obtained, showing a larger Ni–H character in these latter two complexes indicated by the localization of the hydride closer to the optimal position based on steric factors. This suggests that the activation of the Si–H bond by Ni significantly increases going from the 18-electron complex **2**, to the 16-electron complexes **3** and **4**, which is in line with the before mentioned coupling of the  $^{29}\text{Si}$  satellites in  $^1\text{H}$  NMR ( $J_{\text{Hsi}}$  (Hz) **2**: 109, **3**: 18, **4**: ~14) for these complexes. The

different geometry in case of complex **2**, compared to **3** and **4**, is attributed to the decreased bulk at phosphorus, and the four-coordination of the nickel center likely leads to a lesser activation of the Si–H bond.

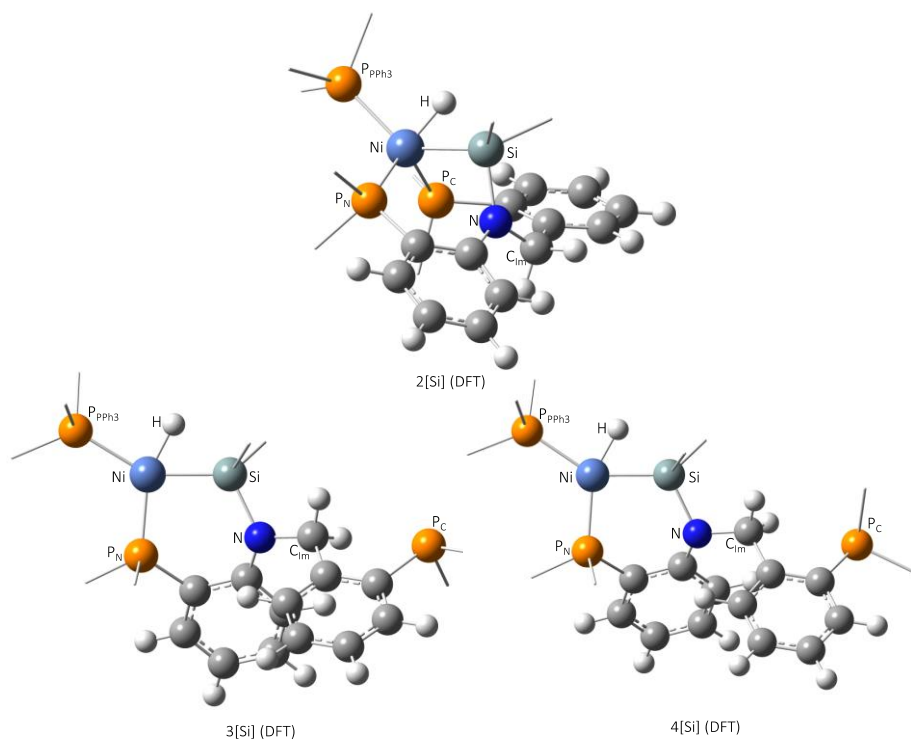


**Figure 5.** DFT calculated structures of **2[Si]**, **3[Si]** and **4[Si]**. Phenyl rings are omitted for clarity, and positioning of the rings are shown. Selected bond distances and angles are shown in Table 1.

**Table 1.** Comparison of selected bond lengths and angles of **2[Si]**-**4[Si]**, as calculated by DFT and the X-ray crystal structures. Bond lengths are given in Å and bond angles in °.

	<b>2[Si]</b> DFT	<b>3[Si]</b> DFT	<b>3[Si]</b> XRD	<b>4[Si]</b> DFT	<b>4[Si]</b> XRD
Ni–H	1.512	1.480	-	1.478	-
Si–H	1.709	1.976	-	1.943	-
Ni–Si	2.243	2.169	2.1864(13)	2.175	2.196(2)
Si–N	1.815	1.838	1.800(4)	1.841	1.781(7)
N–C <sub>im</sub>	1.463	1.472	1.470(6)	1.473	1.492(9)
Ni–PPh <sub>3</sub>	2.297	2.211	2.1852(13)	2.232	2.213(2)
Ni–P <sub>N</sub>	2.243	2.130	2.1194(13)	2.158	2.143(2)
Ni–P <sub>C</sub>	2.343	7.758	7.6617(15)	7.735	7.690(2)
Si–Ni–H	49.60	62.23	-	60.77	-
PPh <sub>3</sub> –Ni–H	87.71	86.16	-	85.18	-

### 6.2.3 DFT calculations

A possible pathway for the C=N hydrosilylation of compound **2** was modelled theoretically. DFT calculations were performed at the B3LYP/6-31G\*\* level of theory with added dispersion correction and a benzene solvent matrix (Chart 1). The first step is the dissociation of the PPh<sub>3</sub> co-ligand from Ni, with a  $\Delta G$  of 25.7 kcal/mol, leaving an open coordination site available for the subsequent addition of Ph<sub>2</sub>SiH<sub>2</sub>. Iluc and Hillhouse<sup>[35]</sup> reported on the oxidative addition of silanes to Ni(0), proposing that this step goes *via* reversible  $\eta^2$ -(Si–H) bonding, which is believed to be the case here as well. Coordination of one of the Si–H bonds of Ph<sub>2</sub>SiH<sub>2</sub> to nickel is exergonic by a  $\Delta G$  of –7.9 kcal/mol. Next, one hydride bound to Si is transferred to the imine carbon atom, resulting in an intermediate Ni-amido complex with coordination of the nitrogen to nickel. This step has a  $\Delta G$  of –18.8 kcal/mol. Formal reductive elimination of the backbone nitrogen and the silane species is proposed to occur next, resulting in the isolated structure **2[Si]** after association of the PPh<sub>3</sub> ligand. This latter structure is slightly uphill compared to the starting structure of **2**, with a  $\Delta G$  of 0.7 kcal/mol, but this is regarded to be within the error margins of the DFT calculations. No concerted transition state for this step could be located, suggesting that it may consist of a more complex sequence of steps possibly involving phosphine decoordination to facilitate N–Si reductive elimination.

Of particular interest is the hydride transfer from the  $\sigma$ -bound H–SiHPh<sub>2</sub> adduct to the imine-carbon, resulting in a –CH<sub>2</sub> moiety and concomitant formation of a nickel-amido bond. For this step, a single, concerted transition state was located at a  $\Delta G$  of +5.11 kcal/mol (Figure 6) in which the hydride is found between the Si and C1 atoms (Figure 6, Si–H1 2.220 Å, C1–H1 1.593 Å), with an additional short contact with the nickel center (Ni–H1 1.501 Å) which assists the hydride shuttling.<sup>[36]</sup> The step corresponding to this transition state can be described as a combination of an oxidative addition of the Si–H bond to Ni and  $\beta$ -insertion of the C=N bond in a single step. Such transition states have been termed ligand-to-ligand hydrogen transfer by Perutz and coworkers and proposed for C–H activation in Ni-catalyzed hydrofluoroarylation of alkynes.<sup>[37]</sup> The overall pathway depicted in Chart 1 constitutes a plausible representation of the mechanism of addition, but alternative pathways involving the dissociation of one of the phosphine side-arms – as observed in compounds **3[Si]** and **4[Si]** – cannot be excluded.



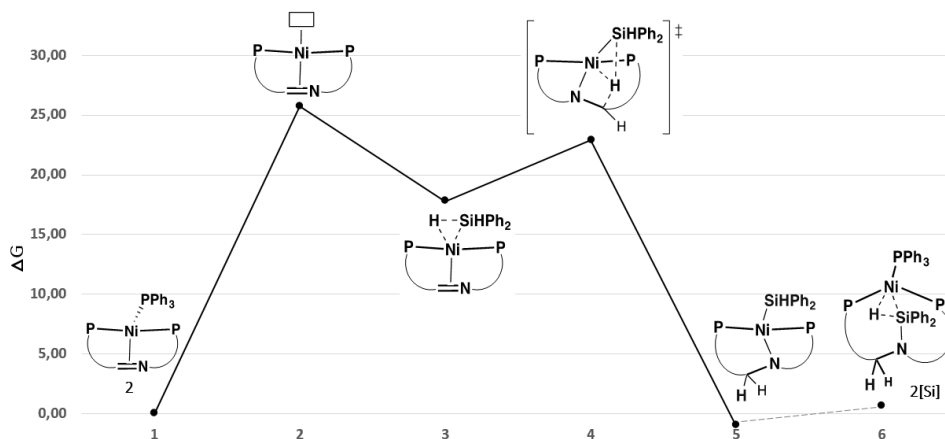


Chart 1. Silane activation pathway on **2** as calculated by DFT.

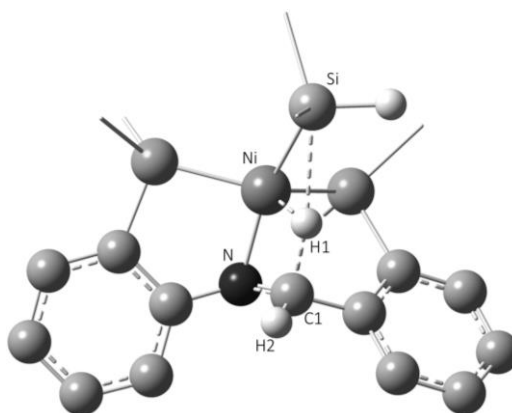


Figure 6. TS between step 3 and 5. The hydride atom is located between the Si and N, transferred from Si to N via Ni-assisted hydrogen shuttling. Calculated at B3LYP/6-31G\*\* level of theory. Ni–Si: 2.269, Ni–N: 1.947, Ni–H1: 1.501, C1–H1: 1.593, C1–H2: 1.094, Si–H1: 2.220, C1–N: 1.375.

### 6.2.4 Silane scrambling

As a means to test the reversibility of the silane addition to compound **2**, one equivalent of  $\text{Ph}_2\text{SiH}_2$  was added to an *in situ* formed sample of **2**[SiD<sub>2</sub>] (Figure 7). Interestingly, a gradual appearance of the Si–H <sup>1</sup>H NMR signal at  $\delta$  –2.72 ppm was observed. The signal integrates to 0.5 H after 1 hour, indicating 50% <sup>1</sup>H incorporation, i.e. statistical distribution (Figure 7; Appendix F, Figure F7). In contrast, no H-incorporation into the backbone –CHD group was observed under the same conditions, ruling out reversible hydrosilylation as a scrambling mechanism. H/D scrambling at the Si–H(D) position could either go *via* exchange of only the

H/D, i.e. *via* activation of the Si–H bond by Ni, or by exchanging the full Ph<sub>2</sub>Si–H fragment *via* Si–N bond cleavage. This question was addressed by using the PhMeSi fragment as a chemical label for the silicon fragment. Addition of Ph<sub>2</sub>SiH<sub>2</sub> to an *in situ* formed sample of **2[SiPhMe]** resulted in a changing <sup>31</sup>P NMR spectrum. Equilibration to a mixture of **2[SiPhMe]** and **2[Si]** was observed, with signals of both species present in a **2[SiPhMe]:2[Si]** ratio of 1:0.8. Performing the opposite reaction, starting from an *in situ* formed sample of **2[Si]** with the addition of PhMeSiH<sub>2</sub>, results in the same product distribution after 3 h, confirming that equilibrium is reached. This demonstrates that the Si–N bond is reversibly cleaved under the reaction conditions, allowing for scrambling of the silyl fragment as a whole.

As both the hydridic position and the silyl fragment can be exchanged, a remaining question is whether these are two distinct processes; in other words, can the hydride position be exchanged independently from the silyl fragment? To address this question, PhMeSiH<sub>2</sub> was added to an *in situ* formed sample of **2[SiD<sub>2</sub>]**. The experiment was followed by <sup>1</sup>H NMR, observing the deuterium/hydride exchange on the Si–H/Si–D position by <sup>1</sup>H NMR, and the exchange of PhMeSiH/Ph<sub>2</sub>SiH in the backbone of the Ni-complex by <sup>31</sup>P NMR. No large difference in scrambling rates were observed: after a reaction time of 10 minutes <sup>1</sup>H NMR indicates a ratio of D/H (**2[SiD<sub>2</sub>]:2[SiPhMe]**) of 6:1, measured by integration of the geminal –CHD signal of **2[SiD<sub>2</sub>]** and the ingrowing Si–H of **2[SiPhMe]**. <sup>31</sup>P NMR indicates a **2[SiD<sub>2</sub>]:2[SiPhMe]** ratio of 5:1 after 8 min.<sup>[38]</sup> A small difference is obtained, likely due to the time of the measurements and error margins due to NMR integration. Taken these differences into account, this suggests that the scrambling rates are similar. Additionally, the observed hydride signals belong mostly to **2[SiPhMe]** at early stages, whereas the hydride signal of **2[Si]** would be expected if a competitive reaction would exchange only the hydride position. Hence, it was reasoned that the two phenomena are likely connected in scrambling of the entire silane fragment.

A plausible mechanism is proposed in Figure 8. Starting from **2[Si]**, dissociation of PPh<sub>3</sub> takes place first. Oxidative addition of the N–SiHPh<sub>2</sub> bond leads to the Ni(II)-amido complex, to which MePhSiH<sub>2</sub> can coordinate *via* an agostic interaction of a Si–H bond. A related reversible cleavage of an Si–N bond has been observed by Calimano and Tilley in related Ir systems.<sup>[39]</sup>  $\sigma$ -Bond metathesis is then proposed to take place in which a hydride is transferred from MePhSiH<sub>2</sub> to SiHPh<sub>2</sub>, resulting in a Si–Ni bond of the former and an agostic interaction with the latter silane. This is related to a phosphine-silyl-Ni(0) system reported by Peters and co-workers, in which both Si–H and H–H were reversibly bound to one Ni center, resulting in ligand exchange *via*  $\sigma$ -bond metathesis.<sup>[40]</sup> Dissociation of SiPh<sub>2</sub>H<sub>2</sub> followed by reductive elimination of the silyl and amido fragments and subsequent association of PPh<sub>3</sub> results in **2[SiMePh]**.

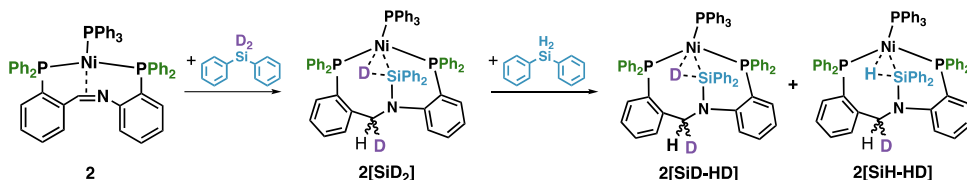


Figure 7. Reactivity of **2** with  $\text{Ph}_2\text{SiD}_2$ . Scrambling of the  $-\text{SiPh}_2\text{H}/-\text{SiPh}_2\text{D}$  fragment.

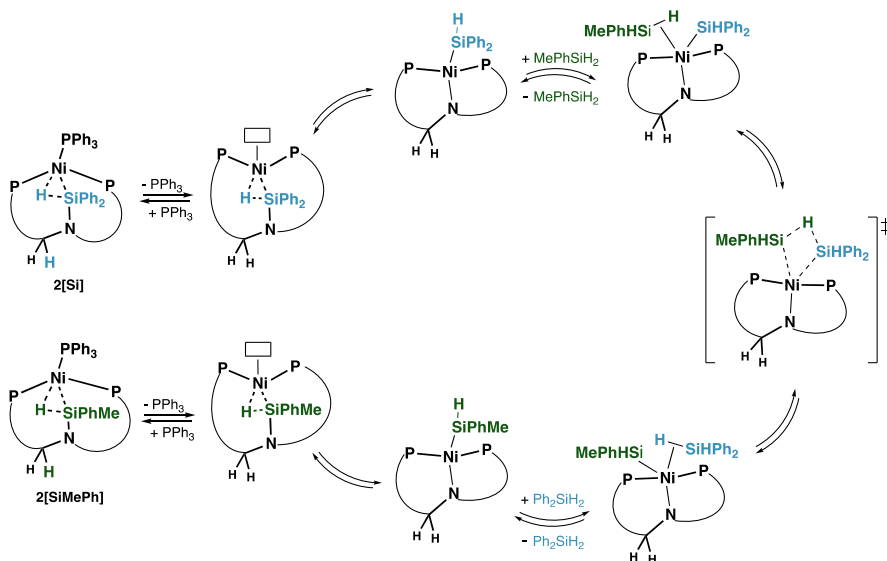


Figure 8. Proposed mechanistic cycle of the scrambling mechanism.

### 6.2.5 Hydrosilylation

Having demonstrated the ability of compounds **2-4** to add a hydrosilane molecule and the ability of the formed aminosilane complex to reversibly activate an external silane, the activity of **2-4** in catalytic hydrosilylation reactions was investigated. The hydrosilylation reaction of 1-octene with diphenylsilane resulted in the selective formation of *n*-octyldiphenylsilane in the presence of 1 mol% of **2-4** (Table 2). Reactions were performed in  $\text{C}_6\text{D}_6$  at room temperature and were monitored by  $^1\text{H}$  NMR spectroscopy. Full conversion of the substrates and quantitative formation of the product was observed in all cases. The time to completion decreases from **2** via **3** to **4**: full conversion with **2** is obtained within 7 h, **3** reaches full conversion within 4 h, and catalyst **4** in only 3 h (Appendix F, Figure F11-13). Compounds **2-4** exhibit full selectivity toward the anti-Markovnikov product, which was demonstrated by APT  $^{13}\text{C}$  NMR,<sup>[41]</sup> and no side-product formation was observed. The catalysts were formed *in situ* prior to addition of the substrates, by reacting 1 equivalent of precatalysts **2-4** with 1.05 equivalents of diphenylsilane in  $\text{C}_6\text{D}_6$ , followed by stirring for one

hour to ensure full conversion to the silane activated compounds. Reaction profiles following the substrate conversion in time by  $^1\text{H}$  NMR displayed an induction period of 1.5 to 3 hours for all reactions, possibly caused by slow dissociation of  $\text{PPh}_3$ . There was no visual evidence for the formation of metallic nickel, but the formation of soluble, catalytically active nanoparticles cannot be fully excluded as another possible explanation for the induction period with the data at hand. The exhibited reactivity by precatalysts **2-4** are in line with the described Ni-systems for the hydrosilylation of 1-octene with diphenylsilane by Shimada<sup>[15]</sup> and Hu (Figure 1).<sup>[16]</sup>

**Table 2.** Hydrosilylation reactions catalyzed with **2-4**.

$$\text{Ph}_2\text{SiH}_2 + \text{CH}_2=\text{CH}(\text{CH}_2)_6\text{CH}_3 \xrightarrow[\text{Y-NMR tube}]{\text{Cat (1 mol\%)} \\ \text{C}_6\text{D}_6, \text{RT}}$$

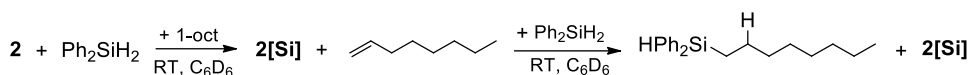
Entry	Catalyst	Time	Conversion 1-octene <sup>[A]</sup>
1	<b>2</b>	6h45min	>99%
2	<b>3</b>	3h45min	>99%
3	<b>4</b>	2h45min	>99%

<sup>[A]</sup> Conversion was determined by  $^1\text{H}$  NMR by integration against internal standard mesitylene.

### 6.2.6 Stoichiometric reactions for mechanistic insights

In the hydrosilylation of 1-octene with diphenylsilane to *n*-octyldiphenylsilane with precatalysts **2-4**, the first step is the activation of one equivalent of diphenylsilane, resulting in the formal hydrosilylation of the imine ligand backbone. This is in line with systems described in literature, which often include a first step where the Si–H bond is activated by Ni, either activated *via* oxidative addition to Ni or in a bifunctional manner by assistance of the ligand.<sup>[24]</sup> Further steps were investigated by stoichiometric reactions. The addition of an equimolar amount of 1-octene to an *in situ* prepared sample of **2[Si]** does not lead to the formation of the hydrosilylation product, also not after a reaction time of 18 h (Scheme 2). However, addition of a second equivalent of  $\text{Ph}_2\text{SiH}_2$  resulted in full conversion of 1-octene to *n*-octyldiphenylsilane. Reactions starting from *in situ* prepared **2[SiD<sub>2</sub>]** or **2[SiPhMe]** exhibit similar behavior: hydrosilylation of 1-octene only occurred upon addition of the second equivalent of the corresponding silane, either  $\text{Ph}_2\text{SiD}_2$  or  $\text{PhMeSiH}_2$ . This suggests that the first silane addition to compound **2** serves to generate the active catalyst **2[Si]**, but transfer of the activated silane as a whole from **2[Si]** to the substrate, regenerating compound **2**, is not taking place under the reaction conditions. This finding is somewhat related to mechanistic investigations of a Ni-catalyzed hydrosilylation with the previously mentioned (salicylaldiminato)methylnickel catalyst published by Shimada and co-workers (Figure 1),<sup>[15]</sup> where the first equivalent of diphenylsilane was proposed to transfer a hydride to a methyl

co-ligand, forming methane, and addition of the remaining silyl to nickel, forming the catalyst.



**Scheme 2.** Stoichiometric addition of diphenylsilane and 1-octene to **2** and subsequent addition of 1 extra equivalent of diphenylsilane, to promote hydrosilylation.

Moreover, during the stoichiometric conversion of 1-octene with **2**[SiD<sub>2</sub>] and additional Ph<sub>2</sub>SiD<sub>2</sub> it was observed that the –CHD <sup>1</sup>H NMR signals of the ligand were unchanged, suggesting that the backbone hydrogen atom is neither transferred to the product nor scrambles with the incoming silane. To verify whether this changes upon multiple turnovers, a catalytic hydrosilylation experiment was performed with *in situ* prepared **2**[SiD<sub>2</sub>]. 40 equivalents of 1-octene and 40 equivalents of Ph<sub>2</sub>SiH<sub>2</sub> were added subsequently. Also after 40 turnovers, hydride incorporation to the geminal –CHD moiety is not observed, indicating no participation in catalysis.

The need of the second silane equivalent to induce hydrosilylation raises a question: which silyl group is preferentially transferred to the olefinic substrate, the silyl group already installed on the catalyst backbone or the incoming silane? Answering this question is complicated by the occurrence of silane scrambling (*vide supra*). A series of stoichiometric crossover experiments were performed (Figure 9). Addition of 1 equivalent of Ph<sub>2</sub>SiH<sub>2</sub> to **2**, forming **2**[Si], and subsequent addition of 1-octene does – again – not lead to hydrosilylation. Only upon addition of a second equivalent of silane does the hydrosilylation reaction proceed. Here, PhMeSiH<sub>2</sub> is added as a chemical label for the silane fragment. If the activated silane in the backbone was transferred during catalysis, the result of the reaction would be the formation of diphenyloctylsilane and **2**[SiPhMe]. In case only the second equivalent of silane was transferred in hydrosilylation, the product of the reaction would be the methylphenyloctylsilane, and unchanged **2**[Si]. Because scrambling of the silyl group is expected to occur as well under these conditions, it is likely that a mixture of both products will be obtained, rendering the interpretation of the results more difficult. This problem could potentially be overcome by performing an additional complementary experiment, i.e. adding Ph<sub>2</sub>SiH<sub>2</sub> to a preformed mixture of **2**[SiPhMe] and 1-octene. If silyl scrambling is fast compared to the hydrosilylation reaction, then the ratio **2**[SiPhMe]:**2**[Si] and that between the two hydrosilylation products at the end of the reaction should be independent of the order of addition of both silanes. Due to peak overlap in the <sup>1</sup>H NMR the hydrosilylation product ratio could not be measured directly; therefore, only the **2**[SiPhMe]:**2**[Si] was measured by <sup>31</sup>P NMR.

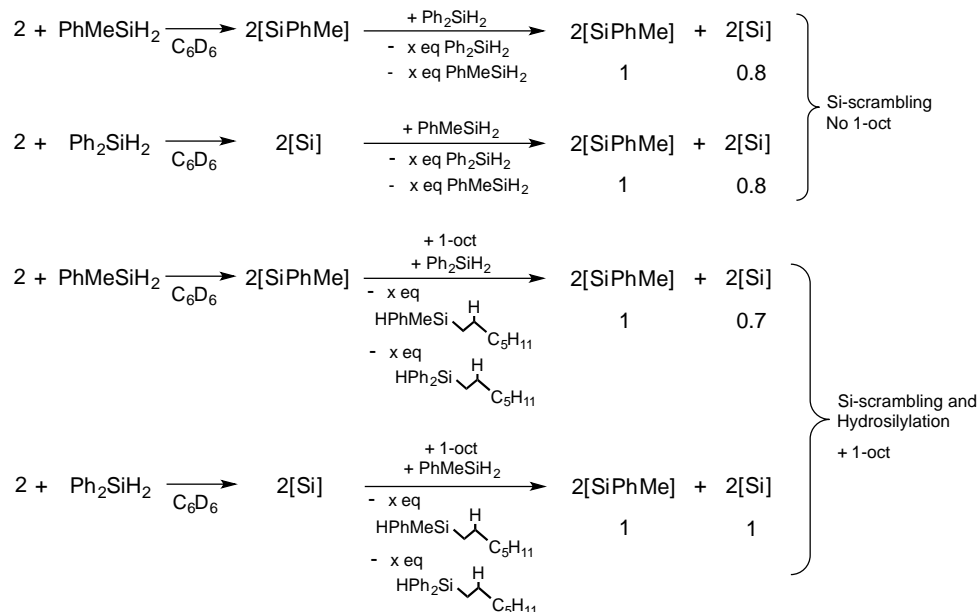


Figure 9. Scrambling reactions.

Addition of one equivalent of  $\text{Ph}_2\text{SiH}_2$  to an equimolar mixture of  $2[\text{SiPhMe}]$  formed *in situ* and 1-octene resulted in a Ni-complex mixture with  $2[\text{SiPhMe}]:2[\text{Si}]$  ratio of 1:0.7 at the end of the reaction, indicating that the incoming  $\text{Ph}_2\text{SiH}$  fragment is transferred in slight excess. The reverse experiment, adding one equivalent of  $\text{PhMeSiH}_2$  to an equimolar mixture of  $2[\text{Si}]$  formed *in situ* and 1-octene resulted in a  $2[\text{SiPhMe}]:2[\text{Si}]$  ratio of 1:1. First of all, these results show that stoichiometric hydrosilylation and silane scrambling are occurring on a similar timescale, since the obtained mixture of Ni-complexes is close to equimolar, implying the formation of both possible hydrosilylation products. The observed  $2[\text{SiPhMe}]:2[\text{Si}]$  ratios after reaction are governed by a combination of the rate of silane scrambling and the relative rates of hydrosilylation with both silanes and cannot readily be interpreted on their own. However, their dependence on the order of addition suggests a slight preference for transfer of the incoming silane over the pre-bound silane. The observed differences are too small for a definitive conclusion to be reached, but suggests a mechanism in which the N-bound silyl group is not directly transferred to the olefinic substrate.

### 6.2.7 Mechanistic proposal

Complexes 2-4 were shown to be precatalysts, generating an active hydrosilylation catalyst after activation by reaction with diphenylsilane, resulting in  $2[\text{Si}]$ ,  $3[\text{Si}]$ , and  $4[\text{Si}]$ . These species contain a Si-H moiety in the catalyst backbone, which continuously scrambles with free silanes *via* reversible cleavage of the Ni-(Si-H) and Si-N bonds. Furthermore, catalytic

hydrosilylation only occurs upon addition of an extra equivalent of silane, and the  $-\text{CH}_2$  group formed by hydrosilylation of the imine was shown to be unreactive under catalytic conditions. This implies for the mechanism that the methylene unit in the supporting ligand does not play a role in the hydrosilylation mechanism and that the hydride which participates in the reaction should be included to the mechanistic cycle *via* reaction with a second equivalent of the silane substrate. Furthermore, crossover experiments suggest a slight preference for incorporation of the incoming silane into the product.

On the basis of these observations, a possible mechanism for the hydrosilylation of 1-octene can be proposed (Figure 10). The first step is the activation of one equivalent of  $\text{Ph}_2\text{SiH}_2$ , resulting in reactive species **2[Si]** as described previously. Then,  $\text{PPh}_3$  dissociates from the metal center (**A**), creating a vacant site for 1-octene addition. This dissociation step is possibly the cause for the observed initiation period in the catalytic runs, although direct evidence is lacking. Alternatively, a free coordination site could also be generated *via* decooordination of one of the phosphine tethers (not included in Figure 10). Next, 1-octene is proposed to bind in an  $\eta^2$ -fashion (**B**), followed by 1,2-insertion, forming an Ni(II) silyl/alkyl complex (**C**), in accord to the Chalk-Harrod mechanism.<sup>[3]</sup>  $\text{Ph}_2\text{SiH}_2$  is proposed to coordinate next, *via* an agostic interaction of a Si–H bond (**D**).<sup>[25]</sup> Hydride transfer *via*  $\sigma$ -bond metathesis (**E**) yields the Ni(II) complex with an  $\eta^2$ -coordinating Si–H backbone and a covalent interaction with the incoming silane (**F**). Reductive elimination of the silyl and octyl moieties results in product formation and the starting Ni(0) complex (**A**).

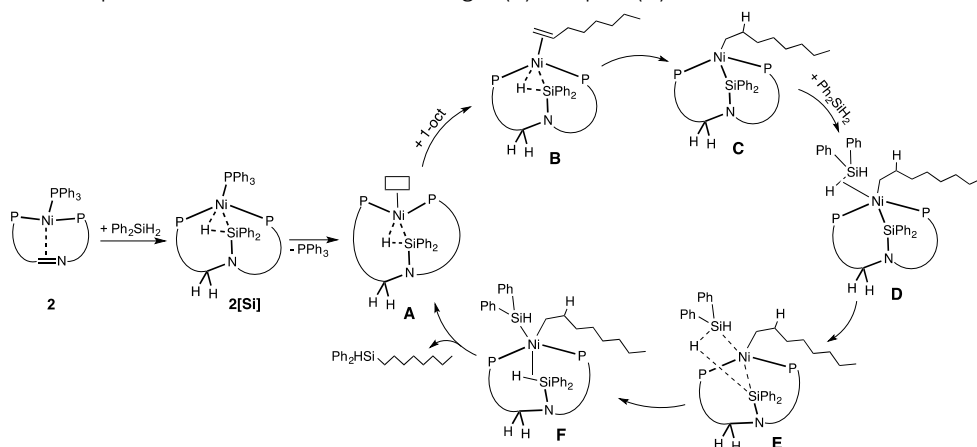


**Figure 10.** Proposed mechanism for the hydrosilylation of 1-octene with  $\text{Ph}_2\text{SiH}_2$  catalyzed by **2**. Ligand is not shown completely for clarity, P =  $\text{PPh}_2$ .

This mechanism preserves the Si–N bond throughout the cycle, consistent with the slight preference for transferring the incoming silane observed in stoichiometric experiments (*vide supra*). However, alternative pathways involving oxidative addition of the Si–N bond, as proposed in the mechanism for silane scrambling (Figure 8), followed by olefin insertion into the formed Ni–Si bond cannot be excluded.

### 6.3 Conclusions

The reactivity toward silanes of Ni(PCNP)-complexes featuring a side-on coordinated imine moiety was studied. Complexes Ni(P<sup>Ph</sup>CNP<sup>Ph</sup>)PPh<sub>3</sub> (**2**), Ni(P<sup>Ph</sup>CNP<sup>oTol</sup>)PPh<sub>3</sub> (**3**) and Ni(P<sup>oTol</sup>CNP<sup>oTol</sup>)PPh<sub>3</sub> (**4**) cleanly activate diphenylsilane, each resulting in a single isolable species, characterized as the product of formal hydrosilylation of the imine-backbone (**2[Si]**-**4[Si]**). Herein, a hydride is added to the imine-carbon atom and the R<sub>2</sub>Si–H moiety binds to the nitrogen atom to form an N-substituted silane, which additionally coordinates to Ni *via* the Si–H bond. The latter bond in complex **2[Si]** coordinates in an η<sup>2</sup>(Si,H)-fashion to nickel, as evident from the <sup>29</sup>Si satellites at 109 Hz in the <sup>1</sup>H NMR spectrum and DFT calculations. In complexes **3[Si]** and **4[Si]** the Si–H bond is activated to a larger extent, as was shown by the <sup>29</sup>Si satellites at 18 and ~14 Hz, respectively, and the DFT calculated structures. The X-ray crystal structures show positioning of the silane between Ni and N, forming an Ni–Si–N structure. Complexes **3[Si]** and **4[Si]** are therefore better described as a Ni(II) center bearing a silyl and a hydride ligand resulting from oxidative addition. A possible pathway for this activation was identified by DFT calculations, suggesting a cooperative Ni-mediated ligand-to-ligand hydride transfer as a key step. Similar to the π-ligand complexes reported by Iluc and Agapie, the imine ligands presented herein act as a hydride acceptor in the activation of silane substrates, albeit irreversibly with the current ligand design.

Compounds **2-4** are efficient precatalysts for the hydrosilylation of 1-octene with diphenylsilane resulting in full conversion within 7 h at room temperature in all cases and high selectivity for the anti-Markovnikov product, in line with reported Ni-catalysts for this reaction. Stoichiometric reactions show that the CH<sub>2</sub> group in the ligand backbone is unreactive in the hydrosilylation reactions. Hence, addition of the alkene substrate 1-octene to **2[Si]**-**4[Si]** or **2[SiPhMe]** does not lead to product formation, and addition of a second equivalent of silane is necessary for reactivity. Scrambling of the R<sub>2</sub>Si–H moiety in compound **2[Si]** occurs spontaneously upon addition of extra silane. This indicates reversible cleavage of the Si–N bond under catalytic conditions. This finding might have general implications for the mechanism of hydrosilylation reactions employing N-containing ligands such as imines or amides in Ni-catalysts, for which the incorporation of this step might be considered. A possible catalytic mechanism is proposed based on the results, in which the N-bound silane moiety acts as a hydride reservoir.

Overall, the possibility of stepwise addition in this system and the clean reactivity lead to complementary insights in the field of Ni-catalyzed hydrosilylation by an improved understanding of the hydrosilylation mechanism. Further investigations to expand the substrate scope of the hydrosilylation reactions and detailed studies into the mechanism and kinetics, both experimentally and computationally, are currently ongoing. Furthermore, the modular nature of the ligand used in these studies allows for prompt ligand variations,



opening up a pathway for synthesis of a large variety of chelating imine-based compounds, for example including ligands for asymmetric catalysis.

## 6.4 Experimental section

### 6.4.1 General considerations

All reagents were purchased from commercial sources and used as received unless stated otherwise. All reactions were performed in a N<sub>2</sub> glovebox and at room temperature unless stated otherwise. Deuterated benzene (C<sub>6</sub>D<sub>6</sub>) was degassed using the freeze-thaw-pump method (4x) and subsequently stored over molecular sieves. Tetrahydrofuran (THF) was distilled over sodium/benzophenone before use, both were degassed by bubbling N<sub>2</sub> through it for 30 minutes and stored over molecular sieves. Dry diethylether (Et<sub>2</sub>O), hexanes and toluene were acquired from a MBRAUN MB SPS-80 solvent purification system and further dried over molecular sieves before use. Ligands **1Ph**, **1<sup>PhTol</sup>**, **1<sup>OTol</sup>** and complexes **2**, **3** and **4** were synthesized according to procedures described in Chapter 5 of this thesis.

<sup>1</sup>H, <sup>13</sup>C, <sup>29</sup>Si and <sup>31</sup>P NMR spectra (respectively 400, 100, 80 and 161 MHz) were recorded on an Agilent MRF400 or a Varian AS400 spectrometer at 25 °C. <sup>1</sup>H and <sup>13</sup>C NMR chemical shifts are reported in ppm relative to TMS using the residual solvent resonance as internal standard. <sup>31</sup>P NMR chemical shifts are reported in ppm and externally referenced to 85% aqueous H<sub>3</sub>PO<sub>4</sub> and <sup>29</sup>Si NMR chemical shifts are externally referenced to TMS. Infrared spectra were recorded using a Perkin Elmer Spectrum One FT-IR spectrometer under a N<sub>2</sub> flow. Compounds were found to be too sensitive for obtaining accurate elemental analysis.

DFT calculations were performed using the Gaussian 09 software package<sup>[42]</sup> using the B3LYP (Becke, three-parameter, Lee-Yang-Parr) functional and the 6-31G\*\* basis set on all atoms. The structures were optimized without any symmetry restraints. Frequency analyses were performed on all calculations to verify that the obtained stationary points are in fact minima, and transition states contained one negative frequency. For the structures described in Chart 1, a dispersion correction using the GD3 parameters was added, and after optimization a single point calculation was performed to add a benzene solvent model.

### 6.4.2 Synthesis

**2[Si]**: Ni(P<sup>Ph</sup>CNP<sup>Ph</sup>)(PPh<sub>3</sub>) (39.4 mg, 0.045 mmol) was suspended in C<sub>6</sub>H<sub>6</sub> (3 mL). While stirring, Ph<sub>2</sub>SiH<sub>2</sub> (9.2 μL, 9.1 mg, 0.050 mmol) was added and the mixture was stirred for 3 h during which the color changed from deep red to clear orange. All solvents were evaporated and the resulting yellow powder was washed with hexanes (4 x 1 mL). The product was extracted using THF (5 mL) and filtered, after which it was dried. Addition of hexanes (1 mL) to the sticky yellow product induced precipitation, and **(2[Si])** was isolated after evaporation of the solvent as a yellow powder with a yield of 85% (40.7 mg, 0.039 mmol). <sup>1</sup>H NMR (C<sub>6</sub>D<sub>6</sub>): δ<sub>H</sub> 8.04 (d, *J* = 8 Hz, 2H, Ar-H), 7.55 (t, *J* = 8 Hz, Ar-H), 7.43 (d, *J* = 7 Hz, Ar-H), 7.38 (dd, *J* = 5, 8 Hz, Ar-H), 7.16-6.92 (m, Ar-H), 6.86 (dt, *J* = 2,7 Hz, Ar-H), 6.82-6.75 (m, Ar-H), 6.73-6.67 (m, Ar-H), 6.60 (t, *J* = 7 Hz, Ar-H), 6.53 (t, *J* = 7 Hz, Ar-H), 6.36 (t, *J* = 7 Hz, 1H, Ar-H), 5.01 (d, <sup>2</sup>*J*<sub>HH</sub> = 15 Hz, 1H, -CH<sub>2</sub>), 4.61 (dd, <sup>2</sup>*J*<sub>HH</sub> = 2, 15 Hz, 1H, -CH<sub>2</sub>), -2.72 (ddd, <sup>2</sup>*J*<sub>HP</sub> = 19, 23, 36 Hz, 1H, Si-H) ppm. <sup>13</sup>C NMR (C<sub>6</sub>D<sub>6</sub>): δ<sub>C</sub> 156.15 (d, *J*<sub>CP</sub> = 18 Hz), 145.27 (d, *J*<sub>CP</sub> = 23 Hz), 144.05 (d, *J*<sub>CP</sub> = 5 Hz), 142.92,

142.47 (d,  $J_{CP} = 12$  Hz), 140.45, 139.86 (m), 139.63 (m), 139.07, 138.77, 136.49, 136.32, 136.16, 135.50, 135.30, 134.96, 134.71, 134.58, 133.79, 133.72, 133.67, 133.59, 133.55, 133.43, 133.32, 133.23, 133.20, 132.56, 132.44, 132.10, 131.78, 129.95 (m), 129.80, 129.51 (m), 128.92, 128.83, 128.60, 128.54, 128.47, 128.39, 128.18, 127.71, 127.42, 127.30, 127.22 (d,  $J_{CP} = 1$  Hz), 127.14, 126.92, 126.73, 126.69, 120.75 (d,  $J_{CP} = 5$  Hz).  $^{31}\text{P}$  NMR ( $\text{C}_6\text{D}_6$ ):  $\delta_{\text{P}}$  32.78 (d,  $^2J_{\text{PP}} = 17$  Hz), 17.06 (dd,  $^2J_{\text{PP}} = 17$ , 45 Hz), 7.82 (d,  $^2J_{\text{PP}} = 45$  Hz) ppm.  $^{29}\text{Si}$  NMR ( $\text{C}_6\text{D}_6$ ):  $\delta_{\text{Si}}$  6.45 (ddd,  $J_{\text{SiP}} = 2$ , 17, 60 Hz, Si-H) ppm. IR  $\text{cm}^{-1}$ : 3052, 2923, 2853, 1955, 1893, 1816, 1664, 1584, 1467, 1433, 1263, 1184, 1117, 1093, 1027, 868, 822, 740, 695, 519, 508, 486.

**3[Si]**:  $\text{Ni}(\text{P}^{\text{oTol}}\text{CNP}^{\text{Ph}})(\text{PPh}_3)$  (17.9 mg, 0.0199 mmol) was suspended in  $\text{C}_6\text{H}_6$  (1 mL). While stirring,  $\text{Ph}_2\text{SiH}_2$  (4.4  $\mu\text{L}$ , 4.4 mg, 0.024 mmol) was added and the mixture was stirred for 2.5 h during which the color changed from deep red to clear orange. All solvents were evaporated and the resulting yellow powder was washed with hexanes (4 x 1 mL). The product was extracted using THF (3 mL) and filtered, after which it was dried. Addition of hexanes (0.5 mL) to the sticky yellow product induced precipitation, and **3[Si]** was isolated after evaporation of the solvent as a yellow powder with a yield of 90% (19.4 mg, 0.018 mmol).  $^1\text{H}$  NMR ( $\text{C}_6\text{D}_6$ ):  $\delta_{\text{H}}$  7.57 (d,  $J = 5$  Hz, Ar-H), 7.34 (t,  $J = 9$  Hz, Ar-H), 7.05-6.99 (m, Ar-H), 6.94-6.77 (m, Ar-H), 6.39 (t,  $J = 7$  Hz, Ar-H), 4.92 (s, broad, -CH<sub>2</sub>), 2.44 (s, 6H, oTol-CH<sub>3</sub>), -4.35 (dd,  $^2J_{\text{HP}} = 90$ , unresolved Hz, Si-H) ppm.  $^{13}\text{C}$  NMR ( $\text{C}_6\text{D}_6$ ):  $\delta_{\text{C}}$  155.10 (d,  $J_{CP} = 10$  Hz), 144.58, 144.38, 136.26, 135.42, 134.19 (d,  $J_{CP} = 15$  Hz), 133.69 (d,  $J_{CP} = 4$  Hz), 132.14, 131.53, 130.41 (d,  $J_{CP} = 5$  Hz), 130.10, 129.27, 129.06, 128.67, 128.60, 128.48, 128.39, 127.62, 127.30 (d,  $J_{CP} = 4$  Hz), 126.61, 126.51, 121.90, 121.39, 120.04, 117.81 (d,  $J_{CP} = 7$  Hz), 50.91 (d,  $J_{CP} = 29$  Hz), 21.39 (d,  $J_{CP} = 22$  Hz) ppm.  $^{31}\text{P}$  NMR ( $\text{C}_6\text{D}_6$ ):  $\delta_{\text{P}}$  27.38, 22.02, -31.67 ppm.  $^{29}\text{Si}$  NMR ( $\text{C}_6\text{D}_6$ ): no signal obtained due to low solubility of the material. IR  $\text{cm}^{-1}$ : 3359, 3312, 3052, 2961, 2920, 2851, 1953, 1857, 1660, 1633, 1581, 1467, 1449, 1434, 1379, 1261, 1231, 1093, 1026, 847, 801, 742, 693, 515, 498, 456.

**4[Si]**:  $\text{Ni}(\text{P}^{\text{oTol}}\text{CNP}^{\text{oTol}})(\text{PPh}_3)$  (16.5 mg, 0.0178 mmol) was suspended in  $\text{C}_6\text{H}_6$  (1 mL). While stirring,  $\text{Ph}_2\text{SiH}_2$  (4  $\mu\text{L}$ , 3.97 mg, 0.022 mmol) was added and the mixture was stirred for 2.5 h during which the color changed from deep red to clear orange. All solvents were evaporated and the resulting yellow powder was washed with hexanes (4 x 1 mL). The product was extracted using THF (3 mL) and filtered, after which it was dried. Addition of hexanes (0.5 mL) to the sticky yellow product induced precipitation, and **4[Si]** was isolated after evaporation of the solvent as a yellow powder with a yield of 71% (14.1 mg, 0.013 mmol).  $^1\text{H}$  NMR ( $\text{C}_6\text{D}_6$ ):  $\delta_{\text{H}}$  7.48-7.44 (m, Ar-H), 7.36 (s, Ar-H), 7.26 (t,  $J = 8$  Hz, Ar-H), 7.19 (s, Ar-H), 7.09-6.98 (m, Ar-H), 6.96-6.80 (m, Ar-H), 6.77-6.73 (m, Ar-H), 6.69-6.66 (m, Ar-H), 6.50 (s, Ar-H), 6.44-6.40 (m, Ar-H), 4.84-4.78 (m, -CH<sub>2</sub>), 4.65-4.60 (m, -CH<sub>2</sub>), 2.57 (s, 3H, oTol-CH<sub>3</sub>), 2.52 (s, 3H, oTol-CH<sub>3</sub>), 2.45 (s, 3H, oTol-CH<sub>3</sub>), 2.33 (s, 3H, oTol-CH<sub>3</sub>), -5.53 (dd,  $^2J_{\text{HP}} = 19$ , 85 Hz, 1H, Si-H) ppm.  $^{13}\text{C}$  NMR ( $\text{C}_6\text{D}_6$ ): quality is poor due to low solubility of the compound.  $^{31}\text{P}$  NMR ( $\text{C}_6\text{D}_6$ ):  $\delta_{\text{P}}$  26.02, 4.85, -31.24 ppm.  $^{29}\text{Si}$  NMR ( $\text{C}_6\text{D}_6$ ): no signal obtained due to low solubility of the material. IR  $\text{cm}^{-1}$ : 3050, 1862 (hydridic signal), 1580, 1467, 1449, 1433, 1377, 1283, 1231, 1095, 1034, 849, 803, 745, 693, 677, 576, 557, 519, 500, 487, 456, 429.

**2[SiPhMe]**:  $\text{Ni}(\text{P}^{\text{Ph}}\text{CNP}^{\text{Ph}})(\text{PPh}_3)$  (14.7 mg, 0.017 mmol) was suspended in  $\text{C}_6\text{H}_6$  (1 mL). While stirring,  $\text{Ph}_2\text{SiH}_2$  (3.3  $\mu\text{L}$ , 3.3 mg, 0.018 mmol) was added and the mixture was stirred for 3 h during which the color changed from turbid red to clear orange. All solvents were evaporated and the resulting powder was washed with hexanes (2 x 1 mL). The solids were dried in vacuum and **2[SiPhMe]** was isolated an

off-white powder in quantitative yield.  $^1\text{H}$  NMR ( $\text{C}_6\text{D}_6$ ):  $\delta_{\text{H}}$  8.04 (d,  $J = 6$  Hz, Ar-H), 7.82 (t,  $J = 8$  Hz, Ar-H), 7.59 (small, broad, Ar-H), 7.51-7.45 (m, Ar-H), 7.40 (t,  $J = 8$  Hz, Ar-H), 7.30-7.18 (m, Ar-H), 7.13-6.77 (m, Ar-H), 6.73-6.69 (m, Ar-H), 6.63-6.57 (m, Ar-H), 6.55-6.49 (m, Ar-H), 6.29 (t,  $J = 6$  Hz, Ar-H), 6.00 (t,  $J = 5$  Hz, Ar-H), 5.02 (d,  $^2J_{\text{HH}} = 15$  Hz, minor species,  $-\text{CH}_2$ ), 4.79 (d,  $^2J_{\text{HH}} = 15$  Hz, major species,  $-\text{CH}_2$ ), 4.53 (d,  $^2J_{\text{HH}} = 15$  Hz, minor species,  $-\text{CH}_2$ ), 4.40 (d,  $^2J_{\text{HH}} = 15$  Hz, major species,  $-\text{CH}_2$ ), 0.68 (s, major species,  $-\text{Me}$ ), 0.44 (s, minor species,  $-\text{Me}$ ),  $-2.52$  (ddd,  $^2J_{\text{HP}} = 35, 24, 11$  Hz, major species, Si-H),  $-2.84$  (ddd,  $^2J_{\text{HP}} = 36, 21, 8$  Hz, minor species, Si-H) ppm. Broadband  $^{31}\text{P}$  decoupled NMR from  $\delta -4$  to  $-2$  ppm:  $-2.52$  (s,  $^{29}\text{Si}$ -satellites:  $J_{\text{HSi}} = 111$  Hz),  $-2.84$  (s,  $^{29}\text{Si}$ -satellites:  $J_{\text{HSi}} = 102$  Hz) ppm.  $^{13}\text{C}$  NMR ( $\text{C}_6\text{D}_6$ ):  $\delta_{\text{C}}$  155.70, 155.54, 145.80, 145.58, 144.79, 144.22, 143.95, 142.71, 142.02, 141.89, 139.88, 139.64, 139.24, 137.68, 135.22, 135.08, 134.76, 134.60, 134.38, 134.25, 133.71, 133.09, 132.59, 132.47, 132.35, 132.23, 129.96, 129.71, 129.35, 128.58, 128.43, 127.71, 127.64, 127.51, 127.39, 127.26, 127.04, 126.71, 125.87, 125.71, 121.46, 120.20, 14.37, 9.20 ppm.  $^{31}\text{P}$  NMR ( $\text{C}_6\text{D}_6$ ):  $\delta_{\text{P}}$  33.29 (A, dd,  $^2J_{\text{PP}} = 3, 16$  Hz), 30.28 (B, dd,  $^2J_{\text{PP}} = 5, 16$  Hz), 17.94 (B, dd,  $^2J_{\text{PP}} = 16, 48$  Hz), 17.52 (A, dd,  $^2J_{\text{PP}} = 16, 45$  Hz), 10.43 (B, dd,  $^2J_{\text{PP}} = 5, 48$  Hz), 7.78 (A, dd,  $^2J_{\text{PP}} = 3, 45$  Hz) ppm.  $^{29}\text{Si}$  NMR ( $\text{C}_6\text{D}_6$ ):  $\delta_{\text{Si}}$   $-3.19$  (dd,  $^2J_{\text{SiP}} = 14, 53$  Hz),  $-8.32$  (ddd,  $^2J_{\text{SiP}} = 4, 15, 43$  Hz) ppm.

**Standard synthesis for isolated deuterated complexes:** The nickel starting complex (**2**, **3** or **4**, 4 to 6 mg) was weighed in a small vial and suspended in  $\text{C}_6\text{H}_6$  (1 mL). While stirring,  $\text{Ph}_2\text{SiD}_2$  (1.05 eq) was added. After 2-3 hours, as indicated by the color and physical change of the mixture from a dark red suspension to an orange solution, the solvent was evaporated. Hexanes (2 mL) was added, if necessary the mixture was cooled to  $-35^\circ\text{C}$ , and removed by decantation followed by evaporation of remaining volatiles in vacuum. All reactions lead to quantitative yields.

**2[SiD<sub>2</sub>]:** Standard procedure followed.  $^1\text{H}$  NMR ( $\text{C}_6\text{D}_6$ ):  $\delta_{\text{H}}$  8.04 (d,  $J = 7.07$  Hz, Ar-H, 2H), 7.55 (t,  $J = 8$  Hz, Ar-H), 7.42 (d,  $J = 7$  Hz, Ar-H), 7.13-6.92 (m, Ar-H), 6.87 (dt,  $J = 2, 7$  Hz, Ar-H), 6.82-6.68 (m, Ar-H), 6.60 (t,  $J = 7$  Hz, Ar-H), 6.53 (t,  $J = 8$  Hz, Ar-H), 6.37 (t,  $J = 7$  Hz, Ar-H, 1H), 4.99 (s,  $-\text{CDH}$ , 0.5H), 4.60 (d,  $J = 2$  Hz,  $-\text{CDH}$ , 0.5H) ppm.  $^2\text{H}$  NMR ( $\text{C}_6\text{D}_6$ ):  $\delta_{\text{H}}$  5.05 ( $\text{Ph}_2\text{SiHD}$ ), 4.55 (broad,  $-\text{CHD}$ ),  $-2.65$  (Si-D-N) ppm.  $^{13}\text{C}$  NMR ( $\text{C}_6\text{D}_6$ ):  $\delta_{\text{C}}$  156.11 (d,  $J = 16$  Hz), 145.25 (d,  $J = 24$  Hz), 143.98, 142.82, 142.41 (d,  $J = 10$  Hz), 139.87, 139.63, 139.07, 138.77, 136.06, 135.31, 134.95, 134.70, 134.58, 133.72, 133.59, 133.19, 132.56, 132.44, 130.56, 130.13, 129.80, 129.33, 128.57, 127.43, 127.30, 127.22, 127.14, 127.06, 126.92, 126.72 (d,  $J = 5$  Hz), 125.70, 120.76 (d,  $J = 4$  Hz), 100.57 ppm.  $^{31}\text{P}$  NMR ( $\text{C}_6\text{D}_6$ ):  $\delta_{\text{P}}$  32.69 (d,  $^2J_{\text{PP}} = 17$  Hz), 17.09 (dd,  $^2J_{\text{PP}} = 17, 45$  Hz), 7.77 (dd,  $^2J_{\text{PP}} = 4, 45$  Hz) ppm.  $^{29}\text{Si}$  NMR ( $\text{C}_6\text{D}_6$ ): no signal obtained due to low solubility of the material. IR  $\text{cm}^{-1}$ : 3052, 2961, 2923, 2854, 1667, 1585, 1556, 1479, 1467, 1433, 1307, 1261, 1184, 1157, 1118, 1090, 1027, 824, 802, 739, 695, 617, 542, 519, 506, 488, 409.

**3[SiD<sub>2</sub>]:** Standard procedure followed.  $^1\text{H}$  NMR ( $\text{C}_6\text{D}_6$ ):  $\delta_{\text{H}}$  7.57 (broad s, Ar-H), 7.33 (t,  $J = 8$  Hz, Ar-H), 7.18-7.10 (m, Ar-H), 7.05-6.99 (m, Ar-H), 6.94-6.79 (m, Ar-H), 6.39 (t,  $J = 7$  Hz, Ar-H), 4.88 (broad s,  $-\text{CH}_2$ ), 2.43 (s, 3H,  $-\text{CH}_3$ ) ppm.  $^{31}\text{P}$  NMR ( $\text{C}_6\text{D}_6$ ):  $\delta_{\text{P}}$  27.44, 21.98,  $-31.64$  ppm.

**4[SiD<sub>2</sub>]:** Standard procedure followed.  $^1\text{H}$  NMR ( $\text{C}_6\text{D}_6$ ):  $\delta_{\text{H}}$  7.46 (broad s, Ar-H), 7.26 (t,  $J = 8$  Hz, Ar-H), 7.19 (broad s, Ar-H), 7.13 (broad s, Ar-H), 7.09-6.80 (broad m, Ar-H), 6.75 (broad s, Ar-H), 6.68 (broad s, Ar-H), 6.50 (broad s, Ar-H), 6.42 (broad s, Ar-H), 4.79 (broad s,  $-\text{CH}_2$ ), 4.61 (broad s,  $-\text{CH}_2$ ), 2.57 (broad s,  $-\text{CH}_3$ ), 2.52 (broad s,  $-\text{CH}_3$ ), 2.45 (broad s,  $-\text{CH}_3$ ), 2.33 (broad s,  $-\text{CH}_3$ ) ppm.  $^{31}\text{P}$  NMR ( $\text{C}_6\text{D}_6$ ):  $\delta_{\text{P}}$  26.09, 4.81,  $-31.25$  ppm.

**Standard synthesis for *in situ* formed complexes and stoichiometric reactions:** the Ni-complex suspended in C<sub>6</sub>H<sub>6</sub> (0.6 mL). While stirring, the silane (1 equivalent) was added using a microsyringe and the mixture was stirred for >30 min, until full color change was observed from deep red to clear orange.

**Standard method for the catalytic runs:** the Ni-complex (**2-4**, 0.004 mmol) was weighed in a vial and suspended in C<sub>6</sub>D<sub>6</sub> (0.3 mL), resulting in a red-suspension (for **2** and **3**) or red solution (**4**). Diphenylsilane was added (1.05 equivalents) and the mixture was stirred for 30 min to form the Si-species, resulting in an orange-red solution. The mixture was transferred to a Young-type NMR tube, and additional C<sub>6</sub>D<sub>6</sub> (0.3 mL) was added. Next, the substrates and internal standard were added using a microsyringe in the following order: mesitylene (50 equivalents, internal standard), 1-octene (100 equivalents) and diphenylsilane (100 equivalents). The mixture was directly moved to the NMR and measured in time, taking an <sup>1</sup>H NMR measurement every 30 minutes. Normal settings for <sup>1</sup>H NMR were applied, with the exception of the number of scans (1 scan) and an acquisition time of 10 seconds.

## 6.5 References

- [1] R. Beck, S. A. Johnson, *Organometallics*, **2012**, *31*, 3599–3609.
- [2] T. Zell, T. Schaub, K. Radacki, U. Radius, *Dalton. Trans.*, **2011**, *40*, 1852–1854.
- [3] a) A. J. Chalk, J. F. Harrod, *J. Am. Chem. Soc.*, **1965**, *87*, 1133–1135. b) D. Troegel, J. Stohrer, *Coord. Chem. Rev.*, **2011**, *255*(13–14), 1440–1459.
- [4] J. L. Speier, J. A. Webster, G. H. Barnes, *J. Am. Chem. Soc.*, **1957**, *79*, 974–979.
- [5] B. D. Karstedt, General Electric Company. U.S. Patent US3775452A, **1973**.
- [6] X. Du, Z. Huang, *ACS Catal.*, **2017**, *7*, 1227–1243.
- [7] Chapter 4 of this thesis: D. G. A. Verhoeven, J. Kwakernaak, M. A. C. van Wiggen, M. Lutz, R. J. M. Klein Gebbink, M. -E. Moret, *to be submitted*.
- [8] J. Sun, L. Deng, *ACS Catal.*, **2016**, *6*, 290–300.
- [9] Examples of Co catalysts: a) M. Brookhart, B. E. Grant., *J. Am. Chem. Soc.*, **1993**, *115*, 2151–2156. b) Z. Mo, Y. Liu, L. Deng, *Angew. Chem. Int. Ed.*, **2013**, *52*, 10845–10849. c) C. Chen, M. B. Hecht, A. Kavara, W. W. Brennessel, B. Q. Mercado, D. J. Weix, P. L. Holland, *J. Am. Chem. Soc.*, **2015**, *137*, 13244–13247. d) C. H. Schuster, T. Diao, I. Pappas, P. J. Chirik, *ACS Catal.*, **2016**, *6*, 2632–2636. e) A. D. Ibrahim, S. W. Entsminger, L. Zhu, A. R. Fout, *ACS Catal.*, **2016**, *6*, 3589–3593. f) X. Du, Y. Zhang, D. Peng, Z. Huang, *Angew. Chem. Int. Ed.*, **2016**, *55*, 6671–6675. g) D. Noda, A. Tahara, Y. Sunada, H. Nagashima, *J. Am. Chem. Soc.*, **2016**, *138*, 2480–2483. h) Gorczyński, M. Zaranek, S. Witomska, A. Bocian, A. R. Stefankiewicz, M. Kubicki, V. Patroniak, P. Pawluc, *Catal. Commun.*, **2016**, *78*, 71–74.
- [10] Examples of Fe catalysts: a) R. Langer, Y. Diskin-Posner, G. Leitnus, L. J. W. Shimon, Y. Ben-David, D. Milstein, *Angew. Chem. Int. Ed.*, **2011**, *50*(42), 9948–9952. b) A. M. Tondreau, C. C. H. Atienza, K. J. Weller, S. A. Nye, K. M. Lewis, J. G. P. Delis, P. J. Chirik, *Science*, **2012**, *335*(6068), 567–570. c) X. Du, Y. Zhang, D. Peng, Z. Huang, *Angew. Chem. Int. Ed.*, **2016**, *55*, 6671–6675.
- [11] X. Du, Z. Huang, *ACS Catal.*, **2017**, *7*, 1227–1243.
- [12] Y. Nakajima, K. Sato, S. Shimada, *Chem. Rec.*, **2016**, *16*, 2379–2387.
- [13] a) M. Kumada, Y. Kiso, M. Umeno, *Chem. Commun.*, **1970**, 611. b) I. Pappas, S. Treacy, P. J. Chirik, *ACS Catal.*, **2016**, 4105–4109. c) Y. Chen, C. Sui-Seng, S. Boucher, D. Zargarian, *Organometallics*,

- 2005, 24, 149–155. d) L. Benitez Junquera, M. C. Puerta, P. Valerga, *Organometallics*, **2012**, 31, 2175–2183. e) T. J. Steiman, C. Uyeda, *J. Am. Chem. Soc.*, **2015**, 137, 6104–6110.
- [14] M. I. Lipschutz, T. D. Tilley, *Chem. Commun.*, **2012**, 48, 7146–7148.
- [15] V. Srinivas, Y. Nakajima, W. Ando, K. Sato, S. Shimada, *Catal. Sci. Technol.*, **2015**, 5, 2081–2084.
- [16] I. Buslov, J. Becouse, S. Mazza, M. Montondon-Clerc, X. Hu, *Angew. Chem. Int. Ed.*, **2015**, 54, 14523–14526.
- [17] I. Pappas, S. Treacy, P. J. Chirik, *ACS Catal.*, **2016**, 4105–4109.
- [18] Chapter 1 of this thesis: D. G. A. Verhoeven, M. -E. Moret, *Dalton Trans.* **2016**, 45, 15762–15778.
- [19] Examples with Ir: a) L. E. Doyle, W. E. Piers, J. Borau-Garcia, *J. Am. Chem. Soc.*, **2015**, 137, 2187–2190. b) L. E. Doyle, W. E. Piers, J. Borau-Garcia, M. J. Sgro, D. M. Spasyuk, *Chem. Sci.*, **2016**, 7, 921–931.
- [20] Example with Ru: M. P. Boone, D. W. Stephan, *J. Am. Chem. Soc.*, **2013**, 135, 8508–8511.
- [21] S. Lin, M. W. Day, T. Agapie, *J. Am. Chem. Soc.*, **2011**, 133, 3828–3831.
- [22] B. J. Barrett, V. M. Iluc, *Organometallics*, **2014**, 33, 2565–2574.
- [23] K. T. Horak, D. G. VanderVelde, T. Agapie, *Organometallics*, **2015**, 34(19), 4753–4765.
- [24] S. N. MacMillan, W. H. Harman, J. C. Peters, *Chem. Sci.*, **2014**, 5, 590–597.
- [25] V. N. Iluc, G. L. Hillhouse, *J. Am. Chem. Soc.*, **2010**, 132, 11890–11892.
- [26] D. Schmidt, T. Zell, T. Schaub, U. Radius, *Dalton Trans.*, **2014**, 43, 10816–10827.
- [27] S. Wu, X. Li, Z. Xiong, W. Xu, Y. Lu, H. Sun, *Organometallics*, **2013**, 32, 3227–3237.
- [28] D. J. Charboneau, D. Balcells, N. Hazari, H. M. C. Lant, J. M. Mayer, P. R. Melvin, B. Q. Mercado, W. D. Morris, M. Repisky, H.-W. Suh, *Organometallics*, **2016**, 35(18), 3154–3162.
- [29] W. Chen, S. Shimada, M. Tanaka, Y. Kobayashi, K. Saigo, *J. Am. Chem. Soc.*, **2004**, 126(26), 8072–8073.
- [30] J. Takaya, N. Iwasawa, *Dalton Trans.*, **2011**, 40(35), 8814–8821.
- [31] Formation of single crystals was attempted multiple times, but did not result in crystals suitable for XRD structure analysis.
- [32] Fe: R. S. Simons, C. A. Tessier, *Organometallics*, **1996**, 15, 2604–2610.
- [33] Ni–Al–H: T. Steinke, C. Gemel, M. Cokoja, M. Winter, R. A. Fisher, *Angew. Chem. Int. Ed.*, **2004**, 43, 2299–2302.
- [34] S. Xu, S. Zhang, H. Sun, *Inorg. Chim. Acta*, **2015**, 430, 161–167.
- [35] V. M. Iluc, G. L. Hillhouse, *Tetrahedron*, **2006**, 62, 7577–7582.
- [36] This transition state could not be optimized with the added dispersion correction. Therefore, the calculation was performed at the B3LYP/6-31G\*\* level of theory, followed by a single point calculation with the added dispersion correction.
- [37] J. Guihaumé, S. Halbert, O. Eisenstein, R. N. Perutz, *Organometallics*, **2011**, 31(4), 1300–1314.
- [38] The scrambling stays related in time; <sup>1</sup>H NMR shows a ratio of D/H (**2[SiD<sub>2</sub>]**: **2[SiPhMe]**) of 2.5:1 after 18 min, corresponding to a **2[SiD<sub>2</sub>]**: **2[SiPhMe]** ratio in <sup>31</sup>P NMR of 1.7:1 after 21 min. NMR spectra are given in Appendix F, Figure A14 to A16.
- [39] E. Calimano, T. D. Tilley, *J. Am. Chem. Soc.* **2009**, 131(31), 11161–11173.
- [40] B. A. Connor, J. Rittle, D. VanderVelde, J. C. Peters, *Organometallics*, **2016**, 35(5), 686–690.
- [41] APT <sup>13</sup>C NMR was taken *in situ* after catalysis reached full conversion, without further isolation of the product. Seven signals for –CH<sub>2</sub> groups were visible, together with one –CH<sub>3</sub> group, observed by the opposite phasing of these signals. For more info, see Chapter 4 of this thesis.

- [42] M. J. Frish, G. W. Trucks, H. B. Schlegel, G. E. Scuseria, M. A. Robb, J. R. Cheeseman, G. Scalmani, V. Barone, B. Mennucci, G. A. Petersson, H. Nakatsuji, M. Caricato, X. Li, H. P. Hratchian, A. F. Izmaylov, J. Bloino, G. Zheng, J. L. Sonnenberg, M. Hada, M. Ehara, K. Toyota, R. Fukuda, J. Hasegawa, M. Ishida, T. Nakajima, Y. Honda, O. Kitao, H. Nakai, T. Vreven, J. A. Montgomery, Jr., J. E. Peralta, F. Ogliaro, M. Bearpark, J. J. Heyd, E. Brothers, K. N. Kudin, V. N. Staroverov, R. Kobayashi, J. Normand, K. Raghavachari, A. Rendell, J. C. Burant, S. S. Iyengar, J. Tomasi, M. Cossi, N. Rega, J. M. Millam, M. Klene, J. E. Knox, J. B. Cross, V. Bakken, C. Amado, J. Jaramillo, R. Gomperts, R. E. Stratmann, O. Yazyev, A. J. Austin, R. Cammi, C. Pomelli, J. W. Ochterski, R. L. Martin, K. Morokuma, V. G. Zakrzewski, G. A. Voth, P. Salvador, J. J. Dannenberg, S. Dapprich, A. D. Daniels, Ö. Farkas, J. B. Foresman, J. V. Ortiz, J. Cioslowski, D. J. Fox, "Gaussian 09 Revision A.02".

## Appendix A: The Crystal Structure of Na[B(Ar<sup>F</sup>)<sub>4</sub>]

### A1. Introduction

Since the publication of the synthesis and use of Na[B(Ar<sup>F</sup>)<sub>4</sub>] (Ar = 3,5-bis(trifluoromethyl)phenyl) by Kobayashi in 1981, it has become a broadly used reagent for organometallic synthesis.<sup>[1]</sup> A safe method for its preparation was reported by Yakelis and Bergman in 2005, improving on the original, hazardous, procedure.<sup>[2]</sup> The [B(Ar<sup>F</sup>)<sub>4</sub>]<sup>-</sup> anion is widely used in inorganic chemistry as a weak or non-coordinating counterion, allowing for the isolation or *in situ* generation of reactive electrophilic species that would otherwise be quenched by coordination.<sup>[3]</sup> The polarizability of the B(Ar<sup>F</sup>)<sub>4</sub> anion aids solvation in organic solvents, and its use in for example halide abstraction<sup>[4]</sup> is benefitted by strong binding of the halide to Na, promoting its removal. One prominent use of non-coordinating anions is the stabilization of active olefin polymerization catalysts often generated *in situ*.<sup>[5]</sup>

Several solvated structures of Na[B(Ar<sup>F</sup>)<sub>4</sub>] are described in literature,<sup>[6,7]</sup> among which the diaqua-analogue [Na(OH<sub>2</sub>)<sub>2</sub>][B(Ar<sup>F</sup>)<sub>4</sub>] in which the sodium center has a slightly distorted octahedral geometry with coordination of four fluorine atoms from -CF<sub>3</sub> groups, each originating from a different borate group, and two water molecules.<sup>[8]</sup> The Na-F interactions are close, with bond lengths between 2.44-2.68 Å. Crystal structures incorporating crown-ethers are also known, for example with 18-crown-6 or related sulfur analogues, as published by Reid and co-workers.<sup>[9]</sup> Remarkably, presumably owing to the weakly coordinating character of the B(Ar<sup>F</sup>)<sub>4</sub><sup>-</sup> anion and ensuing high affinity of Na for solvents, an unsolvated structure of Na[B(Ar<sup>F</sup>)<sub>4</sub>] was hitherto unprecedented.

### A2. Results and discussion

In the course of a study of halide abstraction reactions with Na[B(Ar<sup>F</sup>)<sub>4</sub>] (Chapter 3 of this thesis), crystals of unsolvated Na[B(Ar<sup>F</sup>)<sub>4</sub>] suitable for X-ray diffraction were serendipitously obtained.<sup>[10]</sup> The coordination chemistry of nickel(II) complex Ni(<sup>Ph</sup>dppb)Cl<sub>2</sub> (<sup>Ph</sup>dppb = 2,2'-bis(diphenylphosphino)benzophenone) was explored upon removal of a chloride ligand, resulting in **1**, a dimeric μ-Cl bridging [Ni(<sup>Ph</sup>dppb)Cl]<sub>2</sub> with a k<sup>2</sup>(P,O)-coordination of the diphosphine ketone ligand. A series of crystallization experiments was performed, which in no case lead to the isolation of the dimeric nickel complex. Nevertheless, crystals could be isolated from a slow vapor diffusion setup of hexanes into CH<sub>2</sub>Cl<sub>2</sub>. First, phase separation occurred, resulting in a dense brown oil, immiscible in the CH<sub>2</sub>Cl<sub>2</sub>/hexanes phase, which was identified as a mixture that mainly consists of compound **1**. From this mixture, cubical, colorless crystals grew which were identified as Na[B(Ar<sup>F</sup>)<sub>4</sub>] by X-ray crystal structure determination, without co-crystallization of solvent molecules (Figure 1).

The crystals have a 1:1 ratio of the cation and anion, crystallized in a three-dimensional framework in the P4/n space group. Each B(Ar<sup>F</sup>)<sub>4</sub> anion has an exact crystallographic S<sub>4</sub> symmetry, with the aromatic rings in a propeller-like structure around the centric borane

atom. Each sodium cation is located on a fourfold axis and is coordinated to the aromatic –CF<sub>3</sub> groups in a square antiprism geometry with a coordination number of eight, each interaction originating from an individual borate center. This is a high coordination number for sodium, which is most commonly observed in complexes of crown ethers and related ligands.<sup>[11]</sup> The Na–F bond distances are rather short, with values of Na–F1 2.455(3) Å and Na1–F4<sup>i</sup> 2.648(3) Å. While similarly short Na–F contacts are occasionally found in crystal structures containing the [B(Ar<sup>F</sup>)<sub>4</sub>]<sup>–</sup> anion,<sup>[6–8]</sup> carbon-bound fluorine atoms are generally thought to be very poor ligands<sup>[12]</sup> responsible for the weakly-coordinating character of the anion. Hence it is remarkable that the coordination sphere of Na in the structure *only* consists of such contacts. This constitutes, to the best of our knowledge an unprecedented structural motif that can be related to the recent observation of a remarkable 16-coordinate environment around a cesium cation created by C–F bonds only.<sup>[13]</sup>

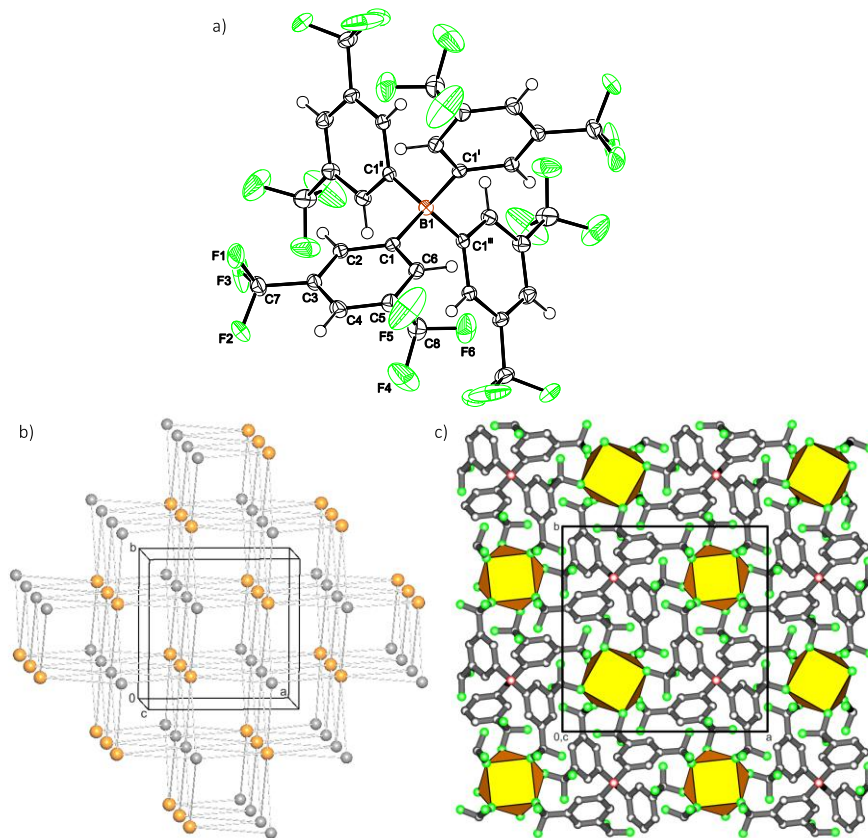


**Figure 1.** a) Displacement ellipsoid plot of the anion of Na[B(Ar<sup>F</sup>)<sub>4</sub>] (50% probability level). View along the *c* axis. Sodium cation is omitted for clarity. Symmetry codes *i*: 1.5-*x*, 0.5-*y*, *z*; *ii*: *y*+0.5, 1-*x*, -*z*; *iii*: 1-*y*, *x*-0.5, -*z*. Selected distances and angles: Na–F1 2.455(3) Å and Na1–F4<sup>i</sup> 2.648(3) Å. C7–F1–Na1 165.0(2), C8–F4–Na1<sup>i</sup> 140.9(2)°. b) Simplified coordination net of Na[B(Ar<sup>F</sup>)<sub>4</sub>] as calculated with the TOPOS software.<sup>[14]</sup> Sodium cations are drawn in orange, simplified anions in grey. All nodes have a coordination number of eight. c) View along the *c* axis on the polymeric structure of Na[B(Ar<sup>F</sup>)<sub>4</sub>]. The eightfold sodium coordination polyhedra are drawn in yellow. The DRAWxtl software was used to prepare the drawing.<sup>[15]</sup>



### A3. Conclusion

The crystal structure of unsolvated Na[B(Ar<sup>F</sup>)<sub>4</sub>] was obtained for the first time. It crystallizes in the high symmetry P4/n space group and displays a high coordination number of eight around the Na-cation originating exclusively from C–F...Na contacts. The aromatic groups surrounding the B-center are positioned in a tetrahedral geometry, in a propeller-like structure, with an exact S<sub>4</sub> symmetry. The structural characterization of a “naked” sodium salt of the widely used weakly-coordinating anion [B(Ar<sup>F</sup>)<sub>4</sub>] provides important insights in potential residual metal–anion interactions in its salts.

### A4. Experimental section

#### A4.1 General considerations

All reagents were purchased from commercial sources and used as received unless stated otherwise. Reactions were performed in a N<sub>2</sub> glovebox and at room temperature unless stated otherwise. Dichloromethane (CH<sub>2</sub>Cl<sub>2</sub>) was distilled over calciumhydride before use, and was degassed by bubbling N<sub>2</sub> through it for 30 minutes and stored over molecular sieves. Dry diethylether (Et<sub>2</sub>O) and hexanes were acquired from a MBRAUN MB SPS-80 solvent purification system, degassed by bubbling N<sub>2</sub> through it for 30 minutes and further dried over molecular sieves before use. Na[B(Ar<sup>F</sup>)<sub>4</sub>] was purchased and further dried under high vacuum for 3 days at 50°C. (Ph<sup>h</sup>dppb)NiCl<sub>2</sub> was synthesized following the literature procedure.<sup>[16]</sup>

**[Ni(Ph<sup>h</sup>dppb)(μ-Cl)]<sub>2</sub>(B(Ar<sup>F</sup>)<sub>4</sub>)<sub>2</sub> (1):** (Ph<sup>h</sup>dppb)NiCl<sub>2</sub> was suspended in Et<sub>2</sub>O (0.5 mL) in a vial in the glovebox. NaB(Ar<sup>F</sup>)<sub>4</sub> was also suspended in Et<sub>2</sub>O (2 mL) and transferred to the [Ni] mixture. The final mixture was stirred overnight at room temperature, after which all solvents were removed in vacuum. Subsequently, Et<sub>2</sub>O (1 mL) and hexanes (3 mL) were added and the formed precipitation was filtered and washed with hexanes (3 x 1 mL). The product was extracted using Et<sub>2</sub>O (3 mL), after which the solvents were removed in vacuum and **1** was obtained as a brown powder (89%, 31.5 mg, 0.0104 mmol). For analysis of compound **1**, see Chapter 3. The remaining brown powder (5-10 mg) was dissolved in CH<sub>2</sub>Cl<sub>2</sub> (1 mL) and filtered into a crystallization setup. Hexanes (2 mL) was placed around it and the mixture was left standing for 2-3 weeks. First, phase separation occurred, resulting in a dense brown oil, immiscible in the CH<sub>2</sub>Cl<sub>2</sub>/hexanes phase, which was identified as a mixture that mainly consists of compound **1**. From this mixture, cubical, colorless crystals grew which were identified as Na[B(Ar<sup>F</sup>)<sub>4</sub>] by X-ray crystal structure determination.

#### A4.2 X-ray crystal structure determination

C<sub>32</sub>H<sub>12</sub>BF<sub>24</sub>Na, Fw = 886.22, colorless block, 0.18 × 0.16 × 0.08 mm<sup>3</sup>, tetragonal, P4/n (no. 85), a = b = 13.3543(7), c = 9.3836(7) Å, V = 1673.4(2) Å<sup>3</sup>, Z = 2, D<sub>x</sub> = 1.759 g/cm<sup>3</sup>, μ = 0.21 mm<sup>-1</sup>. 36485 Reflections were measured on a Bruker Kappa ApexII diffractometer with sealed tube and Triumph monochromator (λ = 0.71073 Å) at a temperature of 150(2) K up to a resolution of (sin θ/λ)<sub>max</sub> = 0.65 Å<sup>-1</sup>. The Eval15 software was used for the integration of the intensities.<sup>[17]</sup> Multiscan absorption correction and scaling

was performed with SADABS<sup>[18]</sup> (correction range 0.65-0.75). 1941 Reflections were unique ( $R_{\text{int}} = 0.061$ ), of which 1491 were observed [ $I > 2\sigma(I)$ ]. The structure was solved with Patterson superposition methods using SHELXT.<sup>[19]</sup> Least-squares refinement was performed with SHELXL-2014<sup>[20]</sup> against  $F^2$  of all reflections. The crystal appeared to be twinned by merohedry, and the twin matrix (0,1,0 / 1,0,0 / 0,0,-1) was included in the refinement. Non-hydrogen atoms were refined freely with anisotropic displacement parameters. All hydrogen atoms were located in difference Fourier maps and refined with a riding model. 133 Parameters were refined with no restraints.  $R1/wR2$  [ $I > 2\sigma(I)$ ]: 0.0589 / 0.1690.  $R1/wR2$  [all refl.]: 0.0818 / 0.1834.  $S = 1.118$ . Twin fraction BASF = 0.171(3). Residual electron density between  $-0.51$  and  $0.60$  e/Å<sup>3</sup>. Geometry calculations and checking for higher symmetry were performed with the PLATON program.<sup>[21]</sup>

The Kitajgorodskij packing index is 68.6%, which is generally expected to be 65-75% for organic compounds.<sup>[22]</sup>

### A4.3 Twinning in the crystal structure

The crystal symmetry of Na[B(Ar<sup>F</sup>)<sub>4</sub>] is  $P4/n$  (point group 4/m). The Na and B atoms are on special positions and they perfectly fulfill the symmetry of space group  $P4/nmm$  (point group 4/mmm). This symmetry is broken if the carbon and fluorine atoms are taken into account. An analysis of all non-hydrogen atoms with the PSEUDO software<sup>[23]</sup> shows a deviation from  $P4/nmm$  which is larger than the chosen tolerance of 2 Å. Still, the metric symmetry of the lattice is 4/mmm and the twin operation can be obtained by a coset decomposition of point group 4/mmm with respect to 4/m:

$$\{1, 2_{001}, 4^+_{001}, 4^-_{001}, -1, m_{001}, -4^+_{001}, -4^-_{001}\}\{2_{010}, 2_{100}, 2_{110}, 2_{1-10}, m_{010}, m_{100}, m_{110}, m_{1-10}\}$$

The operations of the second coset are equivalent twin operations and  $2_{110}$  was arbitrarily chosen for the refinement of Na[B(Ar<sup>F</sup>)<sub>4</sub>]. By this twin refinement the  $R1$  value improves from 0.1383 to 0.0589. More importantly, the variance of scale factors  $F^2_{\text{obs}}/F^2_{\text{calc}}$  improves significantly (Figure 2).

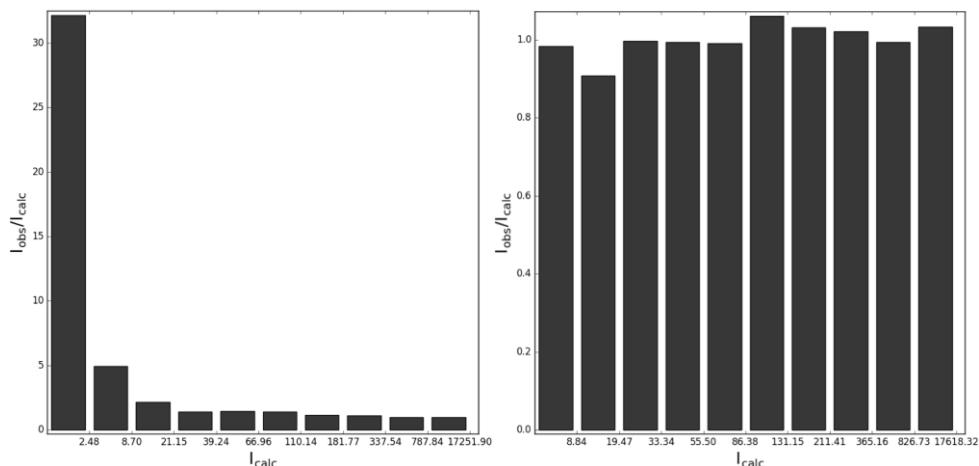


**Figure 2.** Histogram of the scale factor  $k = F^2_{\text{obs}}/F^2_{\text{calc}}$  in a refinement of Na[B(Ar<sup>F</sup>)<sub>4</sub>] without twin contribution (left) and with twin contribution (right). The scale factor  $k$  is expected to be constant over all intensity bins.

## A5. References

- [1] H. Kobayashi, A. Sonoda, H. Iwamoto, M. Yoshimura, *Chem. Lett.*, **1981**, 10(5), 579–580.
- [2] N. A. Yakelis, R. G. Bergman, *Organometallics*, **2005**, 24, 3579–3581.
- [3] a) M. Brookhart, B. Grant, A. F. Volpe Jr., *Organometallics*, **1992**, 11, 3920–3922. b) I. Crossing, I. Raabe, *Angew. Chem. Int. Ed.*, **2004**, 43, 2066–2090.
- [4] a) Y. Ganushevich, V. Miluykov, D. Yakhrov, O. Sinyashin, P. Lönnecke, E. Hey-Hawkins, *Inorg. Chim. Acta* **2011**, 376, 118–122. b) B. J. Barrett, V. M. Iluc, *Inorg. Chem.* **2014**, 53, 7248–7259.
- [5] E. Y. -X. Chen, T. J. Marks, *Chem. Rev.*, **2000**, 100, 1391–1434.
- [6] J. C. Slootweg, P. Chen, *Organometallics*, **2006**, 25, 5863–5869.
- [7] H. B. Mansaray, C. Y. Tang, D. Vidovid, A. L. Thompson, *Inorg. Chem.*, **2012**, 51(23), 13017–13022.
- [8] C. -T. Chang, C. -L. Chen, Y. -H. Liu, S. -M. Peng, P. -T. Chou, S. -T. Liu, *Inorg. Chem.*, **2006**, 45, 7590–7592.
- [9] a) M. J. D. Champion, W. Levason, D. Pugh, G. Reid, *Dalton Trans.*, **2016**, 45, 18393–18416. b) M. Everett, A. Jolleys, W. Levason, D. Pugh, G. Reid, *Chem. Commun.*, **2014**, 50, 5843–5846.
- [10] Chapter 3 of this thesis: D. G. A. Verhoeven, M. A. C. van Wiggen, J. Kwakernaak, M. Lutz, R. J. M. Klein Gebbink, M.-E. Moret, *Chem. Eur. J.*, **2017**, Accepted.
- [11] J. W. Steed, *Coord. Chem. Rev.*, **2001**, 215(1), 171–221.
- [12] J. A. Samuels, E. B. Lobkovsky, W. E. Streib, K. Folting, J. C. Huffman, J. W. Zwanziger, K. G. Caulton, *J. Am. Chem. Soc.*, **1993**, 115(12), 5093–5104.
- [13] D. Pollak, R. Goddard, K. R. Pörschke, *J. Am. Chem. Soc.*, **2016**, 138(30), 9444–9451.
- [14] V. A. Blatov, A. P. Shevchenko, D. M. Proserpio, *Cryst. Growth Des.*, **2014**, 14, 3576–3586.
- [15] L. W. Finger, M. Kroeker, B. H. Toby, *J. Appl. Cryst.*, **2007**, 40, 188–192.
- [16] Chapter 2 of this thesis: B. W. H. Saes, D. G. A. Verhoeven, M. Lutz, R. J. M. Klein Gebbink, M. -E. Moret, *Organometallics*, **2015**, 34, 2710–2713.
- [17] A. M. M. Schreurs, X. Xian, L. M. J. Kroon-Batenburg, *J. Appl. Cryst.*, **2010**, 43, 70–82.
- [18] G. M. Sheldrick, SADABS, Universität Göttingen, Germany, **2008**.
- [19] G. M. Sheldrick. *Acta Cryst.*, **2015**, A71, 3–8.
- [20] G. M. Sheldrick. *Acta Cryst.*, **2015**, C71, 3–8.
- [21] A. L. Spek, *Acta Cryst.*, **2009**, D65, 148–155.
- [22] A.I. Kitajgorodskij, *Molecular Crystals and Molecules*, **1973**, Academic Press (New York).
- [23] C. Capillas, E.S. Tasci, G. de la Flor, D. Orobengoa, J.M. Perez-Mato and M.I. Aroyo, *Z. Kristallogr.*, **2011**, 226, 186–196.

## The Crystal Structure of Na[B(Ar<sup>F</sup>)<sub>4</sub>]

## Appendix B: Additional Experimental Section to Chapter 2

### B1. X-Ray crystal structure determinations

Reflections were measured on a Bruker Kappa ApexII diffractometer with sealed tube and Triumph monochromator ( $\lambda = 0.71073\text{\AA}$ ). X-ray intensities were integrated using the Eval15 software.<sup>[A1]</sup> Absorption correction was performed with SADABS.<sup>[A2]</sup> The structures were solved with direct methods using SHELXS-97<sup>[A3]</sup> (compound **4**) or with Patterson overlay methods using SHELXT<sup>[A4]</sup> (compounds **2-CH<sub>2</sub>Cl<sub>2</sub>**, **2**, and **3**). Least-squares refinement was performed with SHELXL-2014<sup>[A5]</sup> against  $F^2$  of all reflections. Non-hydrogen atoms were refined freely with anisotropic displacement parameters. Hydrogen atoms of the metal complex molecules were located in difference Fourier maps. Hydrogen atoms of the solvent molecules were included in calculated positions. All hydrogen atoms were refined with a riding model. Structure calculations and checking for higher symmetry were performed with PLATON.<sup>[A6]</sup> Further details are given in Table 1. Compounds **2-CH<sub>2</sub>Cl<sub>2</sub>** and **2**: The two crystal forms were obtained from the same crystallization batch. Compound **3**: The crystal was obtained from benzene-d<sub>6</sub>. Compound **4**: The crystal structure is affected by a small contribution of whole-molecule disorder. This has been ignored in the refinement. The co-crystallized diethyl ether molecule is disordered on an inversion center. Restraints have been used for 1,2 and 1,3 distances of the diethyl ether molecule.

**Table B1.** Details of the X-ray crystal structure determinations for complexes **2-CH<sub>2</sub>Cl<sub>2</sub>**, **2**, **3** and **4**.

Parameter	<b>2-CH<sub>2</sub>Cl<sub>2</sub></b>	<b>2</b>	<b>3</b>	<b>4</b>
Chemical formula	C <sub>37</sub> H <sub>28</sub> Cl <sub>2</sub> NiOP <sub>2</sub> ·CH <sub>2</sub> Cl <sub>2</sub>	C <sub>37</sub> H <sub>28</sub> Cl <sub>2</sub> NiOP <sub>2</sub>	C <sub>37</sub> H <sub>28</sub> ClNiOP <sub>2</sub>	C <sub>55</sub> H <sub>43</sub> NiOP <sub>3</sub> ·½ C <sub>4</sub> H <sub>10</sub> O
Formula weight	765.07	680.14	644.69	908.57
Crystal color	Brown	Brown	Red	Dark red
Crystal size [mm <sup>3</sup> ]	0.39 x 0.11 x 0.06	0.29 x 0.29 x 0.06	0.12 x 0.12 x 0.04	0.20 x 0.12 x 0.07
T [K]	150(2)	150(2)	150(2)	150(2)
Crystal system	Orthorhombic	Monoclinic	Monoclinic	Monoclinic
Space group	P2 <sub>1</sub> 2 <sub>1</sub> 2 <sub>1</sub> (no. 19)	P2 <sub>1</sub> /c (no. 14)	P2 <sub>1</sub> /n (no. 14)	P2 <sub>1</sub> /c (no. 14)
a [Å]	9.62126(17)	18.7117(7)	9.8635(3)	13.5071(5)
b [Å]	18.4902(4)	11.2342(4)	35.4023(14)	17.8465(6)
c [Å]	20.0628(5)	15.8601(5)	17.3720(5)	19.8676(6)
$\beta$ [°]	-	110.302(2)	93.340(1)	108.318(2)
V [Å <sup>3</sup> ]	3569.16(13)	3126.83(19)	6055.8(4)	4546.5(3)
Z	4	4	8	4
D <sub>calc</sub> [g/cm <sup>3</sup> ]	1.424	1.445	1.414	1.327
(sin $\theta$ / $\lambda$ ) <sub>max</sub> [Å <sup>-1</sup> ]	0.65	0.65	0.65	0.65
$\mu$ [mm <sup>-1</sup> ]	0.96	0.92	0.86	0.58
Abs. corr.	Numerical	Multi-scan	Numerical	Multi-scan
Abs. corr. range	0.73-0.95	0.68-0.75	0.79-1.00	0.65-0.75
Refl. measured/unique	87198 / 8203	47086 / 7186	63999 / 13906	54739 / 10440
Parameters/restraints	415 / 0	388 / 0	757 / 0	586 / 37
R1/wR2 [ $>2\sigma(I)$ ]	0.0292 / 0.0831	0.0222 / 0.0561	0.0356 / 0.0749	0.0385 / 0.0877
R1/wR2 [all refl.]	0.0314 / 0.0846	0.0255 / 0.0576	0.0640 / 0.0832	0.0614 / 0.0965
Flack x parameter <sup>[A7]</sup>	-0.003(2)	-	-	-
S	1.044	1.039	1.028	1.037
$\rho$ <sub>(min/max)</sub> [eÅ <sup>-3</sup> ]	-0.72 / 1.01	-0.31 / 0.34	-0.43 / 0.43	-0.28 / 0.64

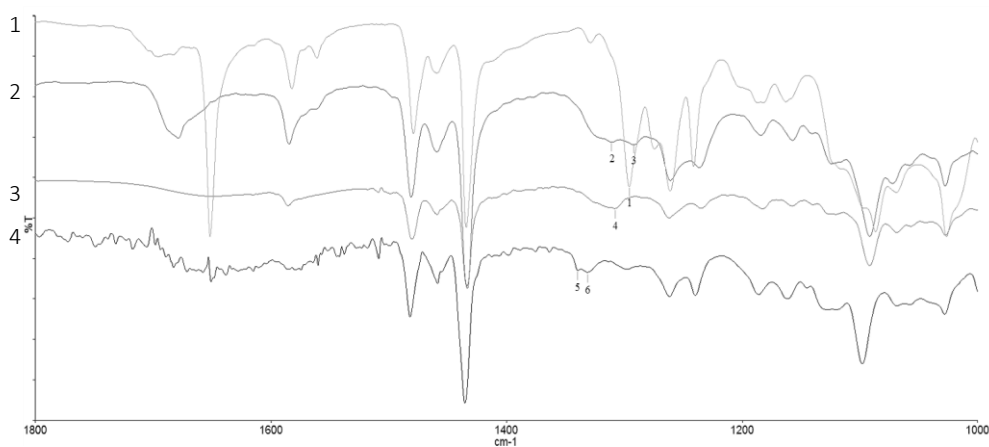
**Table B2.** Comparison of bond lengths [Å] and angles [°] in the crystal structures of **2** and **2·CH<sub>2</sub>Cl<sub>2</sub>**.

	<b>2</b>	<b>2·CH<sub>2</sub>Cl<sub>2</sub></b>
Ni...C	3.4031(12)	3.359(3)
Ni...O	3.1012(10)	3.092(2)
C=O	1.2288(16)	1.223(4)
P–Ni–P	112.996(13)	113.76(3)
Cl–Ni–Cl	133.302(14)	135.80(4)

## B2. IR spectroscopy

**Table A3.** Experimental and calculated C=O vibrational frequencies.

	$\nu_{\text{C=O}}(\text{exp})$ (cm <sup>-1</sup> )	$\nu_{\text{C=O}}(\text{calc})$ (cm <sup>-1</sup> )	Calc. IR Intensity (km/mol)
Phdpbp ( <b>1</b> )	1661	1750	138
(Phdpbp)NiCl <sub>2</sub> ( <b>2</b> )	1634	1695	118
(Phdpbp)NiCl ( <b>3</b> )	1340, 1331	1372	40
(Phdpbp)Ni(PPh <sub>3</sub> ) ( <b>4</b> )	1309	1346	19

**Figure B1.** Overlay of the IR spectra of **1** (top spectrum, 1), **5** (2<sup>nd</sup> spectrum), **4** (3<sup>rd</sup> spectrum) and **3** (bottom spectrum, 4). The region from 1100 to 1800 cm<sup>-1</sup> is shown. Peak signals (in cm<sup>-1</sup>): 1: 1296, 2: 1310, 3: 1292, 4: 1309, 5: 1340, 6: 1331.

### B2.2 Assignment of C=O vibrational frequencies

The assignment of C=O vibrational frequencies is proposed on the basis of a comparison of experimental IR data and predictions from DFT calculations at the B3LYP/6-31G\*\* level. The free ligand **1** exhibits one intense IR absorption at 1661 cm<sup>-1</sup>, which is straightforwardly assigned to the ketone moiety; DFT overestimates it by ca 5% and predicts it at 1750 cm<sup>-1</sup> associated with an IR intensity of 138 km/mol. Upon coordination of **1** to NiCl<sub>2</sub> in complex **2**, the energy of this band decreases to 1634 cm<sup>-1</sup> and it remains intense, which is qualitatively reproduced by DFT (1695 cm<sup>-1</sup>, 118 km/mol). Reasons for this shift may include a weak, presumably electrostatic interaction with the nickel center as well as increased conjugation with the phenyl rings imposed by coordination.

Upon  $\eta^2(\text{C},\text{O})$  coordination to Ni(I) in **3**, DFT predicts a shift of ca  $320\text{ cm}^{-1}$  towards lower energies as compared to compound **2**. This is accompanied by a 3-fold decrease of the calculated IR intensity, likely due to the fact that the C–O oscillator is not terminal anymore but part of a three-membered Ni–C–O cycle. These predictions are consistent with the assignment to C=O vibrations of the two weak IR absorptions observed at  $1340$  and  $1331\text{ cm}^{-1}$  – corresponding to shifts of  $296$  and  $303\text{ cm}^{-1}$  from compound **2**, respectively – as the free ligand does not display strong absorptions in this region. The reason for the doubling of this peak is unclear, but it could arise from the two independent molecules found in the unit cell of **3** in the solid state having different microenvironments or from coupling of the C=O oscillator with aromatic C–H bending modes (See Figure A1).

Finally, moving to Ni(0) in compound **4**, DFT predicts a decrease of the C=O vibrational energy by  $26\text{ cm}^{-1}$  from the Ni(I) compound **3**, consistent with the assignment of the experimental bands at  $1309\text{ cm}^{-1}$  in **4** and at  $1310\text{ cm}^{-1}$  in **5** to this mode.

### B3. EPR spectra

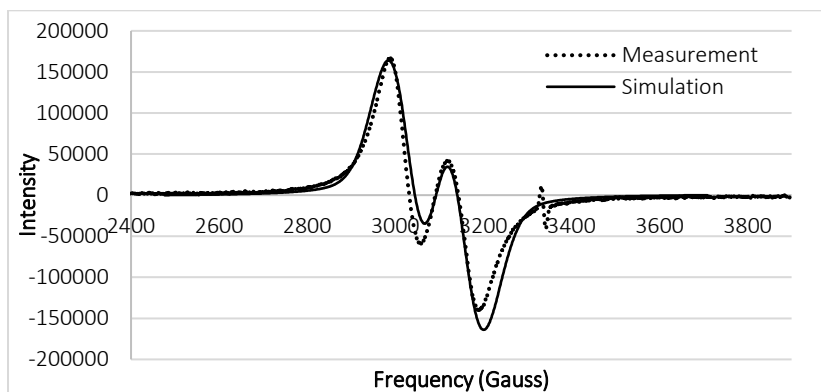


**Figure B2.** X-band EPR spectrum of ( $\text{Phdpbp}$ )NiCl (**3**) in toluene at 300 K (blue) and simulated spectrum (red). Simulation parameters:  $g = 2.325$ ,  $^{31}\text{P1}$  (MHz):  $A = 380$ .

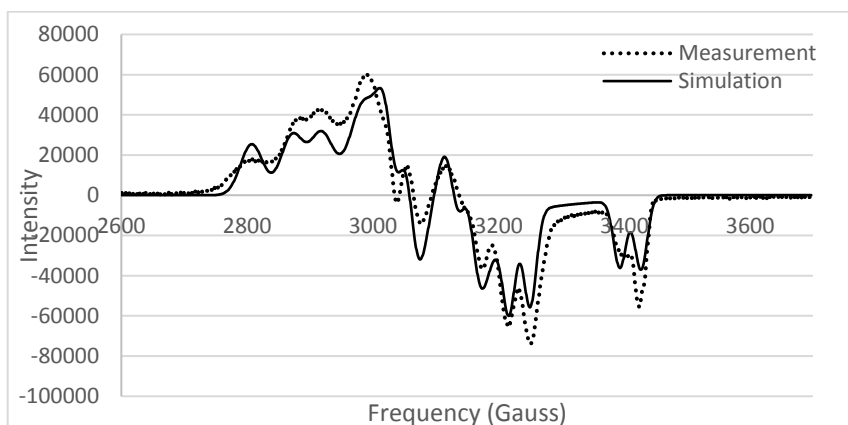
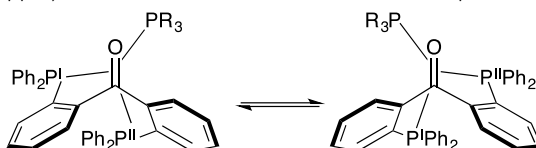


**Figure B3.** X-band EPR spectrum of ( $\text{Phdpbp}$ )NiCl (**3**) in toluene at 100 K (blue) and simulated spectrum (red). Simulation parameters:  $g_x = 2.325$ ,  $g_y = 2.175$ ,  $g_z = 2.026$ ,  $^{31}\text{P1}$  (MHz):  $A(x) = 360$ ,  $A(y) = 300$ ,  $A(z) = 500$ ,  $^{31}\text{P2}$  (MHz):  $A(x) = 210$ ,  $A(y) = 100$ ,  $A(z) = 95$ .

## B4. Fluxionality in compounds **4** and **5**

The  $^{31}\text{P}$  NMR spectrum of  $\text{Ni}_2(\text{Phdpbp})_3$  (**5**) at 100 °C consists of three mutually coupled doublet of doublet signals at 44.4, 21.3, and 5.6 ppm, indicating that the two  $^{31}\text{P}$  nuclei from the Phdpbp ligand are inequivalent in this compound. In contrast, the  $^{31}\text{P}$  NMR spectrum of  $(\text{Phdpbp})\text{Ni}(\text{PPh}_3)$  (**4**) displays a single doublet for these two P atoms. This discrepancy can be resolved by considering that, while inequivalent in the frozen structure, these two P atoms exchange quickly on the NMR timescale *via* a propeller-like inversion of the ligand as depicted in Scheme A1. This exchange mechanism is expected to be considerably slower in a sterically congested structure such as **5**, for which the two P atoms will give two different signals. This interpretation is supported by the fact that the chemical shift assigned to the Phdpbp ligand in **4** (17.9 ppm) is found between those in **5** at room temperature (22.9 ppm, 11.2 ppm).



**Scheme B1.** Inversion of the ligand causing a difference of the phosphorous nuclei in  $^{31}\text{P}$  NMR.

## B5. NMR spectra

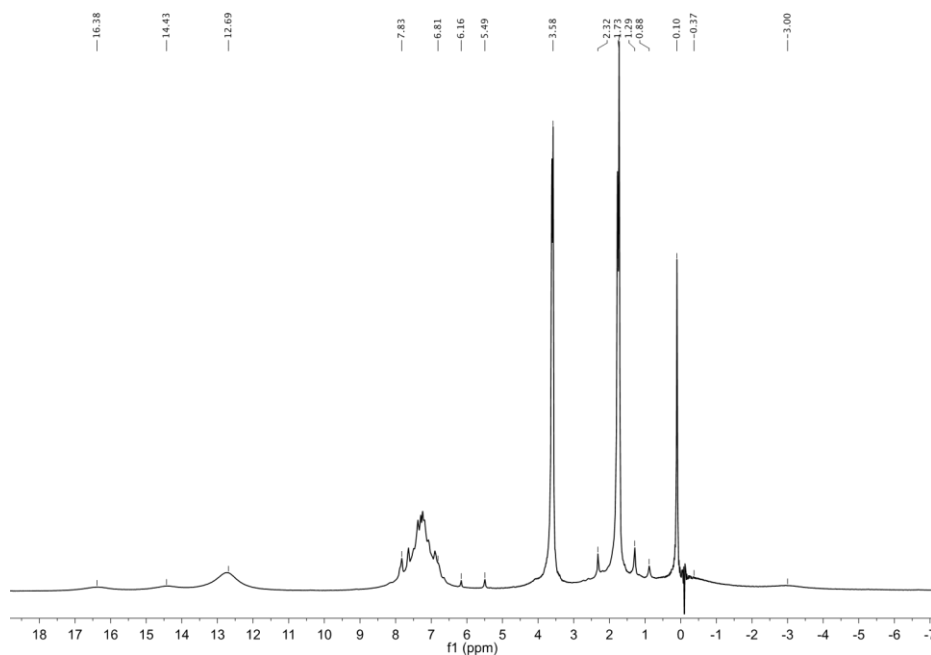


**Figure B4.**  $^1\text{H}$  NMR spectrum of  $(\text{Phdpbp})\text{NiCl}$  (**3**) (*d*-THF). Paramagnetic settings: acquisition time: 0.1 s, relaxation delay: 0.1 s.



## B6. References

- [A1] A. M. M. Schreurs, X. Xian, L. M. J. Kroon-Batenburg, *J. Appl. Cryst.*, **2010**, *43*, 70–82.
- [A2] G. M. Sheldrick, **1999**, SADABS: Area-Detector Absorption Correction, Universität Göttingen, Germany.
- [A3] G. M. Sheldrick, *Acta Cryst.*, **2008**, *A64*, 112–122.
- [A4] G.M. Sheldrick. *Acta Cryst.*, **2015**, *A71*, 3–8.
- [A5] G.M. Sheldrick. *Acta Cryst.*, **2015**, *C71*, 3–8.
- [A6] A.L. Spek, *Acta Cryst.*, **2009**, *D65*, 148–155.
- [A7] S. Parsons, H.D. Flack, T. Wagner, *Acta Cryst.*, **2013**, *B69*, 249–259.



## Appendix C: Additional Experimental Section to Chapter 3

### C1. X-ray crystal structure determination

**2:**  $C_{37}H_{28}Cl_2FeOP_2 \cdot C_7H_8$ , Fw = 769.42, yellow needle,  $0.26 \times 0.11 \times 0.11 \text{ mm}^3$ , orthorhombic, Pbc<sub>a</sub> (no. 61),  $a = 18.0070(4)$ ,  $b = 19.2846(4)$ ,  $c = 21.4460(5) \text{ \AA}$ ,  $V = 7447.3(3) \text{ \AA}^3$ ,  $Z = 8$ ,  $D_x = 1.372 \text{ g/cm}^3$ ,  $\mu = 0.67 \text{ mm}^{-1}$ . 133064 Reflections were measured on a Bruker Kappa ApexII diffractometer with sealed tube and Triumph monochromator ( $\lambda = 0.71073 \text{ \AA}$ ) at a temperature of 150(2) K up to a resolution of  $(\sin \theta/\lambda)_{\max} = 0.65 \text{ \AA}^{-1}$ . The intensities were integrated with the Eval15 software.<sup>[A1]</sup> Multi-scan absorption correction and scaling was performed with SADABS<sup>[A2]</sup> (correction range 0.67-0.75). 8544 Reflections were unique ( $R_{\text{int}} = 0.088$ ), of which 6024 were observed [ $I > 2\sigma(I)$ ]. The structure was solved with Patterson superposition methods using SHELXT.<sup>[A3]</sup> Least-squares refinement was performed with SHELXL-2014<sup>[A4]</sup> against  $F^2$  of all reflections. Non-hydrogen atoms were refined freely with anisotropic displacement parameters. The toluene solvent molecule was refined with a disorder model. Hydrogen atoms were located in difference Fourier maps (metal complex) or introduced in calculated positions (solvent). All hydrogen atoms were refined with a riding model. 515 Parameters were refined with 231 restraints (molecular flatness, distances, angles, and displacement parameters of the disordered toluene).  $R1/wR2$  [ $I > 2\sigma(I)$ ]: 0.0391 / 0.0798.  $R1/wR2$  [all refl.]: 0.0709 / 0.0918.  $S = 1.026$ . Residual electron density between -0.33 and 0.51  $e/\text{\AA}^3$ . Geometry calculations and checking for higher symmetry were performed with the PLATON program.<sup>[A5]</sup>

**3:**  $C_{37}H_{28}Cl_2CoOP_2 \cdot C_4H_8O$ , Fw = 752.47, green needle,  $0.56 \times 0.17 \times 0.05 \text{ mm}^3$ , monoclinic,  $P2_1/c$  (no. 14),  $a = 15.8479(5)$ ,  $b = 10.7277(3)$ ,  $c = 21.1721(6) \text{ \AA}$ ,  $\beta = 94.629(1)^\circ$ ,  $V = 3587.75(18) \text{ \AA}^3$ ,  $Z = 4$ ,  $D_x = 1.393 \text{ g/cm}^3$ ,  $\mu = 0.75 \text{ mm}^{-1}$ . The crystal appeared to be twinned with a twofold rotation about  $hkl = (0,0,1)$  as twin operation. Consequently, two orientation matrices were used for the intensity integration with Eval15.<sup>[A1]</sup> 71764 Reflections were measured on a Bruker Kappa ApexII diffractometer with sealed tube and Triumph monochromator ( $\lambda = 0.71073 \text{ \AA}$ ) at a temperature of 150(2) K up to a resolution of  $(\sin \theta/\lambda)_{\max} = 0.65 \text{ \AA}^{-1}$ . Multi-scan absorption correction and scaling was performed with TWINABS<sup>[A2]</sup> (correction range 0.66-0.75). 15581 Reflections were unique ( $R_{\text{int}} = 0.028$ ), of which 13615 were observed [ $I > 2\sigma(I)$ ]. The structure was solved with Patterson superposition methods using SHELXT.<sup>[A3]</sup> Least-squares refinement was performed with SHELXL-2014<sup>[A4]</sup> against  $F^2$  of all reflections using a HKLF5 file.<sup>[A6]</sup> Non-hydrogen atoms were refined freely with anisotropic displacement parameters. The THF solvent molecule was refined with a disorder model. Hydrogen atoms were introduced in calculated positions. All hydrogen atoms were refined with a riding model. 453 Parameters were refined with 33 restraints (distances, angles and displacement parameters of the disordered THF).  $R1/wR2$  [ $I > 2\sigma(I)$ ]: 0.0301 / 0.0693.  $R1/wR2$  [all refl.]: 0.0372 / 0.0722.  $S = 1.023$ . Twin fraction BASF = 0.4249(5). Residual electron density between -0.59 and 0.46  $e/\text{\AA}^3$ . Geometry calculations and checking for higher symmetry were performed with the PLATON program.<sup>[A5]</sup>

**5:**  $C_{37}H_{28}ClFeOP_2 \cdot C_7H_8$ , Fw = 733.97, red block,  $0.42 \times 0.28 \times 0.08 \text{ mm}^3$ , triclinic, P1 (no. 2),  $a = 9.8065(3)$ ,  $b = 10.0413(2)$ ,  $c = 18.4674(5) \text{ \AA}$ ,  $\alpha = 84.692(2)$ ,  $\beta = 83.314(1)$ ,  $\gamma = 86.462(1)^\circ$ ,  $V = 1795.99(8) \text{ \AA}^3$ ,  $Z = 2$ ,  $D_x = 1.357 \text{ g/cm}^3$ ,  $\mu = 0.62 \text{ mm}^{-1}$ . 47519 Reflections were measured on a Bruker Kappa ApexII diffractometer with sealed tube and Triumph monochromator ( $\lambda = 0.71073 \text{ \AA}$ ) at a temperature of 150(2)

K up to a resolution of  $(\sin \theta/\lambda)_{\max} = 0.65 \text{ \AA}^{-1}$ . The intensities were integrated with the Eval15 software.<sup>[A1]</sup> Multi-scan absorption correction and scaling was performed with SADABS<sup>[A2]</sup> (correction range 0.69–0.75). 8234 Reflections were unique ( $R_{\text{int}} = 0.017$ ), of which 7591 were observed [ $I > 2\sigma(I)$ ]. The structure was solved with Patterson superposition methods using SHELXT.<sup>[A3]</sup> Least-squares refinement was performed with SHELXL-2014<sup>[A4]</sup> against  $F^2$  of all reflections. Non-hydrogen atoms were refined freely with anisotropic displacement parameters. All hydrogen atoms were located in difference Fourier maps and refined with a riding model. 443 Parameters were refined with no restraints.  $R1/wR2$  [ $I > 2\sigma(I)$ ]: 0.0245 / 0.0624.  $R1/wR2$  [all refl.]: 0.0273 / 0.0640.  $S = 1.015$ . Residual electron density between  $-0.28$  and  $0.36 \text{ e/\AA}^3$ . Geometry calculations and checking for higher symmetry were performed with the PLATON program.<sup>[A5]</sup>

**6pTol:**  $\text{C}_{41}\text{H}_{36}\text{ClCoOP}_2$ ,  $F_w = 701.02$ , red-brown needle,  $0.46 \times 0.06 \times 0.05 \text{ mm}^3$ , monoclinic,  $P2_1/c$  (no. 14),  $a = 10.2010(6)$ ,  $b = 19.8405(13)$ ,  $c = 16.9354(10) \text{ \AA}$ ,  $\beta = 92.060(4)^\circ$ ,  $V = 3425.4(4) \text{ \AA}^3$ ,  $Z = 4$ ,  $D_x = 1.359 \text{ g/cm}^3$ ,  $\mu = 0.71 \text{ mm}^{-1}$ . 25316 Reflections were measured on a Bruker Kappa ApexII diffractometer with sealed tube and Triumph monochromator ( $\lambda = 0.71073 \text{ \AA}$ ) at a temperature of  $150(2) \text{ K}$  up to a resolution of  $(\sin \theta/\lambda)_{\max} = 0.56 \text{ \AA}^{-1}$ . The intensities were integrated with the Eval15 software.<sup>[A1]</sup> Numerical absorption correction and scaling was performed with SADABS<sup>[A2]</sup> (correction range 0.82–1.00). 4941 Reflections were unique ( $R_{\text{int}} = 0.116$ ), of which 3208 were observed [ $I > 2\sigma(I)$ ]. The structure was solved with Patterson superposition methods using SHELXT.<sup>[A3]</sup> Least-squares refinement was performed with SHELXL-2016<sup>[A4]</sup> against  $F^2$  of all reflections. Non-hydrogen atoms were refined freely with anisotropic displacement parameters. All hydrogen atoms were included in calculated positions and refined with a riding model. 419 Parameters were refined with no restraints.  $R1/wR2$  [ $I > 2\sigma(I)$ ]: 0.0585 / 0.1038.  $R1/wR2$  [all refl.]: 0.1120 / 0.1206.  $S = 1.031$ . Residual electron density between  $-0.37$  and  $0.72 \text{ e/\AA}^3$ . Geometry calculations and checking for higher symmetry were performed with the PLATON program.<sup>[A5]</sup>

**9:**  $\text{C}_{74}\text{H}_{56}\text{Cl}_2\text{Cu}_2\text{P}_4$ ,  $F_w = 1299.04$ , orange plate,  $0.25 \times 0.17 \times 0.05 \text{ mm}^3$ , monoclinic,  $P2_1/n$  (no. 14),  $a = 13.7486(4)$ ,  $b = 13.2778(4)$ ,  $c = 17.3560(5) \text{ \AA}$ ,  $\beta = 97.406(1)^\circ$ ,  $V = 3141.95(16) \text{ \AA}^3$ ,  $Z = 2$ ,  $D_x = 1.373 \text{ g/cm}^3$ ,  $\mu = 0.91 \text{ mm}^{-1}$ . 53691 Reflections were measured on a Bruker Kappa ApexII diffractometer with sealed tube and Triumph monochromator ( $\lambda = 0.71073 \text{ \AA}$ ) up to a resolution of  $(\sin \theta/\lambda)_{\max} = 0.65 \text{ \AA}^{-1}$ . A temperature of  $230(2) \text{ K}$  was chosen for the data collection because there is a solid-solid phase transition at approximately  $140\text{--}150 \text{ K}$  which destroys the single crystal. The intensities were integrated with the Eval15 software.<sup>[A1]</sup> Numerical absorption correction and scaling was performed with SADABS<sup>[A2]</sup> (correction range 0.85–0.97). 7211 Reflections were unique ( $R_{\text{int}} = 0.031$ ), of which 5959 were observed [ $I > 2\sigma(I)$ ]. The structure was solved with Patterson superposition methods using SHELXT.<sup>[A3]</sup> Least-squares refinement was performed with SHELXL-2014<sup>[A4]</sup> against  $F^2$  of all reflections. Non-hydrogen atoms were refined freely with anisotropic displacement parameters. All hydrogen atoms were located in difference Fourier maps and refined with a riding model. 379 Parameters were refined with no restraints.  $R1/wR2$  [ $I > 2\sigma(I)$ ]: 0.0291 / 0.0712.  $R1/wR2$  [all refl.]: 0.0404 / 0.0762.  $S = 1.038$ . Residual electron density between  $-0.18$  and  $0.38 \text{ e/\AA}^3$ . Geometry calculations and checking for higher symmetry were performed with the PLATON program.<sup>[A5]</sup>

CCDC 1552060 (compound **2**), 1552061 (**3**), 1552062 (**5**), 1552063 (**6pTol**), and 1552064 (**9**) contain the supplementary crystallographic data for this paper. These data can be obtained free of charge from The Cambridge Crystallographic Data Centre via [www.ccdc.cam.ac.uk/data\\_request/cif](http://www.ccdc.cam.ac.uk/data_request/cif).

## C2. NMR spectra

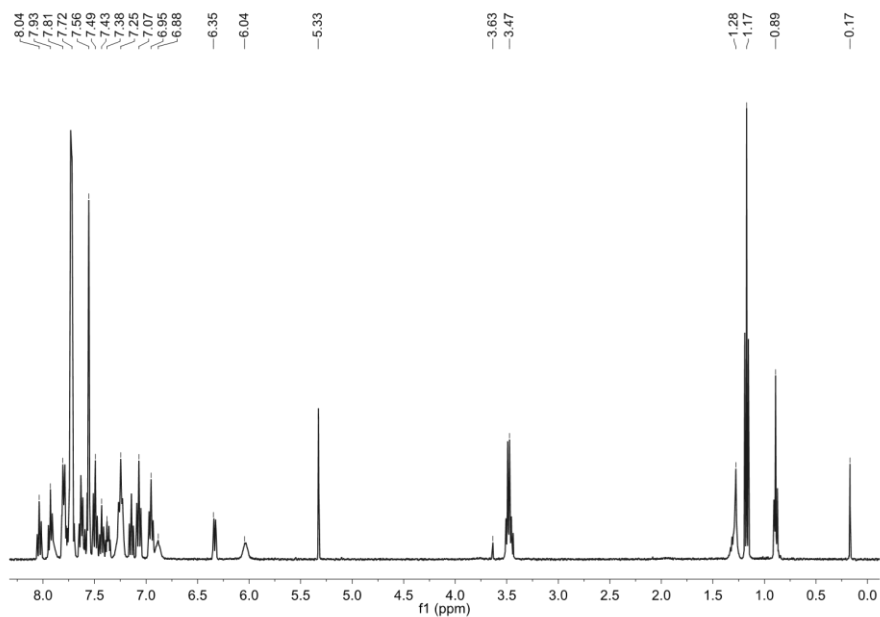


Figure C1. <sup>1</sup>H NMR spectrum of [Ni(Phdpbp)(μ-Cl)]<sub>2</sub>(B(Ar<sup>F</sup>)<sub>4</sub>)<sub>2</sub> (**8**) in CD<sub>2</sub>Cl<sub>2</sub>.

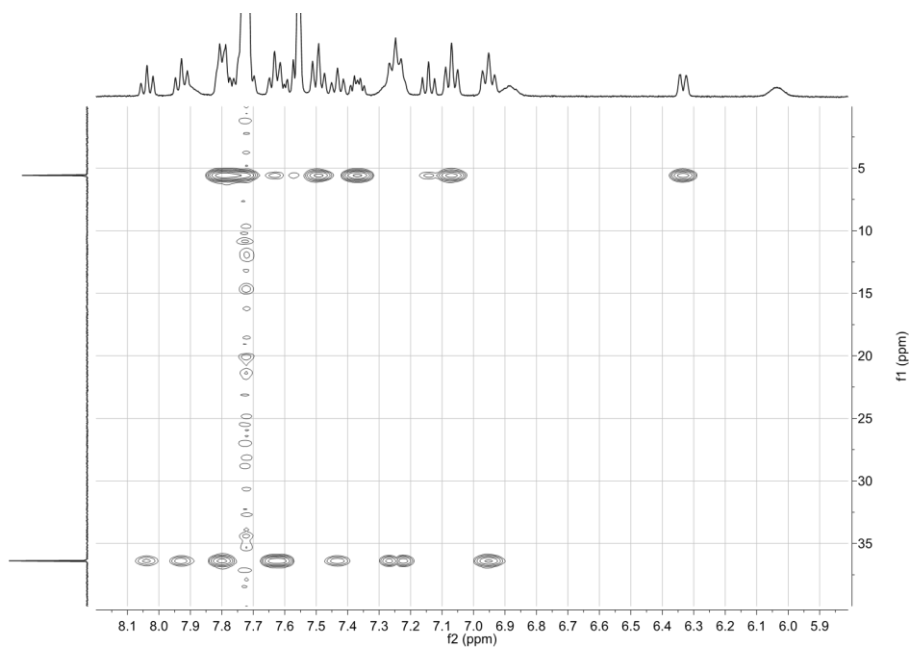


Figure C2. <sup>31</sup>P-<sup>1</sup>H HMBC NMR spectrum of [Ni(Phdpbp)(μ-Cl)]<sub>2</sub>(B(Ar<sup>F</sup>)<sub>4</sub>)<sub>2</sub> (**8**) in CD<sub>2</sub>Cl<sub>2</sub>.

## C3. IR spectra

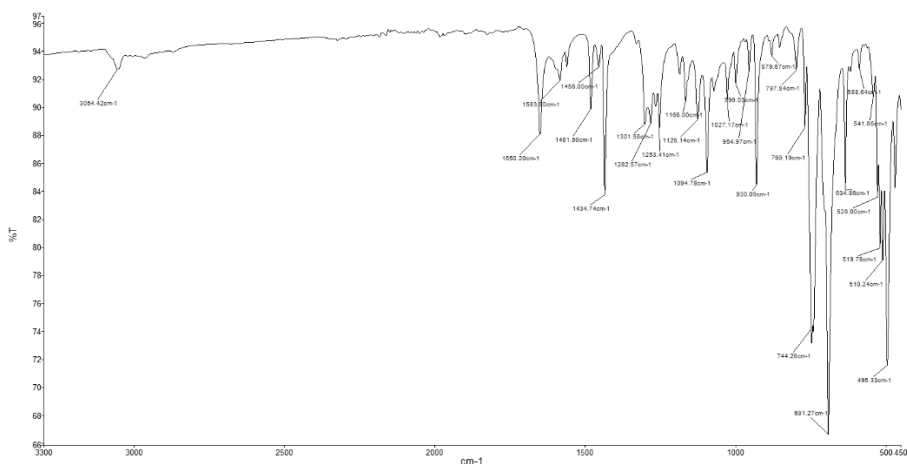


Figure A8. ATR-IR spectrum of  $(\text{Phdbbp})\text{FeCl}_2$  (**2**).

The vibration of the C=O moiety is shifted to a lower frequency, but a smaller signal is still present around the same frequency, i.e.  $1650 \text{ cm}^{-1}$  for **2** and  $1656 \text{ cm}^{-1}$  for **5**. This signal is attributed to either decomposition of the sensitive Fe(I) complex, and so the presence of free ligand or oxidized material, or to overtones of presumably the present aromatic substituents.

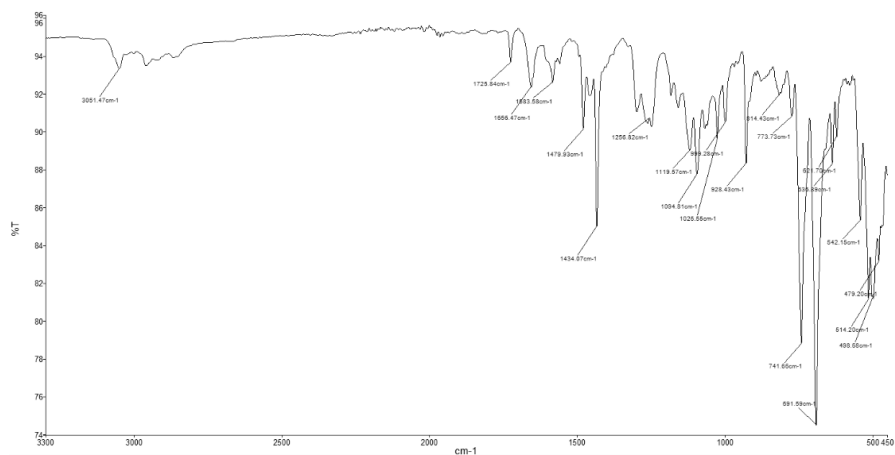


Figure A10. ATR-IR spectrum of  $(\text{Phdbbp})\text{FeCl}$  (**5**).

## C4. DFT computational details

Table A1. Extended version of Table 4.

	<sup>ph</sup> dppb, 1	Fe(I), 5	Co(I), 6	Co(I), 6pTol	Ni(I), 7	Cu(I)
WBI(C–O)	1.78	1.31	1.40	1.40	1.46	1.79
WBI(M–O)	-	0.38	0.31	0.31	0.24	<0.01
WBI(M–C)	-	0.33	0.33	0.33	0.33	<0.01
q(C)	0.56	0.21	0.27	0.27	0.29	0.55
q(O)	-0.52	-0.66	-0.62	-0.63	-0.61	-0.49
q(C+O)	0.04	-0.45	-0.35	-0.36	-0.32	0.06
NSD(M)	-	3.21	2.01	2.06	0.99	-
NSD(CO)	-	-0.34	-0.23	-0.23	-0.14	-
<b>Distances</b>						
C=O DFT	1.214	1.316	1.289	1.289	1.279	1.216
XRD	1.213	1.330	-	1.306	1.310	-
C–M DFT	-	2.178	2.169	2.169	2.109	3.182
XRD	-	2.088	-	2.072	2.006	-
M–O DFT	-	1.943	1.985	1.987	2.039	2.947
XRD	-	1.907	-	1.947	1.974	-
<b>Angles</b>						
P–M–P DFT	-	108.92	112.05	112.20	113.26	120.09
XRD	-	106.35	-	109.62	107.57	-

## C5. EPR analysis

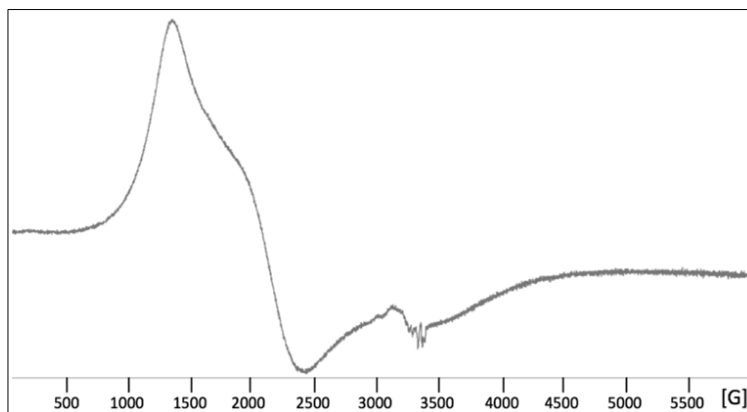


Figure A15. EPR spectrum of  $(^{\text{Ph}}\text{dpbp})\text{FeCl}$  (**5**).

## C6. References

- [A1] A. M. M. Schreurs, X. Xian, L. M. J. Kroon-Batenburg, *J. Appl. Cryst.*, **2010**, *43*, 70–82.
- [A2] G. M. Sheldrick, **2008**, SADABS, Universität Göttingen, Germany.
- [A3] G. M. Sheldrick, *Acta Cryst.*, **2015**, *A71*, 3–8.
- [A4] G. M. Sheldrick, *Acta Cryst.*, **2015**, *C71*, 3–8.
- [A5] A. L. Spek, *Acta Cryst.*, **2009**, *D65*, 148–155.
- [A6] R. Herbst-Irmer, G. M. Sheldrick, *Acta Cryst.*, **1998**, *B54*, 443–449.



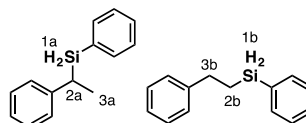
## Appendix D: Additional Experimental Section to Chapter 4

### D1. X-ray crystal structure determination

**2 $\rho$ Tol**: C<sub>41</sub>H<sub>36</sub>Cl<sub>2</sub>CoOP<sub>2</sub> · C<sub>4</sub>H<sub>8</sub>O, Fw = 808.57, green needle, 0.60 × 0.08 × 0.08 mm<sup>3</sup>, orthorhombic, Pbca (no. 61), a = 18.5335(6), b = 17.1819(4), c = 25.6327(9) Å, V = 8162.5(4) Å<sup>3</sup>, Z = 8, D<sub>x</sub> = 1.316 g/cm<sup>3</sup>,  $\mu$  = 0.67 mm<sup>-1</sup>. 90122 Reflections were measured on a Bruker Kappa ApexII diffractometer with sealed tube and Triumph monochromator ( $\lambda$  = 0.71073 Å) at a temperature of 150(2) K up to a resolution of  $(\sin \theta/\lambda)_{\max}$  = 0.65 Å<sup>-1</sup>. The Eval15 software<sup>[A1]</sup> was used for the intensity integration. A numerical absorption correction and scaling was performed with SADABS<sup>[A2]</sup> (correction range 0.78-0.96). 9372 Reflections were unique ( $R_{\text{int}}$  = 0.029), of which 7569 were observed [ $I > 2\sigma(I)$ ]. The structure was solved with Patterson superposition methods using SHELXT.<sup>[A3]</sup> Least-squares refinement was performed with SHELXL-2014<sup>[A4]</sup> against  $F^2$  of all reflections. Non-hydrogen atoms were refined freely with anisotropic displacement parameters. Hydrogen atoms of the metal complex were located in difference Fourier maps. Hydrogen atoms of the THF molecule were introduced in calculated positions. All hydrogen atoms were refined with a riding model. 473 Parameters were refined with no restraints. R1/wR2 [ $I > 2\sigma(I)$ ]: 0.0313 / 0.0836. R1/wR2 [all refl.]: 0.0427 / 0.0906. S = 1.012. Residual electron density between -0.25 and 0.56 e/Å<sup>3</sup>. Geometry calculations and checking for higher symmetry was performed with the PLATON program.<sup>[A5]</sup>

### D2. Analysis of hydrosilylation products

Analysis of styrene hydrosilylation products (Table 3, Entry 1): Hydrosilylation method 2 was used. 0.250 mL of a PhSiH<sub>3</sub>/styrene mixture (0.135 mL, 1.1 mmol/0.115 mL, 1.0 mmol) was used. Upon addition, minor bubbling was observed and a color change from brown to yellow-brown was observed during reaction.



Markovnikov product: <sup>1</sup>H NMR (C<sub>6</sub>D<sub>6</sub>):  $\delta$  7.52-6.98 (m, 12H, Ar-H), 4.45 (t, <sup>3</sup>J<sub>HH</sub> = 3.6 Hz, <sup>2</sup>J<sub>HSi</sub> = 193.1 Hz, 2H, 1a), 2.41 (m, 1H, 2a), 1.33 (d, <sup>3</sup>J<sub>HH</sub> = 7.5, <sup>2</sup>J<sub>HSi</sub> = 127.6, 3H, 3a). <sup>13</sup>C NMR (C<sub>6</sub>D<sub>6</sub>):  $\delta$  144.36-109.98 (Ar-C), 25.26 (CH, 2a), 16.10 (CH<sub>3</sub>, 3a). INEPT <sup>29</sup>Si-NMR (C<sub>6</sub>D<sub>6</sub>):  $\delta$  -21.27 (1a). GC-MS: t: 15.80, m/z: [M]<sup>+</sup> obs. 212.0, calcd. 212.1. anti-Markovnikov product: <sup>1</sup>H NMR (C<sub>6</sub>D<sub>6</sub>):  $\delta$  7.52-6.98 (m, 12H, Ar-H), 4.48 (m, <sup>3</sup>J<sub>HH</sub> = 3.5 Hz, <sup>2</sup>J<sub>HSi</sub> = 195.8 Hz, 2H, 1b), 2.62 (m, <sup>3</sup>J<sub>HH</sub> = 8.4 Hz, 2H, 2b), 1.10 (m, 2H, 3b). <sup>13</sup>C NMR (C<sub>6</sub>D<sub>6</sub>):  $\delta$  144.36-09.98 (Ar-C), 30.98 (CH<sub>2</sub>, 2b), 11.94 (CH<sub>2</sub>, 3b). INEPT <sup>29</sup>Si-NMR (C<sub>6</sub>D<sub>6</sub>):  $\delta$  -31.40 (1b). GC-MS: t: 16.80, m/z: [M-C<sub>6</sub>H<sub>7</sub>]<sup>+</sup> obs. 134.1, calcd. 134.1. GC: Markovnikov product: t: 7.69, 6.1 mg, 0.03 mmol, 3%. Anti-Markovnikov product: t: 7.93, 8.4 mg, 0.04 mmol, 4%. PhSiH<sub>3</sub>: t: 3.61, 89.8 mg, 0.83 mmol, 69%, conv: 31%. Styrene: t: 4.65, 86.7 mg, 0.83 mmol, 83%, conv: 17%. Ph<sub>2</sub>SiH<sub>2</sub>: t: 7.24, 10.1 mg, 0.05 mmol, 5%.

Analysis of allylbenzene hydrosilylation products (Table 3, Entry 3): Hydrosilylation method 2 was used. Amounts: **3 $\rho$ Tol** (14.0 mg, 0.02 mmol), THF (1 mL), 1.9 mL of a PhSiH<sub>3</sub>/allylbenzene mixture (0.961 mL, 7.8 mmol/0.939 mL, 7.1 mmol). Substrate addition caused bubbling and the mixture instantly turned to a clear brown solution. It was stirred further for 72 h. The product was isolated by column chromatography with petroleum ether as eluent. Evaporation of the solvents in vacuum resulted in a

turbid white liquid (1.044 g, 4.61 mmol, 65%).  $^1\text{H}$  NMR ( $\text{C}_6\text{D}_6$ ):  $\delta$  7.48-6.98 (m, 12H, Ar-H), 4.46 (t,  $^3J_{\text{HH}} = 3.7$  Hz,  $^2J_{\text{HSi}} = 191.6$  Hz, 2H), 2.47 (t,  $^3J_{\text{HH}} = 7.6$  Hz,  $^2J_{\text{HSi}} = 126.0$  Hz, 2H), 1.65 (m,  $^2J_{\text{HSi}} = 127.4$ , 2H), 0.77 (m,  $^2J_{\text{HSi}} = 120.5$ , 2H).  $^{13}\text{C}$  NMR ( $\text{C}_6\text{D}_6$ ):  $\delta$  141.84, 135.14, 132.19, 129.45, 128.41, 128.20, 127.93, 125.71, 38.84 ( $\text{CH}_2$ ), 26.92 ( $\text{CH}_2$ ), 9.56 ( $\text{CH}_2$ ). INEPT  $^{29}\text{Si}$ -NMR ( $\text{C}_6\text{D}_6$ ):  $\delta$  -31.10. *Catalytic experiments:* Amounts: 0.267 mL of a  $\text{PhSiH}_3$ /allylbenzene mixture (0.135 mL, 1.1 mmol/0.132 mL, 1.0 mmol). Upon addition, minor bubbling was observed and a color change from brown to yellow-brown was observed during reaction. GC-MS: phenyl(1-phenylethyl)silane: t: 17.99, m/z:  $[\text{M}-\text{C}_6\text{H}_6]^+$  obs 148.1, calcd. 148.1.  $\text{PhSiH}_3$ : t: 3.48, m/z:  $[\text{M}]^+$  obs. 108.0, calcd. 108.0. Styrene: t: 8.01, m/z:  $[\text{M}]^+$  obs. 118.1, calcd. 118.1.  $\text{Ph}_2\text{SiH}_2$ : t: 14.08, m/z:  $[\text{M}]^+$  obs. 184.1, calcd. 184.1. GC: phenyl(1-phenylethyl)silane: t: 8.18, 190.5 mg, 0.84 mmol, 84%.  $\text{PhSiH}_3$ : t: 3.60, 3.4 mg, 0.03 mmol, 3%, conv: 97%. Allylbenzene: t: 5.57, 4.8 mg, 0.04 mmol, 4%, conv: 96%.  $\text{Ph}_2\text{SiH}_2$ : t: 7.24, 7.5 mg, 0.04 mmol, 4%.

### D3. NMR spectra

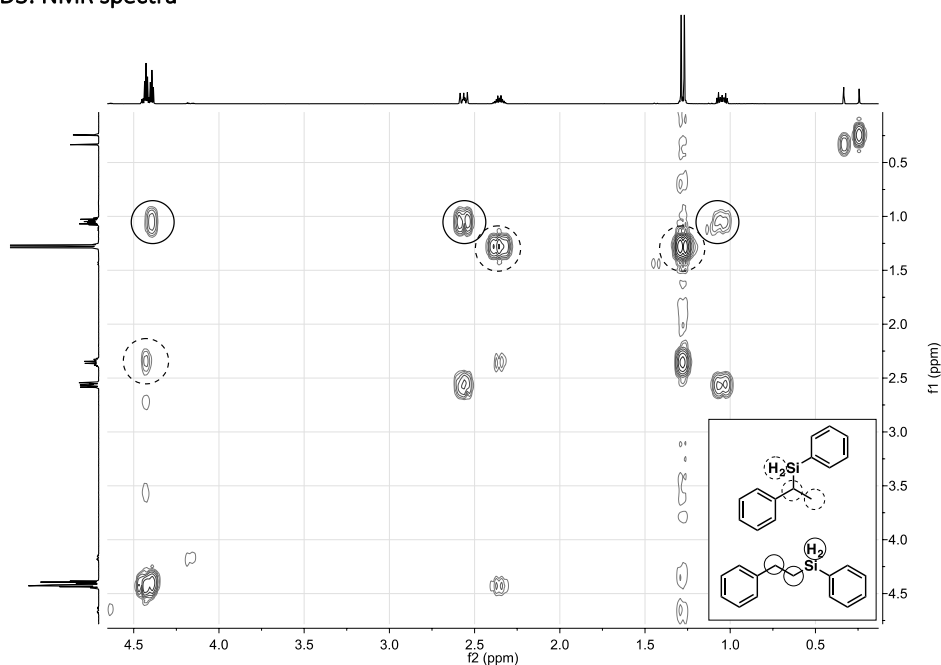
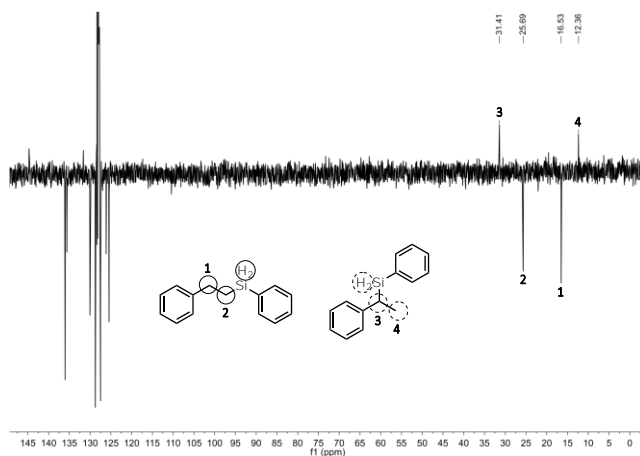
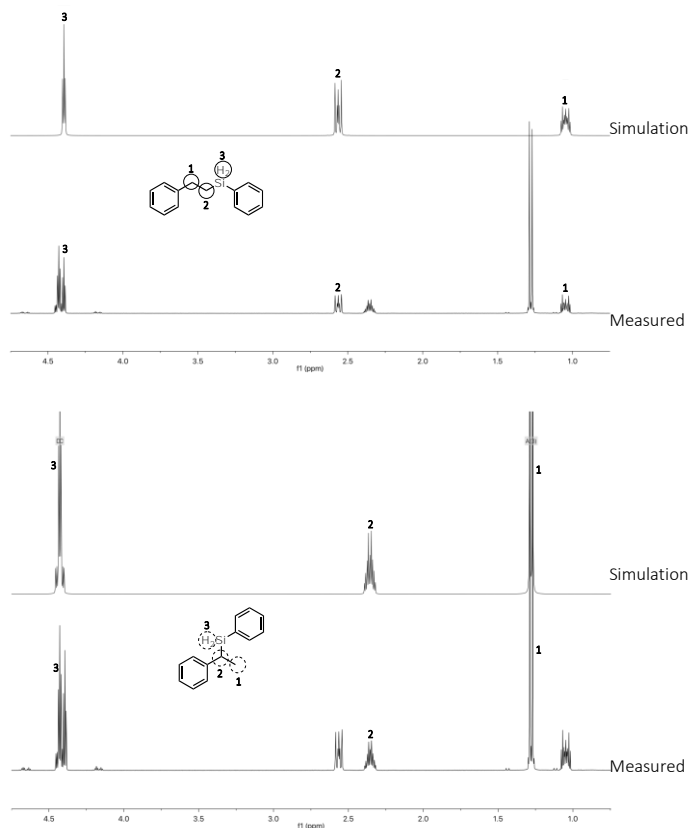


Figure D1. 2D  $^1\text{H}$ - $^1\text{H}$  COSY NMR spectrum of the styrene hydrosilylation reaction.



**Figure D2.** APT  $^{13}\text{C}$  NMR ( $\text{C}_6\text{D}_6$ ) spectrum of styrene hydrosilylation (pos. phase: CH,  $\text{CH}_3$ ; neg. phase: Cq,  $\text{CH}_2$ ).



**Figure D3.** Product mixture of styrene hydrosilylation with  $\text{PhSiH}_3$ . Simulated spectrum by Mestrenova (upper) and measured  $^1\text{H}$  NMR spectrum (in  $\text{C}_6\text{D}_6$ , lower).

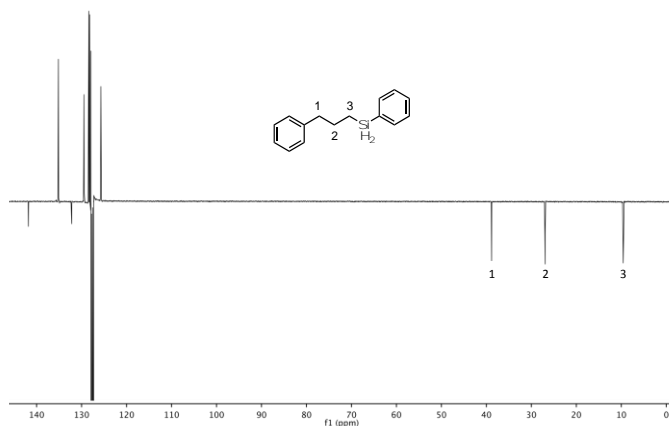


**Figure D4.** APT  $^{13}\text{C}$  NMR spectrum ( $\text{C}_6\text{D}_6$ ) of the hydrosilylation product of allylbenzene (positive phase: CH,  $\text{CH}_3$ ; negative phase:  $\text{C}_q$ ,  $\text{CH}_2$ ).

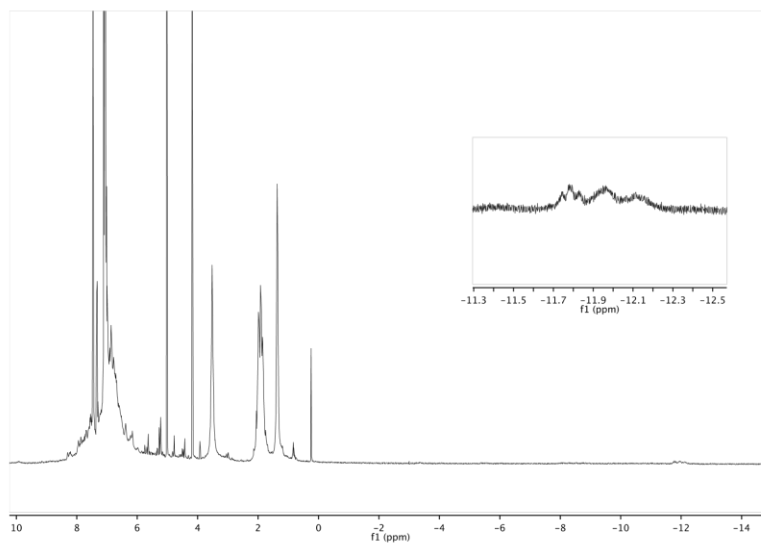


**Figure D5.**  $^1\text{H}$  NMR spectrum ( $\text{C}_6\text{D}_6$ ) of the reaction mixture of 3pTol +  $\text{PhSiH}_3$ , silane activation.

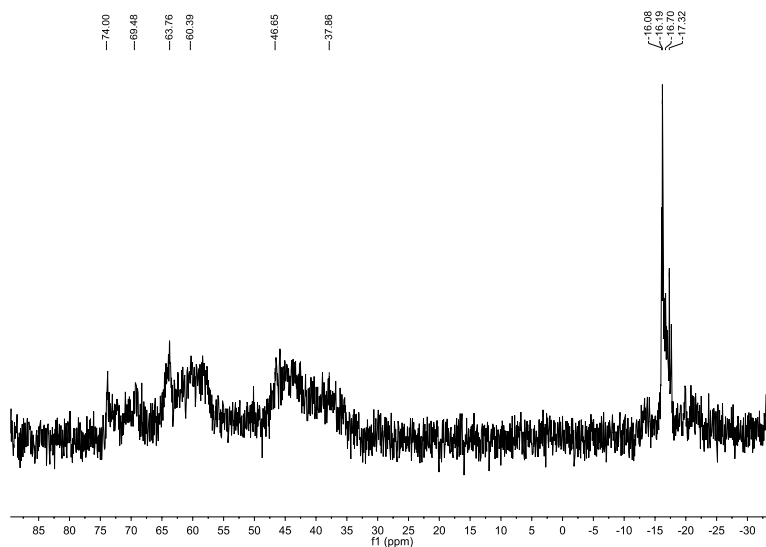


Figure D6.  $^{31}\text{P}$  NMR spectrum ( $\text{C}_6\text{D}_6$ ) of the reaction mixture of  $3\text{P}^{\text{Tot}}$  +  $\text{PhSiH}_3$ , silane activation.

#### D4. References

- [A1] A. M. M. Schreurs, X. Xian, L. M. J. Kroon-Batenburg, *J. Appl. Cryst.*, **2010**, *43*, 70–82.
- [A2] G. M. Sheldrick, SADABS., **2014**, Universität Göttingen, Germany.
- [A3] G. M. Sheldrick, *Acta Cryst.*, **2015**, *A71*, 3–8.
- [A4] G. M. Sheldrick, *Acta Cryst.*, **2015**, *C71*, 3–8.
- [A5] A. L. Spek, *Acta Cryst.*, **2009**, *D65*, 148–155.



## Appendix E: Additional Experimental Section to Chapter 5

### E1. X-ray crystal structure determination

**2:**  $C_{37}H_{29}Cl_2NNiP_2 \cdot 3CH_2Cl_2$ , Fw = 933.94, black plate,  $0.34 \times 0.15 \times 0.04 \text{ mm}^3$ , triclinic,  $P \bar{1}$  (no. 2),  $a = 12.2516(4)$ ,  $b = 12.8555(3)$ ,  $c = 15.4966(5) \text{ \AA}$ ,  $\alpha = 80.183(1)$ ,  $\beta = 72.387(1)$ ,  $\gamma = 62.522(2)^\circ$ ,  $V = 2062.49(11) \text{ \AA}^3$ ,  $Z = 2$ ,  $D_x = 1.504 \text{ g/cm}^3$ ,  $\mu = 1.10 \text{ mm}^{-1}$ . 54078 Reflections were measured on a Bruker Kappa ApexII diffractometer with sealed tube and Triumph monochromator ( $\lambda = 0.71073 \text{ \AA}$ ) at a temperature of  $150(2) \text{ K}$  up to a resolution of  $(\sin \theta/\lambda)_{\max} = 0.65 \text{ \AA}^{-1}$ . The Eval15 software<sup>[A1]</sup> was used for the intensity integration. A multiscan absorption correction and scaling was performed with SADABS<sup>[A2]</sup> (correction range 0.65-0.75). 9468 Reflections were unique ( $R_{\text{int}} = 0.031$ ), of which 7952 were observed [ $I > 2\sigma(I)$ ]. The structure was solved with Patterson superposition methods using SHELXT.<sup>[A3]</sup> Least-squares refinement was performed with SHELXL-2014<sup>[A4]</sup> against  $F^2$  of all reflections. Non-hydrogen atoms were refined freely with anisotropic displacement parameters. Hydrogen atoms were introduced in calculated positions and refined with a riding model. The phosphine ligand is disordered about the imine bond and was refined with two orientations in a ratio of 0.550(6):0.450(6). The coordinated P atoms of the two disorder components were constrained to the same positions. Additional disorder was found in the co-crystallized dichloromethane molecules. 611 Parameters were refined with 480 restraints (distances, angles and displacement parameters of the disordered moieties).  $R1/wR2$  [ $I > 2\sigma(I)$ ]: 0.0368 / 0.0984.  $R1/wR2$  [all refl.]: 0.0472 / 0.1040.  $S = 1.058$ . Residual electron density between  $-0.84$  and  $0.82 \text{ e/\AA}^3$ . Geometry calculations and checking for higher symmetry was performed with the PLATON program.<sup>[A5]</sup>

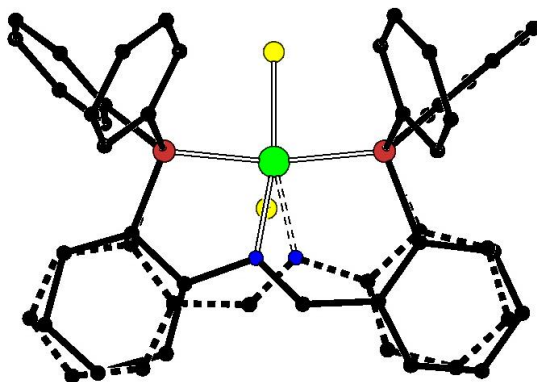


**Figure E1.** Molecular plot of **2** (hydrogen atoms and solvent molecule omitted for clarity). The solid lines show the major component (55%) and the dashed lines the minor component (45%).

**3:**  $C_{55}H_{44}NNiP_3$ , Fw = 870.53, dark red needle,  $0.60 \times 0.03 \times 0.01 \text{ mm}^3$ , triclinic,  $P \bar{1}$  (no. 2),  $a = 12.5025(3)$ ,  $b = 13.9043(4)$ ,  $c = 13.9949(4) \text{ \AA}$ ,  $\alpha = 98.045(2)$ ,  $\beta = 98.593(2)$ ,  $\gamma = 114.259(2)^\circ$ ,  $V = 2137.73(11) \text{ \AA}^3$ ,  $Z = 2$ ,  $D_x = 1.352 \text{ g/cm}^3$ ,  $\mu = 2.02 \text{ mm}^{-1}$ . 42061 Reflections were measured on a Bruker Proteum diffractometer with rotating anode and Helios optics ( $\lambda = 1.54184 \text{ \AA}$ ) at a temperature of  $100(2) \text{ K}$  up to a resolution of  $(\sin \theta/\lambda)_{\max} = 0.57 \text{ \AA}^{-1}$ . The crystal appeared to be broken in two

fragments. Consequently two orientation matrices were used for the integration with the Eval15 software<sup>[A1]</sup> and the reflection data were stored in the HKLF5 format.<sup>[A6]</sup> A multiscan absorption correction and scaling was performed with TWINABS<sup>[A2]</sup> (correction range 0.18-0.46). 6448 Reflections were unique ( $R_{\text{int}} = 0.082$ ), of which 5298 were observed [ $I > 2\sigma(I)$ ]. The structure was solved with Patterson superposition methods using SHELXT.<sup>[A3]</sup> Least-squares refinement was performed with SHELXL-2014<sup>[A4]</sup> against  $F^2$  of all reflections. Non-hydrogen atoms were refined freely with anisotropic displacement parameters. Hydrogen atoms were introduced in calculated positions and refined with a riding model. 542 Parameters were refined with no restraints.  $R1/wR2$  [ $I > 2\sigma(I)$ ]: 0.0594 / 0.1552.  $R1/wR2$  [all refl.]: 0.0721 / 0.1657.  $S = 1.053$ . Batch scale factor BASF = 0.157(6). Residual electron density between -0.79 and 0.74  $e/\text{\AA}^3$ . Geometry calculations and checking for higher symmetry was performed with the PLATON program.<sup>[A5]</sup>

**6:**  $\text{C}_{57}\text{H}_{48}\text{NNiP}_3$ , Fw = 898.58, red needle,  $0.31 \times 0.14 \times 0.04 \text{ mm}^3$ , triclinic,  $\overline{P}1$  (no. 2),  $a = 10.8851(9)$ ,  $b = 11.4437(8)$ ,  $c = 19.2429(13) \text{ \AA}$ ,  $\alpha = 98.018(3)$ ,  $\beta = 94.691(6)$ ,  $\gamma = 108.280(4)^\circ$ ,  $V = 2233.6(3) \text{ \AA}^3$ ,  $Z = 2$ ,  $D_x = 1.336 \text{ g/cm}^3$ ,  $\mu = 0.58 \text{ mm}^{-1}$ . 61890 Reflections were measured on a Bruker Kappa CCD diffractometer with sealed tube and graphite monochromator ( $\lambda = 0.71073 \text{ \AA}$ ) at a temperature of 105(2) K up to a resolution of  $(\sin \theta/\lambda)_{\text{max}} = 0.65 \text{ \AA}^{-1}$ . The crystal appeared to be broken in two fragments. Consequently two orientation matrices were used for the integration with the Eval15 software<sup>[A1]</sup> and the reflection data were stored in the HKLF5 format.<sup>[A6]</sup> A multiscan absorption correction and scaling was performed with TWINABS<sup>[A2]</sup> (correction range 0.50-0.75). 10227 Reflections were unique ( $R_{\text{int}} = 0.078$ ), of which 7310 were observed [ $I > 2\sigma(I)$ ]. The structure was solved with Patterson superposition methods using SHELXT.<sup>[A3]</sup> Least-squares refinement was performed with SHELXL-2016<sup>[A4]</sup> against  $F^2$  of all reflections. Non-hydrogen atoms were refined freely with anisotropic displacement parameters. All hydrogen atoms were located in difference Fourier maps. The hydrogen atom at the coordinated carbon C1 was refined freely with an isotropic displacement parameter. All other hydrogen atoms were refined with a riding model. 566 Parameters were refined with no restraints.  $R1/wR2$  [ $I > 2\sigma(I)$ ]: 0.0507 / 0.1183.  $R1/wR2$  [all refl.]: 0.0860 / 0.1338.  $S = 1.027$ . Batch scale factor BASF = 0.1422(18). Residual electron density between -0.62 and 1.35  $e/\text{\AA}^3$ . Geometry calculations and checking for higher symmetry was performed with the PLATON program.<sup>[A5]</sup>

**7:**  $\text{C}_{59}\text{H}_{52}\text{NNiP}_3 \cdot \text{C}_4\text{H}_8\text{O}$ , Fw = 998.74, red-brown needle,  $0.22 \times 0.04 \times 0.04 \text{ mm}^3$ , monoclinic,  $P2_1/n$  (no. 14),  $a = 9.9759(4)$ ,  $b = 26.7743(10)$ ,  $c = 19.9847(7) \text{ \AA}$ ,  $\beta = 103.5431(18)^\circ$ ,  $V = 5189.4(3) \text{ \AA}^3$ ,  $Z = 4$ ,  $D_x = 1.278 \text{ g/cm}^3$ ,  $\mu = 1.74 \text{ mm}^{-1}$ . 28764 Reflections were measured on a Bruker Proteum diffractometer with rotating anode and Helios optics ( $\lambda = 1.54184 \text{ \AA}$ ) at a temperature of 100(2) K up to a resolution of  $(\sin \theta/\lambda)_{\text{max}} = 0.50 \text{ \AA}^{-1}$ . The Saint software<sup>[A7]</sup> was used for the intensity integration. A numerical absorption correction and scaling was performed with SADABS<sup>[A2]</sup> (correction range 0.70-0.97). 5424 Reflections were unique ( $R_{\text{int}} = 0.066$ ), of which 4188 were observed [ $I > 2\sigma(I)$ ]. The structure was solved with Patterson superposition methods using SHELXT.<sup>[A3]</sup> Least-squares refinement was performed with SHELXL-2016<sup>[A4]</sup> against  $F^2$  of all reflections. Non-hydrogen atoms were refined freely with anisotropic displacement parameters. Hydrogen atoms were introduced in calculated positions and refined with a riding model. The co-crystallized THF molecule was refined with a disorder model. 672 Parameters were refined with 153 restraints (distances, angles and displacement parameters of the disordered THF).  $R1/wR2$  [ $I > 2\sigma(I)$ ]: 0.0423 / 0.0955.  $R1/wR2$  [all refl.]: 0.0634 / 0.1047.  $S = 1.035$ . Residual



electron density between  $-0.37$  and  $0.36$  e/Å<sup>3</sup>. Geometry calculations and checking for higher symmetry was performed with the PLATON program.<sup>[A5]</sup>

**8:** C<sub>74</sub>H<sub>58</sub>N<sub>2</sub>Ni<sub>2</sub>P<sub>4</sub> + disordered solvent, Fw = 1216.52<sup>[\*]</sup>, black needle, 0.23 × 0.12 × 0.06 mm<sup>3</sup>, triclinic,  $\overline{P1}$  (no. 2), a = 13.2569(9), b = 15.5399(12), c = 19.8458(17) Å,  $\alpha$  = 102.640(3),  $\beta$  = 91.222(3),  $\gamma$  = 113.875(4) °, V = 3620.2(5) Å<sup>3</sup>, Z = 2, D<sub>x</sub> = 1.116 g/cm<sup>3</sup><sup>[\*]</sup>,  $\mu$  = 0.65 mm<sup>-1</sup><sup>[\*]</sup>. 54076 Reflections were measured on a Bruker Kappa ApexII diffractometer with sealed tube and Triumph monochromator ( $\lambda$  = 0.71073 Å) at a temperature of 100(2) K up to a resolution of  $(\sin \theta/\lambda)_{\max}$  = 0.61 Å<sup>-1</sup>. The Eval15 software<sup>[A1]</sup> was used for the intensity integration. A multiscan absorption correction and scaling was performed with SADABS<sup>[A2]</sup> (correction range 0.66-0.75). 13475 Reflections were unique (R<sub>int</sub> = 0.093), of which 7947 were observed [ $I > 2\sigma(I)$ ]. The structure was solved with Patterson superposition methods using SHELXT.<sup>[A3]</sup> Least-squares refinement was performed with SHELXL-2014<sup>[A4]</sup> against F<sup>2</sup> of all reflections. The crystal structure contains large voids (1027 Å<sup>3</sup> / unit cell) filled with severely disordered THF solvent molecules. Their contribution to the structure factors was secured by back-Fourier transformation using the SQUEEZE algorithm<sup>[A8]</sup> resulting in 255 electrons / unit cell. Non-hydrogen atoms were refined freely with anisotropic displacement parameters. Hydrogen atoms at the coordinated carbon atoms C1 and C2 were located in difference Fourier maps and refined freely with isotropic displacement parameters. All other hydrogen atoms were introduced in calculated positions and refined with a riding model. 747 Parameters were refined with no restraints. R1/wR2 [ $I > 2\sigma(I)$ ]: 0.0636 / 0.1476. R1/wR2 [all refl.]: 0.1208 / 0.1679. S = 1.032. Residual electron density between  $-0.89$  and  $0.93$  e/Å<sup>3</sup>. Geometry calculations and checking for higher symmetry was performed with the PLATON program.<sup>[A5]</sup> [\*] Derived values do not contain the contribution of the disordered solvent.

**9:** C<sub>76</sub>H<sub>58</sub>N<sub>2</sub>Ni<sub>2</sub>O<sub>2</sub>P<sub>4</sub> · 1.4C<sub>6</sub>H<sub>6</sub> · 0.6C<sub>6</sub>H<sub>14</sub>, Fw = 1433.59, brown needle, 0.35 × 0.07 × 0.01 mm<sup>3</sup>, triclinic,  $\overline{P1}$  (no. 2), a = 10.8492(3), b = 15.2864(6), c = 22.9277(10) Å,  $\alpha$  = 82.943(2),  $\beta$  = 84.132(2),  $\gamma$  = 76.060(2) °, V = 3652.1(3) Å<sup>3</sup>, Z = 2, D<sub>x</sub> = 1.304 g/cm<sup>3</sup>,  $\mu$  = 0.65 mm<sup>-1</sup>. 72208 Reflections were measured on a Bruker Kappa ApexII diffractometer with sealed tube and Triumph monochromator ( $\lambda$  = 0.71073 Å) at a temperature of 150(2) K up to a resolution of  $(\sin \theta/\lambda)_{\max}$  = 0.65 Å<sup>-1</sup>. The Eval15 software<sup>[A1]</sup> was used for the intensity integration. A numerical absorption correction and scaling was performed with SADABS<sup>[A2]</sup> (correction range 0.75-1.00). 16775 Reflections were unique (R<sub>int</sub> = 0.086), of which 10300 were observed [ $I > 2\sigma(I)$ ]. The structure was solved with Patterson superposition methods using SHELXT.<sup>[A3]</sup> Least-squares refinement was performed with SHELXL-2016<sup>[A4]</sup> against F<sup>2</sup> of all reflections. Non-hydrogen atoms were refined freely with anisotropic displacement parameters. Hydrogen atoms were introduced in calculated positions and refined with a riding model. The structure contains a solvent site which is fully occupied by a benzene molecule. A second solvent site is occupied by a mixture of benzene and *n*-hexane. 937 Parameters were refined with 289 restraints (distances, angles, molecular flatness and displacement parameters of the solvent molecules). R1/wR2 [ $I > 2\sigma(I)$ ]: 0.0553 / 0.1186. R1/wR2 [all refl.]: 0.1130 / 0.1407. S = 1.029. Residual electron density between  $-0.44$  and  $0.66$  e/Å<sup>3</sup>. Geometry calculations and checking for higher symmetry was performed with the PLATON program.<sup>[A5]</sup>

## E2. NMR spectra

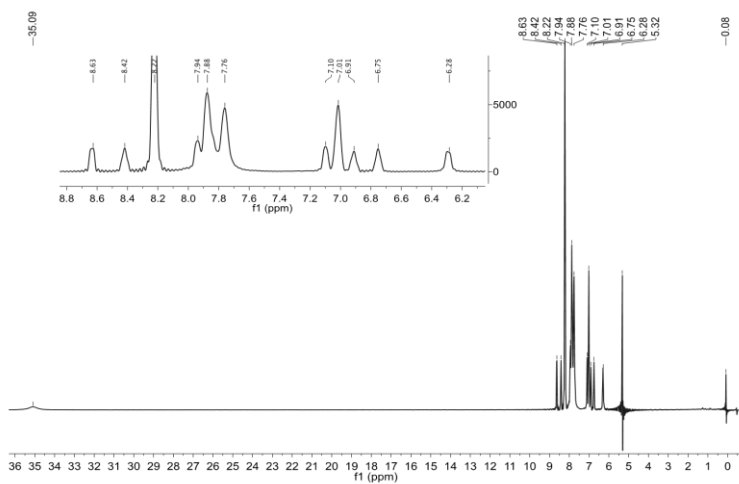


Figure E2.  $^1\text{H}$  NMR spectrum ( $\text{CD}_2\text{Cl}_2$ ) of  $\text{Ni}(\text{P}^{\text{Ph}}\text{CNP}^{\text{Ph}})\text{Cl}_2$  (2) at  $25^\circ\text{C}$

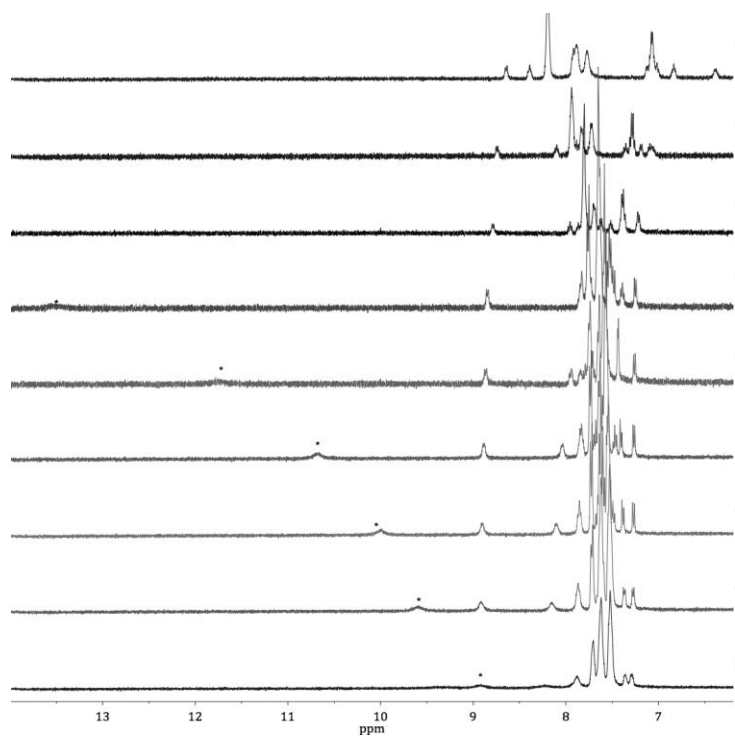
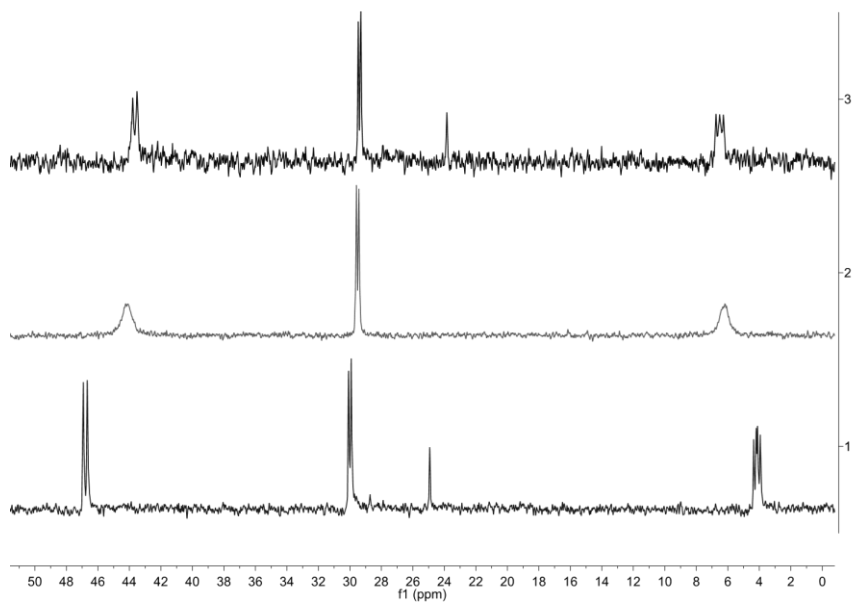
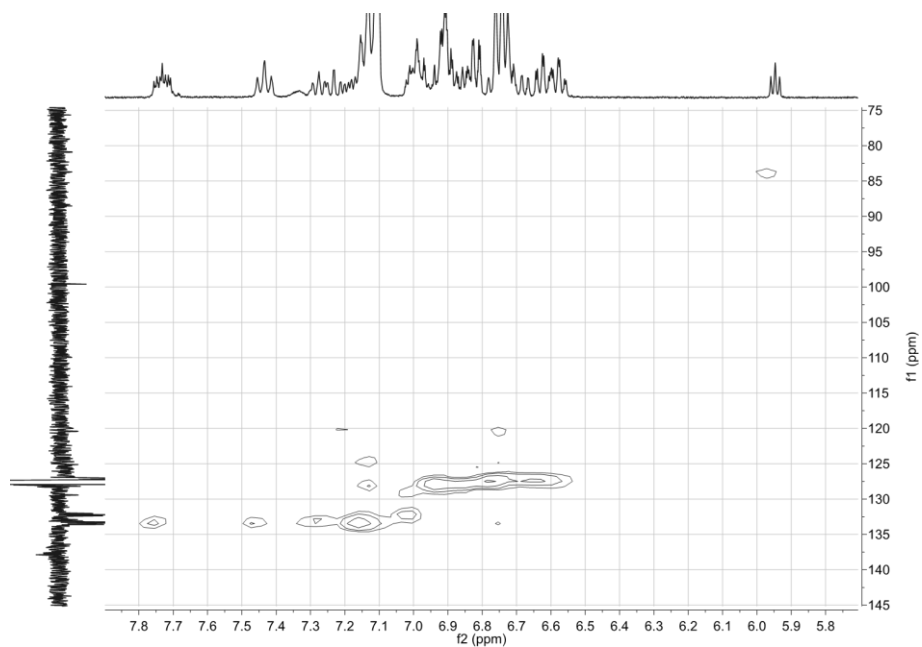


Figure E3. VT  $^1\text{H}$  NMR spectrum ( $\text{CD}_2\text{Cl}_2$ ) of  $\text{Ni}(\text{P}^{\text{Ph}}\text{CNP}^{\text{Ph}})\text{Cl}_2$  (2). Temperatures in  $^\circ\text{C}$  from top to bottom (9 to 1): 10, 0,  $-20$ ,  $-30$ ,  $-40$ ,  $-60$ ,  $-70$ ,  $-80$ .



**Figure E4.**  $^{31}\text{P}$  NMR spectrum of  $\text{Ni}(\text{P}^{\text{Ph}}\text{CN}^{\text{Ph}})(\text{PPh}_3)$  (**3**). Spectrum 1 (bottom):  $-50\text{ }^\circ\text{C}$  ( $\text{C}_7\text{D}_8$ ), 2 (middle):  $25\text{ }^\circ\text{C}$  ( $\text{C}_6\text{D}_6$ ), 3 (top):  $50\text{ }^\circ\text{C}$  ( $\text{C}_7\text{D}_8$ ). Signal at  $\delta = 25$  ppm is an unidentified impurity.



**Figure E5.**  $^1\text{H}$ - $^{13}\text{C}$  ASAPHMQC NMR spectrum ( $\text{C}_6\text{D}_6$ ) of  $\text{Ni}(\text{P}^{\text{Ph}}\text{CN}^{\text{Ph}})(\text{PPh}_3)$  (**3**).

NMR spectra taken from **8** are always from the mixture of **8a** and **8b** because further isolation was unsuccessful.

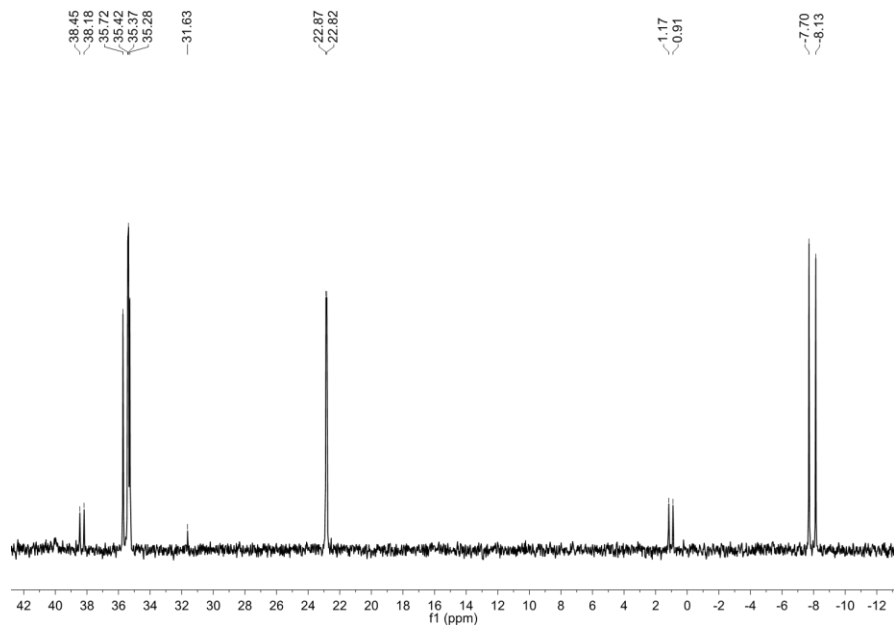


Figure E6.  $^{31}\text{P}$  NMR spectrum ( $\text{C}_6\text{D}_6$ ) of  $[\text{Ni}(\text{P}^{\text{Ph}}\text{CNP}^{\text{Ph}})]_{2n}$  (**8a+8b**). Signal at  $\delta$  -31 ppm is an unknown impurity.

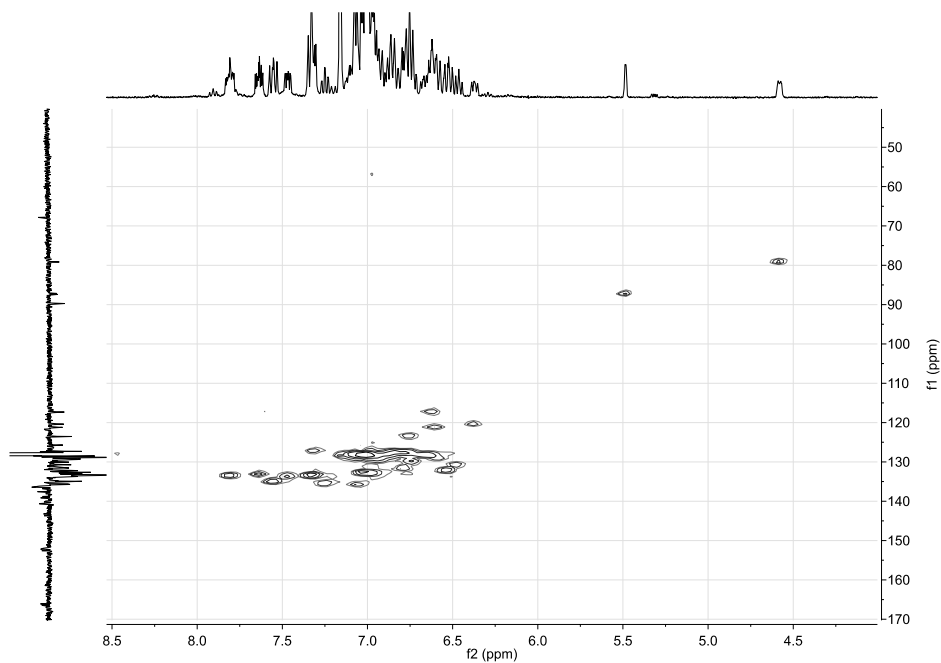


Figure E7.  $^1\text{H}$ - $^{13}\text{C}$  ASAPHMQC 2D NMR spectrum ( $\text{C}_6\text{D}_6$ ) of  $[\text{Ni}(\text{P}^{\text{Ph}}\text{CNP}^{\text{Ph}})]_2$  (**8a+8b**).

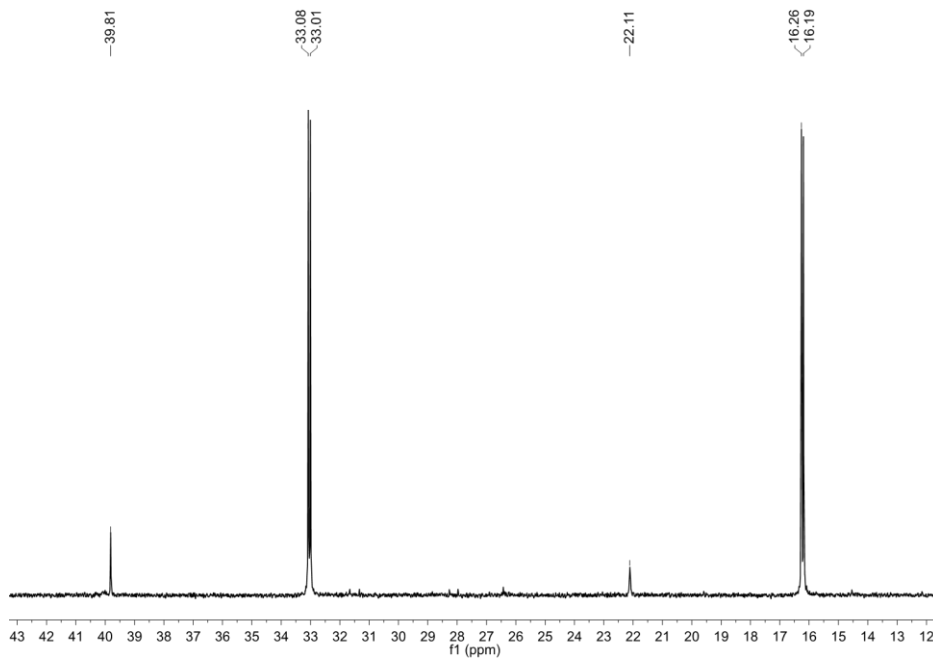


Figure E8.  $^{31}\text{P}$  NMR spectrum ( $\text{C}_6\text{D}_6$ ) of **9a** and **9b** before work-up. Spectrum measured in  $\text{C}_6\text{D}_6$  under a CO atmosphere (1 atm).

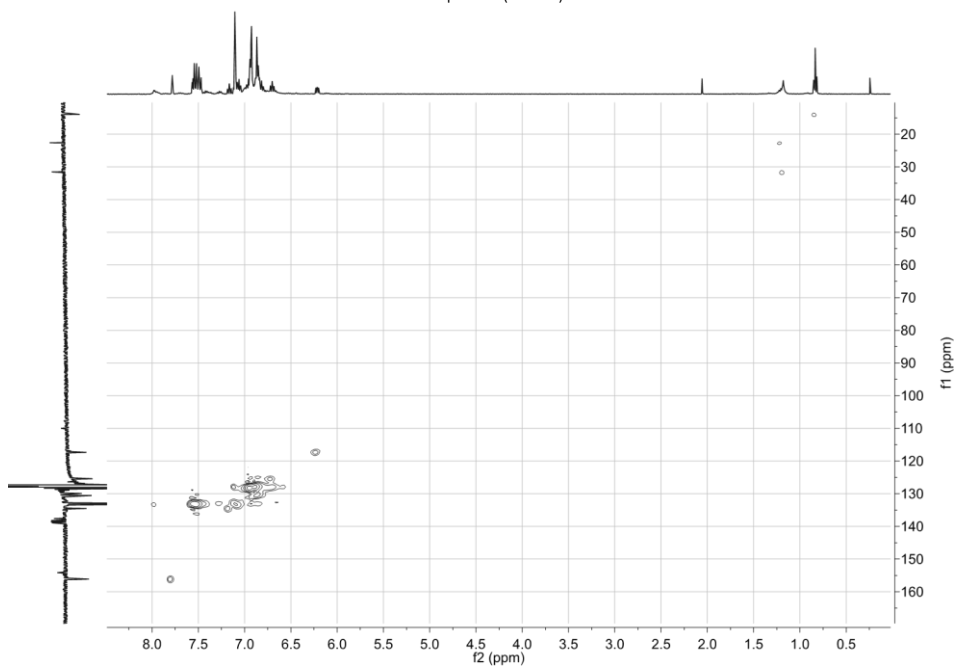


Figure E9. HMQC  $^1\text{H}$ - $^{13}\text{C}$  2D NMR spectrum ( $\text{C}_6\text{D}_6$ ) of **9a**.

### E3. References

- [A1] A. M. M. Schreurs, X. Xian, L. M. J. Kroon-Batenburg, *J. Appl. Cryst.*, **2010**, *43*, 70–82.
- [A2] G. M. Sheldrick, SADABS and TWINABS, **2014**, Universität Göttingen, Germany.
- [A3] G. M. Sheldrick. *Acta Cryst.*, **2015**, *A71*, 3–8.
- [A4] G. M. Sheldrick. *Acta Cryst.*, **2015**, *C71*, 3–8.
- [A5] A. L. Spek, *Acta Cryst.*, **2009**, *D65*, 148–155.
- [A6] R. Herbst-Irmer, G. M. Sheldrick, *Acta Cryst.*, **1998**, *B54*, 443–449.
- [A7] Bruker, **2001**, SAINT-Plus. Bruker AXS Inc., Madison, Wisconsin, USA.
- [A8] A. L. Spek. *Acta Cryst.*, **2015**, *C71*, 9–18.

## Appendix F: Additional Experimental Section to Chapter 6

### F1. X-ray crystal structure determination

**3[Si]:**  $C_{69}H_{60}NNiP_3Si \cdot 0.5C_6H_6$ , Fw = 1121.94, red block,  $0.30 \times 0.24 \times 0.24$  mm<sup>3</sup>, triclinic,  $\overline{P1}$  (no. 2), a = 9.3430(6), b = 12.4727(6), c = 27.2186(14) Å,  $\alpha = 89.538(3)$ ,  $\beta = 81.608(3)$ ,  $\gamma = 68.083(4)^\circ$ , V = 2907.4(3) Å<sup>3</sup>, Z = 2, D<sub>x</sub> = 1.282 g/cm<sup>3</sup>,  $\mu = 0.48$  mm<sup>-1</sup>. 198636 Reflections were measured on a Bruker Kappa CCD diffractometer with sealed tube and graphite monochromator ( $\lambda = 0.71073$  Å) at a temperature of 150(2) K up to a resolution of  $(\sin \theta/\lambda)_{\max} = 0.66$  Å<sup>-1</sup>. The crystal appeared to be broken in several fragments. Five orientation matrices for the major fragments were used for the integration with the Eval15 software<sup>[A1]</sup> and the reflection data were stored in the HKLF5 format.<sup>[A2]</sup> A multiscan absorption correction and scaling was performed with TWINABS<sup>[A3]</sup> (correction range 0.63-0.75). 14521 Reflections were unique ( $R_{\text{int}} = 0.071$ ), of which 10751 were observed [ $I > 2\sigma(I)$ ]. The structure was solved with Patterson superposition methods using SHELXT.<sup>[A4]</sup> Least-squares refinement was performed with SHELXL-2016<sup>[A5]</sup> against  $F^2$  of all reflections. Non-hydrogen atoms were refined freely with anisotropic displacement parameters. The assignment of P versus Si could not be based on the electron density but was taken from the chemical knowledge. Hydrogen atom H2 was refined with distance restraints of 1.66(1) Å to Si2 and 1.49(1) to Ni1. All other hydrogen atoms were included in calculated positions and refined with a riding model. 712 Parameters were refined with 2 restraints (distances of H2). R1/wR2 [ $I > 2\sigma(I)$ ]: 0.0656 / 0.1821. R1/wR2 [all refl.]: 0.0926 / 0.1948. S = 1.112. Batch scale factors BASF = 0.2760(19), 0.195(3), 0.1717(19) and 0.0444(18). Residual electron density between -0.44 and 0.77 e/Å<sup>3</sup>. Geometry calculations and checking for higher symmetry was performed with the PLATON program.<sup>[A6]</sup>

**4[Si]:**  $C_{71}H_{64}NNiP_3Si$  + disordered solvent, Fw = 1110.94<sup>[\*]</sup>, red block,  $0.15 \times 0.07 \times 0.05$  mm<sup>3</sup>, triclinic,  $\overline{P1}$  (no. 2), a = 13.0477(9), b = 13.9732(9), c = 16.6323(10) Å,  $\alpha = 91.756(3)$ ,  $\beta = 93.847(2)$ ,  $\gamma = 90.943(2)^\circ$ , V = 3023.6(3) Å<sup>3</sup>, Z = 2, D<sub>x</sub> = 1.220 g/cm<sup>3</sup><sup>[\*]</sup>,  $\mu = 0.46$  mm<sup>-1</sup><sup>[\*]</sup>. 30962 Reflections were measured on a Bruker Kappa ApexII diffractometer with sealed tube and Triumph monochromator ( $\lambda = 0.71073$  Å) at a temperature of 150(2) K up to a resolution of  $(\sin \theta/\lambda)_{\max} = 0.50$  Å<sup>-1</sup>. The Eval15 software<sup>[A1]</sup> was used for the intensity integration. A multiscan absorption correction and scaling was performed with SADABS<sup>[A3]</sup> (correction range 0.65-0.75). 6313 Reflections were unique ( $R_{\text{int}} = 0.117$ ), of which 3778 were observed [ $I > 2\sigma(I)$ ]. The structure was solved with Patterson superposition methods using SHELXT.<sup>[A4]</sup> Least-squares refinement was performed with SHELXL-2016<sup>[A5]</sup> against  $F^2$  of all reflections. The crystal structure contains large voids (200 Å<sup>3</sup> / unit cell) filled with severely disordered solvent molecules. Their contribution to the structure factors was secured by back-Fourier transformation using the SQUEEZE algorithm<sup>[A7]</sup> resulting in 40 electrons / unit cell. Non-hydrogen atoms were refined freely with anisotropic displacement parameters. The assignment of P versus Si could not be based on the electron density but was taken from the chemical knowledge. One of the P-tolyl groups was refined with a disorder model. Hydrogen atom H2 was refined with distance restraints of 1.66(1) Å to Si2 and 1.49(1) to Ni1. All other hydrogen atoms were included in calculated positions and refined with a riding model. 766 Parameters were refined with 852 restraints (distance restraints for H2 and for the disordered groups, angle restraints for the disordered groups, and restrained displacement parameters for all atoms). R1/wR2 [ $I > 2\sigma(I)$ ]: 0.0644 / 0.1388. R1/wR2 [all refl.]: 0.1264 / 0.1616. S = 1.069. Residual

electron density between  $-0.35$  and  $0.48 \text{ e}/\text{\AA}^3$ . Geometry calculations and checking for higher symmetry was performed with the PLATON program.<sup>[A6]</sup> [\*] derived values do not contain the contribution of the disordered solvent.

## F2. NMR spectra

### F2.1 Characterization of compounds

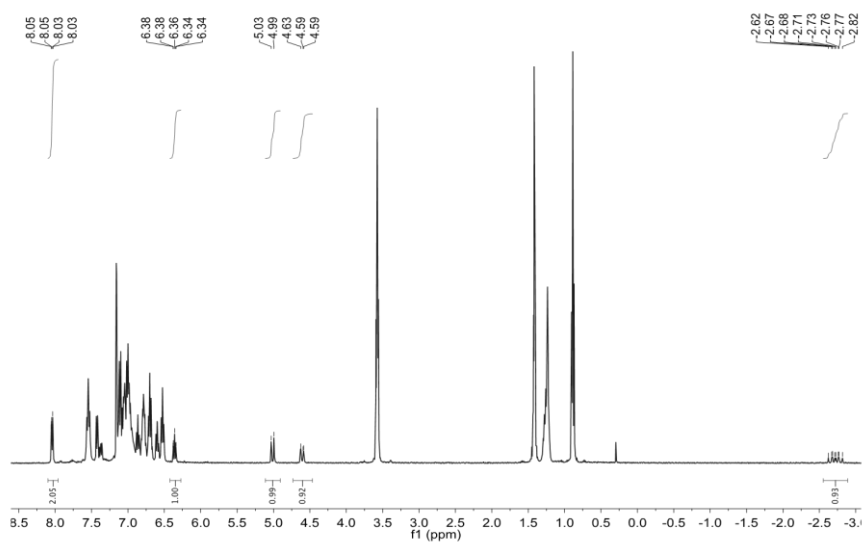


Figure F1.  $^1\text{H}$  NMR spectrum ( $\text{C}_6\text{D}_6$ ) of **2[Si]**.

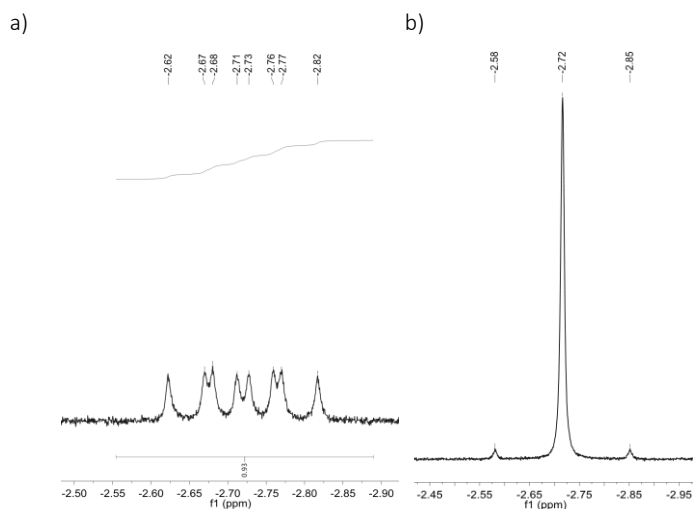
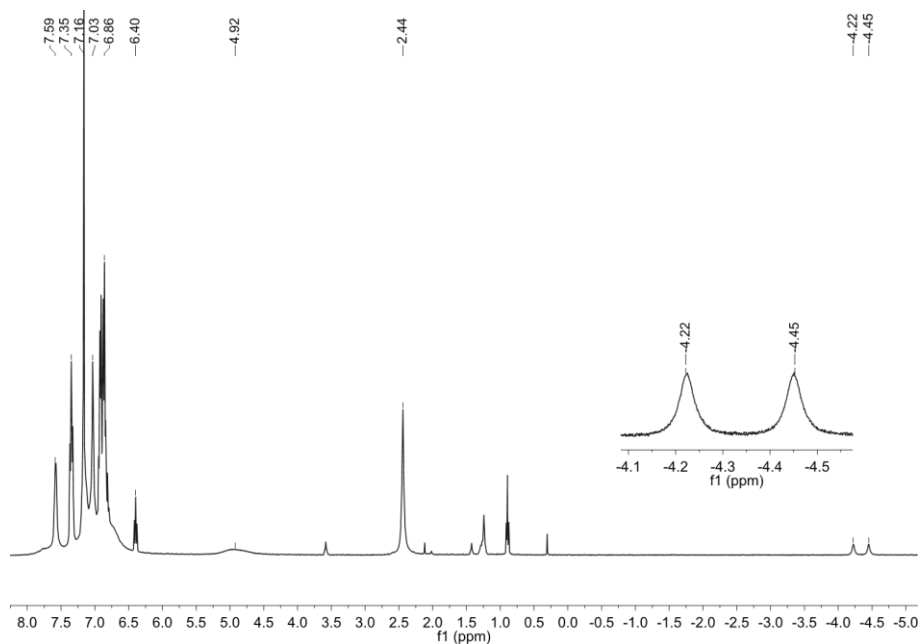
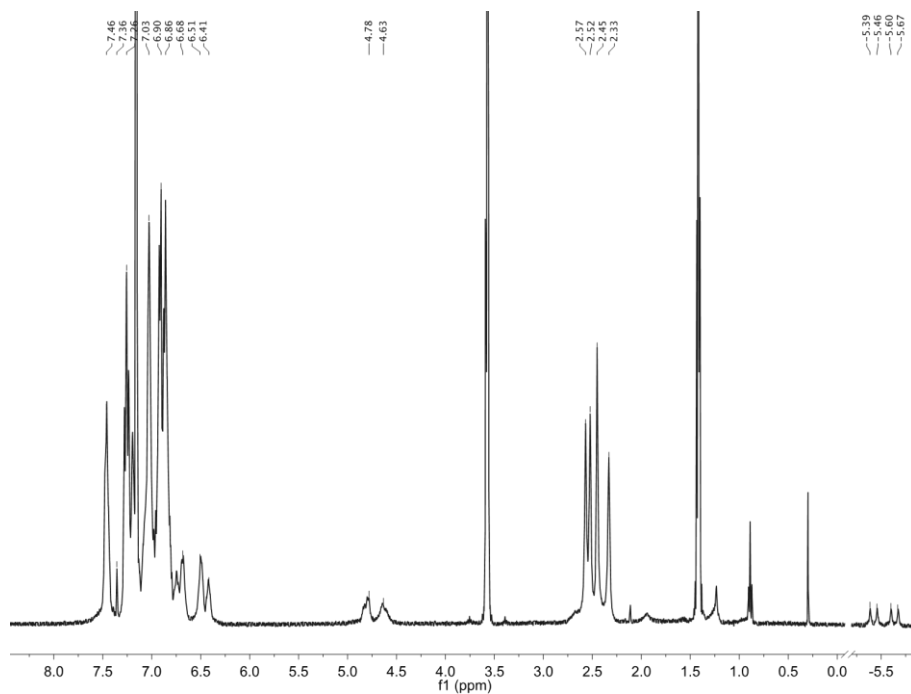


Figure F2. Zoom of the hydride signal  $^1\text{H}$  NMR spectrum ( $\text{C}_6\text{D}_6$ ) of **2[Si]**. a)  $^1\text{H}$  NMR  $^{31}\text{P}$  coupled, b)  $^1\text{H}$  NMR broadband  $^{31}\text{P}$  decoupled.



Figure F3.  $^1\text{H}$  NMR spectrum ( $\text{C}_6\text{D}_6$ ) of **3[Si]**.Figure F4.  $^1\text{H}$  NMR spectrum ( $\text{C}_6\text{D}_6$ ) of **4[Si]**.

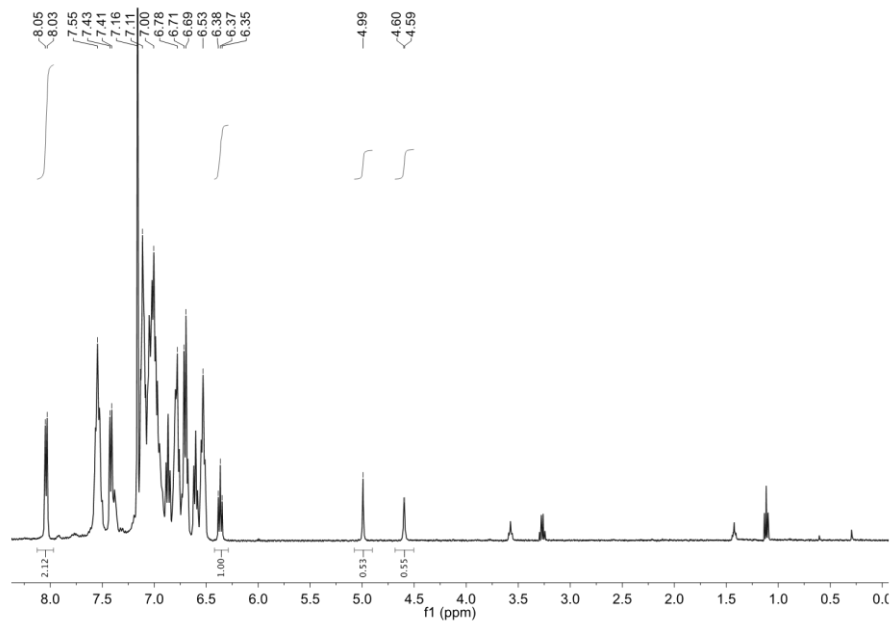


Figure F5.  $^1\text{H}$  NMR spectrum ( $\text{C}_6\text{D}_6$ ) of  $2[\text{SiD}_2]$ .

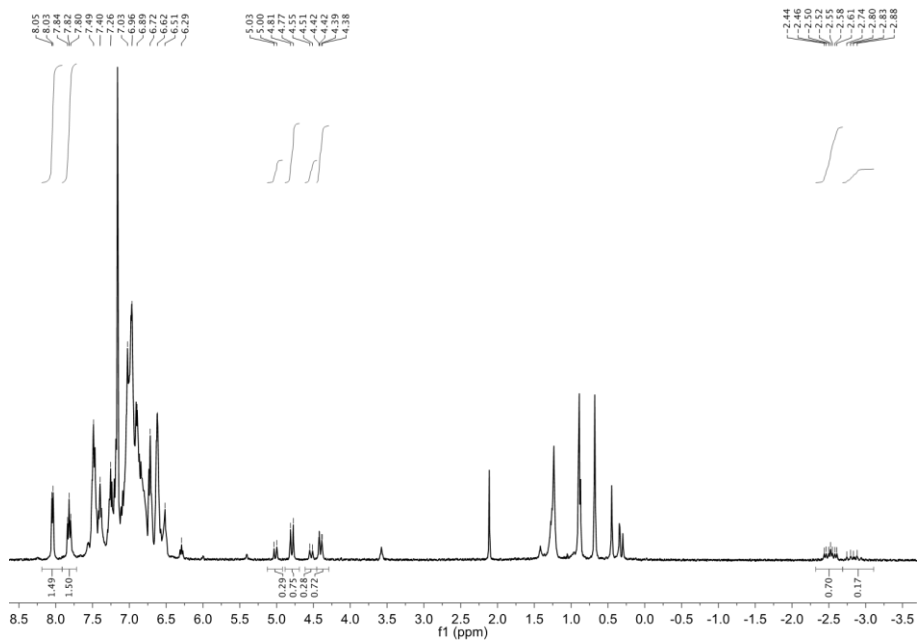


Figure F6.  $^1\text{H}$  NMR spectrum ( $\text{C}_6\text{D}_6$ ) of  $2[\text{SiPhMe}]$ .

## F.2.2 Experiments

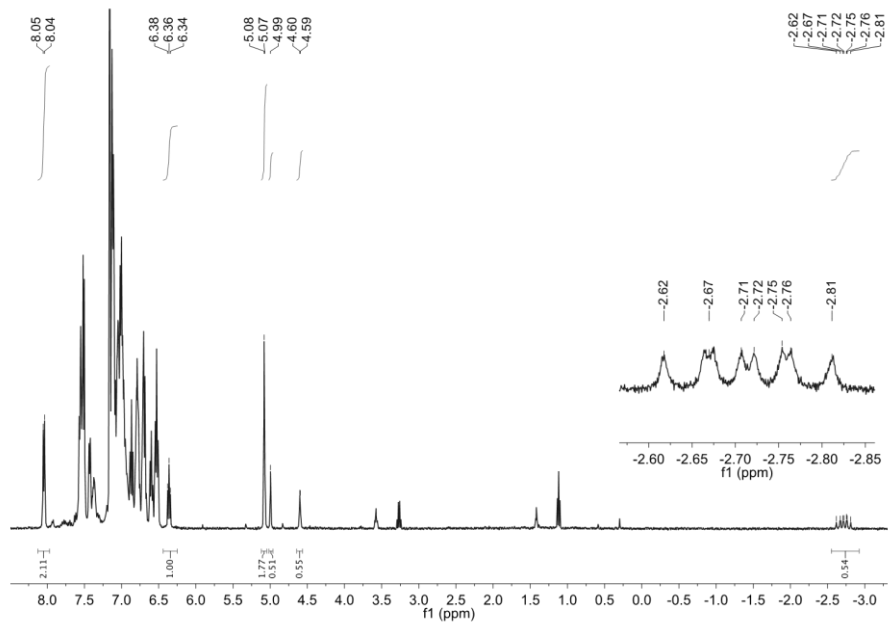


Figure F7.  $^1\text{H}$  NMR spectrum ( $\text{C}_6\text{D}_6$ ) of  $2[\text{SiD}_2] + \text{Ph}_2\text{SiH}_2$  scrambling experiment (time = 2h).

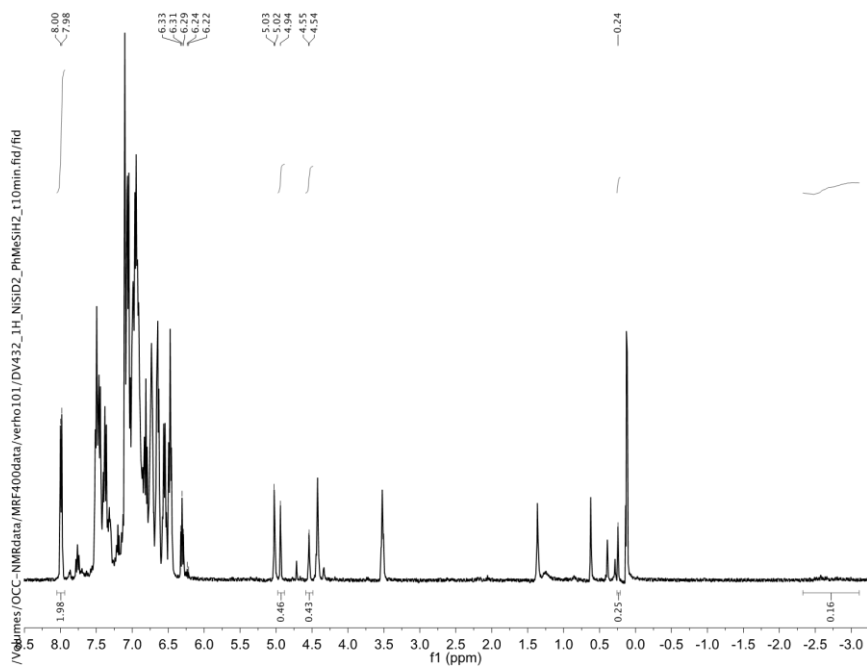


Figure F8.  $^1\text{H}$  NMR spectrum ( $\text{C}_6\text{D}_6$ ) of  $2[\text{SiD}_2] + \text{PhMeSiH}_2$  scrambling experiment (time = 10 min).

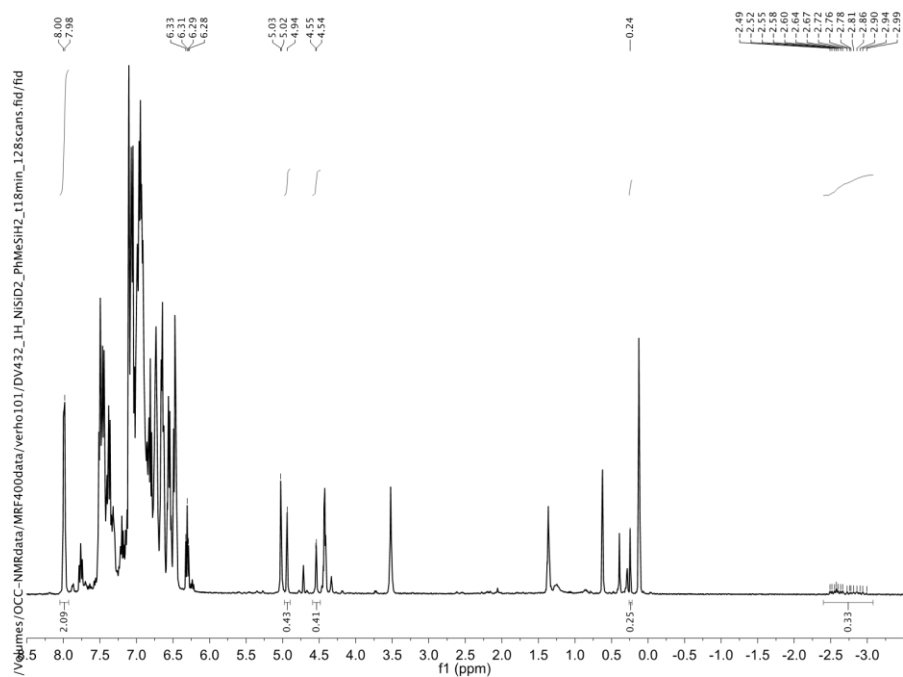


Figure F9.  $^1\text{H}$  NMR spectrum ( $\text{C}_6\text{D}_6$ ) of  $2[\text{SID}_2]$  + PhMeSiH<sub>2</sub> scrambling experiment (time = 18 min).

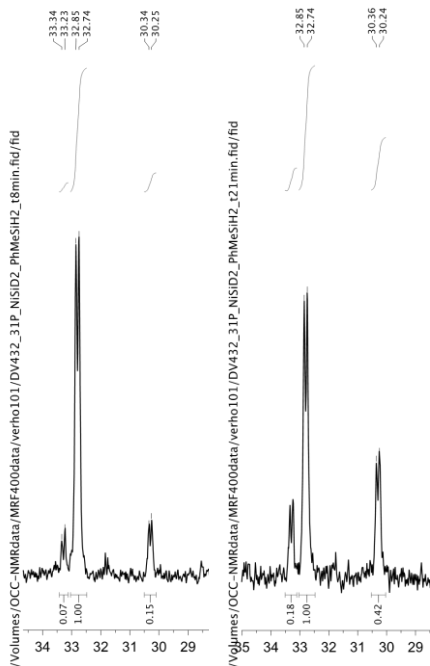


Figure F10.  $^{31}\text{P}$  NMR spectrum ( $\text{C}_6\text{D}_6$ ) of  $2[\text{SID}_2]$  + PhMeSiH<sub>2</sub> scrambling experiment. Left: time = 8 min, right: time = 21 min.

## F3. Hydrosilylation graphs

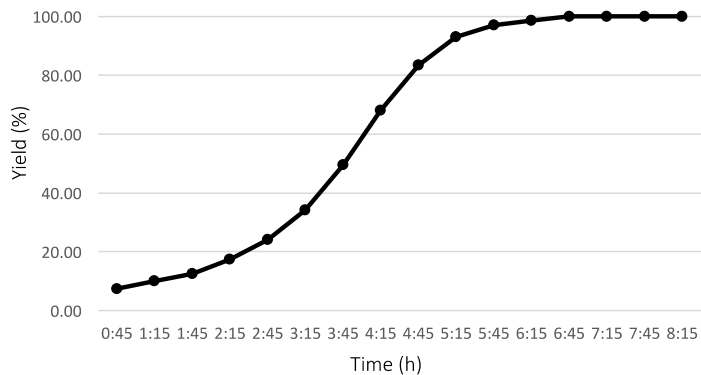


Figure F11. Conversion of 1-Octene + diphenylsilane catalyzed by 2[Si].

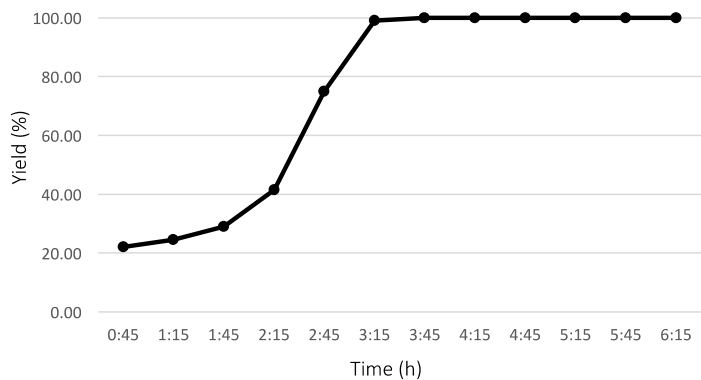


Figure F12. Conversion of 1-Octene + diphenylsilane catalyzed by 3[Si].

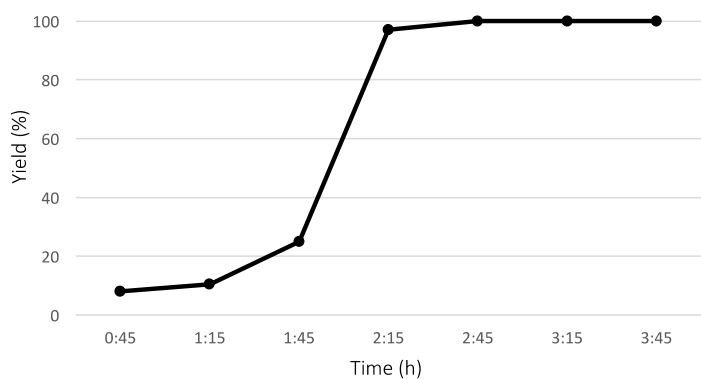


Figure F13. Conversion of 1-Octene + diphenylsilane catalyzed by 4[Si].

#### F4. References

- [A1] A. M. M. Schreurs, X. Xian, L. M. J. Kroon-Batenburg, *J. Appl. Cryst.*, **2010**, *43*, 70–82.
- [A2] R. Herbst-Irmer, G. M. Sheldrick, *Acta Cryst.* **1998**, *B54*, 443–449.
- [A3] G. M. Sheldrick (2014). SADABS and TWINABS. Universität Göttingen, Germany.
- [A4] G. M. Sheldrick. *Acta Cryst.*, **2015**, *A71*, 3–8.
- [A5] G. M. Sheldrick. *Acta Cryst.*, **2015**, *C71*, 3–8.
- [A6] A. L. Spek, *Acta Cryst.*, **2009**, *D65*, 148–155.
- [A7] A. L. Spek. *Acta Cryst.*, **2015**, *C71*, 9–18.

## Summary

Metal-ligand cooperativity is emerging as a powerful tool in the ongoing transition from precious metals to base metals in homogeneous catalysis. The low costs, high abundance and – in most cases – lower toxicity of base metals such as Fe, Co, Ni, and Cu make for a widespread interest in their use. Bond-making and bond-breaking processes, such as oxidative addition and reductive elimination, are often two-electron transformations, which are generally well mediated by late second and third row transition metals, i.e. precious metals. These elementary steps can be complicated when using complexes of base metals, as these metals tend to undergo one-electron redox reactions. Metal-ligand cooperativity is a promising tool to overcome the, often undesired, one-electron pathways by specifically designing and tuning the ligands. It can take a number of forms, of which general classes are: hemilability, redox-activity, and bifunctional activity (Figure 1). The incorporation of  $\pi$ -coordinating ligands to organometallic frameworks, for example by including C=C, C=N or C=O moieties, can induce such reactivity as a result of the versatile possible modes of coordination, generally being noncoordination,  $\eta^1$ -( $\sigma$ -donation) or  $\eta^2$ -coordination. The latter binding mode follows the Dewar-Chatt-Duncanson (DCD) model, described by the metallacycle and side-on bound  $\pi$ -complex resonance structures, and can engage in bifunctional small-molecule activation (Figure 2a,b). Recent advances in the synthesis and reactivity of metal complexes with tethered  $\pi$ -ligands are described in **Chapter 1**, including examples of cooperative behavior that substantiate the potential of such systems in catalysis.

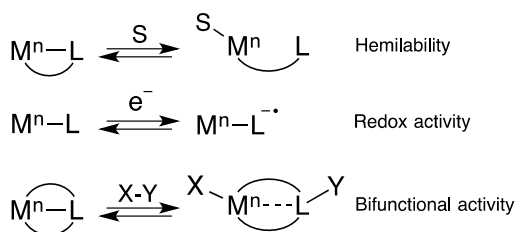


**Figure 1.** General classes of metal-ligand cooperativity.

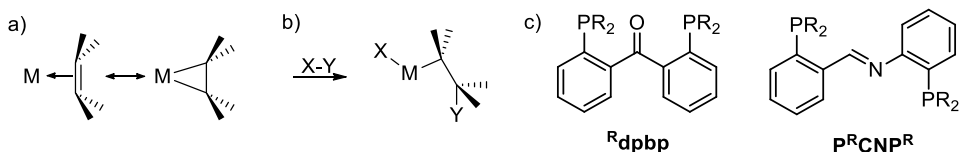
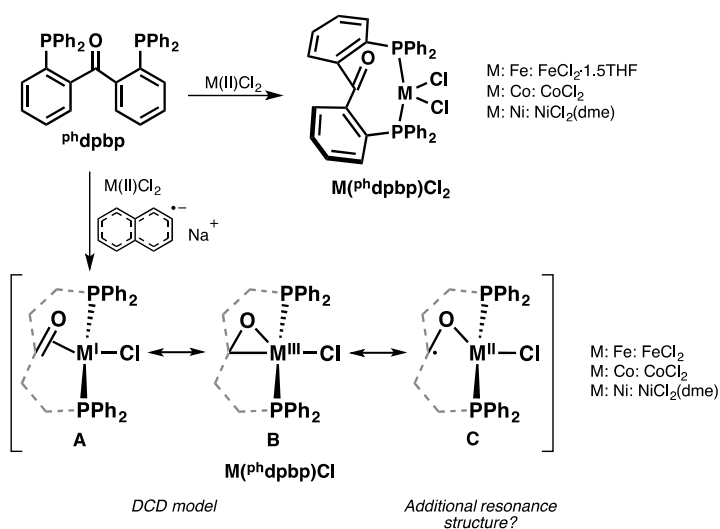


**Figure 2.** a) DCD model resonance extremes, left: side-on, right: metallacycle adduct. b) Addition of X–Y, altering the binding mode forming a  $\sigma$ -bond with one carbon. c) the ketone and imine ligand.

In the following chapters, the synthesis, coordination chemistry, and reactivity in metal complexes of two classes of  $\pi$ -ligands is described (Figure 2c). The ligands contain two

phosphine tethers to ensure a stable chelating structure and to position either a ketone or imine moiety close to the metal center.

The coordination chemistry of the diphosphine-ketone ligand 2,2'-bis(diphenylphosphino)benzophenone (<sup>Ph</sup>dppb) with nickel is investigated in **Chapter 2** (Scheme 1). The synthesized series of Ni-complexes in the oxidation states of II, I, and 0, display hemilabile behavior: the ketone moiety does not bind to Ni(II) in complex (<sup>Ph</sup>dppb)NiCl<sub>2</sub>, whereas reduction to Ni(I) or Ni(0) induces η<sup>2</sup>(C,O) coordination of the ketone to form pseudotetrahedral complexes (<sup>Ph</sup>dppb)NiCl and (<sup>Ph</sup>dppb)Ni(PPh<sub>3</sub>). DFT calculations indicate that the interaction of the ketone to the metal is dominated by π-backdonation, and <sup>Ph</sup>dppb functions as an acceptor ligand in this series of complexes.



**Scheme 1.** Overview of the <sup>Ph</sup>dppb ligand and its base-metal complexes.

The coordination of <sup>Ph</sup>dppb is extended to base metals Fe, Co and Cu, as described in **Chapter 3**. A systematic investigation of the interaction of the ketone moiety throughout this series is performed, providing the possibility to interpret periodic trends. The C=O moiety can adopt several binding modes, i.e. nonbound in the M(II) (M = Fe, Co, Ni) and Cu(I) complexes, η<sup>1</sup>(O) in a Ni(II)<sup>+</sup> cation, and η<sup>2</sup>(C,O) in the M(I) complexes (M = Fe, Co, Ni). Special attention is drawn to the latter structures and their interaction with the metal center. As seen in Chapter 2 for the Ni(I) complex, the ketone ligand in the Fe(I) and Co(I) complexes acts as an accepting ligand and the η<sup>2</sup>(C,O)-coordination is likewise dominated by π-backdonation. The binding is mostly well described by the Dewar-Chatt-Duncanson model, i.e. the π-complex and the metallaoxacycle extreme. Geometric changes in the Fe(I), Co(I) and Ni(I) structures show lengthening of the M–C bond and concomitant shortening of the M–O bond,



accompanied by a slight increase of the C=O bond length, increasing from Ni to Fe. This somewhat unexpected trend can be explained as a minor contribution of the ketyl radical resonance structure  $(\text{C}-\text{O})^{\bullet}-\text{M}(\text{II})$  to the bonding, mostly in the Fe(I) complex (Scheme 1), as supported by computational investigations.

The activity of  $\text{P}^{\text{h}}\text{dppb}$  Co-complexes for the hydrosilylation of unsaturated compounds is described in **Chapter 4**. Homogeneously catalyzed hydrosilylation reactions of unsaturated compounds by first-row transition metals have gained considerable attention in the last years, aiming at substituting precious metal-based catalysts and at insights into the mechanistic pathways. Cobalt complexes of the ketone ligand are shown to be good catalysts for the hydrosilylation reaction of 1-octene with phenylsilane, especially the Co(I) complex of modified ligand  $\text{P}^{\text{t}}\text{ol}\text{dppb}$  (Figure 3). The Co(I) complex is a good precatalyst for the mentioned reaction under mild conditions at 1 mol% catalyst, 1 h, room temperature, and without solvent, yielding 84% of octylphenylsilane. Investigation of the substrate scope shows lower performance of the catalyst in styrene hydrosilylation, but excellent results with allylbenzene (84%) and acetophenone (>99%). NMR data suggests that the active catalyst is possibly a Co-H species. Further mechanistic details for this system are unclear due to the high reactivity of this system, but more insight on such mechanisms is afforded by using Ni-imine systems in **Chapter 6**.

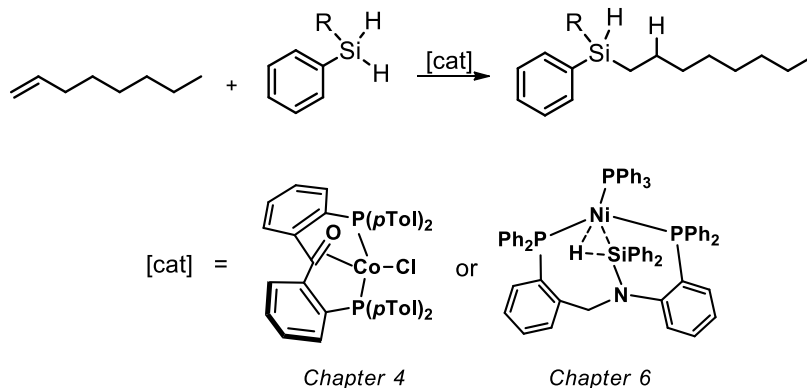
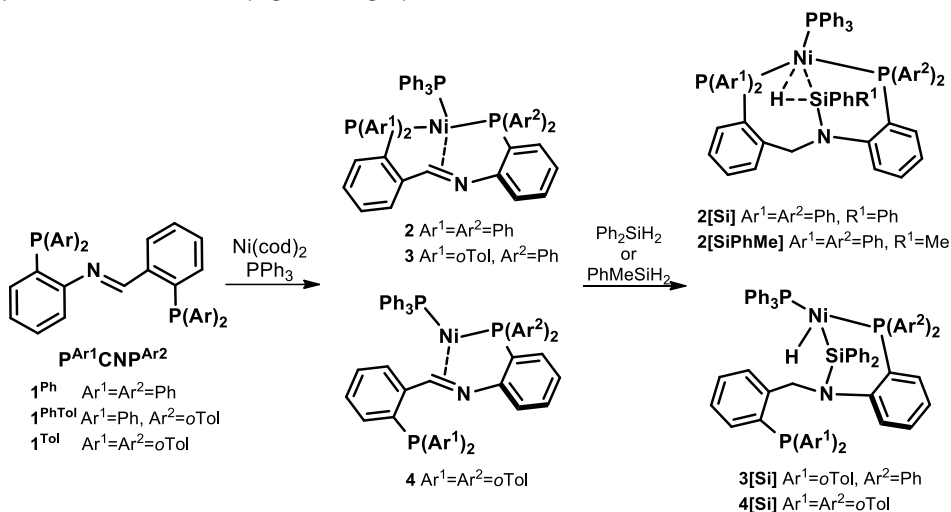


**Figure 3.** Top: hydrosilylation of 1-octene with a silane, R = H/Ph. Bottom: explored catalytic systems.

In **Chapter 5** the imine ligand PCNP is investigated, consisting of diphosphine substituted *o*-phenylene linkers bound to the C=N backbone (Scheme 2, **1**). The PCNP ligand is readily synthesized *via* an imine condensation of the diphenylphosphine substituted aldehyde and amine compounds, and its coordination to nickel is investigated. The imine functionality of this chelating ligand binds in an  $\eta^1(\text{N})$ -fashion in the Ni(II) complex  $\text{Ni}(\text{P}^{\text{h}}\text{CNP}^{\text{h}})\text{Cl}_2$ . The less common  $\eta^2(\text{C},\text{N})$ -interaction is obtained in Ni(0) complexes with addition of a  $\text{PPh}_3$  co-ligand (Scheme 2, **2**). The design of the ligand allows for rapid incorporation of R-groups, forming even mixed ligands, as the building blocks of the imine condensation can be adjusted. Incorporation of more bulky groups by substituting the phenyl substituents for *o*-tolyl groups

leads to different coordination of the ligand to nickel. In the less bulky tetra-phenyl (**2**) and mixed di-phenyl/di-*o*-tolyl substituted complexes (**3**) both phosphine tethers are bound, next to the  $\eta^2(\text{C},\text{N})$ -coordinating  $\text{C}=\text{N}$  and a  $\text{PPh}_3$  co-ligand, whereas one phosphine arm remains unbound when using a tetra-*o*-tolyl substitution (**4**). Interesting behavior on the imine ligands is obtained in the absence of a co-ligand in the synthesis of dimeric Ni complexes, resulting in the formation of a  $\mu\text{-}\eta^1(\text{N})\eta^2(\text{C},\text{N})$ -coordinating complex (Figure 4, left), in a mixture with a species which is suggested to be formed by a coupling of the imine moieties, resulting in a new C–C bond in a Ni(0)Ni(II) species. Evidence for this latter structure arises from isolation of a crystalline CO derivative (Figure 4, right).



Scheme 2. Overview of the imine-ligands and Ni-complexes.

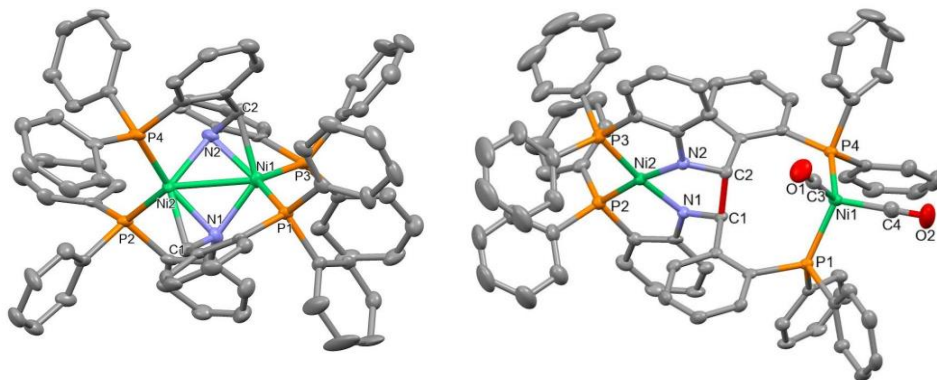
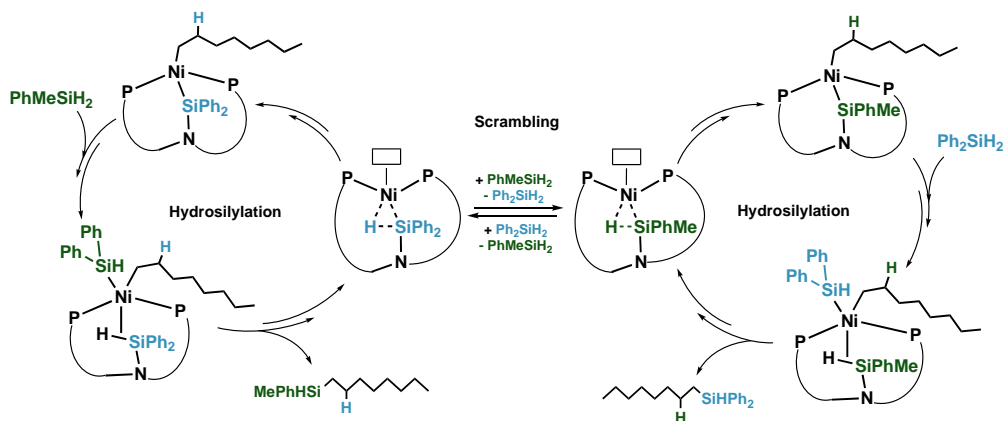


Figure 4. XRD crystal structures of the  $\mu\text{-}\eta^1(\text{N})\eta^2(\text{C},\text{N})$ -coordinating complex and the CO derivative, in which the new C–C bond is shown in red.

The reactivity of imine complexes **2–4** toward silanes is described in **Chapter 6**. The complexes can cleanly activate diphenylsilane, each resulting in a single isolable species, characterized as

the product of formal hydrosilylation of the imine-backbone (Scheme 2, **2[Si]-4[Si]**). A hydride is added to the imine-carbon atom and the  $R_2Si-H$  moiety binds to the nitrogen atom to form an *N*-substituted silane, which additionally coordinates to Ni *via* the Si-H bond. The Si-H bond in complex **2[Si]** is activated and coordinates in an  $\eta^2(Si,H)$ -fashion to Ni. In the electronically unsaturated complexes **3[Si]** and **4[Si]**, which are identified by XRD analysis, the Si-H is strongly activated and the complexes are better described as a Ni(II) center bearing a silyl and a hydride ligand resulting from oxidative addition. The mechanism of this reaction is investigated by DFT calculations, suggesting a Ni-mediated ligand-to-ligand hydride transfer mechanism and cooperative activation of the silane by Ni. Furthermore, compounds **2-4** are efficient precatalysts for the hydrosilylation of 1-octene with diphenylsilane, resulting in high conversion within 7 h at room temperature in all cases, and full selectivity toward the anti-Markovnikov product. Stoichiometric reactions show that the  $CH_2$  group, originating from addition of a hydride to the imine-C, is unreactive in the hydrosilylation reactions. Hence, addition of the alkene substrate 1-octene to **2[Si]-4[Si]** or **2[SiPhMe]** (Scheme 2) does not lead to product formation, and addition of a second equivalent of silane is necessary for reactivity. Scrambling of the  $R_2Si-H$  moiety in compound **2[Si]** occurs spontaneously upon addition of extra silane. This indicates reversible cleavage of the Si-N bond under catalytic conditions. This finding might have general implications for the mechanism of hydrosilylation reactions employing N-containing ligands, such as imines or amides, in Ni-catalysts, for which the incorporation of this step might be considered. A possible mechanism is proposed based on the results, in which the *N*-silane moiety acts as a hydride reservoir (Scheme 3).



**Scheme 3.** Schematic proposed mechanism of concomitant hydrosilylation and silane scrambling reactions.

### Future perspectives

The application of earth abundant metals to catalysis is of considerable interest, not only to replace precious metals, but also to discover new reaction pathways and new reactivity.

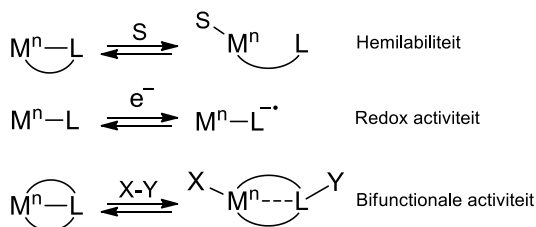
Careful design of the ligands can make for their optimal use in cooperation with the metal center, optimizing the use of both parts in the catalyst. Incorporation of metal-ligand cooperativity can lead to new elementary steps that make use of ligand centered reactivity as well, opening up new pathways in chemistry. For example, storage at the ligand backbone of substrate fragments, such as hydrogen, hydride, electrons or heterolytically added substrates, are key features for cooperativity in a system. The understanding of ligand centered reactivity is herein a key step for the development of efficient systems, and warrants further research.

The incorporation of two polar  $\pi$ -ligands in base metal complexes was developed in this work, namely a ketone and an imine functionality. Both ligands contain two strongly binding phosphine tethers, which are important to ensure the stability of the complexes, but are also flexible linkers and can create lability for ongoing reactivity. Both ligands, <sup>R</sup>dppb and PCNP, exhibit versatile coordination chemistry involving several coordination modes, and show interesting reactivity toward hydrosilanes. Hydrosilylation reactions are important in industry, for example in the synthesis of silicon-based polymers, oils and resins, as well as in the production of organosilicon reagents for fine chemicals, for which the utilization of systems based on earth abundant metals is of interest to replace the often-used Pt-catalysts. The systems described herein should be further developed in the direction of hydrosilylation reactions – as good to excellent reactivity was shown – but also in different reactions, such as the hydrogenation of alkene and carbonyl groups. The clean reactivity of particularly the Ni(PCNP) systems allows for in-depth characterization of possible reaction intermediates, creating a promising basis for fundamental research, both experimental and computational, aiming at cooperative processes in small-molecule activation and catalysis.

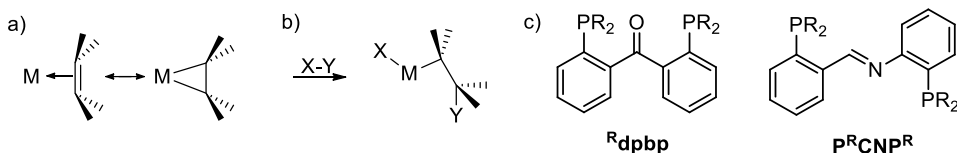
In the long run, metal-ligand cooperativity is envisioned to become a key-feature in the design of earth abundant metal complexes. The performed research on the coordination and reactivity of  $\pi$ -ligands offers a better understanding of these ligands and their reactions, and will hopefully inspire future research regarding new avenues in metal-ligand cooperativity.

## Samenvatting

Metaal-ligand coöperativiteit krijgt almaar meer aandacht als een belangrijke methode in de voortdurende overgang van edelmetalen naar onedele metalen in de homogene katalyse. De lage kosten, overvloedige aanwezigheid en veelal lagere toxiciteit van onedele metalen zoals Fe, Co, Ni en Cu zorgen voor een algemene interesse in hun gebruik. Reacties waarin bindingen gemaakt en verbroken worden, zoals oxidatieve addities en reductieve eliminaties, zijn veelal twee-elektronen transformaties. Deze reacties vinden over het algemeen plaats met behulp van late tweede- en derde-rij overgangsmetalen, oftewel edelmetalen. Deze elementaire stappen zijn minder voorkomend wanneer er gebruik wordt gemaakt van onedele metaalcomplexen, aangezien deze de neiging hebben om één-elektron redoxreacties uit te voeren. Metaal-ligand coöperativiteit is een veelbelovende strategie om deze vaak ongewilde één-elektron-reacties te omzeilen. Metaal-ligand coöperativiteit kan verschillende vormen hebben, veelal binnen drie algemene groepen: hemilabiliteit, redox-activiteit en bifunctionele activiteit (Figuur 1). Het inbouwen van  $\pi$ -coördinerende liganden in een organometaalcomplex, bijvoorbeeld door het invoeren van C=C, C=N of C=O groepen, kan dit soort reactiviteit bevoordelen als een gevolg van de verschillende wijzen waarop deze groepen aan een metaal kunnen coördineren. Over het algemeen zijn de manieren van interactie: niet-bindend, via  $\eta^1$ -( $\sigma$ -donatie) of via een  $\eta^2$ -coördinatie. Deze laatste manier volgt het Dewar-Chatt-Duncanson (DCD) model, die wordt beschreven door twee resonantiestructuren: het metallocycclus complex en het zijdelings gebonden  $\pi$ -complex. Deze bindingswijze kan positief bijdragen aan de bifunctionele activering van kleine moleculen (Figuur 2a,b). Recente ontwikkelingen in de synthese en reactiviteit van metaalcomplexen met chelerende  $\pi$ -liganden zijn beschreven in **Hoofdstuk 1**. Typische voorbeelden van coöperatieve systemen of systemen met het potentieel tot coöperativiteit in homogene katalyse worden in dit hoofdstuk beschreven.



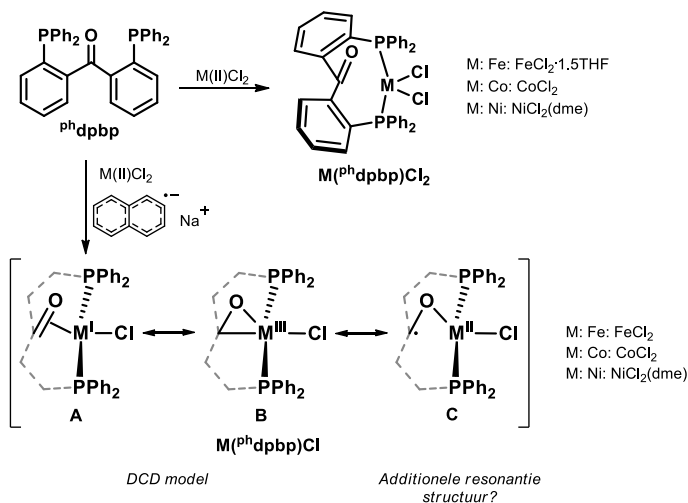
**Figuur 1.** Algemene vormen van metaal-ligand coöperativiteit.



**Figuur 2.** a) Resonantie-extremen van het DCD model, links: het zijdelings gebonden  $\pi$ -complex, rechts: het metallocyclus adduct. b) Additie van X-Y, waarbij de manier van binden wordt veranderd, resulterend in een  $\sigma$ -bindend koolstofligand. c) het keton en imine ligand beschreven in dit proefschrift.

In de hierop volgende hoofdstukken worden de synthese, coördinatiechemie en reactiviteit in metaalcomplexen van de twee typen liganden beschreven (Figuur 2c). De liganden bezitten twee fosfine groepen, die als armen dienen om een stabiel metaalcomplex te creëren met een chelerende structuur. Daarnaast zorgen zij voor de positionering van de keton- ofwel imine-groep dichtbij het metaalcentrum.

De coördinatiechemie van het difosfine-ketonligand 2,2'-bis(difenylfosfino)benzofenon ( $^{\text{Ph}}\text{dppb}$ ) met nikkel is beschreven in **Hoofdstuk 2** (Schema 1). De verkregen serie Ni-complexen met oxidatietoestanden II, I en 0 vertonen hemilabel gedrag: de ketongroep bindt niet aan Ni(II) in het  $(^{\text{Ph}}\text{dppb})\text{NiCl}_2$  complex, terwijl reductie van het complex naar Ni(I) of Ni(0) resulteert in een  $\eta^2(\text{C},\text{O})$  coördinatie van het keton. De gesynthetiseerde  $(^{\text{Ph}}\text{dppb})\text{NiCl}$  en  $(^{\text{Ph}}\text{dppb})\text{Ni}(\text{PPh}_3)$  complexen hebben een pseudo-tetraëdrische structuur. DFT-berekeningen wijzen op een dominerende  $\pi$ -backbonding in de interactie van de ketongroep met het metaal. Daarbij heeft het  $^{\text{Ph}}\text{dppb}$  ligand een elektronaccepterende functie in de gehele serie van de complexen.

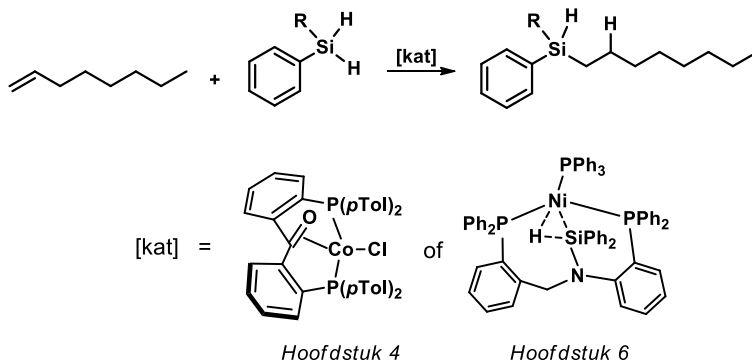


**Schema 1.** Overzicht van het  $^{\text{Ph}}\text{dppb}$  ligand en diens Fe-, Co- en Ni-complexen.

In **Hoofdstuk 3** is de coördinatiechemie van het  $^{\text{Ph}}\text{dppb}$  ligand aan andere onedele metalen beschreven. Een systematisch onderzoek in deze serie van complexen is

uitgevoerd, waarbij de interactie van het ketonfragment met Fe, Co, Ni en Cu is onderzocht. De C=O groep kan zijn binding met het metaal op verschillende manieren aanpassen: niet-gebonden in de M(II) (M = Fe, Co, Ni) en Cu(I) complexen,  $\eta^1(\text{O})$  in het Ni(II)<sup>+</sup> kation en  $\eta^2(\text{C,O})$  in de M(I) complexen (M = Fe, Co, Ni). Speciale aandacht is geschonken aan de interactie van het keton met het metaalcentrum in de laatstgenoemde structuren. Het ketonligand heeft ook in de Fe(I) en Co(I) complexen dezelfde accepterende functie als voor het Ni(I) complex in Hoofdstuk 2, en ook hier wordt de  $\eta^2(\text{C,O})$ -interactie gedomineerd door  $\pi$ -backbonding. De binding wordt grotendeels correct beschreven door het Dewar-Chatt-Duncanson model, met de resonantie-extremen van het  $\pi$ -complex en de metallocycclus. Geometrische veranderingen in de Fe(I), Co(I) en Ni(I) structuren laten de verlenging van de M–C binding zien, tezamen met een korter wordende M–O binding en een iets langere C=O binding. In alle gevallen worden de trends sterker van Ni naar Fe. Deze trends zijn onverwachts, maar kunnen uitgelegd worden door een kleine bijdrage van een ketylradicaal resonantiestructuur  $(\text{C}=\text{O})^{\bullet-}\text{M}(\text{II})$  aan de algehele bindingstructuur. Deze is met name in het Fe(I) complex aanwezig (Schema 1) en is bevestigd met berekeningen.

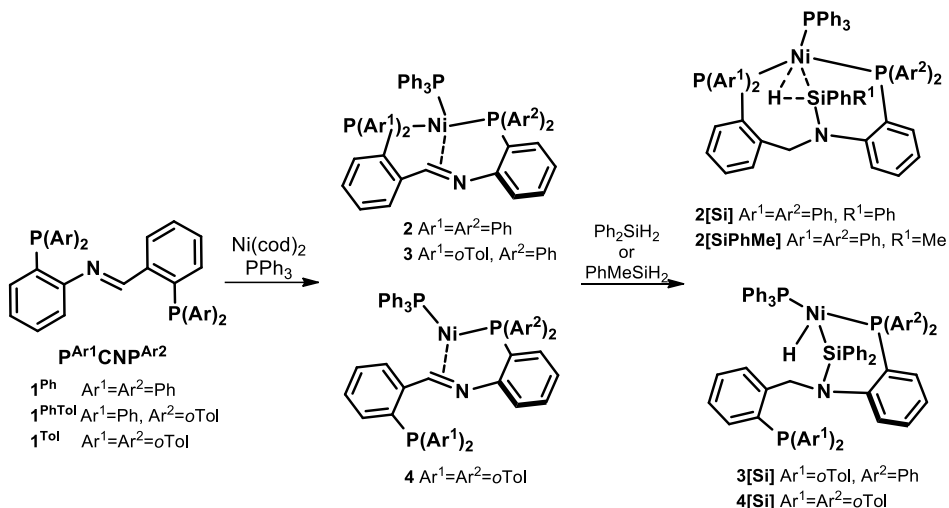
De reactiviteit van de <sup>Ph</sup>dppb Co-complexen in de hydrosilylering van alkenen is beschreven in **Hoofdstuk 4**. De hydrosilylering van alkenen met homogene katalysatoren gebaseerd op eerste-rij overgangsmetalen heeft in de afgelopen jaren veel aandacht gekregen, met als doel de katalysatoren gebaseerd op edelmetalen te vervangen en om meer inzicht te verkrijgen in het mechanisme van de reactie. Kobaltcomplexen van het ketonligand zijn goede katalysatoren voor de hydrosilyleringsreactie van 1-octeen met fenylsilaan, waarbij voornamelijk het Co(I) complex van het gemodificeerde <sup>pTol</sup>dppb ligand goede resultaten geeft (Figuur 3). Dit Co(I) complex is een goede pre-katalysator voor bovengenoemde reactie onder milde condities, te weten: 1 mol% complex, 1 uur, kamertemperatuur en zonder toevoeging van een oplosmiddel. Dit resulteert in een opbrengst voor het product octylfenylsilaan van 84%. Onderzoek naar de activiteit van het complex met andere substraten toonde een lager rendement in de hydrosilylering van styreen. Desalniettemin worden in de hydrosilylering van allylbenzeen (84%) en acetofenon (>99%) goede resultaten behaald. Met behulp van NMR-spectroscopie zijn aanwijzingen gevonden dat de actieve katalysator mogelijk een kobalthydride (Co–H) bevat. Verdere details met betrekking tot het mechanisme van de katalyse zijn nog onduidelijk als gevolg van de hoge reactiviteit van het systeem.



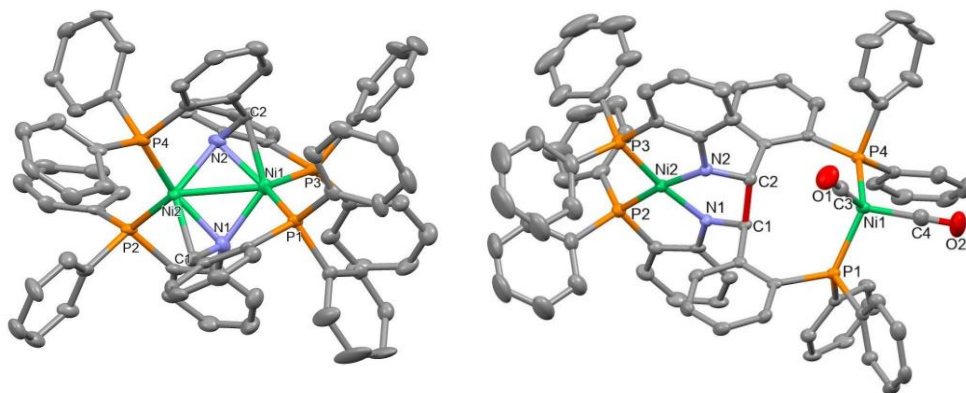
**Figuur 3.** Katalytische hydrosilylering van 1-octeen met een silaan, R = H, Ph.

De nikkel-coördinatiechemie van het imineligand PCNP is onderzocht in **Hoofdstuk 5**. Het ligand bestaat uit difenylfosfine-gesubstitueerde *o*-fenyleengroepen die gebonden zijn aan een C=N-groep (Schema 2, **1**). Het PCNP-ligand kan gemakkelijk worden gesynthetiseerd door middel van de iminecondensatie van een aldehyde en een amine, die ieder gesubstitueerd zijn met een difenylfosfinegroep. De iminegroep van dit chelerende ligand bindt met een  $\eta^1(\text{N})$ -coördinatie in het Ni(II) complex  $\text{Ni}(\text{P}^{\text{Ph}}\text{CNP}^{\text{Ph}})\text{Cl}_2$ . Een  $\eta^2(\text{C,N})$ -coördinatie, een minder voorkomende coördinatiewijze, vindt plaats in de Ni(0) complexen waarbij trifenylfosfine toegevoegd is als coligand (Schema 2, **2**). Door het specifieke ontwerp van het ligand is het gemakkelijk om verschillende R-groepen te introduceren, aangezien de bouwstenen van de iminecondensatie aangepast kunnen worden. Hiermee kunnen ook gemixte liganden gemaakt worden. Grotere, omvangrijkere groepen zijn ingebouwd door de substitutie van de fenylgroepen met *o*-tolyl groepen, wat leidt tot een verandering in de coördinatie rondom nikkel. In de complexen van de liganden met minder grote substituenten, te weten het tetra-fenyl (**2**) en het gemende difenyl/*di-o*-tolyl (**3**) ligand, zijn beide fosfine-armen gebonden aan nikkel, tezamen met de  $\eta^2(\text{C,N})$ -gecoördineerde iminegroep en een  $\text{PPh}_3$  coligand. In het complex van het zeer omvangrijke tetra-*o*-tolyl gesubstitueerde ligand (**4**) is daarentegen slechts één van de fosfine-armen gebonden. Interessante reactiviteit is gevonden met dimere nikkelcomplexen van het imine ligand, welke zijn gevormd via dezelfde syntheseroute, maar zonder toevoeging van een coligand. In dit dimere complex zijn de iminegroepen op een  $\mu\text{-}\eta^1(\text{N})\eta^2(\text{C,N})$ -wijze gecoördineerd aan beide nikkelcentra (Figuur 4, links). Dit complex wordt gevormd in een mengsel samen met een complex waarin de iminegroepen een koppelingsreactie zijn aangegaan, waardoor een nieuwe C–C binding is gevormd in een Ni(0)Ni(II) complex. Bewijs voor deze laatstgenoemde structuur is verkregen aan de hand van het analoge, CO-gebonden complex (Figuur 4, rechts).





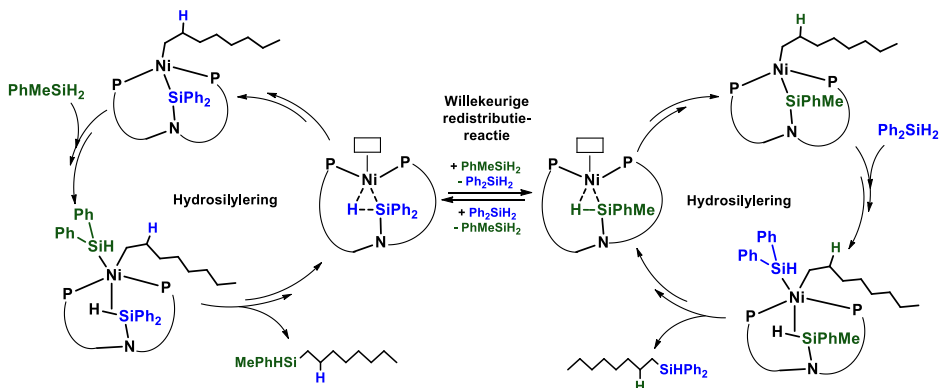
Schema 2. Overzicht van de PCNP-imineliganden en nikkelcomplexen.



Figuur 4. Kristalstructuren van het dimere  $\mu\text{-}\eta^1(\text{N})\eta^2(\text{C},\text{N})$ -gecoördineerde complex en het CO-complex, waarbij de nieuwe C–C binding is weergegeven in het rood.

De reactiviteit van iminecomplexen **2-4** met silanen is beschreven in **Hoofdstuk 6**. De complexen reageren op een schone manier met difenylsilaan, allen resulterend in complexen die zijn gekarakteriseerd als de producten van een formele hydrosilylering van de iminegroepen (Schema 2, **2[Si]**-**4[Si]**). De additie van een hydride heeft hierbij plaatsgevonden aan het koolstofatoom van het imine en de  $\text{R}_2\text{Si-H}$ -groep is gebonden aan het stikstofatoom, resulterend in een *N*-gesubstitueerd silaan. Deze laatstgenoemde groep coördineert daarnaast ook nog via de Si–H-binding aan nikkel. De Si–H binding in het **2[Si]** complex heeft een relatief lange bindingsafstand en heeft een  $\eta^2(\text{Si},\text{H})$ -coördinatie met nikkel. De elektronisch onverzadigde **3[Si]** en **4[Si]** complexen zijn onder andere geïdentificeerd met behulp van XRD-analyse. De Si–H-binding van deze structuren is sterk

geactiveerd en hierdoor worden deze beter beschreven als het product van oxidatieve additie, als Ni(II) complexen met een silyl- en een hydride-ligand. Het mechanisme van deze activeringsreactie is onderzocht met behulp van DFT-berekeningen en lijkt te verlopen via een nikkel-gemedieerde hydride-overdracht van ligand naar ligand en coöperatieve activering van het silaan over de Ni–N-binding. Daarnaast zijn complexen **2-4** efficiënte pre-katalysatoren voor de hydrosilylering van 1-octeen met difenylsilaan, waarmee hoge opbrengsten behaald worden. De reactie verloopt bij kamertemperatuur binnen 7 uur en met volledige selectiviteit voor het anti-Markovnikov product. Stoichiometrische reacties laten zien dat de CH<sub>2</sub>-groep van het ligand, die ontstaat in de hydride-additie aan het imine-koolstofatoom, niet deelneemt aan de hydrosilyleringsreacties. Hierdoor leidt de toevoeging van het alkeensubstraat 1-octeen aan **2[Si]-4[Si]** of **2[SiPhMe]** (Schema 2) niet tot de vorming van het hydrosilyleringsproduct en is een tweede equivalent van het silaan nodig voor de productvorming. De willekeurige redistributie van de R<sub>2</sub>Si–H-groep in **2[Si]** vindt spontaan plaats zodra extra silaan wordt toegevoegd. Dit laat zien dat reversibele vorming van de Si–N-binding plaats vindt onder dezelfde condities als de katalyse. Dit gegeven heeft mogelijk verdere algemene implicaties omtrent het mechanisme van gekatalyseerde hydrosilyleringsreacties waarbij gebruik gemaakt wordt van stikstof-bevattende liganden zoals imines of amides in combinatie met nikkel. De resultaten verkregen in dit hoofdstuk laten zien hoe een N-silaangroep dienst kan doen als hydridereservoir in dergelijke reacties (Schema 3).



**Schema 3.** Voorgesteld mechanisme van de tegelijdige hydrosilyleringsreactie en de willekeurige redistributiereactie van silanen door Ni-PNCP-complexen.

### *Toekomstperspectieven*

Het gebruik van onedele metalen in de katalyse is van aanzienlijk belang, niet alleen voor het vervangen van edelmetalen, maar ook voor de ontdekking van nieuwe mechanismen en reacties. Het nauwkeurig ontwerpen van liganden kan leiden tot een optimaal gebruik en

samenwerking van beide delen van een homogene katalysator, d.w.z. het ligand en het metaalcentrum. Het introduceren van metaal-ligand coöperativiteit kan tot nieuwe elementaire stappen leiden waarbij mede gebruik wordt gemaakt van reactiviteit die gecentreerd is op het ligand. Dit opent de deur naar nieuwe methodes binnen de homogene katalyse. Een belangrijke functie van coöperativiteit in een katalysator is bijvoorbeeld het opslaan van delen van substraten op het ligand, zoals waterstofatomen, hydriden, elektronen of heterolytisch geactiveerde substraten. Het algemene begrip van ligand-gecentreerde reactiviteit speelt hierbij een belangrijke rol in de verdere ontwikkeling van efficiënte katalysatoren en vraagt om verder onderzoek.

In dit proefschrift is de introductie van twee polaire  $\pi$ -liganden in onedele metaalcomplexen ontwikkeld. Naast een  $\pi$ -gecoördineerd keton- of iminefunctionaliteit bevatten beide liganden twee sterk-bindende fosfine-armen, die belangrijk zijn voor het garanderen van de stabiliteit van de complexen, maar daarnaast ook flexibiliteit waarborgen waarmee ruimte wordt gecreëerd voor reactiviteit. De beide liganden ( $^R$ dpbp en PCNP) vertonen een veelzijdige coördinatiechemie, die verschillende coördinatiewijzen omvat en leidt tot interessante, katalytische reactiviteit met hydrosilanen. Hydrosilyleringsreacties zijn van groot belang in de industrie, bijvoorbeeld in de synthese van siliconenpolymeren en smeermiddelen, maar ook in de productie van organosiliciumreagentia in de industriële fijnchemie. Hiervoor is het introduceren van katalytische systemen gebaseerd op onedele metalen van groot belang om de vaak gebruikte platina-katalysatoren te vervangen. Gezien hun goede tot excellente reactiviteit zijn de systemen beschreven in dit proefschrift interessant voor verdere ontwikkeling en toepassing in hydrosilyleringsreacties en andere hydro-additiereacties van alkenen en carbonylverbindingen, zoals bijvoorbeeld hydrogeneringen. De selectieve reactiviteit van voornamelijk de Ni(PCNP) complexen biedt daarnaast mogelijkheden voor de uitgebreide karakterisering van mogelijke reactie-intermediären. Dit creëert een veelbelovende basis voor fundamenteel onderzoek, zowel experimenteel als op basis van berekeningen, gericht op de coöperatieve activering van kleine moleculen en coöperatieve processen in homogene katalyse.

Op de lange termijn wordt metaal-ligand coöperativiteit gezien als een belangrijke methode voor het ontwerpen van katalysatoren gebaseerd op onedele metalen. Het uitgevoerde onderzoek in de richting van de coördinatie en reactiviteit van  $\pi$ -liganden draagt bij aan een verbeterd begrip van dit type liganden en de bijbehorende reactiviteit en zal hopelijk nieuw onderzoek omtrent metaal-ligand coöperativiteit inspireren.



*Happiness is only real when shared.*

- Christopher J. McCandless

## Dankwoord

I believe that science is a team effort. Many minds think and work together in creative ways to understand fundamental problems. Out of curiosity, love for chemistry, environmental needs or to personally be enlightened. I also believe that science can greatly benefit from teamwork, two heads are better than one, and maybe we can even make an analogy here with the work performed in this thesis, two parts of a catalyst work better in collaboration, the metal and the ligand. To not be isolated, but to share knowledge, ideas, views, and tips-and-tricks is of endless importance for me as a person and as a scientist, and I am grateful to the people who were willing to work with me and who welcomed me in their teams.

After writing this thesis, four years of labwork, numerous presentations, group meetings, work discussions, paper revisions and much more, I want to thank the people who contributed in many ways, made this work possible, and helped me throughout the project. During the last years I have been able to learn and grow, and much of this is thanks to the people around me. Supervisors, students, colleagues, family and friends, I could not have done this without you.

**Marc-Etienne**, you are the first and foremost person I would like to thank. Under your supervision and guidance, I was able to grow as a scientist, a researcher and as a person. Your love for organometallics and your eye for details always made me enthusiastic after a meeting, I always felt more enlightened, and motivated to do an extra step. I am honored to be your first PhD student. It was a joy for me to see how quickly you grew into your new role of the leader of your own research group. Your door was always open, and the freedom I got in deciding myself when I wanted to have a meeting was very important for me to become independent. You care for your students, for our projects and also for our personal well-being. Thank you for believing in me in this project, for inspiring me in our meetings and for being a great supervisor.

**Bert Klein Gebbink**, bedankt voor de supervisie in mijn onderzoek en de waardevolle discussies in de group meetings en werkbesprekingen. Jouw visie en kijk op het onderzoek hebben mij nieuwe inzichten gegeven en motiveerden mij om dingen uit te zoeken, uitgebreid na te denken over theoretische aspecten en meer te lezen, en jouw soms kritische vragen hielden mij 'on top of my game'. Bedankt dat ik een deel kon zijn van de fantastische OCC-groep en bedankt voor de samenwerking.

**Leo Jenneskens**, bedankt voor je input en interessante discussies, vaak over fundamentele aspecten van het onderzoek. **Martin Lutz**, thank you for measuring all the XRD structures in

this thesis. Your expertise in the practical and theoretical aspects has brought this research many important insights on the structure and chemistry of the complexes.

**Milka**, bedankt voor al jouw inzet om de OCC-groep draaiende te houden en alles soepel te laten verlopen voor ons. Als moeder van de groep zorg je altijd erg goed voor ons en kunnen we altijd bij je terecht met onze papierwerk-problemen en een praatje. Ook **Johann** wil ik hiervoor bedanken en daarnaast ook voor de speciale NMR lessen die ik mocht hebben. NMR is een van de belangrijkste analysetechnieken geweest in mijn proefschrift en ik ben dan ook erg dankbaar voor al jouw hulp. **Henk**, bedankt voor alle technische hulp, ESI-MS spectra en gezellige koffiepauzes. Geniet van je welverdiende pensioen. **Jord** en **Adri**, ook jullie bedankt voor de technische assistentie op de groep. Jord, het is jammer dat je niet meer bij de groep bent en ik hoop dat je het naar je zin hebt met je huidige baan. Adri, wat een ongelooflijke kennis en liefde voor katalyse heb jij. Bedankt voor jouw enthousiasme voor mijn onderzoek en inzichten die je me hebt gegeven. **Ad vd Eerden**, bedankt voor de hulp met mijn eerste CO-experimenten op het ICC lab.

I want to especially thank the students that worked with me in this project. Our collaborations are invaluable to me. You all contributed to this project in your own way. While guiding you in science, you guided me personally. **Richt**, your hard work and love for chemistry combined with your intellect made a very challenging project possible. The research you started is still ongoing in the group, and even with the hard work of many people, it is still a challenge. You always made for nice, funny and serious conversation in the group, with an endless interest for the people around you. What I think we all remember are your original expressions, with 'als-een-malle-bever' and 'dikke prima' as my own favorites. On a more personal note: I had some tough times in personal situations in the course of our collaboration, thank you for always having a listening ear. You stay positive and realistic, which is a great combination to me. I am proud of you for always pushing yourself to the next level in your career. Good luck with your PhD in Göttingen. Then **Maxime** joined as well, and 'team Dide' was born (Maxime, keep reading on the next page). Richt and Maxime, the combination of you two at the lab was fantastic, no subject was too weird and no conversation too personal, and it was a pleasure for me to see how you two became such good friends. Laughing so much throughout the days when we were all together at the lab made everything go better and easier. **Joost**, you greatly combined hard work in the lab and your sports and work at Olympos. Your work on the cobalt complexes was the continuation of your friend Maxime's work, and in your hands the catalysis came to life. Your contributions are present in two *Chapters*, numbers 3 and 4, of which mainly Chapter 4 greatly got its shape thanks to you. You have a calmed personality and you work especially hard when you are motivated, I hope you will find a suiting job for all your potential after the Master. **Bart**, secretly I always count you also in this list. It was such a pleasure that you were already working in the ketone-project in a very early phase when I started my PhD,

thank you for the nice collaboration. The Ni-project was very fruitful, with a nice publication and a prominent spot in this thesis in *Chapter 2*.

The bachelor students who worked in this project: **Jochem**, you worked on the Cu-ketone complexes with great enthusiasm. The product of the continuation of your work is shown in *Chapter 3*. It is nice to see you around in the coffee corner from time-to-time and I hope you are enjoying your masters project at ICC. **Hidde**, your project was about the synthesis and coordination of the imine ligand, and this was a great success. The flawless synthesis of the ligand and subsequent coordination resulted in two crystal structures that are present in this thesis in *Chapter 5*, and all of this in less than 8 weeks at the lab. You are an enthusiastic and hard-working chemist, thank you for your help and keep on going. I would also like to thank my second-year bachelor students **Jilles**, **Willeke** and **Mirjam**. We learned a lot on how to make – and also on how not to make – the imine version of the ketone ligand in your short projects. Thanks for the persistence and motivation, and for the great interest you all had in the project.

**Annet** and **Christian**, I would like to thank both of you for your literature essays which helped to shape the background of this thesis.

**Maxime**, when you started your project you were afraid of your vacuum pump, when you finished your project you were maintaining the glovebox and taught people how to use it. I think this is a perfect example of how I saw you grow. I am proud of you and the chemist you are. Thank you for all your help, which is reflected in two chapters, in *Chapters 3* and *4*. Besides my student, you are my friend and *paranymph*. I love your free character and your hilarious stories about which you laugh the hardest. I like how you asked me the most difficult questions as a student, about chemistry and the project background, but also on why the master in general is shaped the way it is, why we do this research, why I do what I do, and why you do the things you do. Your curiosity is bigger than only the lab. Life keeps throwing things at you and I keep on being impressed on how you manage it all. I am grateful for the fact that you will stand next to me on this important occasion. Thank you for all of this.

Major thanks go out to the Organic Chemistry and Catalysis group. I very much enjoyed all the social activities in the group: lunches, coffee breaks, Friday borrels, dinners at the Greek restaurant, BBQs in the park, Christmas dinners, group outings, 90s now's, queens/kings nights, the *woordgrapjes*, and of course the OCC campingtrips.

**Basje**, for the three years we were sitting across of each other we shared basically everything that was happening at the group. Thank you for the good, hilarious, and also deep conversations about the PhD, life, the projects (mold on your paint samples?) and so much more. My favorite part was always to read you the 'opmerkelijke' news items when one of us had a set-back (the best one was obviously the crocodile story). Your down-to-earth mentality kept me with both feet on the ground, also in the difficult moments. **Alessio**, thank you for the discussions and collaborations. I think we made a perfect team-ketone and team-glovebox. I am happy to see the progress in your work which has shown very nice examples of

cooperativity in the nickel systems. Stay 25 years for the rest of your PhD, dat klopt! **Charl**, we spent a long time on the lab together, already having our fumehoods next to each other the first days of my master project. Thank you for all the good discussions, nice conversations and, most importantly, for the numerous perfect puns. It was always nice to receive a slow-clap from you. I look forward to reading your thesis! **Leon**, we have been studying together for more than ten years and I have so many things to thank you for. Especially, thank you for teaching me the basics of DFT calculations in which your patience helped me to persist in the difficult beginning. After all this time, our ways are now actually going to part after your defense in April. Good luck, also in your new job. **Jacco**, your Brabant-ness made me feel at home in the group instantly and thank you for being the stable factor in the group who was (and will be) always around. **Emily**, for your friendship, thank you for all of our nice conversations, the great Pinkpop-adventures and the nice evenings downtown. **Jianming**, for making all of us laugh at unexpected moments. **Peter J**, for teaching the group some nice physics. **Serhii**, your unique character adds knowledge and cats to the group. **Edu**, for your calmed and very kind conversations. **Jing**, for your kind help, always and anytime. **Pradip**, for helping me with DFT calculations, your knowledge has helped me on several occasions, of which a nice example is shown in the orbital diagrams in Chapter 3. **Martine, Maria**, good luck and enjoy continuing the projects. **Thomas** for your fantastic stories and recently organizing the borrels, and also for your enthusiastic help as technician (hopefully you will not encounter more chemical orders with so much bad luck anymore!).

Some of my former colleagues who I want to thank especially: **Suresh**, thank you for your help at the lab, and for all the fun at the OCC campingtrips. **Stefan**, it was a joy to work with you again after such a long time. Also thanks to **Emma, Richard, Matthias, Peter S** and **Yuxing** for the earlier phases of my PhD.

Students keep the atmosphere in the group lively and often come up with fantastic idea's. I want to thank the Bachelor and Master students of the group: **Marc, Cody** (voor al je goede grapjes), **Kirsten, Rohland, Roel, Yoni, Yuri, Daniël, Raoul, Sam, Laurens V, Desmond, Dirk-Jan, Laura, Stella, Laurens B, Cecilia**, and all the other former and current students. Also **Hung-Kun (Mr H)** and **Esther**, who were there during the master and in the first weeks.

Mijn lieve vriendinnen, **Lindy, Linda, Lizzy, Larissa** en **Shirley**, wat is het toch heerlijk om met jullie bij te kletsen, uit te gaan, wijntjes te drinken en zo veel meer. Ik ben jullie dankbaar dat jullie mijn gezwets over wetenschap zo af-en-toe aan kunnen. We gaan allemaal way-back en ik vind het super en bijzonder dat we elkaar nog steeds zien. **Lindy**, zolang als we leven zijn we al vriendinnen (en zeker nog tot in het bejaardentehuis). Je laat mij me altijd welkom en thuis voelen en je bent er altijd, dankjewel.

**Dayinta**, je hebt me enorm geholpen met mijn master waar we zo vaak samen studeerden en ook al kunnen we elkaar niet erg vaak zien, ik waardeer jouw vriendschap heel erg. Dank je dat



je altijd zo leuk, eerlijk en positief bent, ook in mijn PhD gaf je me soms echt goede inzichten waar ik nog steeds heel veel aan heb. Ik kan niet wachten op jouw promotie! En ook **Rutger** bedankt!

**Maarten**, jouw vriendschap was voor mij heel bijzonder en dierbaar, zeker in de laatste maanden toen we beide een PhD waren begonnen hebben we hele fijne gesprekken gehad. Jouw hervonden kijk op het leven, het enorme genieten, was en is inspirerend. Het is nog steeds niet te bevatten dat mijn proefschrift hier nu wel ligt, ik wil deze graag aan jou opdragen.

Familie is bijzonder voor mij. De band waarmee we met elkaar verweven zijn zorgt dat we elkaar nooit uit het oog verliezen. Ik ben jullie enorm dankbaar.

**Olda** en **Toon**, jullie zijn van onschatbare waarde geweest tijdens mijn PhD. Jullie hebben mij in alles gesteund, staan altijd achter de keuzes die ik maak en juichen harder dan wie dan ook. Vanuit de opvoeding leerden wij al om door te zetten en op onze eigen benen te staan, dit in een lieve en vertrouwde omgeving. Ik denk dat jullie jezelf wel een schouderklopje kunnen geven, want jullie hebben nu twee gepromoveerde dochters. Olda, niemand zo trots als jij. Je zei weleens: 'ik heb vandaag weer even naast mijn schoenen gelopen', zo trots als een pauw. Wat er ook gebeurde, jouw steun was en is er altijd. En haalde ik een onvoldoende, dan zei je altijd 'meer als je best kan je niet doen'. Dit maakt dat ik altijd een vertrouwde plek heb en me onvoorwaardelijk gesteund voel. Zo sterk en zo liefdevol, dankjewel. Toon, van jou heb ik geleerd dat eigenlijk alles altijd wél kan. En die instelling in het leven brengt ons naar vele plekken. Van jongs af aan heb jij mij steeds een beetje kennis laten maken met Natuur en wetenschap, van het spelen met knex en op een bureaustoel rondraaien met een fietswiel, tot het uitleggen waarom de lucht blauw is, hoe een regenboog ontstaat en wat geluid of elektriciteit is. Vragen stellen en nieuwsgierig zijn was altijd goed. Later legde je mij wis- en natuurkunde uit, en nu vertel ik jou over chemie. We vinden elkaar ook altijd met avontuurlijke bezigheden, mooie vakanties en uitgebreide etentjes. Ik wil jullie beide bedanken voor dit alles. Beide hebben jullie weer een nieuwe jeugd gevonden, vol nieuwe avonturen en liefde. **Frans**, als echte kunstenaar heb jij een bijzondere kijk op het leven. Ik kan enorm genieten van onze gesprekken waarin wij elkaar treffen op onverwachtse momenten. Bedankt dat je met mij het avontuur aan wilde gaan om de omslag van mijn thesis te ontwerpen, en wat ben ik blij met het resultaat. Samen met Olda zie ik je genieten, van muziek, uitgaan, gezelligheid en familie, ook daarvoor een dankjewel. **Hanneke**, voor jou is niks te gek, skiën, klimmen, reizen, alles is goed. We genieten van het samen winkelen en we moeten toch altijd een beetje gebelen als mensen weer eens niet begrijpen wat onze relatie nou precies is. Samen met Toon kan je de wereld aan en wij zijn altijd uitgenodigd om mee te genieten. Bedankt voor alle leuke avonturen en we blijven genieten. **Familie Boek** heb ik er als cadeautje bijgekregen, die ik ook allemaal wil bedanken. In het bijzonder **Oscar**, mijn soort-van-broertje wat al heel snel vertrouwd voelde, bedankt voor jouw steun en vriendschap.

**Aukje**, als ervaringsdeskundige kan je mij als geen ander begrijpen en adviezen geven over het werk. Jouw motivatie kent geen einde en met jouw oog voor detail en zorgzaamheid heb je alle touwtjes in handen. Je grijpt altijd alle kansen met beide handen aan en dat is een voorbeeld voor ons allemaal. Geniet van je nieuwe baan in Parijs samen met **Sam**. Bedankt voor al jouw steun en alle leuke en mooie avonturen van de afgelopen jaren. Sam, jij bent absoluut Aukje's rots en het is fantastisch dat jullie samen alles aan kunnen.

Ook wil ik mijn sportieve **familie Verhoeven** en de altijd gezellige **familie Couwenberg** bedanken.

**Manuel**, supervisor, colleague, friend, love, family, paronymph: you are important in so many ways. You inspire me to be a better person, friend, scientist and chemist. You guided me during my master and beyond, and you bring so much beautiful moments and laughter. I admire your view on the world, your skills to see the good in various situations and in people, your love for creativeness in life, music and art, your love for Science. Our chemistry is extraordinary. We met in the lab and up until this day it is an always present common love. Life is precious and with you I can truly be myself. You believe in me, you care for me and you get me better than I do. In my wandering universe you are my home, my rock, my *pale blue dot*. Thank you.

**Dide**

## Résumé

Dide Verhoeven was born on 3 September 1990 in Utrecht. After finishing the HAVO education at high school in the areas of Nature & Health and Nature & Technique in 2007 at the Cals College in Nieuwegein, she did her HBO bachelor Organic Chemistry at the University of Applied Sciences, Hogeschool Utrecht (HU) which she finished in 2011. Within the bachelor program she did a six-month junior research internship at the Molecular Inorganic Chemistry group at the University of Amsterdam (UVA) with Prof. Dr. C. J. Elsevier and Dr. P. Hauwert on zero-valent palladium N-heterocyclic carbene complexes. She performed her bachelor research in the group of Inorganic Chemistry & Catalysis with Prof. Dr. Ir. B. Weckhuysen and Dr. J. J. Zakzeski on the oxidation of kraft lignin with a nickel catalyst in ionic liquids. Within the last year of the bachelor, she also followed the pre-master program at Utrecht University for the master Nanomaterials: Chemistry and Physics, which she started in 2011. She performed her master research in the group of Organic Chemistry & Catalysis (OCC) under supervision of Prof. Dr. R. J. M. Klein Gebbink and Dr. M. Basauri Molina on the synthesis of artificial metalloenzymes for olefin metathesis in water. After graduating the master education in 2013 she started her PhD studies in the same year at Utrecht University in the OCC group under supervision of Dr. M. -E. Moret. The most important results of the research are presented in this thesis. Several parts of this thesis have been presented in national and international conferences, such as EUCOMC XXI and XXII, COST CARISMA meeting, International Symposium on Relations between Homogeneous and Heterogeneous Catalysis, Netherlands' Chemistry and Catalysis Conference and CHAINS.



## Publication list

**D. G. A. Verhoeven**, M. A. C. van Wiggen, J. Kwakernaak, M. Lutz, R. J. M. Klein Gebbink, M. -E. Moret, 'Periodic Trends in the Binding of a Phosphine-Tethered Ketone Ligand to Fe, Co, Ni and Cu', *Chem. Eur. J.*, **2017**, DOI: 10.1002/chem201703254.

**D. G. A. Verhoeven**, M. -E. Moret, 'Metal-Ligand Cooperation at Tethered  $\pi$ -Ligands', *Dalton Trans.*, **2016**, *45*, 15762–15778.

B. W. H. Saes, **D. G. A. Verhoeven**, M. Lutz, R. J. M. Klein Gebbink, M. -E. Moret, 'Coordination of a Diphosphine-Ketone Ligand to Ni(0), Ni(I), and Ni(II): Reduction-Induced Coordination', *Organometallics*, **2015**, *34*(12), 2710–2713.

### *Previous research*

M. Basauri-Molina, **D. G. A. Verhoeven**, A. J. van Schaik, H. Kleijn, R. J. M. Klein Gebbink, 'Ring-Closing and Cross-Metathesis with Artificial Metalloenzymes Created by Covalent Active Site-Directed Hybridization of a Lipase', *Chem. Eur. J.*, **2015**, *21*, 15676–15685.

